GREEN AROMATICS FROM BIOMASS FAST PYROLYSIS AND CATALYSIS

By

Shantanu Kelkar

A DISSERTATION

Submitted to
Michigan State University
in partial fulfillment of the requirements
for the degree of

Biosystems Engineering – Doctor of Philosophy

Chemical Engineering – Doctor of Philosophy

2013

ABSTRACT

GREEN AROMATICS FROM BIOMASS FAST PYROLYSIS AND CATALYSIS

By

Shantanu Kelkar

The green synthesis of aromatic chemicals is especially important due to their high volume in making fuels and chemicals. Biomass pyrolysis integrated with catalysis provides one renewable route for creating these aromatics like benzene, toluene and xylenes. To this end, several biomass types and catalyst preparations were examined for yield performance using analytical pyrolysis–GC/MS. In addition, MSU-MFI, a mesoporous zeolite with intracrystal mesopores, was synthesized using silane-modified polymers as mesopore-generating agents. Due to higher yields and lower coke formation when compared with the conventional ZSM-5 catalyst, MSU-MFI offers an improved option for making non-oxygenated aromatic chemicals from photosynthetic biomass. Biomass fast pyrolysis was also demonstrated on a pilot-scale using a compact, transportable, screw conveyor reactor for producing bio-oil.

Dedicated to my loving family and dearest friends

ACKNOWLEDGEMENTS

My utmost gratitude and indebtness to my advisor, Dr. Chris Saffron, for his strong and unstinting support during my doctoral degree; for his amazing patience and optimism. Thanks to my co-advisor in Chemical Engineering, Dr. Dennis Miller, for his guidance and time; for being patient during the many meetings for my quest to understand diffusion in catalysts. Dr. James (Ned) Jackson for serving on my committee, for his kindness and for teaching us organic chemistry through his lab meetings and discussions. Dr. David Hodge for serving on my committee, for guidance on data analysis and for giving me an opportunity to work with him and his lab group. Dr. Tom Pinnavaia for advice and support with catalysis work. I am blessed with one of the best doctoral program committee and will always be grateful for all that I learnt.

A sincere thank you to Dr. Robert Kriegel, Mr. Mike Schulthies and The Coca-Cola Company for generous and patiently supporting this exciting project. Thanks also to U.S. Department of Transportation through the Northeast Sungrant Initiative for support.

Thanks also to Dr. Kirk Dolan, Dr. Janice B. Harte and Dr. Muhammad Siddiq for the many opportunities to work with them, for their friendship, advice and support in times of need.

Very special thanks go to Kristine Van Winkle, who as a lab assistant made things work; for her friendship. Thanks to Kevin Andreassi for helping with experiments throughout my research; for his efficiency and reliability. Without your help Kristine and Kevin, this research would not been possible. Thanks to group members and friends, especially Dr. Zhenglong Li for his friendship, for setting the example of an ideal researcher and exemplary work ethic; Jon Bovee for his friendship and help on many projects, Mahlet Garedew, Chai Li and Tom Stuecken. Thanks to the post-doctoral scholars, Dr. Somnath Bhattacharjee, Dr. Soumitra

Chatterjee and Dr. Ambareesh Mukute. Thanks also to Dan Swanson and Pastor Hurtado, Kara Vossler, Brandon Kovnat, Akua Nkrumah for their contribution and help with many many experiments.

Sincere thanks are due to the technical staff that helps behind the scenes and were always available: Dr. Michael McGilvary from Shimadzu for his advice and friendship and Terry Hohenwater from CDS Analytical. Thanks also to Dr. Hodge's lab group: Tongjun Liu, Glen Li, Crystal Li and especially, Ryan Stoklosa and Dan Williams. Dan and Ryan made the lab a fun and good place to be at; their contribution towards this work was indirect but important. Also thanks to Aaron Oberg who was always available when his help was needed, and Dr. Xianfeng Ma, Dr. Lars Peereboom. Special thanks to Dr. Joel Dulhebohn and Dr. Seoung-Soo Kim from the Pinnavaia lab for advice with catalysis work, and Dr. Ibrahim Greiby for his collaboration.

Heartfelt thanks and gratitude to my family for their support during my education and life; for being there through the thick and the thin, for loving me through the few highs and the many many lows. Friends played a very very important role, tolerated my idosyncracies and cheered me on through rough times, saved me when my family was away. Special thanks to Bhupinder Kumar, Rahul and Prajakta Deshpande, Lovelesh Chawla, Madison Hall, Sonali Kand and Maya Patel, without all of whom, the journey would have been impossible. Thanks also to these awesome friends: Maulik Dhandha, Brajesh Tripathi, Nikhil Mehrotra, Mahesh Khurana, Rabiha Binti Sulaiman and Girish Kasat.

TABLE OF CONTENTS

LIST OF TABLES

LIST OF FIGURES

KEY TO SYMBOLS AND ABBREVIATIONS

Abbreviations

ZSM5: ZSM-5, zeolite catalyst

Worm: (2%) Al-MSU-S, worm geometry catalyst

Foam: (2%) Al-MSU-S, foam geometry catalyst

SZ: sulfated zirconia catalyst

MSZ: Mesoporous (20%) sulfated zirconia

RM: Red mud

Symbols

A = area of cross-section of micropore,

A_m= area of cross-section of macropore,

C_A = concentration of reactant (1^{st} order reaction) in micropore,

C_{AS}=reactant concentration at micropore-macropore interface,

C_{AM} = concentration in macropore = C_{AS},

C_{bulk} = bulk conc., D = effective diffusivity in micropore,

D_m = effective diffusivity in macropore,

H = third dimension of catalyst, D_m = effective diffusivity in the macropore, k=rate constant,

k=rate constant,

L=length of pore,

S = surface area,

V_p = pore volume,

X=length of macropore,

x= distance along macropore length,

z= distance along length L.

Greek symbols

λ = dimensionless quantity equal to z/X,

λ' = dimensionless quantity equal to x/X,

Φ = Thiele modulus, subscript m for macropore,

η = effectiveness, subscript m for macropore,

ε_m = volume occupied by macropores, macroporosity,

ε_{mic} =volume occupied by micropores, microporosity (fixed),

ε_s = volume occupied by solid, solid density

CHAPTER 1. INTRODUCTION AND BACKGROUND

1.1 Introduction

The fluctuating supply and cost of fossil fuels and the environmental effects due to their use has put the spotlight on more sustainable sources of energy such as the production of fuels and chemicals from biomass feedstock. Other green sources of energy for heat and electricity, such as hydroelectricity, wind and solar, exist. However, plant and plant-derived biomass represents the only sustainable source of organic carbon as an alternative to the carbon fuel obtained from petroleum-based sources [1]. Plant biomass based energy and chemicals can provide local heat and power, but also use existing infrastructure (fuel processing, vehicles, CHP), give impetus to the local economy and increase energy independence of communities, while being carbon neutral or negative. For an efficient transition to a bio-based economy, it is necessary to select cheap and abundant source of biomass.

Renewable feedstock may be used to meet the U.S. energy demands as well as to promote national energy independence and security. Biological or chemical strategies of converting biomass into green fuels and chemicals are being studied worldwide; however these methods involve multiple steps and long residence times. Aromatic hydrocarbons such as benzene, toluene, ethylbenzene and xylenes (BTEX) are important petrochemicals used in the chemical industry (e.g. for the production of polymers and plasticisers or as fuel additives). Producing aromatics and olefins from bio-based chemicals requires additional petroleum-based processing. Bio-based aromatic molecules can also be produced from carbohydrates using aqueous phase processing and catalysis. However, to produce aromatic hydrocarbons from lignocellulosic biomass such as wood, grasses agricultural residue and food waste, thermochemical methods such as fast pyrolysis combined with catalysis need to be used. Pyrolysis technologies offer a potentially less expensive route to aromatics with minimal

modifications required to the existing petroleum infrastructure. Fermentation-based processes have been extensively considered, but they suffer from high cost, limited scalability, and incompatibility with the existing hydrocarbon-based infrastructure. Instead, liquefaction of terrestrial plant matter via biomass fast pyrolysis may be a more practical first step.

Proposed is a simple process for converting plant-derived biomass into aromatics such as BTEX, which are intermediates for many chemicals and polymers. This process, consisting of pyrolysis and catalysis, will transform renewable feedstocks and waste streams into value-added products. Pyrolysis can be used to transform feedstocks and waste streams such as poplar, switchgrass, algae, coffee bean waste, or any of the sources of lignocellulosic biomass described in the "billion-ton" study [1]. Historically, low selectivity is the barrier limiting the application of pyrolysis, as hundreds of compounds are produced from lignocellulosic materials. To mitigate the low selectivity of pyrolysis, shape-selective catalysis can be used to convert this complex mixture into a simpler mixture enriched in aromatics. This process will exhibit simplicity in concept and flexibility across an array of plant biomass feedstock, cost-competitiveness when compared to the current petro-based supply chain is expected as is a reduction in environmental impacts associated with climate change. Products and co-products will be locally generated and distributed to the communities providing the resources supporting the supply chain.

If deployed, positive socio-economic benefits include domestic and international jobs creation, capital retention and investment in rural communities, and increased profitability resulting from waste conversion into valuable chemicals. This simple and flexible process may offer a profitable way to benefit the global environment and to advantage lesser developed regions through jobs creation in biomass supply chains.

1.2 Fast pyrolysis

An organic material or recent biological origin is defined as biomass [2]. Plant-based biomass are composed of three polymers – hemicellulose 20-40%, cellulose 40-60% and lignin 10-25% by weight. These organic polymers decompose thermally when heated the absence of oxygen. This irreversible process is known as pyrolysis and it produces numerous chemical species in the form of vapors, aerosols and solid residue.

Conventional or slow pyrolysis has been known since ancient times and was used to produce solid charcoal from biomass. To maximize char formation, the process uses low heating rates (<50°C/min) and long vapor residence times (Table 1.1). Researchers in the early 1980's found that rapid heating of biomass to moderate temperatures (about 500°C has been found to be optimum) and immediate quenching of the emerging pyrolysis vapors shifted the product towards maximum liquid yield, known as bio-oil. This process is termed as fast pyrolysis. Another process called as flash pyrolysis approaches gasification by utilizing high temperature and produces gaseous species as major product [2].

Table 1.1 Thermochemical conversion processes

Process product yields (%) dry wood basis	***Liquid***	***Char***	***Gas***
Fast pyrolysis (Moderate temp.: ~ 500 °C, short residence time)	70	15	15
Carbonization (low temp., < 350 °C long residence time)	30	35	35
Gasification (high temp., > 700 °C short residence time)	5	10	85

Fast pyrolysis converts low-value, low-density biomass in a single step to a denser liquid product, bio-oil, at yields in excess of 70% by weight. Biomass fast pyrolysis involves the rapid heating of biomass (~500 °C/sec) in an inert atmosphere to intermediate temperatures (~500 °C).

The products include a solid char, non-condensable gases and a condensable product, bio-oil. Bio-oil may be futher upgraded to transportation fuels or chemicals [3].

The condensation of pyrolysis vapors and aerosols produces a dark brown colored liquid with a smoky odor called as bio-oil. Non-condensable fraction of pyrolysis vapors consists of gaseous species such as carbon monoxide, carbon dioxide, methane and hydrogen. Solid reidue from pyrolysis is known as char. Char is product of dehydration, condensation and re-polymerization of the non-volatile fragments of hemicellulose, cellulose and lignin produced during pyrolysis. The relative proportions of these three solid, liquid and gas product fractions significantly vary depending upon the process and reactor conditions.

Figure 1.1 Products and applications of fast pyrolysis of biomass. For interpretation of the references to color in this and all other figures, the reader is referred to the electronic version of this dissertation.

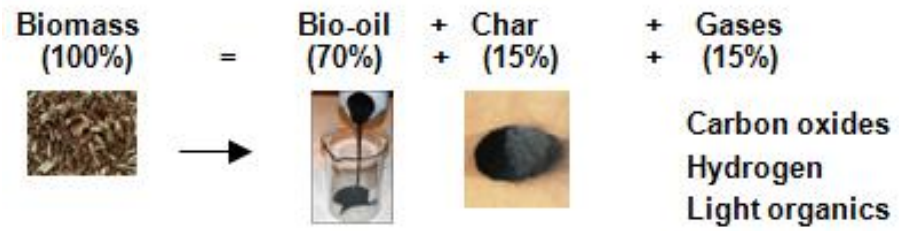

A wide range of reactor configurations have been operated, including fluidized-bed reactor, circulating fluidized-bed reactor (CFB), transported bed reactor, rotating cone reactor, ablative reactor, auger reactor, vacuum moving bed reactor and entrained flow reactor, etc (Table 1.2) . Among these reactors, fluidized-bed reactor and circulating fluidized-bed reactor are the most popular configurations due to their ease of operation and ready scale-up. However, these two types of reactors require a heat transfer medium (sand) to increase the heat transfer rate and need high amounts of inert gas to fluidize the biomass. The operation cost is increased due to energy input for heating the sand and the cost from using inert gas.

Table 1.2 Overview of fast pyrolysis reactor characteristics for bio-oil production [4]

Property	Status	Bio-oil (wt%)	Complexity	Feed size	Inert gas need	Specific size	Scale Up
Fluid bed	Comm	75	Medium	Small	High	Medium	Easy
CFB	Pilot	75	High	Medium	High	Large	Easy
Entrained	None	65	High	Small	High	Large	Easy
Rotating cone	Demo	70	High	Very small	Low	Small	Medium
Ablative	Lab	75	High	Large	Low	Small	Hard
Vacuum	Demo	60	High	Large	Low	Large	Hard

Comm: commercial (>3000 Kg/h). Demo: demonstration (300-3000 Kg/h). Pilot: pilot plant (30-300 Kg/h). Lab: laboratory (1-30 Kg/h).

1.3 Catalytic upgrading

Low selectivity limits the application of pyrolysis, as hundreds of compounds are produced from pyrolysis of biomass constituents and their interaction. Pyrolysis products are a complex and reactive mixture of non-condensable gases such as CO, CO_2, CH_4, highly oxygenated compounds such as carboxylic acids, carbonyl group compounds, furans, phenolics and sugars and a significant amount of water.

Hydrogen at high pressure may be employed during pyrolysis (hydro-pyrolysis) or post-pyrolysis to reduce oxygenated molecules (hydrotreating). In these processes, pyrolysis compounds are deoxygenated with hydrogen at high pressures and moderate temperatures to form hydrocarbons and water. In the absence of hydrogen, pyrolysis vapors may be reacted with a catalyst at atmospheric pressure. The quality and selectivity of pyrolysis products can be altered and improved by using heterogeneous catalysts, at atmospheric pressure, and without hydrogen requirement. Catalysts may be employed at three stages: 1) pyrolysis of biomass is performed in the presence of catalyst, i.e. catalytic fast pyrolysis (CFP) or co-pyrolysis and catalysis; 2) immediately post-pyrolysis of biomass, where the vapor products (condensable and non-condensable) react on a catalyst bed, i.e. catalytic vapor cracking (CVC), or sequential

pyrolysis and catalysis; 3) condensed liquid product, bio-oil, is passed over a catalyst bed in vapor or liquid form, i.e. bio-oil upgrading.

Catalytic upgrading of pyrolysis products removes oxygen in the form of coke and non-condensable gases such as CO, CO_2, and H_2O and gives a product richer in hydrocarbons. Consequently, the liquid yield (bio-oil) decreases to as low as 45-50% while gas and coke (on catalyst) production increase rapidly. Thermochemical conversion of biomass to bioenergy has many advantages: as it is possible to employ small on-site fast pyrolysis units to rapidly convert biomass to a condensed form of energy in the form of bio-oil. The solid by-product, char, may be used a source of energy, an adsorbent, fertilizer or for carbon sequestration. Energy from non-condensable may be recovered and re-used in the process. Thus, solid biomass may be directly converted into liquid product rich in aromatics in a simple, single or two-step continuous process with short residence times, without use of hydrogen, high pressure, complicated multi-step processes or high capital cost. Catalytic fast pyrolysis produces higher quality bio-oil and reduces the cost and intensity of downstream refining processes.

In addition to reduced emissions due to use of renewable biomass, significant carbon reductions are anticipated upon deployment of the proposed process as the solid bio-char co-product can be land applied to sequester carbon or used as a source of energy. As the carbon in bio-char mineralizes to carbon dioxide at very slow rates, this process can become “carbon negative” when bio-char is returned to agricultural or silvicultural systems as a nutrient amendment [5]. Also, the carbon credits acquired in a cap and trade system for sequestering carbon as bio-char can further enhance the economic viability of this process [6].

1.4 Goal and Objectives

Aromatic hydrocarbons may be produced from renewable resources, as opposed to fossil fuels, by using thermochemical methods such as pyrolysis with catalysis. The project goal is to develop a process that is locally deployable for producing aromatics from plant biomass. The objectives of this project are as follows:

- Screen biomass-catalyst combinations for aromatics production
- Formulate new catalysts for increasing aromatics
- Design and operate a pilot-scale process

To this end, we begin with the pyrolysis of biomass components, specifically, hexoses (Chapter 2). The structural features of these hexoses that influence the production of two major products upon pyrolysis, anhydropyranoses and 5-hydroxymethylfurfural, were studied. Then, we move to experiments with whole biomass. Eight North-American grass species, all belonging to the Poaceae tribe, were selected to study the effect of their composition on the distribution of pyrolysis products (Chapter 3). In Chapter 4, the study was expanded to include different feedstock in an attempt to identify the best feedstock for producing aromatics from biomass pyrolysis. A similar study was repeated with six different catalysts in order to compare their product yields and identify the best for aromatics production (Chapter 5). When catalysts are used in an industrial environment, they are in the form of pellets which are microporous-macroporous structures. Therefore, in Chapter 6, a theoretical study on the effect of these macropores on the mass transfer within a pellet was carried out and a simple 2D model was proposed for a first-order reaction. From the results of these studies, it was hypothesized that a mesoporous-microporous catalyst with a metal dehydrogenating functionality may have greater aromatic yields and lower coke production than conventional catalysts. In Chapter 7, the

synthesis of such a bifunctional mesoporous catalyst and its application in biomass pyrolysis was demonstrated. Chapter 8 expands the application of this bifunctional mesoporous catalyst to hydrocarbon reactions, specifically, conversion of bio-derived isobutylene gas to aromatics. Finally, in a scale-up experiment, pyrolysis of spent coffee grounds was demonstrated in a 10 kg/hour screw-conveyor reactor (Chapter 9). Response surface design of experiments was used to determine the optimum reactor tempereature and screw speed for maximum liquid product yield.

CHAPTER 2. ANALYTICAL FAST PYROLYSIS OF HEXOSES AND THEIR MIXTURES WITH BIOMASS

Somnath Bhattacharjee, Shantanu Kelkar, Soumitra Chatterjee,
Robert Kreigel, Christopher M. Saffron and James E. Jackson

2.1 Abstract

Fast pyrolysis of hexoses, namely, glucose, galactose, mannose and their α- and β-methyl pyranosides gives anhydropyranoses and 5-hydroxymethylfurfural as major products. For the parent sugars, the yields of 1,6-anhydropyranose products decrease in the order glucose > galactose > mannose. Displacement of the glycosidic substituent (-OH or -OMe) by the C-2 hydroxyl group is thought to form an intermediate epoxide which, in turn, is opened by attack of the primary -OH group at C-6, to produce 1,6-anhydropyranoses. Glucose and mannose are C-2 epimers, with their –OH groups oriented equatorial or axial, respectively. We propose that the above reactivity order reflects formation of 1,2-epoxy intermediate from glucose rather than from mannose, leading to a higher 1,6-anhydropyranose yield. The stereochemistry of the C-4 position also affects 1,6-anhydropyranose formation; pyrolysis of galactose (C-4 epimer of glucose) forms less 1,6-anhydropyranose than glucose. Our studies indicate that fast pyrolysis of the methyl α/β-gluco/galacto and α-manno-pyranosides produce more 1,6-anhydropyranoses than the underivatized parent sugars, demonstrating the importance of the leaving group (-OMe vs –OH) in 1,6-anhydropyranose formation.

2.2 Introduction

Greenhouse gas emissions and fast depletion of petroleum sources are major concerns in today's world. There has been a growing interest in the utilization of biomass, the only renewable carbon source, for carbon-neutral production of fuels and chemicals [7]. Fast pyrolysis is a thermochemical process that consists of rapid heating in the absence of oxygen to

temperatures between 400 and 800°C. This process breaks down biomass, which mainly consists of biopolymers such as cellulose, hemicellulose and lignin, into smaller molecules with higher energy content such as furans [8], [9]. Cellulose, a linear homopolymer of glucopyranose linked by β-1,4-glycosidic bonds, typically accounts for the largest fraction of biomass by weight. A detailed understanding of the mechanistic pathways of cellulose pyrolysis is important for widespread commercialization of biomass conversion to meet the energy and chemical needs [10].

Due to the great potential as feedstocks for fuels and chemicals production, mechanistic pathways of cellulose pyrolysis have been extensively investigated [11], [12], [13]. To understand the pyrolytic behavior of cellulose, chemicals produced from cellulose pyrolysis under moderate or high temperatures are identified by advanced tools such as GC/MS, NMR, FTIR. The pyrolysis of these carbohydrates is a complex process and the relevant mechanistic pathways are somewhat controversial, despite much effort dedicated to their elucidation [4], [13], [14], [15], [16], [17], [18].

Levoglucosan is one of the major products obtained from fast pyrolysis of cellulose and glucose. It is well established that levoglucosan formation entails cleavage of the cellulose chain at the macromolecule's 1,4 glycosidic linkages, accompanied by intramolecular rearrangement of the glucose monomer units [15], [19], [20]. However, the precise mechanism of anyhydropyranoses such as levoglucosan formation remains controversial. As shown in Figure 2.1, two primary paths have been suggested: (a) a direct homolysis mechanism, in which cleavage of the glycosidic bond to form a C-1 radical is the initial step; [21], [22] and (b) heterolytic cleavage, in which conversion starts with formation of an oxacarbenium ion intermediate, followed by nucleophilic attack by the primary –OH group at C-6 position [13],

[14], [23], [24], [25], [26], [27]. Additionally, some reports indicated that formation of levoglucosan occurs through the SN^2 via intermediate epoxide [17]. Ponder proposed a two-step mechanism with an ionic intermediate to yield levoglucosan[23]. More recently, Broadbelt theorized a concerted mechanism [28] with an ionic intermediate to yield levoglucosan [29]. Many others have proposed cellulose conversion to levoglucosan through diradical formation [4], [15], [30], [31]. Overall, further research is necessary in order to better understand the transformation of cellulose and glucose into levoglucosan.

Figure 2.1 Proposed initial intermediates in homolytic and ionic mechanisms for levoglucosan formation from cellulose

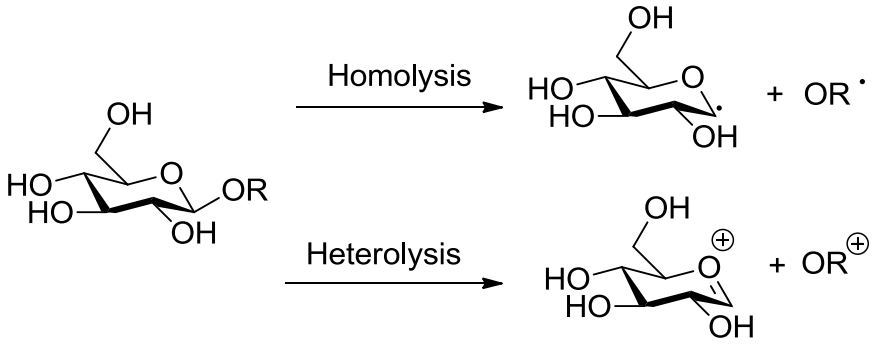

Furans, particularly 5-hydroxymethylfurfuraldehyde (HMF), are also major products from fast pyrolysis of cellulose and glucose. Reports indicate that furans form directly from cellulose without small-molecule production [32]. Several free glucose can be an intermediate in the conversion as observed in low temperature (100–200 ^oC) aqueous-phase processes [33], [34]. Like levoglucosan, there are competing furan formation mechanisms which have been reported. Dauenhauer et al. proposed that furan rings can form from interior monomers without the need for a reducing end group or glucose intermediate [32]. Others report that furan compounds can form from glucose and probably from the reducing end of cellulose through a ring opening mechanism [35], [36], [37]. Additionally, a secondary reaction was claimed to be responsible for

the conversion of major cellulose pyrolysis products such as levoglucosan to furans, light oxygenates, char and gases [38]. Conversely, Shanks, Brown et al. and Dauenhauer et al. stated that levoglucosan is relatively stable and does not undergo further pyrolysis reactions [39]. Our preliminary results are consistent with Shanks and Dauenhauer in that levoglucosan is relatively stable in the absence of inorganic minerals as catalysts.

2.3 Objectives

Therefore the primary objective of the present study is to gain insight into the fundamental chemistry of hexose pyrolysis as further study is needed to the better understand the mechanisms of cellulose pyrolysis. As such, we subjected glucose (the monomer unit of cellulose), mannose (the C-2 epimer of glucose), galactose (the C-4 epimer of glucose), their α- and β-methyl pyranosides and 2-deoxy-d-glucose (absence of –OH at C-2 position) under fast pyrolysis conditions by rapidly heating to 600 ˚C while maintaining very low vapor residence time. We carefully chose different isomers of glucose to understand fast pyrolysis mechanism. For example, we envisioned that fast pyrolysis of glucose; galactose and mannose would produce similar products. However, the products distribution of glucose and other isomers should differ from each other because of their structural differences. Additionally, we anticipated 2-deoxy-d-glucose should produce product different from glucose, galactose and mannose

In order to understand the complex reactions of pyrolysis, glucose and cellulose are used as model compounds to better understand actual biomass as a substrate. These carbohydrates can be mixed with biomass samples to probe the balance between inter- and intra-molecular processes in the pyrolysis reaction. Furthermore, the use of isotopically labeled small molecules may reveal reaction path details despite the overall complexity of the process. Therefore, the secondary objective focuses on the more relevant realm of real plant matter and the development

and characterization of methodologies to mix ^{13}C-labeled defined small molecule probe (in this case, 13C-labelled glucose) with Poplar (DN-34, *Populus euramericana cv. Eugenei*) and *Arabidopsis thaliana.*

2.4 Experimental section

2.4.1 Materials

D(+) Glucose (≥99.5%), D(+) galactose (≥99.0%), D(+) mannose (≥99.0%), methyl-α-D-glucopyranoside (≥99.0%), methyl-β-D-glucopyranoside (≥99.0%), methyl-α-D-galactopyranoside (≥98.0%), methyl-β-D-galactopyranoside(≥98.0%), methyl-α-D-mannopyranoside (≥99.0%), 2-deoxy-D-glucose (≥98.0%) were purchased from Sigma-Aldrich and used as received. All standards were purchased from Sigma-Aldrich and used without further purification. Quartz wool, pyrolysis tubes were bought from CDS Analytical (Bellafonte, PA).

The plant materials used for this research were with Poplar (DN-34, *Populus euramericana* cv. Eugenei) and *Arabidopsis thaliana*. Poplar chips were obtained from Michigan State University's Forest Biomass Innovation Center near Escanaba, MI. The chips were dried to less than 10% moisture by weight and milled to a particle size of less than 1 mm (US mesh #35) using a Willey Mill (Standard Model No.3, Arthur H. Thomas, Philadelphia, PA).

Arabidopsis thaliana (ecotype Columbia) embryonic suspension cell line T87-C33 cells were obtained from the lab of Dr Kenneth Keegstra at the MSU-DOE Plant Research Laboratory. The procedure for growth of *Arabidopsis* cells is described elsewhere. For the sampling, 50 mL of two-week old suspension culture was centrifuged at 3000 rpm for 3 minutes. The cell pellet obtained was dried at ~80 °C to get ~3g of dried *Arabidopsis* cells.

Both biomass were washed with hot water using Sohxlet apparatus for 12 h, filtered and oven dried at 60 ^{o}C for 24 h. Anhydrous D-glucose (Acros), 13C-labelled glucose (Cambridge

Isotopes), Avicel Cellulose (Fluka) and Galactose & (Sigma-Aldrich Co., St Louis, MO) were used without additional purification. Powdered reactants were prepared by physically mixing in the following ratios: 1:9, 3:7 and 1:1 (approximately). Then weighed amount of those premixed samples (300-500 μg) were packed into quartz tubes containing quartz wool.

2.4.2 Analytical Pyrolysis-GC/MS

Experiments were conducted using a microscale pyrolysis unit, CDS Pyroprobe 5250 (CDS Analytical Inc, Oxford, PA) interfaced to a Shimadzu QP-5050A gas chromatograph /mass spectrometer (Shimadzu Corp, Columbia, MD). Glucose sample was pre-mixed with poplar and *Arabidopsis Thaliana* respectively with different physical ratios (1:9, 3:7, 1:1 approximately). Then weighed amount of those premixed samples (300-500 μg) were poured into quartz tubes containing quartz wool. These samples were pyrolized at 600 ^{o}C pyroprobe for 10 s and vapor line was directly attached to a GC-MS. Sample vapors were analyzed in GC and each peak was determined by mass-spectrometer. Possible compounds from mass-spectrometer were separately injected to GC to validate the presence of that compound.

For hexoses, approximately 0.5-1 mg samples were packed between quartz wool in a quartz tube with a filler rod. The pyroprobe was set at 600 °C with a hold time of 10 s at a heating rate of 1000°C/s. The GC used a Restek Rtx-1701 column (Restek, Bellefonte, PA), 60 m x 0.25 mm with a 0.25 μm film thickness. The column gas flow was 1 cm/s with a split ratio of 1:100. The GC oven temperature program begins with 1 minute at 40 °C followed by heating at 8 °C/min to 270 °C. The injector and detector temperature were set at 280 °C. The mass spectra were recorded in electron ionization mode for *m/z* of 28 to 400. Compounds were identified by comparing the retention time and mass spectra of commercially available pure compounds, reported mass spectra in references [13], [32] and/or most probable matches in

NIST library. Some peaks remain unidentified. Percent of peak area was calculated by equation 1. Peaks appeared at retention time below 4.0 min were not included in Table 1A in Supporting Information because those peaks correspond to light gases. Additionally, the amount of char produced during fast pyrolysis was not included in Table 1 or 1A. Peak area percentages below 0.4 % were not listed in the Table 1 as the total of these peaks only contributed about 5 %. Three replicates of each sample were run, and the values represent in the table are the difference between the average and standard deviation.

$$\% \text{ of peak area} = \frac{\text{each peak area}}{\text{total peak area}} \text{ X } 100 \qquad (1)$$

2.5 Result and discussion

2.5.1 Hexoses to anhydrosugars: 1,6-anhydrosugar formation from the fast pyrolysis of parent sugars

Pyrolysis of aldohexoses produces 1,6-anhydrosugers as major products. Formation of 1,6-anhydrohexopyranose from glucose (**1**), galactose (**2**), mannose (**3**), α/β-gluco/galacto and α-manno-pyranoside (**5**, **6**, **7, 8** and **9** respectively) requires an energetically unfavorable change in conformation. The thermal energy available during fast pyrolysis is sufficient to effect such a change. Byrne in the early 60's followed by more recent work [17] reported the formation of carbenium ions as intermediates during the conversion of monosaccharides to anhydrocompounds under fast pyrolysis conditions. However, the stabilization of carbenium ions by solvation presumably cannot occur at high temperature (600 ^{o}C) during pyrolysis. Fast pyrolysis of compounds **1-9** was conducted employing a microscale pyrolysis unit and products were characterized by GC/MS. Products distribution for the fast pyrolysis of compounds **1-9** is

summarized in Table 2.1 shows a product distribution which indicates that the yields of 1,6-anhydropyranose decrease in the order glucose > galactose > mannose.

We propose that conversion of **1** (R = H) to 1,6-anhydropyranose (**10**) follows a concerted mechanism via intermediate epoxide formation as shown in

. Glucose exists mostly in its anomeric pyranose forms, with small amounts in the 1,4-furanose forms and the open-chain aldehyde form also present in very small quantity at room temperature [40]. The cleavage of the α and β-glycosidic substituent of respective glucopyranose may occur via anchimeric assistance of the C-2 hydroxyl group to form epoxide **11**, which subsequently could undergo ring opening by the C-6 hydroxyl group to yield **10**. The proposed epoxide formation during conversion of **1** to **10**, is in agreement with what was suggested by Shafizadeh et al [41], [42]. Additionally, α-glucopyranose may also be converted to compound **10** via direct displacement of the α-glycosidic substituent –OH by the C-6 hydroxyl group [30]. This two-step path via epoxide intermediate **11** might be more favorable for both α and β anomers than the direct cyclization by C6-OH which is only favorable for the α anomer.

Table 2.1 Major product distribution (anhydrosugars and furans) of fast pyrolysis of hexoses

Compounds	1	2	3	4	5	6	7	8	9
1,6 Anhydropyranose	10±3	5±0.3	1.6±0.5	-	12±6	19±10	9.4±0.5	17±2	16±4
Dianhydro Compounds	2±0.3	-	0.4±0.1	-	1±0.2	1±1	-	-	-
Other Anhydro Pyranoses & Furanoses	2.5±0.7	2±0.2	-	-	2±1	2±2	3.7±0.5	4±0.5	3.5±.3
Hydroxymethylfurfural (HMF)	11±0.4	7±0.3	11.3±1	-	1±0.8	1.2±1.3	0.9±0.2	0.6±0.2	2±0.3
1-(2-Furanyl)-1,2-Ethanediol	-	-	-	18.5±2.5	-	-	-	-	-
1,4-Anhydro-d-mannitol	-	-	-	2.1±0.5	-	-	-	-	-
Methyl Furan	1±0.5	1±0.1	1±0.1	-	1±0.3	1±0.2	1±0.1	1±0.1	1.2±0.3
Methyl Furfural	0.5±0.1	-	-	5.3±0.6	-	-	-	-	-
Furan Methanol	-	-	-	1.5±0.3	-	-	-	-	-
Furfural	5±0.2	4.2±0.2	5.6±0.6	-	0.8±0.1	1±1	1.1±0.2	1±0.2	1.4±0.1
Furfural alcohol	-	-	-	12.6±4.2	-	-	-	-	-
Furan	1±0.2	0.7±0.1	0.5±0.5	3±1	-	-	-	-	-
Furanone	2.3±0.3	5±0.5	5.5±0.5	0.4±0.02	1±0.3	1±1	3.5±0.3	6±1	3.5±1
Pyran Compounds	-	-	1±0.02	-	0.8±0.02	0.7±0.5	-	-	1.4±0.4
Glyoxylic acid	10.6±0.3	18.3±4.1	18.3±4	-	8.3±0.3	7.1±2	13.3±0.1	9.3±3.5	8.2±1
Glycolaldehyde	1.2±0.6	6.7±1.4	4.8±1.2	5.6±1.4	5.1±0.7	5.7±2.9	5.9±1.1	6.8±0.7	5.4±0.4
Methylglyoxal	2.7±0.5	2.6±0.3	2.9±0.5	-	2.4±0.2	1.9±0.4	2.5±0.1	2.7±0.8	1.6±0.3
Acetic acid	1.1±0.5	1±0.5	1.3±0.4	-	-	-	1.1±0.5	-	-
Acetol	1.3±0.1	1.2±0.2	1.3±0.1	-	1.8±0.8	1.7±0.5	2.7±0.5	1±0.1	1.3±0.1
Butanedial	-	-	-	3.8±0.3	-	-	-	-	-
Methanol	-	-	-	-	18.3±0.4	18±5.4	17.6±1.2	19.4±3.5	16.6±1
Gases	19.6±1.2	24.2±4.3	24.6±4.8	15.9±1.7	17.1±1	21.2±3.3	24.4±6.6	21.6±4	20.7±2.1
Unreacted	-	-	0.7±0.3	6.2±1.3	3.7±1.6	3.8±1.3	-	-	-
Unidentified compounds	7.7	5.2	9	11.3	5.1	3.8	2.1	3.5	8.7

List of hexoses: glucose (**1**), galactose (**2**), mannose (**3**), α/β-gluco/galacto and α-manno-pyranoside (**5**, **6**, **7, 8** and **9** respectively)

Figure 2.2 Possible pathway for the conversion of glucopyranose 1 (R = H) to levoglucosan 10

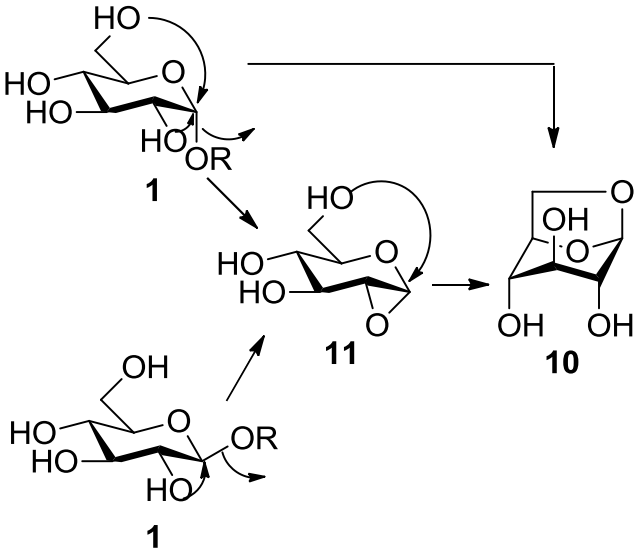

Table 2.2 shows that the yields of 1,6-anhydropyranose decrease in the order glucose > galactose > mannose. The percent of 1,6-anhydropyranose produced by pyrolysis of glucose is two times higher than from galactose and six times higher than from mannose. Figure 2.2 shows that displacement of the glycosidic hydroxyl group by the C-2 -OH forms the intermediate epoxide for the α and β-anomers which are opened in the subsequent step by the attack of the primary -OH group at C-6, to yield 1,6-anhydropyranoses.

Glucose and mannose are C-2 epimers, with their –OH groups oriented equatorial and axial, respectively. We propose that mannose also converts to corresponding 1,6 anhydromannopyranose via a similar concerted mechanism as shown in Figure 2.3 Possible pathway for the conversion of mannopyranose, 3 (R = H) to 1,6-anhydropyranose, 13

Compound **3** first converts into intermediate **12** via formation of epoxide where the α anomer is more favorably oriented than the β anomer due to trans orientation of the –OH at C-2. However, the orientation of the epoxide ring in intermediate **12** presumably opposes the

subsequent attack of the C6 –OH, leading to low 1,6-anhydropyranose yield. Additionally, α-mannopyranose may also convert to compound **13** via direct displacement of the α-glycosidic substituent by the C-6 hydroxyl group. By comparison, the production of 1,6-anhydropyranose from glucose and mannose supports the idea of epoxide formation as a significant pathway during fast pyrolysis, enabled by the subsequent unrestricted opening of the epoxide ring which favors 1,6-anhydropyranose formation as a major product for glucose in comparison with mannose.

Figure 2.3 Possible pathway for the conversion of mannopyranose, 3 (R = H) to 1,6-anhydropyranose, 13

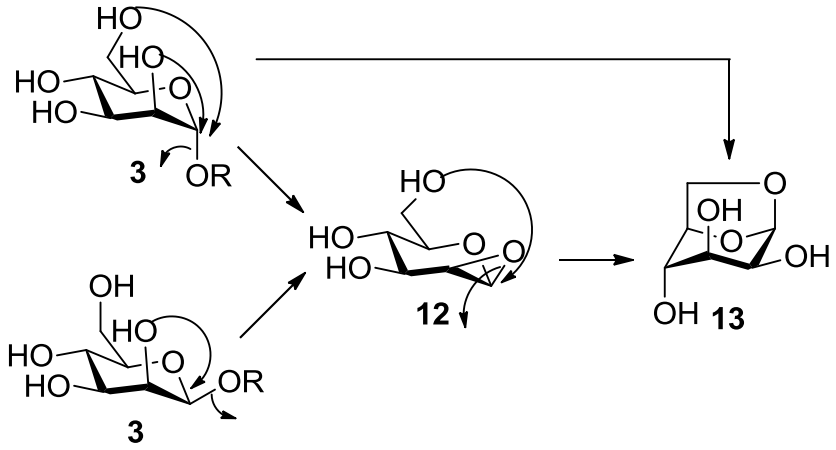

Glucose and galactose are C-4 epimers, where –OH groups at C-4 are oriented equatorial or axial, respectively. Results suggest that the orientation of the –OH group at C-4 is important in producing 1,6 anhydropyranose. We suggest that for the fast pyrolysis of **1**, an intermediate epoxide **11** may form first due to the displacement of the glycosidic hydroxyl group by the –OH group at C-2 which subsequently converts to 1,6-anhydropyranoses, **10** through another intermediate **14**. Intermediate **14** may form via a ring opening of epoxide followed by formation of a five-membered ring through a boat like transition state as shown in Figure 2.4. The hydroxyl group at C-4 is axial in galactose and is unfavorably oriented to form a five-membered ring

containing intermediate similar to **14** and can't stabilize the transition state further. However, glucose consists of –OH at C-4 that is equatorial and presumably forms **14**. Consequently, galactose produces less 1,6-anhydropyranose than glucose. This results supports our hypothesis that the correct stereochemistry of hydroxyl group at C-4 is also important to stabilize the intermediate that enhances production of 1,6 anhydrosugar.

Figure 2.4 Possible contribution of –OH at C-4 to form intermediate 14 **during conversion of glucopyranose,** 1 **(R = H) to levoglucosan,** 10 **under fast pyrolysis condition**

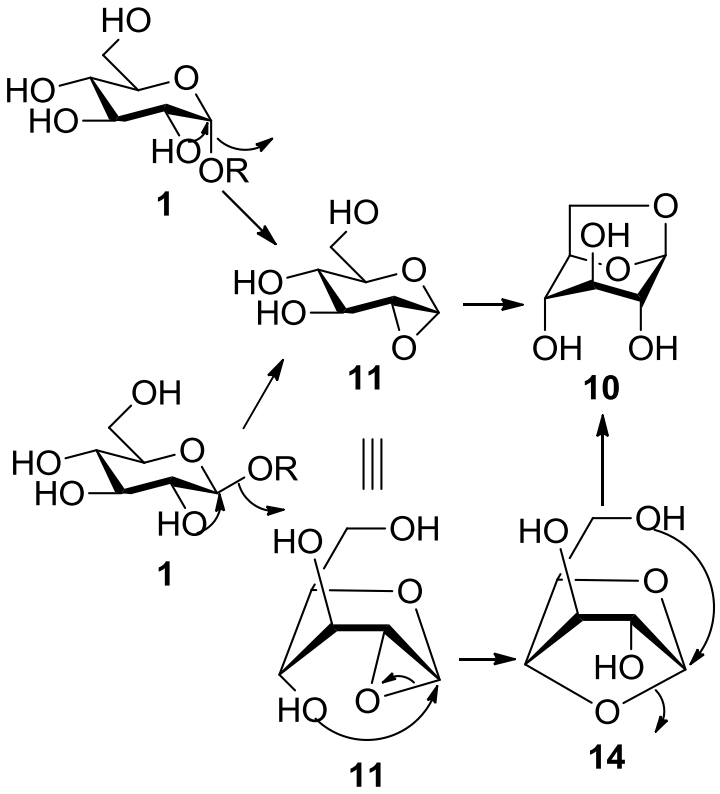

To gain further mechanistic insight we chose 2-deoxy-d-glucose (**4**) for pyrolysis and characterized the products by GC/MS. The reason for selecting **4** is that compounds **4** and **1** have similar structures except for the absence of the –OH at C-2 in compound **4**. Thus a concerted mechanism involving the –OH at C-2 through the formation of an epoxide intermediate to produce 1,6 anhydropyranose from **4** is not possible. Experimental results in Table 2.1 confirm that 1,6 anhydrosuger is not formed from **4**. Additionally, Table 2.1 suggests that galactose,

produces more 1,6-anhydropyranose than does mannose which are C-4 and C-2 epimer of glucose respectively. These results agree with our hypothesis that the presence of –OH at C-2 is more important than at C-4 particularly for the formation of 1,6 anhydrosuger from monosaccharides.

2.5.2 Hexoses to furans: HMF formation from the fast pyrolysis of parent sugars

Furans can be formed by dehydration of the furanose forms of carbohydrates such as fructose. Nonetheless, some carbohydrates such as glucose, which exist primarily in pyranose forms, still form considerable quantities of furans upon pyrolysis. Specifically, HMF, **17** is the major furan compound arising from α and β-glucopyranose. We propose that **17** forms from **1** through an epoxide followed by ring opening of the epoxide to form an energetically stable five-membered ring as shown in Figure 2.5 Formation of the epoxide intermediate **15** from compound **1** is favorable, because it involves breaking a six-membered ring which is facilitated by the antiperiplanar orientation of the two C-O bonds involved in the bond breaking and bond formation process. In turn, **15** rearranges to furan **16**, a stable five-membered ring, as depicted in Figure 2.5. Dehydration of **16**, enabled by the aldehyde moiety, gives **17** as a major product from fast pyrolysis of glucose.

Figure 2.5 Possible pathway for the conversion of α-glucopyranose, 1 (R = H) to 5-hydroxymethylfurfuraldehyde 17

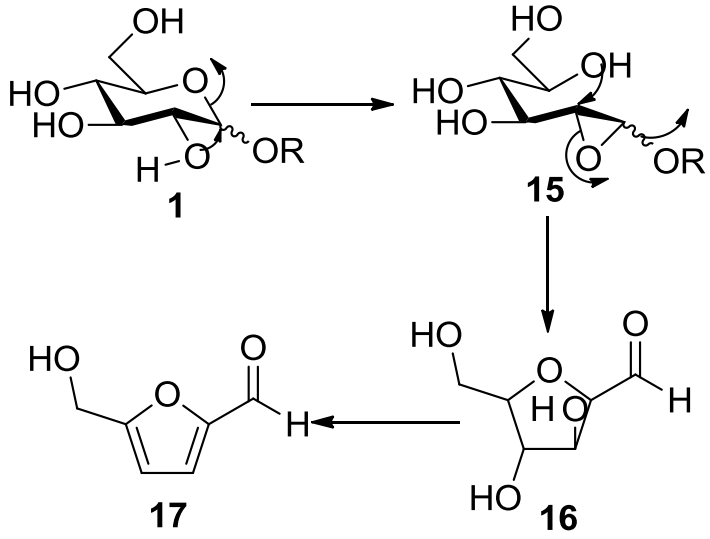

Table 2.2 shows that mannose, which is a C-2 epimer of glucose produces about 1.2 and 1.4 times more furans (HMF and furanones) than glucose and galactose respectively upon fast pyrolysis. Previous studies show that HMF forms as a result of pyrolysis and subsequently breaks down to different furans [36]. The amount of HMF produced from mannose pyrolysis is about 1.0 and 1.6 times higher than that of glucose and galactose respectively. We propose that mannose first converts to intermediate epoxide **18** as shown in Figure 2.6 via a similar event suggested in Figure 2.5

Compound **3** is the C-2 epimer of **1** and thus stereochemistry of intermediate **15** and **18** differs. Glucose and mannose produces similar amount of HMF (Table 2.1) suggesting that the axial or equatorial orientation of –OH at C-2 is not important for the conversion of intermediate **16** from **15** and **18,** unlike 1,6 anhydrosugar formation from the two epimers. Nonetheless, compound **3** gives more furans than **1**, which indicates that **3** prefers to produce furan over 1,6 anhydrosugar and support our hypothesis that the stereochemistry of –OH at C-2 is important in determining the product distribution. Additionally, Table 2.1 suggests that galactose, which is the C-4 epimer of glucose, produces less HMF than mannose and glucose. We speculate that

equatorial –OH at C-4 is presumably important in stabilizing the transition state which leads to the production of more HMF from the pyrolysis of mannose than galactose.

Figure 2.6 Possible pathway for the conversion of mannopyranose, 3 (R = H) to HMF, 17

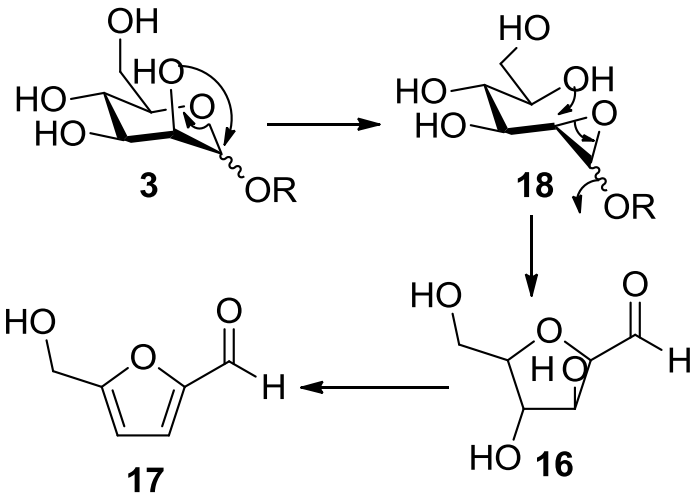

2.5.3 Importance of –OH group at C-2 of Hexoses: Pyrolysis of 2-deoxy-D-glucopyranose

Our results indicate that parent sugars, under pyrolysis conditions, convert into high and low molecular weight compounds (Table 2.2). Parent sugars have different orientation of –OH at C-2 and C-4. The fast pyrolysis conversion of hexoses to high molecular weight compounds appears to occur through a concerted mechanism via neighboring group participation where –OH at C-2 contributes significantly. To confirm the importance of –OH functional group's presence at C-2 for conversion of 1,6 anhydrosugar from hexoses, 2-deoxy-d-glucopyranose which doesn't have –OH at C-2,was subjected to pyrolysis and the products were analyzed. As shown in Table 2.2, 1-(2-furanyl)-1,2-ethanediol (**19**) is produced as a major product. Small amounts of 1,4-anhydro-d-mannitol were produced and would not convert into **20**. We suggest that **4** converts into **19** via a concerted mechanism involving a boat-like transition state by the formation of a five-membered ring simultaneously breaking up a six-membered ring as depicted

in Figure 2.7. Intermediate **19** finally undergoes dehydration which was facilitated by high temperature to give **20** as a major product. Formation of **19** is facilitated by the relative stereochemistry of both C-O bonds involved in the transition state. In principle, there should be another pathway through which the 2-deoxy-1,6-anhydropyranose might have been formed. Formation of compound **20** as a major product as well as and the notable absence of anhydrosugars as products from pyrolysis of compound **4** agree with our hypothesis. Formation of **19** as a major product from compound **4** which does not contain -OH at C-2 further confirmed that a concerted mechanism involving –OH at C-2 is an important feature in the formation of anhydropyranoses from parent sugar.

Figure 2.7 Possible pathway involving 4-OH in a bicyclic intermediate for stepwise conversion of α-2-deoxy-D-glucose, 4 **(R = H) to 1-(2-furanyl)-1,2-Ethanediol,** 20

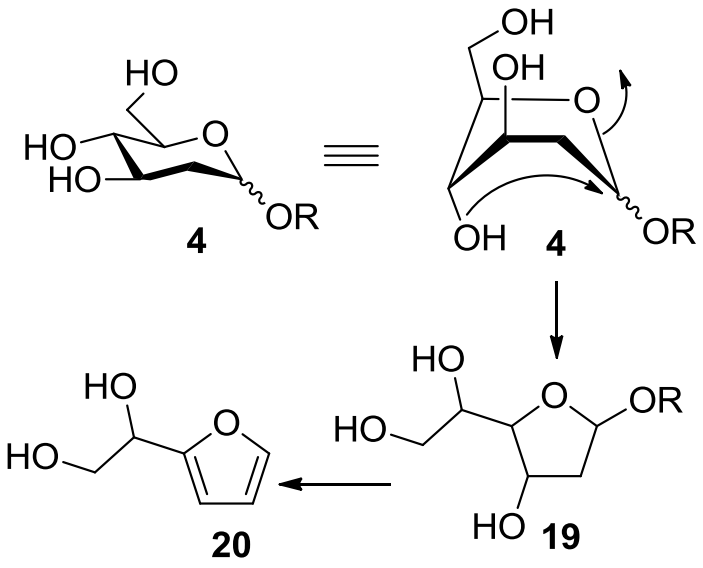

2.5.4 Glucose-biomass mixture pyrolysis

In previous sections, we showed that more anhydrosugars are produced from hexoses such as glucose as compared to maltose or galactose. Cellulose is a polymer of β-1, 4 linkages of glucose. Poplar is a biomass with cellulose as one of its components. We pyrolyzed poplar, its

polysaccharide cellulose, the monosaccahride glucose, and their mixtures using analytical pyroprobe-GC/MS. Levoglucosan was also pyrolyzed to find out if secondary products were formed. In addition, mixtures of glucose with poplar and cellulose were evaluated to probe the nature of the interaction between glucose and polymeric components of biomass. The pyrograms from these experiments and the percent peak area responses are presented in Table 2.2.

Table 2.2 Pyrolysis-GC/MS Data for peak area responses of some common products

	Glucose	Cellulose	Levoglucosan	Poplar	Glc:P 1:1	Cellulose:P 1:1
Methyl glyoxal	5.4	5.9	0.8	6.2	-	-
Hydroxy acetaldehyde	15.9	19.4	1.7	24	21.2	18.1
Acetic Acid	1	-	-	14.3	11.7	10.2
Acetol	1.2	1	0.4	1.5	1.9	1.7
Furfural	4	2.9	1.5	1.5	4.2	2.7
3/4-Hydroxy cyclohexanone	0.9	1.8	0.5	4	2.4	3.1
Hydroxymethyl furfural (HMF)	7.2	4.6	0.5	1.8	8.2	3.5
Anhydrogalactosan /mannosan	3.9	11.9	0.8	3.2	1.7	4.6
Levo glucosan	26.1	18.7	67.1	9.4	13.5	23.9
2,6-Dimethoxy-4-allylphenol	-	-	-	3.3	2.3	3.7

Differences amongst peak responses, especially in the production of levoglucosan were observed. The amount of levoglucosan produced from cellulose was much higher than glucose. Levoglucosan remained unchanged upon pyrolysis yielding mostly the same anhydrosugar in GC/MS analysis. If cellulose decomposed to glucose upon pyrolysis which further decomposes in to anhydrosugar products, then the products of glucose-cellulose mixtures should reflect this by showing an additive effect. Spiking glucose or cellulose to poplar at different ratios showed that the amount of levoglucosan produced form cellulose and poplar separately is significantly

less that the 1:1 mixture of the two. Glucose and cellulose as probe molecules were found to play an interactive role as opposed a simple additive role (Appendix). On the other hand, glucose produced large amounts of furans such as HMF and furfural compared to cellulose. Therefore, it was concluded that levoglucosan formation is the major pathway of cellulose pyrolysis whereas small molecules were mostly a product of monomeric glucose pyrolysis. Other studies have also observed an interactive effect of lignin on cellulose pyrolysis [43], [44].

2.5.5 Hexose derivatives pyrolysis

Our experiements and prior reports indicate that the amount of levoglucosan from cellulose pyrolysis is higher than from glucose [10], [15]. Shanks and Brown et al. observed that levoglucosan production follows a trend according to the degree of polymerization, i.e. polysaccharides > oligosaccharides > disaccharides > monosaccharide [13]. It appears that the reactions occurring in glucose differ from those in cellulose during pyrolysis. The decreased levoglucosan yield from glucose pyrolysis indicates that formation of levoglucosan from glucose and cellulose is either mechanistically different or the size of the leaving group on results in high levoglucosan yields. We subjected methyl-α/β-gluco/galacto and α-manno-pyranosides to fast pyrolysis to determine the effects of –OMe vs. –OH as a leaving group. We anticipated that compounds **5**-**9** should produce more 1,6-anhydropyranoses than the underivatized parent sugars **1**-**3** due to the presence of a more easily removed leaving group. Additionally, direct displacement of the glycosidic –OMe by –OH at C-6 could be another important pathway to yield desired product particularly for the α anomer as proposed by Sakaki [45]. Moreover, retro-aldol condensation is a known pathway for sugar pyrolysis to low molecular weight compounds. This pathway happens to be restricted for α/β-gluco/galacto and α-manno-pyranosides. The

summarized results in Table 2.1 suggest that fast pyrolysis of the methyl α/β-gluco/galacto and α-manno-pyranosides produce more 1,6-anhydropyranoses than the underivatized parent sugars, demonstrating the importance of the leaving group (-OMe vs –OH) in 1,6-anhydropyranose formation. Our results also indicate that the β-gluco/galacto pyranosides produce more anhydrosugars than do the α-anomers. This result our hypothesis that intermediate epoxide formation is major pathway from sugar derivatives to 1,6 anhydrosugar. It is important to note that Table 2.1 indicates that methyl α-manno-pyranosides produce more anhydrosugar than the underivatized parent sugar, and the methyl α-gluco/galactopyranoside. Direct displacement of the glycosidic substituent (-OMe) by the primary –OH at C-6 could be a more probable pathway than through the formation of an epoxide intermediate to afford 1,6 anhydrosugar from the pyrolysis of methyl α-mannopyranosides. This may be due to the stereochemistry of the -OH at C-2 as discussed previously, or perhaps because –OMe is a more apt leaving group than –OH. Additionally, the close proximity of the axial –OH at C-2 may help the C-6-OH act as a nucleophile. Hydrogen-bond formation enhances the rate of the SN2 reaction to produce a higher amount of 1,6 anhydrosuger than expected.

2.6 Conclusion

We used glucose, galactose, mannose, their derivatives, and 2-deoxy-D-glucopyranose under fast pyrolysis condition to show that high molecular weight products form via a concerted mechanism. We determined that epoxide and furan intermediates form in the transition state involving C-2 and C-4 –OH. Our study shows that the stereochemistry of the C-2 and C-4 –OH plays an important role in product distribution. Glucose and cellulose played an interactive role as opposed a simple additive role when spiked as molecular probes to biomass. Levoglucosan formation is the major pathway of cellulose pyrolysis whereas small molecules were mostly a

product of monomeric glucose. We also observed that fast pyrolysis of the hexose derivatives produce more 1,6-anhydrosugar than the underivatized parent sugars, demonstrating the importance of the leaving group (-OMe vs –OH) in 1,6-anhydropyranose formation. Additionally, β-gluco/galacto pyranosides produce more of the corresponding 1,6-anhydropyranoses than do the α-anomers, further supporting our hypothesis that the intermediate epoxide formation is the major pathway from sugar derivatives to 1,6 anhydrosugar.

CHAPTER 3. FAST PYROLYSIS OF BIOMASS: EFFECT OF FEEDSTOCK COMPOSITION AND TAXONOMY ON PYROLYSIS PRODUCTS

Shantanu Kelkar, Zhenglong Li, Jonathan Bovee,
Kurt D. Thelen, Robert Kriegel, Christopher M. Saffron

3.1 Abstract

In the Midwest of the U.S., several members of the Poaceae family can be grown as bioenergy crops. Besides Miscanthus and switchgrass, which have been extensively studied, native Midwestern grasses such as big bluestem, coastal panicgrass, deertongue, indiangrass, sandreed and sideoats grama can be grown in monoculture or polyculture plantations. In addition to climate, soil fertility and water availability, the selection of bioenergy crops depends on the choice of conversion technology. One such technology, fast pyrolysis, is a thermochemical approach for converting biomass into a liquid product known as bio-oil, a hydrocarbon fuel intermediate. In this research, the eight aforementioned grass varieties were characterized by fiber and metal analyses as well as calorimetry and thermal gravimetry. Conversion by analytical pyrolysis showed that although variability exists, all eight grasses produced a similar spectrum of chemical compounds. Principal component analysis of pyrolysis-GC/MS data detected statistically significant differences amongst the grass varieties on the basis of six key chemical markers: glycolaldehyde, acetic acid, acetol, methyl glyoxal, 4-vinylphenol and levoglucosan. Though taxonomic classification was not found to affect product composition, correlation analysis verified that biomass composition and thermal properties might be responsible for the differences in pyrolysis products.

3.2 Introduction

Plant biomass is the only renewable feedstock for making the hydrocarbon fuels that are compatible with the current U.S. energy infrastructure. One strategy for making hydrocarbon fuels involves fast pyrolysis, which is a technology that rapidly heats biomass in the absence of oxygen to create a liquid fuel intermediate known as bio-oil. Through catalytic upgrading, bio-oil can be transformed into hydrocarbon fuels like gasoline, diesel or jet fuel. Though fast pyrolysis and catalytic upgrading can convert a wide variety of plant species into fuels, certain feedstocks may have advantages for this strategy on the basis of feedstock composition. As many different plant species can serve as bioenergy feedstocks, compositional variability should be exploited to select those that are most readily converted into products with desirable qualities. This is contrary to those who claim their processes are "feedstock agnostic," as clearly the composition of the reactants affects the quality of the products. In this study, the magnitude and origins of compositional variability are investigated for eight grass species in order to improve species selection for bioenergy production.

In the Midwest of the U.S., several members of the grass family (Poaceae) can be cultivated as bioenergy crops. In the Billion Ton Study Update, the USDA identifies switchgrass, which can be grown in yields greater than 8 dry tons per acre, and Miscanthus, which can be grown in yields in excess of 15 dry tons per acre, as energy crops because of these high production levels [1], [46]. In addition to switchgrass and Miscanthus, big bluestem, coastal panicgrass, deertongue, indiangrass, sandreed, and sideoats grama are native in the Midwest and can be cultivated with low nitrogen input and low water input due to C4 photosynthetic metabolism. Tilman et al. showed that biofuels from low-input high-diversity mixtures of native grassland perennials produced bioenergy yields 238% greater than

monoculture over a ten year period[47]. Cultivation on marginal lands has also been investigated with positive implications for the ongoing "food vs. fuel" argument.

Fast pyrolysis is a thermochemical approach for converting biomass to a liquid known as bio-oil at yields in excess of 60% by weight. Bio-oil is a complex mixture of water, highly oxygenated compounds such as carboxylic acids, aldehydes, ketones, furans, sugars and phenolics derived from the pyrolysis of cellulose, hemicellulose, lignin, extractives, and their interaction with each other[4]. Secondary products from cross-reactions of primary pyrolysis products and their reaction with the original biomass are also produced. However, the presence of carbonyl and carboxylate containing compounds in bio-oil leads to storage instability and limits its early adoption as a transportation fuel[3]. Biomass constituents such as lignin, ash, and inorganic salts dramatically alter the speciation of pyrolysis products and produce reactive compounds that cause storage instability[4], [43], [48], [49]. Previous studies have demonstrated the effect of inorganic minerals (especially alkali and alkaline earth metals) on the array and amounts of products produced by pyrolysis [48], [50], [51], [52], [53], [54], [55], [56], [57], [58], [59], [60], [61].

The aim of this study was to assess the magnitude and origin of the variability observed upon the pyrolysis of biomass. To this end, the composition and properties of eight grass species native to North America, namely big bluestem, coastal panicgrass, deertongue, indiangrass, Miscanthus, sandreed, sideoats grama and switchgrass, were examined. With the exception of switchgrass and Miscanthus, the fast pyrolysis of many native warm-season grasses has not been extensively researched [62], [63], [64]. As compositional data for grass species is limited, the characterization of potential feedstocks such as native grasses will help identify biomass varieties suitable for pyrolysis and assist in predicting the properties of bio-oil produced

from these grasses [65]. As the degree of genetic relatedness may provide the origin and explain the magnitude of the distribution of pyrolysis products, all eight species were taxonomically categorized into their respective tribes. It was hypothesized that species belonging to the same tribe would create a similar array of pyrolysis products, otherwise environmental factors such as access to soil minerals are implicated in product distribution [4]. Distinctions amongst plant species after pyrolysis were made using principal component analysis, which has been previously used to simplify complex pyrolysis data, identify major products and to observe commonalities amongst species [66], [67], [68], [69]. Statistical correlation analysis was used to observe relationships amongst feedstock components, physical properties and pyrolysis products. These tools were used to take the first step towards establishing a context for selecting grass species for pyrolysis and catalysis to create hydrocarbon fuels.

3.3 Materials & Methods

3.3.1 Feedstock composition analysis

The plant materials used for this research were obtained from the Crop and Soil Science Research Farm on the Michigan State University campus. Plant samples were common native warm-season grasses found in Michigan and other Midwestern states and were as follows: big bluestem, coastal panicgrass, deertongue, indiangrass, Miscanthus, sandreed, sideoats grama and switchgrass. All eight grasses exhibit C4 metabolism. All biomass samples were dried to less than 10% moisture by weight at room temperature and milled to a particle size of less than 0.5 mm (US mesh #35) using a Willey Mill (Standard Model No.3, Arthur H. Thomas, Philadelphia, PA). Samples were stored at room temperature.

Neutral detergent fiber (NDF), acid detergent fiber (ADF), and acid detergent lignin (ADL) were measured using Van Soest fiber analysis[70]. NDF, and ADF were used to calculate

cellulose and hemicellulose. Lignin was also estimated using the National Renewable Energy Laboratory's (NREL) procedure for determination of lignin in biomass [71]. Acetyl groups on hemicellulose contribute to acetic acid production upon pyrolysis. Therefore, the % acetylation of biomass was measured in the form of acetic acid using the NREL method for determining structural carbohydrates and acetylation [71]. This data is not reported in Table 3.1. Analysis of inorganic constituents such as potassium, sodium, magnesium, calcium, and iron was done at Dairyone Labs (Ithaca, NY) using Inductively Coupled Plasma (ICP) Radial Spectrometry after microwave digestion. Chloride ion concentration was evaluated using potentiometric titration. All standards and chemicals were purchased from Sigma-Aldrich, St. Louis, MO. Moisture content in the grass species was measured using ASTM D4442-07 and the ash content was measured using the ASTM D1102 method[72], [73] . The high heating value of biomass was determined using a Parr 1341 Plain Jacket Calorimeter (Parr Instrument Co., Moline, IL) [74].

3.3.2 Thermogravimetric analysis

A Mettler-Toledo thermogravimetric analyzer (TGA, CH-8603 model, Mettler-Toledo, Schwerzenbach, Switzerland) was used to plot the weight loss curves and derivative curves for all samples. Nitrogen was used as the purge gas with a cell and furnace flow rate of 20 mL/min. The furnace was initially purged with nitrogen for 10 minutes at the beginning of each experiment, and samples were then dried in the furnace for 25 minutes at 105 °C. The data from TGA was plotted as differential thermo-gravimetric (DTG) curves using a temperature profile of 10 °C/min, from 105°C - 800°C, directly following the drying phase.

3.3.3 Pyrolysis-GC/MS

Experiments were conducted using a microscale pyrolysis unit, CDS Pyroprobe 5250 (CDS Analytical Inc, Oxford, PA) interfaced to a Shimadzu QP-5050A gas chromatograph/mass

spectrometer (Shimadzu Corp, Columbia, MD). Approximately 0.5 mg of ground biomass sample was packed between quartz wool in a quartz tube with a filler rod. Six replicates of each sample were run. Pyrolysis proceeded by setting the pyroprobe at 600°C with a hold time of 10 s at a heating rate setting of 1000°C/s. The GC used a Restek Rtx-1701 column (Restek, Bellefonte, PA), 60 m x 25 mm with a 0.25 μm film thickness. The column gas flow was 1 cm/s with a split ratio of 1:100 so as to not overwhelm the mass spectrometer. The GC oven temperature program began with a 1 minute hold at 40°C followed by heating at 8°C/min to 270 °C. The injector and detector temperature was set at 280°C. The mass spectra were recorded in electron ionization mode for *m/z* 28 to 400. Identification of compounds was performed by comparing the mass spectra of the peaks with standard spectra of other compounds using the NIST library to obtain the most probable matches. Pure compounds (Sigma-Aldrich Co., St Louis, MO) were then used to confirm the peak identities based on matching of retention times and mass spectra. Quantification was performed using external standards in acetonitrile and a four-point calibration curve was constructed relating concentration to peak area response.

3.3.4 Statistical Analysis

Principal Component Analysis (PCA) of data allows for simplification of vast amounts of data and for observing trends. This simplification is achieved by finding correlated chemical species or markers that may be expressed in the form of a linear combination by a new single variable, known as a principal component (PC). Chemical species affect each new variable, i.e. PC, by a value known as the "loading." When a chemical is highly correlated, either positively or negatively, with a PC, they have a high loading for that PC. Thus, PCA reduces the dimensions of a dataset consisting of a large number of variables to a new set of variables, i.e. PCs, which are ordered such that the first few components retain most of the variation present in all of the

original variables. PCA was performed on the percentage peak area responses of more than 50 variables (chemical species) from the collected set of pyrograms using the MATLAB R2010a (Mathworks Inc, Natick, MA) and the JMP (SAS Institute, Cary, NC) software. The data was not scaled or normalized. The average chromatographic peak areas from the replicates were used for PCA. Mean values for each grass species were selected to avoid inclusion of the experimental variation in the model [69]. Orthogonal rotation of principal component axes allows interpretation of data along the principal components in the same direction where the most significant variables can be formed and is used to identify differences amongst samples. Correlation analysis was used to examine the relationship between the key chemical markers and independent variables, that is, the biomass composition and property data, using Excel (Microsoft Corporation, Redmond, WA). The correlation coefficient measures the linear association between two variables on a scale of -1 to +1.

3.4 Results and Discussion

3.4.1 Feedstock composition and properties

As seen in Table 3.1**,** the cellulose content ranged from 35.2 to 50.2% weight of dry biomass (db), hemicellulose ranged from 27.3 to 32.8% db and lignin ranged from 13.5 to 23.6% db for the eight grass species. These results are typical of grasses grown in the Midwestern region of the United States. The higher heating values (HHV), measured by bomb calorimetry, were found to be in the range 18.4 to 21.2 MJ/kg on a dry biomass basis. Holocellulose is the sum of cellulose and hemicellulose in biomass and is measured after the extractives and the lignin are removed. Grass species with a high holocellulose to lignin ratio (Ho:L) produced a lower HHV. Fahmi et al. (2007) suggested that a lower ash, lower Ho:L cultivar may be better suited for combustion processes rather than a high Ho:L biomass, which may be better for

fermentation processes[75]. Coastal panicgrass, with the highest HHV of the grasses studied, lowest ash and a relatively low Ho:L ratio is more suitable for combustion and pyrolysis applications. Sideoats grama and deertongue, with the lowest HHV, highest ash and Ho:L ratio have a higher potential for biofuel production from sugars by fermentation-based routes.

The ash content varied linearly with HHV which is similar to observations by Jenkins et al. (2006) for washed straw[76]. Although the ash yield itself provides limited information about a feedstock, it has been used as an indicator of the bulk inorganic matter such as alkali and alkaline earth metals (AAEM) that cause slagging, fouling and sintering[60]. However no correlation between ash yield and presence of AAEM was observed in this study. Elemental analysis showed that of the AAEM, potassium was the most significant, measuring 0.5 to 0.86% db. Calcium constituted between 0.19 to 0.40% weight of dry biomass while magnesium varied between 0.1 to 0.2% db. Sodium constituted less than 0.01% db while iron was present in the 45-112 ppm range. Increasing levels of AAEM have been shown to increase the yield of char and gases upon pyrolysis and a decrease the amount of condensable products such as bio-oil [48], [50], [51], [52], [53], [54], [55], [56], [57], [58], [59]. Considering all of the species studied, Miscanthus and big bluestem were found to have the highest cellulose and lignin content whereas switchgrass and coastal panicgrass had the highest AAEM.

Thermogravimetric analysis

The differential thermogravimetry (DTG) curves for each grass sample are shown in Figure 3.1. The DTG curve for each biomass is influenced by its composition [77]. The maximum rate of weight loss was observed between 320-355 °C for all eight samples. This peak represents the thermal decomposition of cellulose and corresponds with that observed by Varhegyi et al. in their experiments with Avicel cellulose[78]. Miscanthus showed the highest

weight loss rate which corresponded with the high cellulose content (50%) determined for this grass. A second smaller peak or shoulder-like feature was observed between 290-300 °C. This smaller peak is partially related to the hemicellulose content of biomass, which decomposes at a lower temperature than cellulose. Lignin decomposition occurs over a wide temperature range, contributing to the cellulose and hemicellulose decomposition peaks [77], [79]. Inorganic minerals may aid biomass pyrolysis by catalyzing reactions necessary for breakdown of biomass components such as lignin and cellulose at a lower temperature [50], [59]. Many studies have reported the effect of inorganic minerals on the shift in biomass weight loss temperature identified by DTG analysis [52], [53], [55], [59]. Thus, indiangrass, with the lowest potassium content (0.52% db), followed by sandreed, big bluestem and miscanthus showed the highest peak temperature for the cellulose weight loss peak. Switchgrass, sideoats grama and coastal panicgrass, with high potassium content (>0.8% db), showed the smallest peaks with the lowest degradation temperature. Switchgrass and sideoats grama, which also had a low cellulose, high hemicellulose and potassium content showed an early peak for cellulose decomposition at 320-325 °C, as well as the lowest weight loss rate. Coastal panicgrass showed a distinct, early peak for hemicellulose decomposition at 290 °C. Potassium levels of 0.8% db or higher may be responsible for lowering the decomposition temperature of biomass components during pyrolysis.

Table 3.1. Chemical composition of grasses [a]

Grass	Big bluestem	Coastal panicgrass	Deertongue	Indiangrass	Miscanthus	Sandreed	Sideoats grama	Switchgrass
% Cellulose	45.100	35.900	35.200	40.700	50.200	42.400	38.100	37.500
%Hemicellulose	28.500	29.700	27.300	28.600	27.000	32.800	31.500	32.400
% Lignin	23.600	20.800	13.500	18.500	22.200	21.900	15.000	16.300
HHV (MJ/kg) [b]	19.700	21.200	18.800	19.400	20.300	20.300	18.400	19.800
% Ash	4.100	3.100	5.300	4.300	3.300	3.700	6.200	4.100
Ho: L [c]	3.100	3.200	4.600	3.700	3.500	3.400	4.700	4.300
% K	0.580	0.860	0.500	0.520	0.600	0.530	0.840	0.800
% Ca	0.350	0.200	0.260	0.300	0.240	0.320	0.190	0.400
% Mg	0.140	0.130	0.130	0.040	0.040	0.070	0.070	0.250
% Na	0.003	0.013	0.005	0.004	0.005	0.005	0.005	0.004
% Chloride	0.120	0.200	0.150	0.120	0.080	0.120	0.180	0.130
% P	0.140	0.170	0.090	0.090	0.060	0.150	0.070	0.230
Fe (ppm)	68	45	51	110	110	68	112	92
AAEM (%) [d]	1.073	1.203	0.895	0.864	0.885	0.925	1.105	1.454
% Char yield	23.6	26.3	25.7	23.9	23.8	24.1	26.5	26.8

a All values are also per oven dry weight of biomass and mean of two or more replicates.

b HHV is on a dry biomass basis and a mean of 10 readings

c Ho:L is the ratio of holocellulose (sum of cellulose and hemicellulose) to lignin

d AAEM is total alkali and alkaline earth metals

Figure 3.1. DTG curve for pyrolysis of eight native grasses using a heating rate of 10 K/min. Markers correspond to (x) Miscanthus, (*)indiangrass, (Δ) sandreed, (□)deertongue, (◊) coastal panicgrass, (○) sideoats grama, (+)switchgrass, and (−)big bluestem.

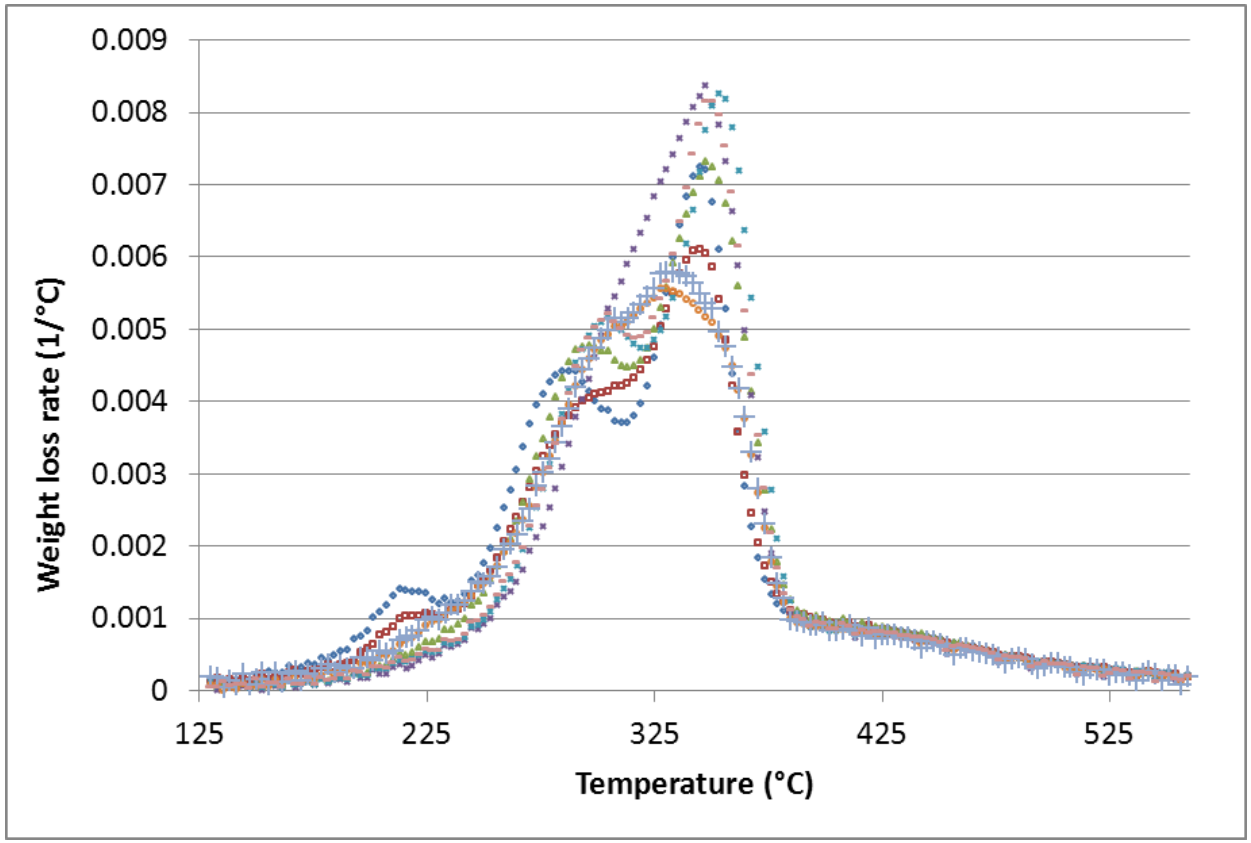

Figure 3.2. Representative pyrogram (switchgrass pyrolysis) with major chemical species found in products of pyroprobe GC/MS analysis.

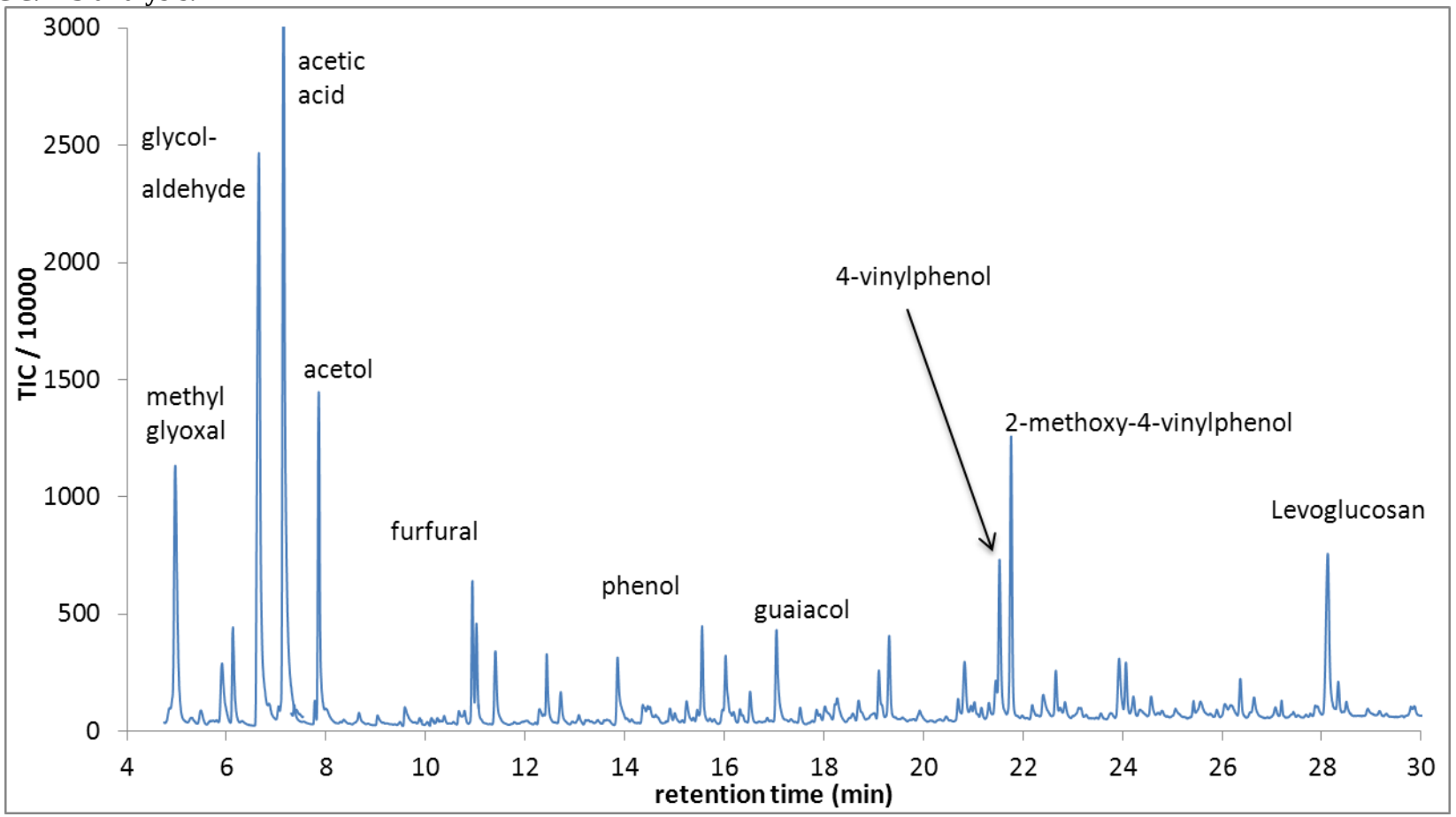

3.4.2 Analytical pyrolysis-GC/MS and PCA

Pyrolysis yields a reactive mixture of water carboxylic acids, hydroxyaldehydes, hydroxyketones, furancarboxaldehydes, sugars, and phenolics such as guaiacols, catechols, syringols, vanillins and isoeugenol. Each of the eight grass species in this study produced a similar mixture of chemical species upon pyrolysis as presented inFigure 3.2. Data is presented from 4.5 min to exclude large single peak for non-condensable gases. List of compounds in condensable product (bio-oil) are listed below as follows: (Retention time) Chemical compound, (4.8) Methyl glyoxal,(5.7) 2,3-Butanedione, (6.4) Glycolaldehyde, (7.0) Acetic acid, (7.9) Acetol, (11.5) Furfural, (13.9) 2-methyl-cyclopenten-1-one, (14.4) Heptanol, (15.3) γ – Crotonolactone, (15.5) Phenol, (17.1) o-Guaiacol, (19.1) p-Methylguaiacol, (19.4) Unknown, (20.7) p-Ethylguaiacol, (21.2) 2,3-Anhydrogalactosan, (21.2) α-D-Glucopyranose, (21.5) γ-Butyrolactone, (21.6) 4-Vinylphenol, (21.8) 2-Methoxy-4-vinylphenol (4-vinylguaiacol), (22.7) 2,6-Dimethoxyphenol (Syringol), (23.9) trans-Isoeugenol, (24.1) Vanillic acid, (26.4) 4-Vinylsyringol, (28.1) 1,6-anhydro-β-glucopyranose (Levoglucosan), (28.3) Methoxyeugenol.

In order to identify differences amongst the pyrolysis products between the plant species, the pyrolysis data was subjected to principal component analysis. Principal component analysis of percentage peak area responses of more than fifty variables (chemical compounds) revealed three major principal components (figure 3.3) These three PCs account for close to 90% of the variability in grass pyrolysis products. In general, variability between plant species was greater than the sum of the variability within plant species plus that introduced by experimental error. The most significant loadings for the first three PCs are shown in Table 3.2.

PCA analysis showed that only a small subset of the chemical compounds identified by GC/MS, namely, methyl glyoxal, glycolaldehyde, acetic acid, acetol, 4-vinylphenol and

levoglucosan had a significant effect on the first three PCs. These are the only six chemicals that had a loading value of greater than 0.1 or less than -0.1 for the first three PCs. The production of these compounds upon fast pyrolysis was the highest and most variable between plant species, a combination that led to the distribution (separation amongst species) observed on the principal component plot (Figure 3.3). Thus, it may be possible to explain most of the variability between grasses using only these six chemical markers which will simplify the analysis of complex pyrolysis data from grasses. Each of these six chemicals was quantified using external standards and the results expressed as weight percentage of total dry biomass are presented in Table 3.3.

The first two principal components (PC) are shown as the abscissa and ordinate in Figure 3.3. The first PC accounted for 54.3% of the variability in the pyrolysis data while the second PC accounted for 20.7%. Compounds such as acetic acid, acetol, 2,3-butanedione, cyclopropanemethanol, succinicaldehyde, 2,6-dimethoxyphenol (syringol), vanillin, and others have a positive loading (positive correlation, therefore, along positive x-axis) for PC1 while 1,6-anhydro-β-glucopyranose (levoglucosan), glycolaldehyde, furfural, 4-vinylphenol, 4-vinylguaiacol, 1,3-anhydrogalactosan have a negative loading (negative x-axis). Species (i.e. grass pyrolysis products) orient along the x-axis according to their tendency to produce a greater proportion of either acetic acid and acetol or levoglucosan and glycolaldehyde upon pyrolysis. Thus, sideoats grama, which produces the most acetic acid but least glycolaldehyde is along the positive x-axis while switchgrass and indiangrass, which produce less acetic acid but more glycolaldehyde are away from the positive x-axis. Samples in the 1st quadrant, sandreed and side oats, have a greater tendency to produce carboxyl and carbonyl group molecules such as acetic acid, acetol and glycolaldehyde than levoglucosan and furans. Similarly, big bluestem, switchgrass and indiangrass showed a greater tendency to produce levoglucosan and 4-

vinylphenol than acetic acid or acetol. Production of acetic acid and acetol was accompanied with a decrease in production of levoglucosan. Previous literature shows that smaller carbonyl and carboxyl group compounds may be formed at the expense of levoglucosan due to presence of AAEM [48]. Although Miscanthus exhibited a high cellulose and lower inorganic mineral content compared to other grasses, it did not produce more levoglucosan upon pyrolysis. Repeated experiments not only confirmed this observation but also revealed that Miscanthus produced the highest amount of 2-methyl-2-cyclopenten-1-one, cresols (dimethylphenols), 4-vinylguaiacol, 4-vinylsyringol and vanillic acid. Methoxy phenols are derivatives of lignin, which had a high value for Miscanthus. Cyclopentenone, methyl and dimethyl phenol derivatives have been detected in products of cellulose and levoglucosan pyrolysis in the presence of potassium [53]. Therefore, potassium-catalyzed pyrolysis of cellulose and levoglucosan from Miscanthus may be leading to cyclopentenone and phenol derivatives at the expense of levoglucosan yield.

Table 3.2. PCA loadings for key chemical markers

Chemical Marker	RT (min)	*PC1*	*PC2*	*PC3*
Variability explained (%)		54.3	20.7	12.9
Methyl glyoxal	4.8	-0.1	-0.4	0.35
Glycolaldehyde	6.5	-0.64	0.75	0.1
Acetic Acid	7.0	0.89	0.22	0.34
Acetol	7.9	0.88	0.1	-0.1
4-Vinylphenol	21.6	-0.41	-0.35	-0.1
Levoglucosan	28.1	-0.8	-0.24	0.41

Table 3.3 Quantification of key chemical markers in grass pyrolysis products

Weight % of dry biomass	*Methyl glyoxal*	*Glycol-aldehyde*	*Acetic Acid*	*Acetol*	*4-vinylphenol*	*Levoglucosan*
Big bluestem	2.7	5.8	7.5	2.7	1.8	2.7
Coastal panicgrass	2.5	6.1	7.8	2.7	2.1	2.5
Deertongue	2.8	4.7	8.5	3.1	1.9	2.8
Indiangrass	2.8	6.4	7.6	2.7	1.9	2.8
Miscanthus	2.3	5.9	7.9	3.3	2.4	2.5
Sandreed	2.7	6.6	8.7	2.8	1.6	2.7
Sideoats grama	2.9	5.4	9.0	3.6	1.5	2.9
Switchgrass	2.9	6.3	7.0	2.4	1.7	2.9

Figure 3.3. A plot of the first two principal components that are formulated to describe the variability between different feedstock. Biomass varieties are placed in the four quadrants, labeled 1st through 4th, in arrangements nearest to the chemicals that they produce in abundance, and furthest from the chemicals that are least produced.

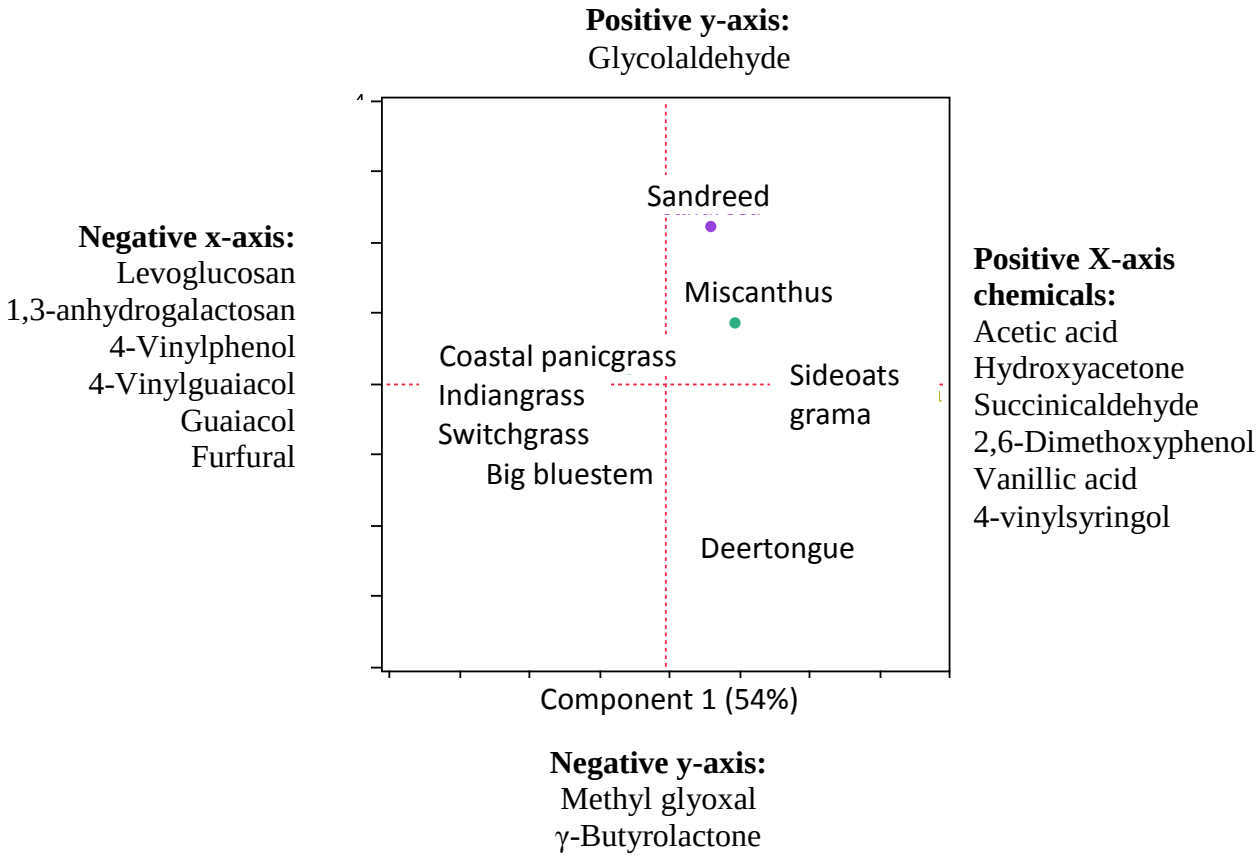

3.4.3 Taxonomy

The taxonomic classification for each grass variety was compared in an attempt to explain the observed variability between pyrolysis products. Using the USDA Plant Database, big bluestem, indiangrass and Miscanthus belong to the Andropogoneae tribe, while coastal panicgrass, deertongue and switchgrass are of the Paniceae tribe (Table 3.4). The Paniceae grasses had a lower cellulose content (35.2 to 37.5% db) when compared with other grasses. Two Paniceae, switchgrass and coastal panicgrass, also had high potassium and AAEM content. Though differences at the species rank are clearly observed, grasses belonging to the same tribe did not cluster on PCA plots of the first three PCs in Figure 3.3. No relationship between a grass variety's tribe and the pyrolysis product profile can be drawn from the PCA.

Table 3.4. Taxonomic classification of grasses

Common Name	Scientific Name	Family	Tribe	Subtribe
Big bluestem	*Andropogon gerardii (Vitman)*	Poaceae	Andropogoneae	Andropogoninae
Coastal panicgrass	*Panicum amarum (Elliott)*	Poaceae	Paniceae	Setariinae
Deertongue	*Dichanthelium clandestinum (L.) Gould*	Poaceae	Paniceae	NA
Indiangrass	*Sorghastrum nutans (L.) Nash*	Poaceae	Andropogoneae	Sorghinae
Miscanthus	*Miscanthus x giganteus*	Poaceae	Andropogoneae	Saccharinae
Sandreed	*Calamovilfa longifolia (Hook.) Scribn*	Poaceae	Eragrostideae	NA
Sideoats grama	*Bouteloua curtipendula (Torr.)*	Poaceae	Cynodonteae	Boutelouinae
Switchgrass	*Panicum virgatum (L.)*	Poaceae	Paniceae	Setariinae

3.4.4 Correlations between alkali and alkaline earth metals and pyrolysis products

A correlation matrix was constructed to relate the six key chemicals identified by PCA—methyl glyoxal, glycolaldehyde, acetic acid, acetol, 4-vinylphenol and levoglucosan—with biomass composition and property data (Table 3.5). In this matrix, +1 represents a 100% positive relationship amongst two variables while -1 represents a 100% negative relationship.

Cellulose did not show a strong (statistically significant) correlation with the production of any of the key chemical markers even though levoglucosan is derived from dehydration of polysaccharides such as cellulose. The dominating and interactive effect of inorganic minerals on pyrolysis products may be responsible for this absence of an obvious relationship. Increasing hemicellulose levels correlated with the production of acetic acid and acetol as well as char yield. It is well known that acetyl groups bound to xylans in hemicellulose are cleaved by pyrolysis to form acetic acid [80]. As expected, higher heating value showed a strong negative relationship with ash and Ho:L ratio and a positive correlation with the amount of lignin.

Amongst the chemical species, levoglucosan showed negative correlations with acetic acid and acetol, which themselves were positively related. Levoglucosan also showed a negative correlation with hemicellulose but this may have been coincidental since acetic acid is strongly correlated with hemicellulose while it is negatively correlated with levoglucosan. However, the direct measurement of acetyl groups in biomass showed that this value did not correlate with the amount of acetic acid produced upon pyrolysis. One explanation for this lack of correlation is that acetic acid may be produced from a combination of hemicellulose degradation as well as catalytic cracking of biomass due to inorganic minerals. In the presence of inorganic salts, levoglucosan production is inhibited by competing primary reactions to produce small molecules such as glycolaldehyde and acetol [48], [81]. Even though glycolaldehyde and levoglucosan are believed to be competing reaction products from cellulose, they exhibited a positive correlation together and a strong negative correlation with lignin. Principal component analysis showed that levoglucosan and glycolaldehyde, both had negative loadings for PC1 (Table 3.2), unlike acetic acid and acetol (Figure 3.3). The interaction between cellulose and inorganic minerals in the presence of lignin has been shown to promote production of glycolaldehyde [43]. It has also been

postulated that C_2-C_3 scission of intermediates from levoglucosan may generate glycolaldehyde [82], [83]. Therefore, it is speculated that glycolaldehyde may have been produced due to cracking of intermediates from levoglucosan.

Elemental analysis of the eight grass species showed potassium to be a major inorganic constituent (Table 3.1). Potassium correlated with a decrease in the amount of levoglucosan, a product of de-polymerization of biomass, and an increase in acetic acid and acetol. Potassium was also negatively related to the peak reaction temperature in TGA analysis. Ash and inorganic minerals present in the grasses catalyze cracking reactions reducing the temperature for peak reaction rate [50]. Chloride levels, an indicator of the inorganic constituents, correlated with char yields. Although sodium showed strong negative correlation with some chemicals, this effect may be coincidental as sodium was not present in significant quantity (a tenth of potassium by weight) and was not significantly variable between species.

The presence of calcium ions has been shown to increase yields of levoglucosan from polysaccharides [81]. Addition of iron, in the form of sulfate, or other transition metals to acid-treated cation-free biomass has been shown to help increase levoglucosan in pyrolysis products [84], [85]. However no such observations for calcium or iron could be made from the data in this study or from correlation analysis. Many of the previous studies have been conducted with biomass or neat polysaccharides that were water or acid-washed to make them cation-free and then spiked with single, inorganic minerals, often at levels significantly higher than found in the native grasses. Contradictory results on the effect of AAEM in pyrolysis products have also been presented. Kawamoto et al. have reported that alkaline earth metal chlorides ($MgCl_2$, $CaCl_2$) substantially decreased the levolgucosan yield in cellulose pyrolysis at 400 °C and that their effect was more significant than alkali metals[86]. Varhegyi et al. reported that $MgCl_2$ (0.01

mol/mol of glucose-unit) did not have a significant effect on cellulose pyrolysis while Muller-Hagedorn et al. also reported that cellulose decomposition was not affected significantly by impregnation of $CaCl_2$ (0.5 wt%) to hornbeam wood[52], [78]. Conversely, Pan and Richards (1989) concluded that potassium, but not calcium, was a strong catalyst in pyrolytic reactions producing gases from polysaccharides and acetic acid from hemicelluloses[87]. Nowakowski and others concluded that calcium, magnesium and iron have a small catalytic effect, while potassium promoted heterolytic fission of biomass to small molecules at the expense of anhydrosugars[53], [61].

Results of this study show that calcium, magnesium, sodium and iron do not significantly affect pyrolysis of native North American grass species. Grasses in this study were neither pre-treated to remove inorganics nor spiked with these minerals. These grasses also contained insignificant quantities of metals such as sodium or iron. These two factors combined with the interactive effect of biomass constituents with different minerals may have been responsible for the absence of trends or strong correlations with regard to specific markers such as calcium, magnesium, sodium and iron.

3.5 Summary

Several members of the Poaceae family are potential feedstocks for conversion to liquid fuels by pyrolysis. As the quality of the bio-oil intermediate is a function of the feedstock composition and properties, eight grass species were screened to detect differences in their pyrolysis products. Because of the complexity of the py-GC/MS dataset that was generated, PCA was used to identify variability in the pyrolysis products amongst these grass species. PCA determined that significant variability exists, however no connection can be made between this variability and the taxonomic tribe to which each grass belongs. Though taxonomic

categorization may play a role in determining a grass's pyrolysis products, no such claim is supported by the dataset collected.

Instead, biomass composition and thermal and pyrolysis properties data were used to explain the observed differences seen on the PCA plots. Correlation analysis was performed to relate the composition and property data to the six chemical compounds that are most responsible for the variability seen after pyrolyzing plant tissue. As expected, the higher heating value of the dry grass tissue correlated positively with lignin and negatively with ash content. Hemicellulose correlated positively with acetic acid and acetol production and negatively with levoglucosan. The total ash content did correlate positively with glycoaldehyde formation, but only weakly with the other chemical products of pyrolysis. Of the metals included in the analysis, potassium was found to reduce the decomposition temperature and increase the char yield. However, potassium was not strongly correlated with any of the six chemical compounds identified by PCA, perhaps due to the low levels of potassium in these plant tissues (<0.9 wt.% d.b.). Further, no significant relationships between the total AAEM content and key pyrolysis chemicals were observed, probably due to the low variability in the inorganic mineral content. The catalytic effect of calcium, magnesium and iron was insignificant, as has been demonstrated in some previous studies.

As for selecting amongst grass species to identify future candidates for bioenergy production by pyrolysis, composition analysis of the eight grass species suggests that coastal panicgrass, with the highest HHV, lowest ash and low Ho:L ratio may be suitable for pyrolysis applications. Sideoats grama and deertongue, with the lowest HHV, highest ash and Ho:L ratio may be better suited for fermentation based processes. Switchgrass, indiangrass and big bluestem cluster together on the PCA plot and showed less tendency to produce small carbonyl

and carboxylate compounds, which implies that the pyrolysis products may be less chemically reactive, less corrosive to metal surfaces and more stable during storage. Conversely, sideoats grama and sandreed, produced higher levels of acetic acid and acetol, which may be unsuitable for producing stable bio-oil that can readily be transported and stored for further chemical upgrading.

Table 3.5. Correlation analysis between biomass composition and pyrolysis chemicals. For each variable, Pearson correlation coefficients are presented in the first row and significance p-value in the second row. Cells with statistically significant correlations are highlighted.

	HHV	% Ash	% Lignin	% Cellulose	% Hemi-cellulose	Ho:L	% K	% Ca	% Mg	% Na	% Chloride
HHV	1	-0.95	0.71	0.24	0.05	-0.79	0.16	0.04	0.08	0.62	-0.06
		0	0.05	0.57	0.91	0.02	0.7	0.92	0.86	0.1	0.9
% Ash		1	-0.77	-0.42	0.1	0.83	0.06	-0.22	-0.04	-0.39	0.33
			0.03	0.3	0.82	0.01	0.89	0.6	0.92	0.34	0.42
% Lignin			1	0.72	-0.1	-0.95	-0.18	0.16	-0.25	0.1	-0.42
				0.04	0.81	0	0.67	0.71	0.55	0.81	0.31
% Cellulose				1	-0.32	-0.53	-0.39	0.13	-0.46	-0.39	-0.81
					0.44	0.17	0.34	0.76	0.25	0.34	0.01
% Hemicellulose					1	0.16	0.45	0.29	0.33	0.01	0.28
						0.71	0.26	0.49	0.43	0.97	0.51
Ho:L						1	0.18	-0.14	0.2	-0.28	0.27
							0.66	0.75	0.64	0.5	0.52
% K							1	-0.3	0.4	0.53	0.65
								0.48	0.33	0.17	0.08
% Ca								1	0.56	-0.58	-0.51
									0.14	0.13	0.2
% Mg									1	0.02	0.22
										0.96	0.59
% Na										1	0.67
											0.07
% Chloride											1

Table 3.5 (cont'd)

	% P	Fe (ppm)	AAEM (%)	TGA peak	Char yield	Methyl glyoxal	Glycol-aldehyde	Acetic acid	Acetol	4-Vinylphenol	Levo-glucosan
HHV	0.46	-0.38	0.14	0.58	-0.16	0.26	-0.86	0.03	0.31	0.03	-0.31
	0.25	0.35	0.73	0.13	0.7	0.54	0.01	0.94	0.46	0.94	0.45
% Ash	-0.4	0.26	0.01	-0.66	0.37	-0.18	0.72	0.2	-0.18	-0.12	0.22
	0.33	0.54	0.97	0.07	0.37	0.68	0.04	0.63	0.68	0.78	0.61
% Lignin	0.11	-0.1	-0.23	0.7	-0.7	0.37	-0.52	-0.13	0.03	-0.32	-0.08
	0.8	0.81	0.59	0.05	0.06	0.37	0.19	0.76	0.94	0.44	0.84
% Cellulose	-0.35	0.43	-0.52	0.51	-0.79	0.29	0.18	-0.48	-0.36	-0.36	0.1
	0.4	0.29	0.19	0.2	0.02	0.49	0.67	0.23	0.38	0.39	0.8
% Hemicellulose	0.59	0.05	0.56	-0.41	0.41	-0.35	-0.26	0.8	0.9	-0.07	-0.77
	0.12	0.9	0.15	0.31	0.31	0.39	0.54	0.02	0	0.88	0.02
Ho:L	-0.19	0.28	0.2	-0.72	0.63	-0.34	0.68	0.11	-0.05	0.19	0.08
	0.65	0.51	0.64	0.04	0.09	0.41	0.06	0.8	0.9	0.66	0.86
% K	0.38	0.06	0.84	-0.56	0.77	-0.27	-0.28	0.38	0.26	0.21	-0.46
	0.35	0.89	0.01	0.15	0.03	0.51	0.51	0.35	0.54	0.62	0.25
% Ca	0.62	0	0.2	0.11	-0.2	-0.58	-0.04	-0.21	0.38	0.48	-0.09
	0.1	1	0.63	0.8	0.63	0.13	0.92	0.62	0.35	0.22	0.83
% Mg	0.83	-0.37	0.81	-0.18	0.59	-0.53	-0.24	-0.05	0.41	0.69	0.01
	0.01	0.37	0.01	0.67	0.12	0.17	0.57	0.9	0.32	0.06	0.98
% Na	0.21	-0.51	0.31	0.12	0.4	0.35	-0.73	0.35	0.17	-0.03	-0.21
	0.63	0.2	0.45	0.79	0.32	0.4	0.04	0.4	0.69	0.94	0.62
% Chloride	0.19	-0.42	0.54	-0.43	0.73	0.03	-0.35	0.6	0.24	0.01	-0.13
	0.66	0.29	0.17	0.29	0.04	0.94	0.4	0.12	0.56	0.98	0.75

Table 3.5 (cont'd)

	% P	Fe (ppm)	AAEM (%)	TGA peak	Char yield	Methyl glyoxal	Glycol-aldehyde	Acetic acid	Acetol	4-Vinylphenol	Levo-glucosan
% P	1	-0.41	0.76	-0.01	0.39	-0.47	-0.63	0.25	0.74	0.52	-0.4
		0.32	0.03	0.97	0.34	0.25	0.09	0.55	0.04	0.18	0.33
Fe (ppm)		1	-0.16	-0.53	-0.15	-0.43	0.64	-0.17	-0.31	0.03	-0.35
			0.71	0.18	0.72	0.29	0.09	0.68	0.45	0.95	0.4
AAEM (%)			1	-0.48	0.79	-0.53	-0.34	0.29	0.48	0.51	-0.37
				0.23	0.02	0.18	0.41	0.48	0.23	0.2	0.37
TGA Peak				1	-0.64	0.68	-0.41	-0.31	-0.07	-0.32	0.41
					0.09	0.07	0.31	0.45	0.88	0.43	0.31
Char yield					1	-0.34	-0.06	0.37	0.31	0.38	-0.22
						0.41	0.89	0.37	0.45	0.35	0.6
Methyl glyoxal						1	-0.18	0.07	-0.18	-0.79	0.4
							0.67	0.87	0.67	0.02	0.33
Glycoaldehyde							1	-0.36	-0.53	-0.04	0.34
								0.38	0.17	0.92	0.41
Acetic Acid								1	0.75	-0.41	-0.64
									0.03	0.31	0.09
Acetol									1	-0.03	-0.65
										0.95	0.08
4-vinylphenol										1	-0.03
											0.94
Levoglucosan											1

Table 3.5 (cont'd)

	HHV	% Ash	% Lignin	% Cellulose	% Hemi-cellulose	Ho:L	% K	% Ca	% Mg	% Na	% Chloride	% P
HHV	1	-0.95	0.71	0.24	0.05	-0.79	0.16	0.04	0.08	0.62	-0.06	0.46
		0	0.05	0.57	0.91	0.02	0.7	0.92	0.86	0.1	0.9	0.25
% Ash		1	-0.77	-0.42	0.1	0.83	0.06	-0.22	-0.04	-0.39	0.33	-0.4
			0.03	0.3	0.82	0.01	0.89	0.6	0.92	0.34	0.42	0.33
% Lignin			1	0.72	-0.1	-0.95	-0.18	0.16	-0.25	0.1	-0.42	0.11
				0.04	0.81	0	0.67	0.71	0.55	0.81	0.31	0.8
% Cellulose				1	-0.32	-0.53	-0.39	0.13	-0.46	-0.39	-0.81	-0.35
					0.44	0.17	0.34	0.76	0.25	0.34	0.01	0.4
% Hemicellulose					1	0.16	0.45	0.29	0.33	0.01	0.28	0.59
						0.71	0.26	0.49	0.43	0.97	0.51	0.12
Ho:L						1	0.18	-0.14	0.2	-0.28	0.27	-0.19
							0.66	0.75	0.64	0.5	0.52	0.65
% K							1	-0.3	0.4	0.53	0.65	0.38
								0.48	0.33	0.17	0.08	0.35
% Ca								1	0.56	-0.58	-0.51	0.62
									0.14	0.13	0.2	0.1
% Mg									1	0.02	0.22	0.83
										0.96	0.59	0.01
% Na										1	0.67	0.21
											0.07	0.63
% Chloride											1	0.19
												0.66

CHAPTER 4. A SURVEY OF FEEDSTOCKS FOR AROMATICS FROM BIOMASS PYROLYSIS

4.1 Introduction & Background

Chemicals and liquid fuels may be derived from conversion of renewable feedstock to fuels and chemicals using thermochemical methods such as fast pyrolysis. Many different biomass types are available as potential feestock for conversion to energy using pyrolysis. In the United States, 33% of the land area is forest land, 26% as grassland pasture and range, 20% as cropland, 8% as special uses (e.g., public facilities), and 13% as miscellaneous other uses, such as urban areas, swamps, and deserts [4]. More than 50% of the land in America may be used for cultivating biomass without affecting the environment.

Biomass is approximately 50% cellulose, 15-25% hemicellulose, and 15-30% lignin (mass basis). In addition, it also contains water, extractives and inorganic minerals. Cellulose is a long-chain linear polymer composed of crystalline and amorphous regions. The cellulose polymers are arranged in the form of micro fibrils [88]. These are further organized into fibrils which combine into cellulose fibres, which give a fibrous nature to biomass. Hemicelluloses are branched amorphous polymers, shorter than cellulose polymers and composed of of five or six-carbon sugars. The cellulose fibrils are embedded in a matrix of lignin and hemicellulose where the hemicellulose acts as a connector between cellulose and lignin. Lignin is a three-dimensional polymer formed from phenyl propane units (coumaryl, coniferyl and sinapyl alcohol) with different types of linkages between the building blocks. Softwood lignin is almost exclusively made of coniferyl alcohol. Extractives are organic and inorganic compounds that are extractable from the biomass using polar and nonpolar solvents [88]. Examples are terpenes, fats and waxes, proteins, phenolic compounds, hydrocarbons and sugars. Sodium and potassium salts, also water-soluble, are examples of inorganic extractives. Herbaceous crops like grasses biomass

typically contains significant amounts of inorganics (up to 15 wt%) and extractives (up to 20 wt%) compared with woody biomass (~ 0.3–0.4 wt% inorganics, ~ 2–3 wt% extractives) [88]. Hardwoods (deciduous) and herbaceous crops (switchgrass, corn stover etc) predominantly consist of D-xylose units that make up the hemicellulose while D-mannose, D-xylose and D-galactose make up the hemicellulose in coniferous (softwood).

4.1.1 Aromatics from biomass – stoichiometric yields and H/O molar ratios

The main biomass fractions of cellulose, hemicellulose and lignin react differently at different temperatures to yield different spectra of products upon pyrolysis [4].

The stoichiometric yields (mass basis) for converting glucose, xylose, and p-coumaryl alcohol to toluene are 28%, 28%, and 67% respectively. Bridgwater et al. have proposed that conversion of whole biomass to aromatics ($CH_{1.2}$) using zeolite catalysts could achieve a 42% mass yield or 82% carbon yield [3], [89].

$(C_{3.8}H_{6.5}O_{2.8})_n \rightarrow n(3.1CH)_{1.2} + n(0.7CO_2) + n(1.4H_2O)$ $Y_{CH1.2} = 0.422$ g/g

Thus, there is potential to produce significant amounts of aromatic chemicals using the biomass pyrolysis – catalysis process. During pyrolysis, homogeneous reactions of thermal decomposition of biomass produce smaller oxygenated molecules. The small molecules diffuse into the catalyst pores and react at the active sites through a series of cyclo-oligomerization, decarbonylation and dehydration reactions to produce aromatics, CO, CO_2 and water [90]. However, the maximum yield reported for biomass is only 14% (carbon basis) from catalytic pyrolysis of sawdust in a fluidized bed reactor with ZSM-5 catalyst [91]. These low yields are a result of the highly oxygenated nature of biomass, which leads to production of carbon oxides and oxygenated aromatics such as phenolics instead of hydrocarbon aromatics.

The relative content oxygen and hydrogen in different feedstock not only affects the aromatic yields but also the composition of products produced upon pyrolysis. A Van Krevelen diagram is a plot of the molar ratio of hydrogen to carbon as the ordinate and oxygen-to-carbon ratio as the abscissa [92]. The plot was originally devised for bulk elemental analysis of coal and since its introduction in 1950, has been widely applied in geochemistry to characterize different fossil fuels [93]. Chen's effective H/C ratio is similar in concept to the Van Krevelen plot and is determined from the hydrogen lost from biomass when oxygen is removed in the form of water. Chen et al. proposed an effective hydrogen index (EHI) which is defined as equal to (H-2O-3N-2S)/C where C,H,O,N,S are in moles [94]. Recent studies have defined Chen's ratio as $(H/C)_{eff}$ =(H-2O)/C [95], [96]. Thus, for methanol the effective H/C ratio is 2, for petroleum-based fuels, it is between 1 to 2, while for pyrolysis oil it is below 0.5 and for glucose and cellulose, zero. Most lignocellulosic biomass $(H/C)_{eff}$ between 0 to 0.3 [96]. Feedstocks with H/C_{eff} ratios less than 1 produce more coke and rapidly deactivate the catalyst, making production of high yields or aromatics difficult.

4.1.2 Degradation of biomass upon pyrolysis

Numerous chemical compounds (over 400) in quantities that vary by order of magnitudes, have been observed in products of pyrolysis. These compounds are derived from depolymerization and fragmentation reactions of the three key building blocks of lignocellulose: cellulose, hemicellulose, and lignin, and the secondary reactions between them. Lignin yields guaiacols and syringols while cellulose and hemicellulose produce oxygenates, sugars, and furans. Secondary reactions of these oxygenates, sugars and furans in the presence of heat and inorganic minerals leads to their decomposition to esters, acids, alcohols, ketones, and aldehydes [97].

Cellulose is the largest component of lignocellulosic biomass. Therefore, its decomposition has been extensively studied and a number of models have been proposed including Brodio-Shafizadeh, Waterloo, Diebold, Varhegyi and Antal and Wooten-Hajaligol [42], [82], [98], [99], [100]. The cellulose pyrolysis reaction in endothermic and first-order. Many of these models propose the conversion of cellulose to a depolymerized, but oligomeric form called active cellulose, a rate-limiting step, as identified by NMR analaysis. Active cellulose decomposes to glucose which can dehydrate to levoglucosan (1,6-anhydroglucose, levoglucosan, carbohydrates, or other compounds containing methyl, aromatics, ketones, or other functional groups are derived from from acid or alkali-catalyzed decomposition and dehydration of glucose [99]. Glucose, due to its acyclic or open-ring forms can decompose to molecules such as 5-hydroxymethylfurfuraldehyde which can decompose further into smaller moelcules such as formic acid and lactones. Glycolaldehyde, dihydroxyacetone, glycolaldehyde, and erythrose may be produced from retro-aldol reactions of fructose and glucose. These intermediates react further to form pyurvaldehyde, glcolaldehyde, and acids. Hemicellulose undergoes analogous reaction pathways [99]. Acetic acid is also produced from acetyl groups bound to xylans. Lignin depolymerizes to produce oligomers first, which then pyrolyze to precursor monomers such as coniferyl and sinapyl alcohol and their derivatives such as isoeugenol, vanillin, vinylguaiacol, methyl guaiacol, guaiacol, and catechol. Lignin and hemicellulose pyrolysis are not first-order reactions although the pyrolysis of lignocellulosic biomass may be modeled as a combination of three first order reactions [101].

Pure cellulose, upon pyrolysis, yields mainly levoglucosan, up to 60% from intramolecular condensation and sequential depolymerization of the glycosidic units [66]. Inorganic impurities significantly influence the product composition. Many biomass with

cellulose concentrations greater than 50% (e.g. Miscanthus in our studies) produce low yields of levoglucosan, due to catalytic effect of inorganics. Inorganic minerals may have a greater influence on the pyrolysis product profile than even pyrolysis reaction temperature and biomass characteristics such as crystallanity [48]. The addition of extremely small amounts (0.1 %) of alkali such as K, Li, Ca to pure cellulose shifts the mechanism and the final product selectivity so that glycolaldehyde is the stable reaction intermediate instead of levoglucosan [48], [97]. A probable mechanism by which trace quantities of alkali salts may be having a catalytic effect on biomass pyrolysis is presented in the references [66], [97].

In our studies and those by other groups, alkali cations increased the rate of reaction during pyrolysis (see Chapter 3). If lignocellulose can be pretreated to remove alkali salts by ion-exchange or acid-washing prior to pyrolysis, the yields of levoglucosan can be increased drastically (27% from wood, 45% from cellulose) [84].

4.1.3 Upgrading of pyrolysis products to aromatics

Not only do the types of chemical species produced upon pyrolysis differ according to feedstock but these products of pyrolysis also react differently with catalysts giving dissimilar yields. When pyrolysis products react with a catalyst, the catalyst break down large molecules found in pyrolysis products, for example, to smaller hydrocarbon fragments in zeolite catalyst, forming a ‘hydrocarbon pool’ [102]. These intermediate oxygenates then diffuse into the catalyst pores and are condensed into aromatic molecules and olefins from the hydrocarbon pool due to the oligomerization and cyclization functionalities of the catalyst [91]. Wang et al. [103], [104] have suggested that reactive hydrocarbon pool for the methanol to olefins process is between 5.7 and 6.0 Å, i.e. similar to the kinetic diameters of benzene, indene, 2-furanmethanol

and 4-methylfurfural. The intermediate oxygenates may exist in the hydrocarbon pool in the form of polymethylbenzene or benzenium cations or carbenium ions or naphtenes in pseudo-equilibrium[105], [106]. The product, monocyclic aromatics, and their reaction with other oxygenates leads to the production of naphthalenes and other polycyclic aromatics.

Olefins are precusors to producing aromatic molecules and many studies have shown that increasing the olefin content in catalyst feed increases the aromatics in catalysis products [91], [107], [108], [109]. However acidic catalysts are more selective towards cracking rather than dehydrogenating to produce olefins. Lewis acids sites may have a synergistic effect with Bronsted acid sites by converting a greater amount of alkanes to olefins for conversion to coke and aromatics. In the absence of these sites, free hydrogen ions may be attacking carbenium and benzenium ions and producing light olefins though β–scission, and eventually coke [105], [110]. Aromatics and coke production from polymerization of furans have been suggested to be the major competing reactions[91]. Tagliabue has proposed that the that thermodynamics of catalytic reactions of hydrocarbon pool to aromatics is such that olefins production is preferred over aromatics and there is a greater tendency towards coke formation [108]. It is also speculated that coke is produced from acid catalyzed polymerization of furans to oligomers [111], [112].

Gayubo et al. found that alcohols undergo dehydration at low temperatures (<250 °C) to form olefins, which were converted into alkanes and aromatics at higher temperatures[113]. Acetaldehyde formed significant amount of coke, acetone was converted to isobutene and to heavier olefins, aromatics and alkanes at higher temperatures while acetic acid ketonized to acetone and CO_2[114]. Willams and Horne observed that acetic acid and other low molecular weight bio-oil compounds over ZSM-5 catalyst give large amount of aromatic hydrocarbons[107].

Taarning et al. noted that alcohols and phenols lose oxygen in the form of H_2O, aldehydes, formates and carbohydrates in the form of CO and H_2O and carboxylic acids lose oxygen as CO_2 and H_2O [95]. They concluded that acetic acid was important for hydrocarbon generation as it improves the H/C ratio of pyrolysis products by removing oxygen in the form of CO_2, leading to less coke deposition.

Phenolic compounds produce low yields of aromatics and higher coke than non-phenolic molecules [95], [115]. Phenol was found to be less reactive and only partially converted to propene and butenes at temperatures of 400 °C, while 2-Methoxyphenol formed coke but did not decompose significantly over ZSM-5 at 450 °C [113]. Mullen and Boateng suggested that simple phenolics like phenol do not lead to aromatics and may lead to coke production instead [116]. They also suggested that highly acidic sites (present inside ZSM5 pores, and therefore not accessible to phenolics) were necessary to crack lignin derivatives into olefins and allenes needed for aromatics production. Gayubo too, suggested removal of aldehydes and phenolics from the pyrolysis oil before zeolite catalysis to reduce coking [117].

4.1.4 Objectives

Thus, the chemical composition of products from biomass pyrolysis is affected by feedstock composition. Additionally, differences in product composition influence the yield and selectivity for aromatics from the susequent catalysis step. To understand these interactions, the present study surveys several feedstocks and analyzes their composition, pyrolysis products as well as aromatics from their catalytic reactions. Correlations between products and feedstock properties are studied in order determine strategies for selecting feedstock for thermochemical conversion to fuels and chemicals.

4.2 Materials and Methods

4.2.1 Feedstock varieties and composition analysis

The plant materials were selected to represent a diverse class of biomass (Table 4.1). Large biomass particles were milled to a particle size of less than 1 mm (U.S. mesh #35) using a Wiley Mill (Standard Model No.3, Arthur H. Thomas, Philadelphia, PA). All biomass samples were dried to less than 10% moisture by weight in an 80° C drying oven.

Table 4.1. Biomass varieties

Type	Name	Source
Woody	Poplar (hardwood) DN34	MSU Forest Biomass Innovation Center near Escanaba, MI
	Pine (softwood)	MSU Forest Biomass Innovation Center near Escanaba, MI
Herbaceous	Switchgrass	MSU Crop & Soil Science Research Farm
	Miscanthus	MSU Crop & Soil Science Research Farm
	Corn Stover	Dr. Bruce Dale's lab
Food waste	Coffee Beans	The Coca-Cola Co.
	Spent Coffee Grounds	The Coca-Cola Co.
	Roasted Beans	The Coca-Cola Co.
	Citrus peels	The Coca-Cola Co.
	Spent tea leaves	The Coca-Cola Co.
Model compounds	Cellulose (Avicel)	The Sigma Aldrich Co.
	Lignin (poplar)	The Sigma Aldrich Co.
Algae	Chlamydomonas reinhardtii	Dr. Susie Liu's lab
	Duckweed (freshwater)	Dr. Dawn Reinhold's lab
	Nannochloropsis sp.(saltwater)	Dr. Yair Saichar Hill's lab
Treated waste	Anaerobic Digestate (manure)	Dr. Wei Liao's lab
	AFEX-treated lignin (low MW)	Dr. Bruce Dale's lab
	AFEX-treated lignin (high MW)	

Table 4.2. Analytical methods

Characteristic	Method	Remarks
Cellulose Hemicellulose Lignin Acetylation	Van Soest Method NREL method for carbohydrates and lignin	ADF/NDF Acid hydrolysis
Moisture	ASTM D4442-07	
Ash	ASTM D1102 ASTM E1755-01	Wet ashing Dry ashing
High heating value	ASTM D2015	Bomb calorimetry
Elemental analysis	Various ASTM methods Such as ICP-AES	C-H-O-N-S Cl-K-Na-Ca

Neutral detergent fiber (NDF), acid detergent fiber (ADF), and acid detergent lignin (ADL) (Dairy One Labs, Ithaca, NY) were used to estimate cellulose, hemicellulose, and lignin content (Table 4.2). Cellulose and hemicellulose are determined by the differences of %ADF–%ADL and %NDF–%ADF, respectively. Fiber analysis of non-forage samples was re-evaluated using the National Renewable Energy Laboratory's Analytical Procedure, Determination of Structural Carbohydrates and Lignin in Biomass [71]. Mono-sugar concentrations including cellobiose, glucose, xylose, galactose, arabinose and mannose were determined using a Agilent HPLC with a Bio-rad Aminex HPX-87P analytical column (300 × 7.8 mm, catalog number 125-0098) and a refractive index detector. The mobile phase was Millipore water with a flow rate of 0.6 mL/min and column temperature of 60 °C.Lignin content was expressed by ADL. The minerals Fe, Ca, P, Mg, K, and Na were analyzed using Inductively Coupled Plasma (ICP) Radial Spectrometry after microwave digestion and the chloride ion concentration was determined using potentiometric titration (Dairy One Labs, Ithaca, NY). The elemental composition was performed by combustion using automatic analyzers (Atlantic Microlabs Inc, Norcross, GA).

4.2.2 Thermogravimetric analysis

A TGA/DSC1 (CH-8603 model, Mettler-Toledo, Schwerzenbach, Switzerland) was used to characterize the weight loss curves and derivative curves for all samples. Nitrogen was used as the purge gas with a cell and furnace flow rate of 20 mL/min. The furnace was initially purged with nitrogen for 10 minutes at the beginning of each experiment, and samples were then dried in the furnace for 25 minutes at 105°C. The TGA and DTG curves were determined using a temperature profile of 10 °C/min, from 105°C - 800°C, directly following the drying phase.

4.2.3 Analytical fast pyrolysis and catalysis of biomass

Analytical fast pyrolysis is used to produce pyrolysis gas, which is the intermediate product of this process. The components of the pyrolysis gas were separated by gas chromatography and identified by mass spectrometry. A pyroprobe-GC/MS method was developed to study fast pyrolysis of biomass on the analytical scale. Experiments were conducted using a microscale pyrolysis unit, CDS Pyroprobe 5250 (CDS Analytical Inc, Oxford, PA) interfaced to a Shimadzu QP-5050A gas chromatograph /mass spectrometer (Shimadzu Corp, Columbia, MD). Approximately 0.5 mg of biomass was packed between quartz wool in a quartz tube with a filler rod. Three replicates of each sample were run. The pyroprobe was set at 650 °C with a hold time of 20 s at a heating rate setting of 1000°C/s. For catalytic pyrolysis experiments, the biomass sample was packed between layers of the catalyst and quartz wool. Identification of compounds was performed by comparing the mass spectra of the peaks with standard spectra of other compounds using the NIST library to obtain the most probable matches. Pure compounds (Sigma-Aldrich Co., St Louis, MO) were then used to confirm the peak identities based on

matching of retention times and mass spectra. Quantification was performed using external standards in acetonitrile.

Figure 4.1. Analytical fast pyrolysis-GC/MS unit and method

Pyrolysis conditions
650°C for 20 s
Heated transfer line at 300°C
GC/MS parameters
Split ratio:100
1 ml/min of He carrier gas
Restek 1701 column, 60 m x 0.25 mm x 0.25 μm
Oven program: 40 to 260°C @ 8°C/min
Detector limits: m/z: 40-400

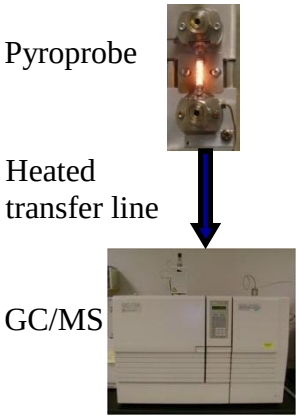

4.2.4 Statistical Analysis

Principal Component Analysis (PCA) of data allows for simplification of vast amounts of data and for observing trends. This simplification is achieved by finding correlated chemical species or markers that may be expressed in the form of a linear combination by a new single variable, known as a principal component (PC). Chemical species affect each new variable, i.e. PC, by a value known as the "loading". When a chemical is highly correlated with a PC, they have a high positive or negative loading for that PC. Thus, PCA reduces the dimensions of a dataset consisting of a large number of variables to a new set of variables, i.e. PCs, which are ordered such that the first few components retain most of the variation present in all of the original variables. PCA was performed on the percentage peak area responses of more than 50 variables (chemical species) from the collected set of pyrograms using the MATLAB R2010a (Mathworks Inc, Natick, MA) and the JMP (SAS Institute, Cary, NC) software. The data was not scaled or normalized. The average chromatographic peak areas from the replicates were used for PCA. Mean values for each grass species were selected to avoid inclusion of the experimental

variation in the model [69]. Orthogonal rotation was used to identify differences. Orthogonal rotation of principal component axes for alignment with the most important variables (by maximizing the variance of the squared loadings along the rotated PCs) and allows interpretation of data along the principal components in the same direction where the most significant variables can be formed. Correlation analysis was used to examine the relationship between the key chemical markers and independent variables, that is, the biomass composition data, using Excel (Microsoft Office 2011). The correlation coefficient measures the linear association between two variables on a scale of -1 to +1.

4.3 Results and Discussion

4.3.1 Biomass selection: Feedstock composition

The composition and elemental analysis of several feedstocks are presented in (Table 4.3 and Table 4.4). Cellulose and lignin were obtained from Sigma-Aldrich Co. and were assumed to be pure; they were not subjected to compositional analysis. Algae and pine were not available in sufficient quantity and were not analyzed as well.

Table 4.3. Chemical Composition (weight% of dry biomass)

Type	% Ash	% ADL (lignin)[1]	% AH Lignin[2]	% Cellulose	% Hemicellulose
Poplar DN34	0.55	11.4	27.2	54.6	13.5
Pine	0.23	-	15.9	57.4	19.0
Switchgrass	4.1	8.15	21.9	37.5	32.4
Miscanthus	3.3	11.1	24.5	50.2	27
Corn stover	-	5.95	18.3	37.2	28.9
Spent tea	3.81	10.2	31.7	34.0	9.5
Green coffee beans	5.7	3.5	27.9	37.7	25.3
Spent coffee grounds	1.52	13.9	29.3	47.3	19
Roasted coffee powder	6.55	7.1	27.5	37.5	19.5
Citrus waste	-	2.65	03.7	36.5	6.05
Duckweed	-	-	13.1	-	-

1 ADL or acid-detergent lignin is an indicator of lignin content in biomass
2 Acid-hydrolysis lignin (soluble + insoluble lignin)

Table 4.4. Elemental analysis (weight% of dry biomass)

Type	%C	%H	%N	%S	%O	% Ca	% P	% Mg	% K	% Na	% Cl	Fe (ppm)
DN34	47.5	6.1	0.2	0.2	46.1	0.2	0.04	0.04	0.02	0.01	0.06	38
Pine	47.8	6.4	0.0	0.0	45.8	-	-	-	-	-	-	-
Switchgrass	44.6	6.1	0.6	0.0	48.8	0.4	0.23	0.25	0.8	0.004	0.13	92
Miscanthus	45.2	6.1	0.4	0.0	48.2	0.25	0.06	0.04	0.6	0.005	0.08	110
Corn Stover	42.1	5.8	0.5	0.0	51.6	0.225	0.265	0.14	1.5	0.031	-	120
Spent Tea	48.7	6.4	4.6	0.4	39.9	0.395	0.4	0.17	1.02	0.018	0.1	105
Green coffee beans	47.4	7.1	2.4	0.2	43.0	0.11	0.19	0.21	1.835	0.017	0.09	56
Spent coffee grounds	52.2	7.7	2.0	0.2	37.9	0.1	0.07	0.1	0.21	0.013	0.04	69
Roasted coffee powder	51.6	6.8	2.8	0.1	38.8	0.1	0.018	0.22	2.02	0.015	0.11	49
Citrus waste	40.3	6.5	1.0	0.0	52.1	1.335	0.09	0.12	0.865	0.017	-	46
Duckweed	36.7	5.2	5.0	0.6	52.5	-	-	-	-	-	-	-
Cellulose	42.6	6.3	0.0	0.0	51.1	-	-	-	-	-	-	-
Lignin	44.4	5.4	3.8	0.2	46.5	-	-	-	-	-	-	-

The cellulose, hemicellulose and acid-detergent lignin as estimated by the Van Soest fiber analysis were in a wide range of values. The lignin values were re-evaluated using the acid hydrolysis method for determining soluble and insoluble lignin. The ash content of woody biomass, poplar and pine was much lower than herbaceous crops such as switchgrass, miscanthus and corn stover. Food wastes had a high ash content with the exception of spent coffee grounds (SCG). SCG are processed using hot water extraction, which reduced the level of inorganic constituents [118]. Elemental analysis showed that spent tea and coffee grounds had lower amount of oxygen and higher carbon and hydrogen content. Although the ash yield by itself provides limited information about a feedstock, it has been used as an indicator of the bulk inorganic matter such as alkali and alkaline earth metals (AAEM) that cause slagging, fouling and sintering [60]. Elemental analysis showed that of the AAEM, potassium was the most significant, measuring 0.02 to 2.02% weight of dry biomass (wdb). Calcium constituted between 0.10 to 0.40% wdb while magnesium varied between 0.04 to 0.25% wdb. Sodium content was

less than 0.03% wdb while iron was present in the 38-120 ppm range. Poplar had the lowest potassium content while coffee beans and grounds had the highest. Hot water extraction to produce spent coffee grounds removed the AAEM from this feedstock; thus spent coffee grounds had significantly lower levels of these metals. Increasing level of AAEM has been shown affect pyrolysis products with an increase in the yield of char and gases and a decrease in the amount of condensable chemicals that constitute bio-oil. However such catalytic activity may be desirable for conversion of biomass pyrolysis to aromatics if the cracking reactions lead to greater production of carboxylic acids (section 4.1.2). Carboxylic acids have a higher H:C molar ratio and increase aromatics production; however if production of aldehydes and furans increases, it may lead to coke formation on catalyst through polymerization and resin formation on the external and internal acidic sites of catalysts [91], [95], [114].

Van Krevelen diagrams are used in the coal and petroleum industries to gauge the quality of these carbonaceous fuels [93]. Catalytic pyrolysis experiments with various feedstocks have shown that biomass composed of a high H:C molar ratio produces more hydrocarbons. Thus, a comparison of the H/C molar ratio of biomass before any further experimentation may provide valuable pointers to the quality of hydrocarbons obtained upon catalytic fast pyrolysis (Table 4.5). The Van Krevelen diagram in reveals a range of O/C and H/C ratios that corresponds to desirable levels of aromatics, specifically, BTEX production upon pyrolysis and catalysis (discussed later in section 4.3.4). Similar to the Van Kreveln plot, Chen et al. proposed an effective hydrogen index (EHI) or H/Ceff of biomass [94]. Feedstocks with H/Ceff ratios less than 1 produced more coke and rapidly deactivate the catalyst, making production of high yields or aromatics difficult. Spent coffee grounds had a high H/Ceff of 0.68 while corn stover and

digestate had really low values, suggesting that these feedstocks may not be the most suitable candidates for hydrocarbon aromatics from catalytic pyrolysis.

Table 4.5 Molar ratios for Van Krevelen plot and Chen's effective ratios (EHI and H/Ceff)

Material	*H/Ceff, ref.*[96]		
Methanol	2		
Petroleum based feedstock	1.0 – 1.5		
Bio-oil	0.3 – 0.5		
Lignocellulosic feedstock	0.0 – 0.3		
Biomass	O/C	H/C	H/Ceff
Poplar	0.73	1.54	0.08
Switchgrass	0.82	1.63	-0.01
Miscanthus	0.80	1.62	0.02
Corn Stover	0.92	1.64	-0.20
Digestate	0.94	1.57	-0.31
Spent Tea	0.61	1.59	0.36
Citrus waste	0.97	1.94	0.00
Ground Coffee Beans	0.68	1.81	0.44
Ground Roasted Beans	0.56	1.58	0.45
Spent Coffee Grounds	0.54	1.77	0.68

Note: Data are means of measurements in duplicate.

4.3.2 TGA results

The differential thermogravimetry (DTG) curves for each grass sample are shown in Figure 4.2. The DTG curve for each biomass is influenced by its composition [77]. The maximum rate of weight loss was observed over a wide range of 275-350 °C for all samples. This peak represents the thermal decomposition of cellulose and corresponds with that observed by Varhegyi et al. in their experiments with Avicel cellulose [78]. Poplar and Miscanthus showed the highest weight loss rate which corresponded with the high cellulose content (47.5 and 50% respectively). A second smaller peak or shoulder-like feature was observed between 290-300 °C. This smaller peak is partially related to the hemicellulose content of biomass, which decomposes at a lower temperature than cellulose. Lignin decomposition occurs over a wide temperature range, contributing to the cellulose and hemicellulose decomposition peaks [77],

[79]. Inorganic minerals may aid biomass pyrolysis by catalyzing reactions necessary for breakdown of biomass components such as lignin and cellulose at a lower temperature [50], [59]. Many studies have reported the effect of inorganic minerals on the shift in biomass weight loss temperature identified by DTG analysis [52], [53], [55], [59]. Thus, coffee beans and ground roasted coffee powder showed similar DTG curves while spent coffee grounds show a slightly larger peak at a higher temperature. Spent coffee grounds have less inorganic minerals and greater lignin content per dry weight of biomass. All three coffee-based biomass showed shoulder-like peak at temperature of 375-410 °C which may be due to lignin breakdown or cracking of fatty acid/esters due to cracking activity of inorganic minerals left behind in the solid biomass residue. Citrus peels with their high hemicellulose content showed multiple peaks are lower temperatures than other biomass. Spent tea leaves also exhibited smaller, multiple peaks. Cellulose and lignin DTG curves show how the presence of these biomass components influences the TGA of biomass. Cellulose shows a sharp, tall peak at 325 °C while lignin produces a much smaller peak at the same temperature. A majority of lignin gets converted to char due to cracking and condensation reactions between phenolics produced upon lignin pyrolysis as well as phenolics and inorganic minerals [116].

The TGA data is useful in determining temperature for pyrolysis, especially of the three heating zones in the MSU pilot-scale screw conveyor reactor. Thermogravimetric analysis showed that temperatures in excess of 300 °C were necessary to initiate pyrolysis and decomposition of biomass,. For example, poplar decomposed almost completely at 500 °C while the same event was observed for spent coffee grounds around 600 °C.

4.3.3 Py-GC/MS

4.3.3.1 Biomass pyrolysis

Pyrolysis of the biomass produced non-condensable and condensable vapors, a mixture of over a hundred compounds, but negligible quantities of monocyclic aromatics such as BTEX (benzene, toluene, ethyl benzene and xylenes). Predominantly, oxygenated molecules such as carboxyl and carbonyl groups, saccharides and phenolic compounds were produced (Figure 4.4). Analytical pyrolysis-GC/MS of biomass feedstock revealed chromatograms with over a 100 different chemicals. These chemicals and their concentration in the condensable GC detectable fraction of pyrolysis vapors is given in the Appendix.

The following were key chemical species that were unique or abundant to the corresponding biomass:

Table 4.6 Most abundant chemicals in different feedstock

Biomass	Key Chemical Markers
Poplar (DN34)	Acetic acid, methoxyeugenol, levoglucosan, Syringols
Pine	Levoglucosan, Glycolaldehyde, Methyl glyoxal, Methyl pyruvate, Guaicols
Switchgrass,Miscanthus Corn Stover,Digestate	Acetic acid, Acetol, Furfural, Cyclopenten derivatives, Guaicols, Cyclopropanemethanol, 4-Vinylphenol, 4-Vinylguaiacol, Levoglucosan (corn stover)
Roasted coffee powder	Furfuryl alcohol, Phenol, Cyclopropanemethanol, Hydroquinone, Palmitic acid, Caffeine; Aliphatic hydrocarbons and levoglucosan
Green coffee beans	
Spent coffee grounds	
Tea	Phenol, Cresol, Methoxyeugenol, Levoglucosan, Caffeine
Citrus	Acetic acid, Acetol, Furfural, 5-Hydroxymethylfurfural
Lignin	Methyl glyocal, Phenol, Guaicol, 4-Vinylguaicol
Cellulose	Anhydrosugars (Levoglucosan etc.)
C. reinhardti Duckweed Nannochloropsis sp.	Toluene, alkene, C10+ alcohols/ketones, aliphatic hydrcarbons

Figure 4.2 Comparison of weight loss data from TGA of various feedstock

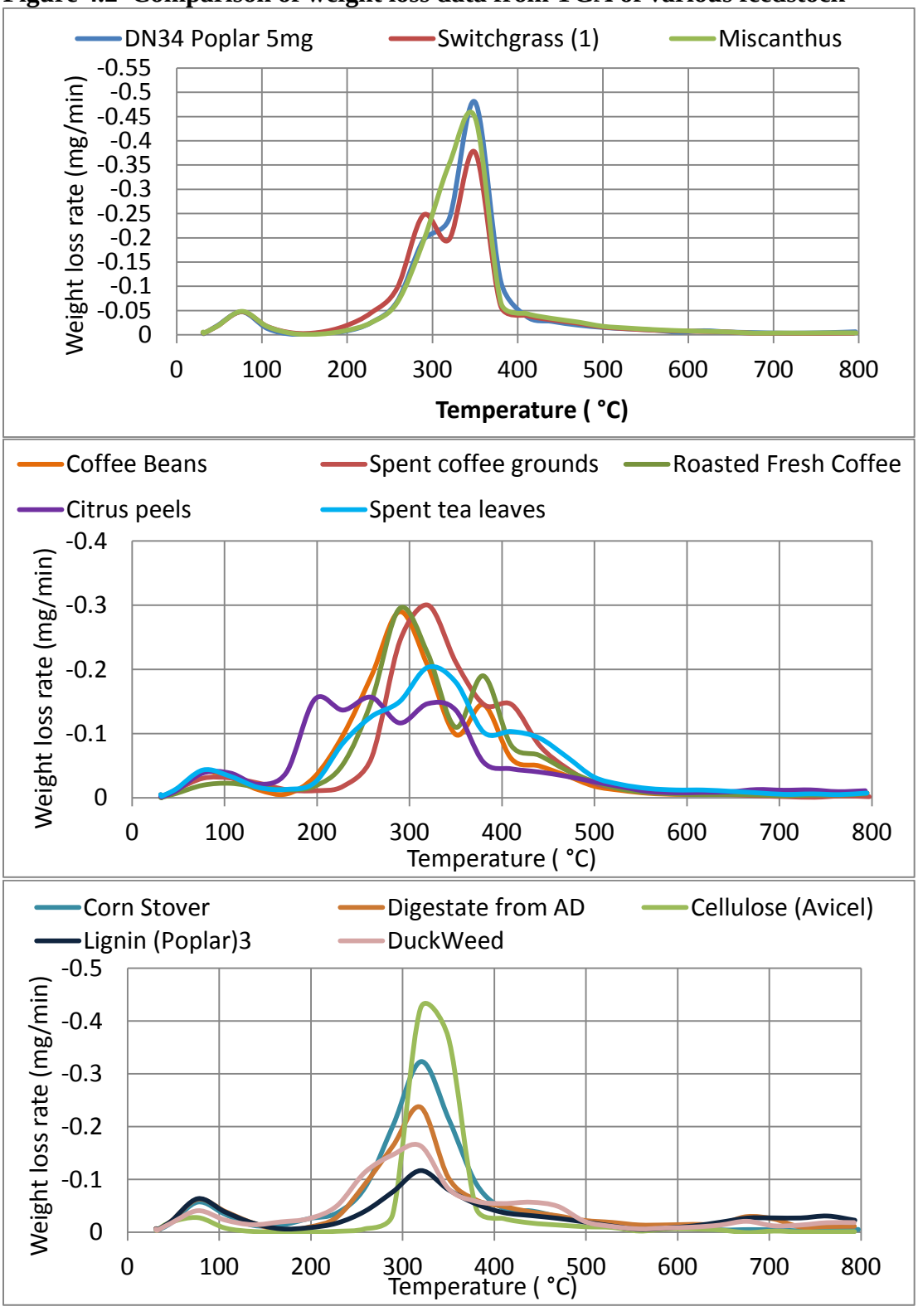

Figure 4.3 Comparison of GC/MS chromatograms from (A) pyrolysis and (B) catalytic pyrolysis (catalyst: ZSM-5) of spent coffee grounds

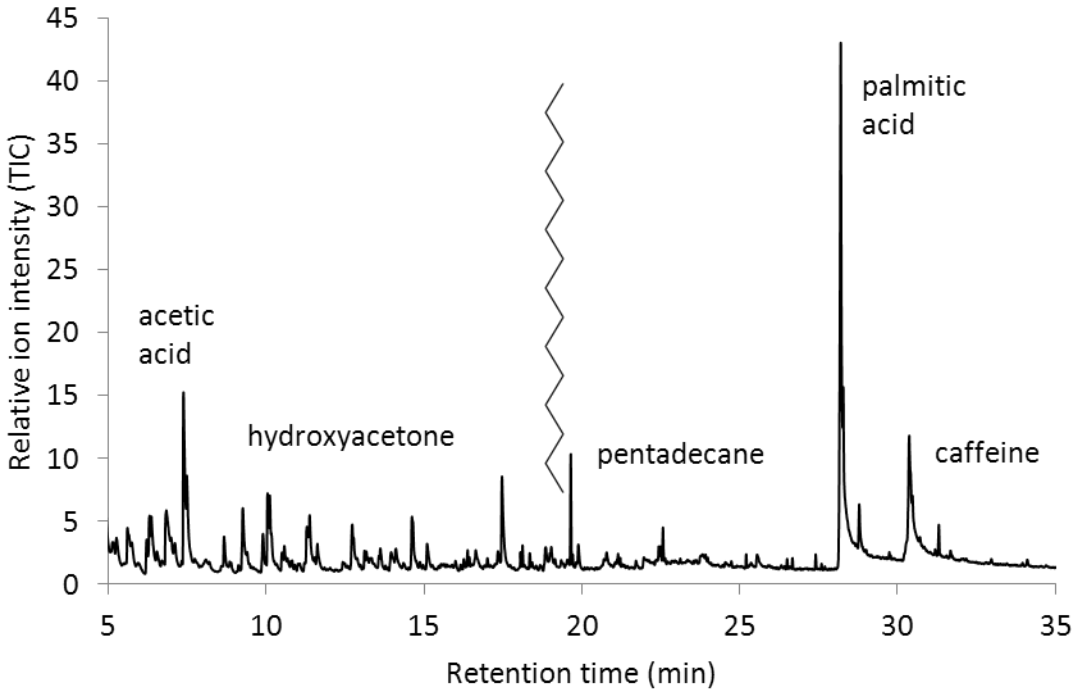

Compounds detected with retention times are as follows: (retention time)compound name, (7.1) Acetic acid, (7.6) Toluene, (7.7) 1-hydroxy-2-Propanone(Acetol), (11.5) 1-Nonanol, (12.0) 3-methyl-Butanoic acid, (12.1) 2-Furanmethanol (furfuryl alcohol), (12.2) 3-methyl-2-Butanone, (12.4) 2-methyl-2-Cyclopenten-1-one, (13.6) Undecane, (13.7) octyl-Cyclopropane, (14.1) Propanoic acid, ethenyl ester, (14.2) 2-Butanone, 1-(acetyloxy)-, (14.7) Butyrolactone, (15.7) Tridecane, (15.8) 1-Undecene, (15.8) 1,2-Cyclopentanedione, 3-methyl-, (17.7) Tridecane, (17.7) 1-Dodecene, (18.0) Phenol, 4-methyl-, (19.1) Pentanal, (19.5) Tridecane, (19.6) 1-Tetradecene, (21.3) Pentadecane, (21.3) 1-Hexadecene, (22.9) Hexadecane, (23.0) 1-Hexadecene, (24.3) 8-Heptadecene, (24.4) Eicosane, (26.8) 1-Tetradecanol, 14-chloro- , (28.7) Hexadecanoic acid, methyl ester, (30.6) n-Hexadecanoic acid (palmitic acid), (30.7) Octadecanoic acid, 2-propenyl ester, (31.5) 1H-Purine-2,6-dione, 3,7-dihydro-1,3,7-trimethyl- (caffeine), (33.3)12-Methyl-E,E-2,13-octadecadien-1-ol,(34.6)Palmitic acid vinylester

Figure 4.3 (cont'd)

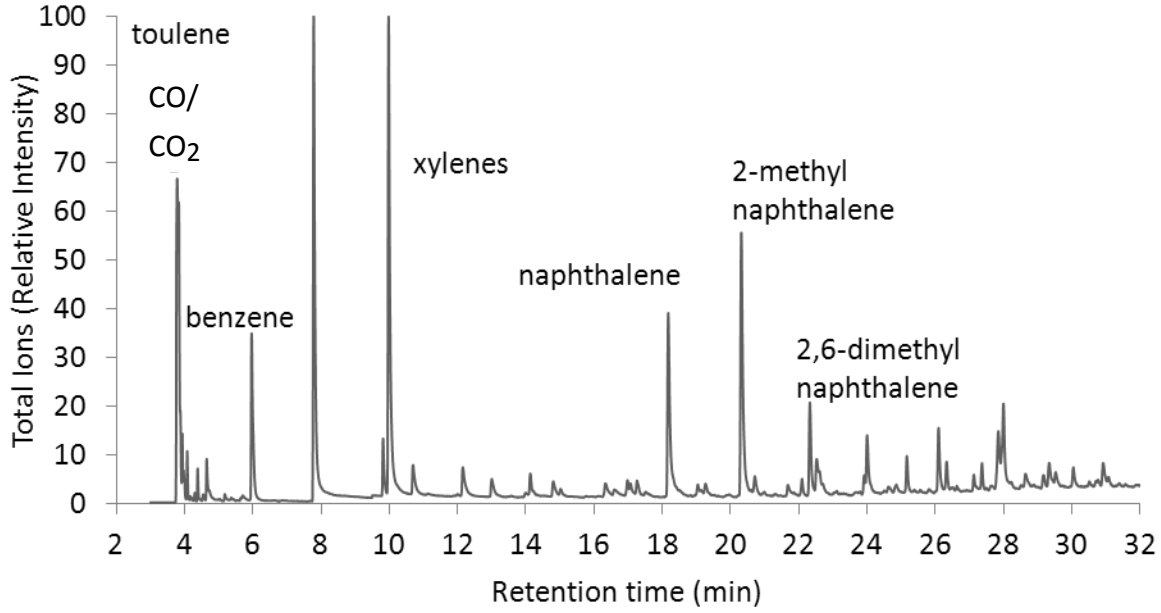

Compounds detected with retention times are as follows: (retention time)compound name, (3.6) Oxygen, (3.9) Carbon dioxide, (4.1) Formic acid, ethenyl ester, (4.2) Methanol, (4.5) Ethanol, (4.7) Acetone, (6.0) Benzene, (7.1) Acetic acid, (7.8) Toluene, (9.8) Ethylbenzene, (10.0) p-Xylene, (10.6) o-Xylene, (12.0) Benzene, 1-ethyl-3-methyl-, (12.2) Benzene, 1,2,3-trimethyl-, (12.8) Benzene, 1,2,3-trimethyl- ,(13.7) Benzene, 1,2,4-trimethyl- , (14.0) Indane, (14.7) Indene, (14.8) Indene, (14.9) 1H-Indene, 2,3-dihydro-2-methyl- , (16.2) 1H-Indene, 2,3-dihydro-5-methyl- , (16.9) 1H-Indene, 1-methyl- , (17.0) 1H-Indene, 2,3-dihydro-4,7-dimethyl-, (18.1) Naphthalene, (20.3) Naphthalene, 2-methyl-, (20.6) Naphthalene, 1-methyl- , (22.0) Naphthalene, 2-ethyl-, (22.3) Naphthalene, 2,6-dimethyl- , (22.5) Naphthalene, 2,6-dimethyl- , (22.6) Naphthalene, 2,6-dimethyl-

4.3.3.2 Internal Bed Catalytic Pyrolysis-GC/MS (Experimental Setup 1)

Catalytic pyrolysis-GC/MS experiments (internal bed or in-situ catalysis) were performed for biomass varieties with HZSM-5, a well-studied acidic zeolite. Biomass samples (0.5 mg) were packed between two layers of HZSM-5 catalyst using the method described before. The biomass to catalyst ratio was 1:5. HZSM-5 was chosen because it is known to be an effective catalyst for cracking, deoxygenating and synthesis of aromatic hydrocarbons [68], [91], [107], [109], [119], [120].

Figure 4.4 displays a typical chromatogram generated upon the catalytic fast pyrolysis of plant biomass, in this case, spent coffee grounds. The prominent chemical markers unique to pyrolysis of specific biomass feedstock are listed in Table 4.6 while a complete list chemicals produced upon biomass pyrolysis is presented in the Appendix. A comparison of aromatic yields relative to poplar is presented in Table 4.7. Spent coffee grounds produced the maximum aromatic compounds of all biomass tested for catalytic fast pyrolysis with HZSM-5 catalyst. With the exception of spent coffee grounds, the yields are in a narrow range for most biomass types (wood, grass, agricultural waste, algae).

Table 4.7. Comparison of aromatic yields for various biomass relative to poplar.

Biomass	Relative yield of aromatics
Anaerobic digester digestate	0.53
Corn Stover	0.56
Citrus waste	0.77
Duckweed	0.84
Spent tea leaves	0.85
Saltwater Algae (Nannochloropsis sp.)	0.85
Cellulose	0.89
Poplar (DN34)	1.00*
Pine	1.00
Switchgrass	1.02
Miscanthus	1.02
Roasted coffee powder	1.19
Freshwater Algae (*C. reinhardtii*)	1.22
Green coffee beans	1.34
Spent coffee grounds	1.83

*Yield for poplar in this experiment was ~ 3.8 % w/w dry biomass. Aromatic yields are an average of three to six replicates. For poplar DN34, BTEX aromatics yield was ~ 4 weight % (HZSM-5 catalyst, catalyst: biomass ratio of 5:1, pyroprobe temperature: 650 °C). The yields are approximate and presented for comparison purposes only. Due to small sample size used in analytical microscale pyrolysis experiments and changes in biomass during storage, the yields may be variable.

4.3.4 Statistical analysis to compare the results of wet chemistry, pyrolysis and catalysis

Multivariate statistical tools, such as Principal Component Analysis (PCA), are being used to make observations from this complex dataset. Figure 4.5 contains a plot of the first two principal components that are formulated to describe the variability between different feedstocks. PCA of the pyrolysis-GC/MS data revealed that small carbonyl compounds such as acetic acid, acetol, and furans, long-chain fatty acid, phenolics were responsible for most of the variability (differences) in pyrolysis products. These observations are not intended to be axiomatic and they are valid only for the set of feedstock in this study. No volatile aromatic molecules were detected except small quantities of toluene in the algae, coffee-based feedstock and lignin. Biomass that eventually produced more monoaromatics showed traces of toluene.

Key chemical markers in Figure 4.5 with their weights are in green (positive x and y axes labels) and red (negative x and y axes labels). Biomass feedstocks (blue) are placed in the four quadrants in arrangements nearest to the chemicals that they produce in abundance, and furthest from the chemicals that are least produced. The main differentiator along the x-axis was the production of medium and long-chain C8+ alcohols and ketones that were observed in algae but not in other biomass. Biomass with high cellulose or other polysaccharides and high inorganic mineral content produced more carbonyl compounds such as acetic acid, acetol, furfural and cyclopenten derivatives. The feedstocks cellulose, lignin and pine were not greatly influenced by the same chemical markers that produced variability in other biomass. Hence, they were observed closest to the center point, that is, they did not show variability for the major chemicals that influenced this analysis. Pine, which is a softwood, produced large amount of levoglucosan, due to its high cellulose and low alkali and alkaline earth metal content [48], and was observed to be separate from other woody and herbaceous crops on the plot.

Along the y-axis, the three coffee-based biomass produced large amount of palmitic acid, aliphatic hydrocarbons and also caffeine, which were absent in other biomass. Therefore the spread along y-axis was severely affected by these chemicals. The production of phenolics was highest in Poplar (DN-34), and DN-34 was placed farthest from the center point of the y-axis. Again, it is important to note that the plot and observations are not axiomatic. The observations mentioned here may be true for the collection of biomass tested, but if some feedstock were removed or others added to the analysis, the plot may change drastically. Note that woody and herbaceous crops produced similar type of compounds; the coffee products produced more fatty acids and alkanes than phenolics. Although very little or none of the desired aromatics were produced, some of these molecules are important precursors to BTEX as shown in section 4.3.5.

Figure 4.4 A plot of the first two principal components formulated to describe the variability between feedstock. Clammy=*C. reinhartii* and Nanno=*Nannochlropsis sp.*

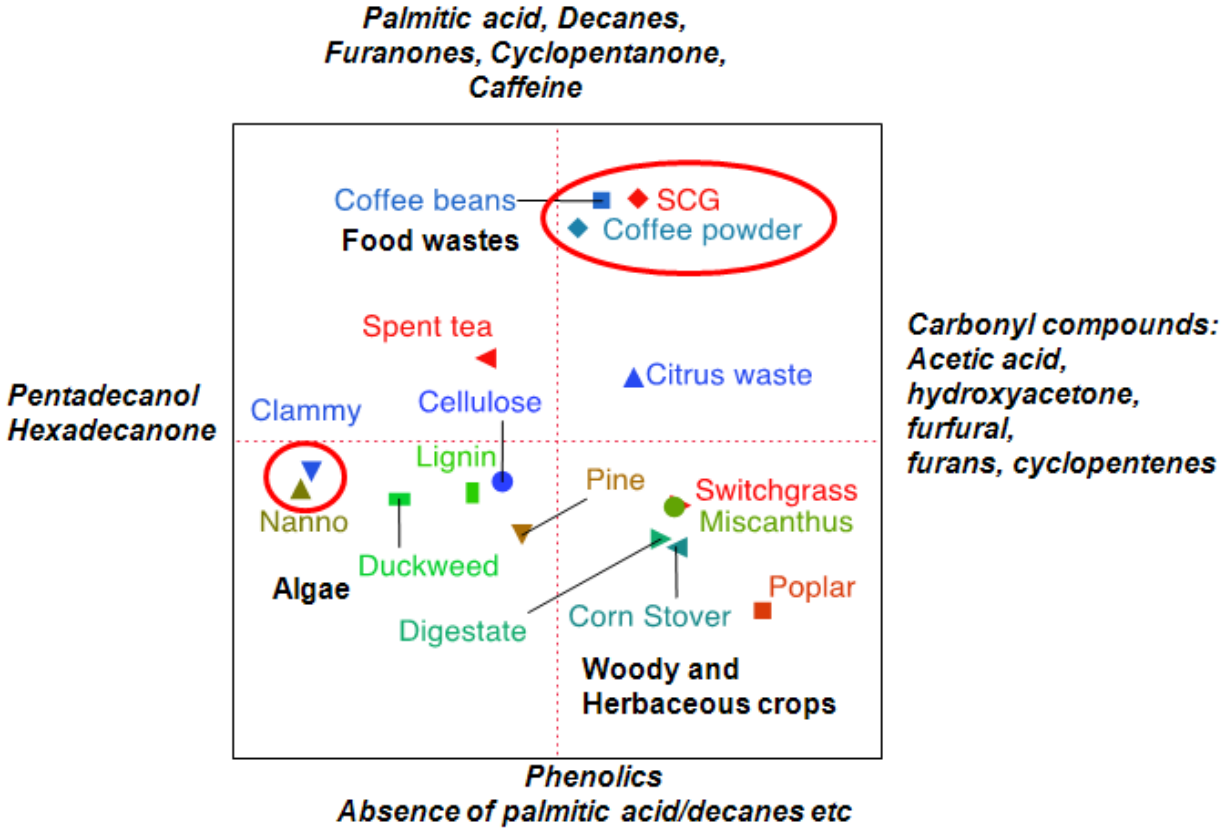

Figure 4.5 Hierarchical cluster diagram of connections between biomass based on the spread of products they generated upon pyrolysis. The length of the connector line increases with decrease in commonality

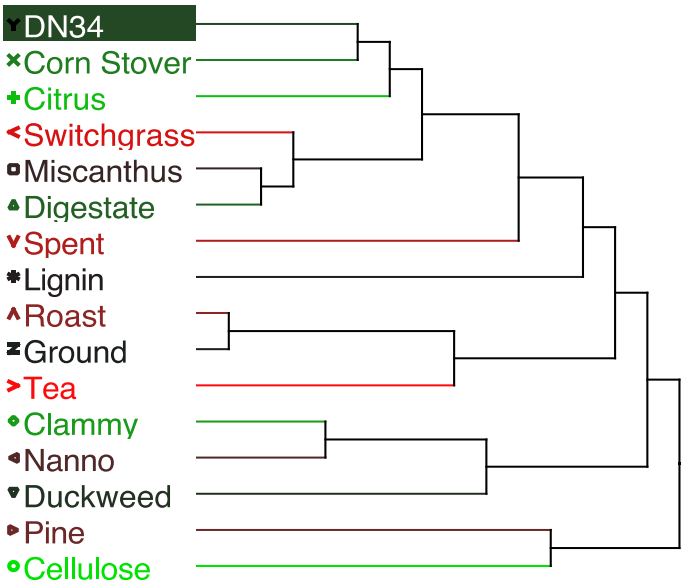

A hierarchical cluster analysis presents information similar to that obtained from principal component analysis in a dendogram plot shown in Figure 4.5. Biomass that produce the most similar products are connected by the shortest lines. Thus, green coffee beans and roasted coffee powder are most similar in terms of their pyrolysis products; so are the two algae. Digestate, the solid left over waste from anaerobic digestion is most similar to herbaceous crops, miscanthus and switchgrass.

However, a comparison of the catalytic pyrolysis results show that similarity between pyrolysis products do not necessarily affect aromatic yields after catalysis. Upon catalytic pyrolysis, all biomass produce the aromatic hydrocarbons with similar product distribution; however their aromatic and catalyst coke yield are very different (Appendix). Therefore a correlation analysis between the feedstock composition and aromatics yields was required to

understand relationships between them. Correlation analysis showed that aromatics yield was heavily influenced by the H:C and O:C ratio as well as lignin content of biomass.

The Van Krevelen diagram (Figure 4.6) in reveals a range of O/C and H/C ratios that corresponds to desirable levels of BTEX (hydrocarbon aromatics) production upon pyrolysis and catalysis (Van Krevelen diagrams are used in the coal and petroleum industries to gauge the quality of these carbonaceous fuels. Catalytic pyrolysis experiments with various feedstocks have shown that biomass composed of a high H/C molar ratio produces more hydrocarbons. Thus, a comparison of the H/C molar ratio of biomass before any further experimentation may provide valuable pointers to the quality of hydrocarbons obtained upon catalytic fast pyrolysis.

In order to enhance the H/C ratio of the feed and produce more hydrocarbons, Dao and co-workers co-fed model bio-oil compounds with a hydrogen-rich compound, methanol and found that the yield of hydrocarbons increased from below 10% to 40 wt.%[121]. Gao et al. studied aromatization over Ga-ZSM-5 catalysts and observed that the oxygen content of the feed was a far more significant factor in influencing aromatic yields than the hydrogen content [122]. Recently, Srinivasan et al. tested torrefied pine wood with zeolite catalyst and observed that torrefaction improved the O:C ratio and initiated decomposition of lignin[123]. When used as a feedstock for catalytic pyrolysis, the lignin in torrefied wood decomposed to smaller monomer and oligomer fragments and produced significantly higher yields of monoaromatics as well as phenolics over non-torrefied pinewood.

In our experiments with AFEX-treated lignin, the low MW lignin had a much higher H:C ratio and produced greater aromatic yields compared with the higher MW lignin. Thus, concluding, it is important to select feedstock with a low oxygen content and a high H:C molar ratio for high aromatic yields from biomass pyrolysis-catalysis.

Figure 4.6. The Van Krevelen diagram for the biomass feedstocks included in this study

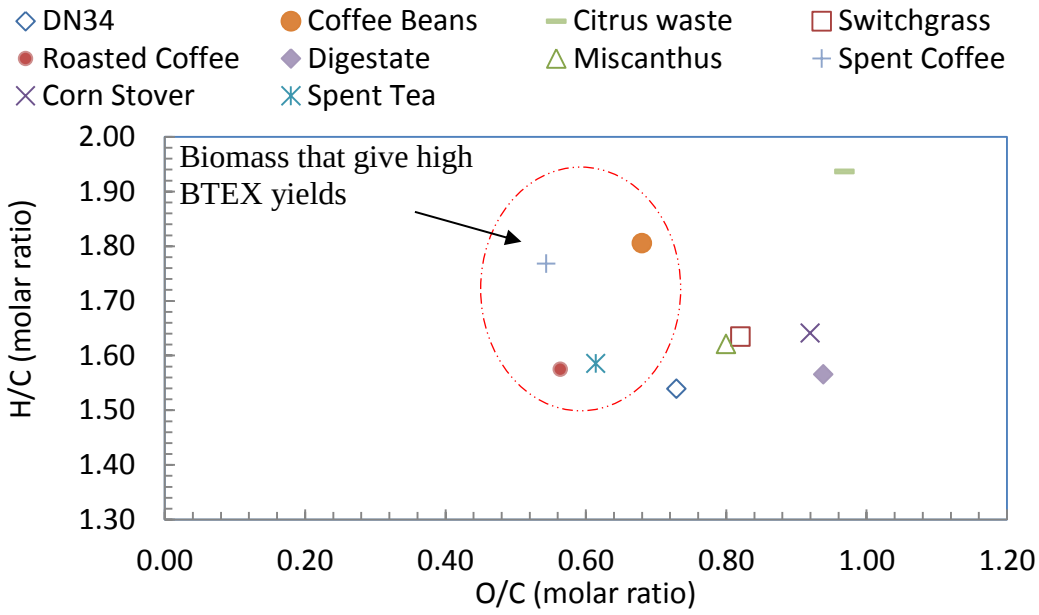

4.3.5 Catalytic pyrolysis of neat compounds

The major chemical species found in pyrolysis products of biomass that gave high aromatic yields were acetic acid, hydroxyacetone (in woody and herbaceous biomass) and palmitic acid (in coffee biomass). To explore the fate of these molecules upon catalysis, neat palmitic acid, acetic acid and hydroxyacetone (acetol) were pyrolyzed with and without catalyst (HZSM-5) using the pyroprobe-GC/MS setup.

Pyrolysis of palmitic acid produced only palmitic acid (Figure 4.7). When palmitic acid is reacted with HZSM-5 catalyst at pyrolysis conditions, aromatic molecules such as benzene, toluene, xylenes, naphthalenes were observed. No alkanes or alkenes were detected.

Figure 4.7. Pyrolysis of palmitic acid with and without catalyst. Dotted line shows the two products without catalyst, while the continuous line shows products after catalysis.

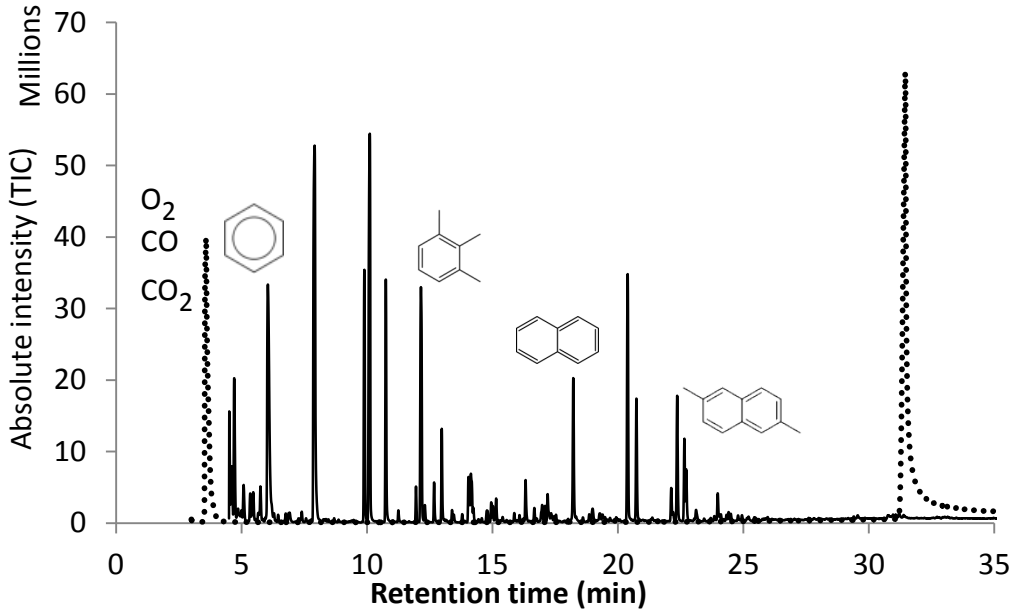

Acetic acid produced large peaks of monoaromatics upon reaction with zeolite catalyst (Figure 4.8). Acetol (hydroxyacetone) dehydrated to a large amount of methylenesuccinic acid/anhydride compound during pyrolysis (Figure 4.9). Methylenesuccinic acid is a building block in production of styrene-butadiene-acrylonitrile and acrylate latexes that have applications in the paper and architectural coating industry. The remaining acetol reacted with the catalyst to produce aromatics. 4-Vinylphenol (herbaceous crops) and caffeine (coffee biomass) also produced aromatics upon catalytic reaction, although the peak areas were much smaller.

Figure 4.8. Pyrolysis of acetic acid with (dark line) and without (dotted line) catalyst.

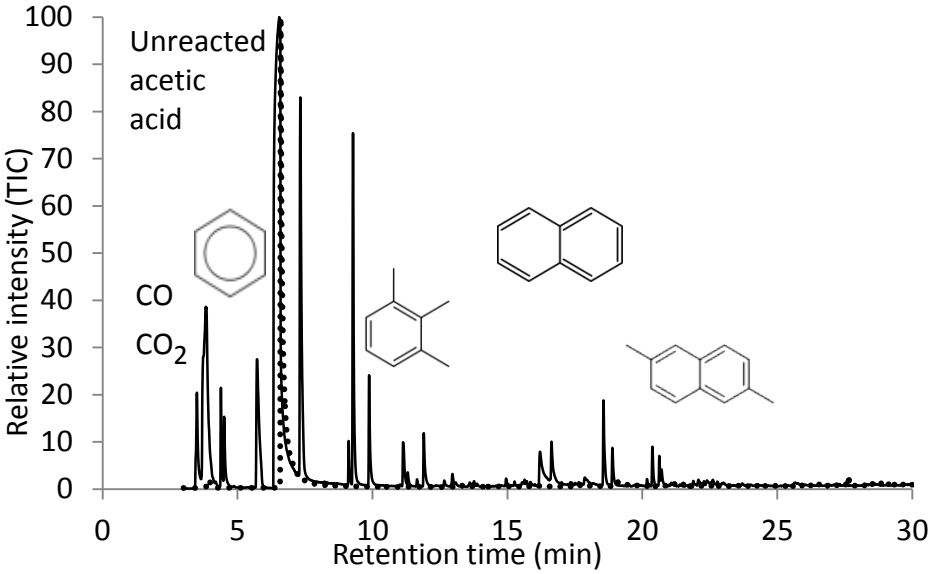

Figure 4.9. Pyrolysis of hydroxyacetone (acetol) with (dark line) and without (dotted line) catalyst.

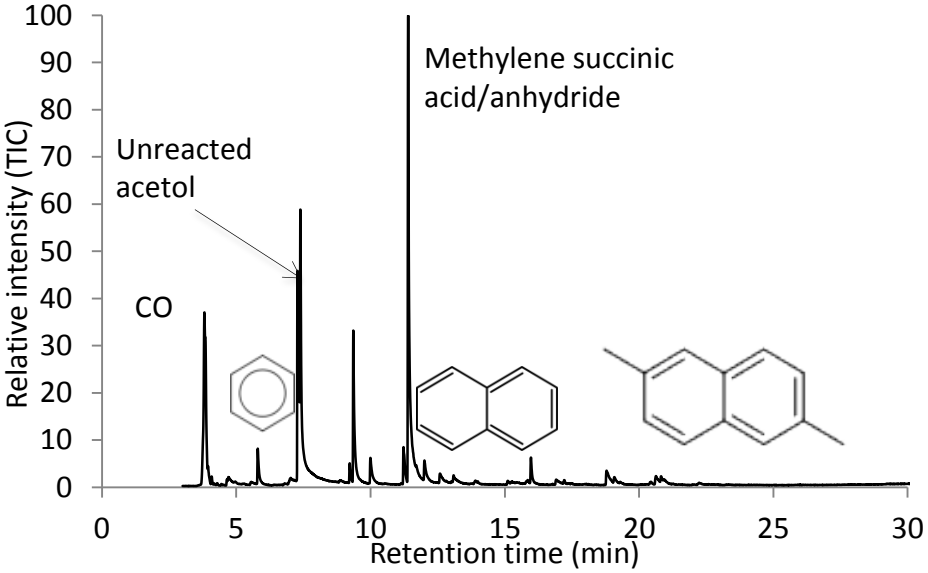

4.3.6 Spent coffee grounds as feedstock

From experiments described in the sections above, spent coffee grounds (SCG) was identified as the feedstock with the potential to produce the most aromatics with HZSM-5

catalyst. In the following section, SCG was used a model biomass to test selected catalysts for the biomass pyrolysis reaction and compare their yields. The catalysts were as follows:

Table 4.8. Catalysts for analytical pyrolysis experiments

Catalyst	Reason for selection
HZSM-5	FCC catalyst, high acidity, shape selectivity
Red mud	Inexpensive byproduct, hazardous waste
$SO_4^{2-}ZrO_2$	High acidity
(20%) SO_4^{2-} ZrO_2 MCM-41	mesoporosity, high pore volume, acidic
(2%) Al-MSU-S Foam	Hexagonal framework, high pore volume, largest pore
(2%) Al-MSU-S Worm	Worm-hole geometry, high pore volume

In early experiments, the pyroprobe was used for catalytic pyrolysis experiments. The pyroprobe may be described as an internal bed or in-situ experiment (setup 1) and is common for studying catalytic pyrolysis. But the technique has many deficiencies such as lack of control over the catalyst bed temperature or control of residence time. In addition, the catalyst temperature is an unknown and may vary over the course of the catalytic pyrolysis experiment. It is also not possible to separate coke from char using the internal-bed method. Therefore, another setups that simulated an external catalyst bed was tested.

4.3.6.1 External catalyst bed experiments (Setup 2: GC Liner)

In order to separate pyrolysis and catalysis reactions and enable an independent study of catalysts, a novel technique was adopted [124]. The catalyst was packed in the inlet liner of the GC following the pyroprobe (Setup 2). The pyrolysis vapors coming from the pyroprobe reacted with a known quantity of catalyst in the inlet of the GC before the products were analyzed quantitatively and qualitatively. Multiple samples of pyrolysis vapors (12 samples of 1 mg spent coffee each) were passed over a known weight of a catalyst and product yields were monitored. Toluene, within the aromatic group of compounds, was observed in the largest concentration for

all catalysts examined. Significant amounts of coking were also observed was all catalysts. Sulfated zirconia catalysts showed low aromatic yields and heavy coke production. Al-MSU-S catalysts produced a small quantity of monoaromatics and higher alkanes. The foam catalyst produced a large quantity of acetic acid and acetol while the worm catalyst generated acetic acid but no acetol. Red mud reduced the intensity of acyl group peaks (organic acid, ketones and aldehydes). Red mud has been previously shown 'active' at temperatures of over 330°C for reducing oxygenated organic compounds. It produced very small quantities of monoaromatics at a GC inlet (catalyst bed) temperature of 280 °C or at 350 °C.

HZSM-5 at 350 °C showed the highest monoaromatics production; however the yields were small compared to pyroprobe reactions. When measured on a weight % of biomass basis, monoaromatics yields from GC liner experiments were significantly lower when compared with previous catalytic pyrolysis studies with the pyroprobe. Experiments with pyrolysis of standard compounds such as fluoranthene and poly(α-methylstyrene) showed that there are no losses or tailing due to use of the liner setup. The large difference was probably a result of low catalyst temperatures (insufficient catalyst activity, condensation of pyrolysis vapors, aerosols and large oligomers leading to heavy coke generation). It is also possible that such a technique may have interfered with the gas splitting operation in the GC inlet. In addition, the inlet was limited with a set point temperature of 350 °C and the actual catalyst bed temperature may have been lower. Although the liner experimental setup (setup 2) is a more accurate representation of large-scale upgrading of pyrolysis vapors than in-situ catalytic pyrolysis (setup 1), and were useful in comparing catalysts, it was desired to test the activity of these catalysts at higher temperatures.

Table 4.9. BTEX yields from GC liner experiment. Yields are relative to HZSM5 analysis at liner temperature of 280 °C (SETUP 2)

Liner temp: 280°C Catalyst type	Pyroprobe Temp.	Catalyst: Biomass ratio	Relative BTEX yield
HZSM5	650 °C	10	1
SO_4^{2-}-ZrO_2	650 °C	10	0.78
(20%) $SO_4^{2-}$$ZrO_2$ MCM-41	650 °C	10	0.78
Red Mud	650 °C	10	0.50
(2%) Al-MSU-S Foam	650 °C	10	0.67
(2%) Al-MSU-S Worm	650 °C	10	0.72
Liner temp: 350 °C Catalyst type	Pyroprobe Temp.	Catalyst: Biomass ratio	Relative BTEX yield
HZSM5	650 °C	10	4.72
SO_4^{2-}-ZrO_2	650 °C	10	2.72
(20%) $SO_4^{2-}$$ZrO_2$ MCM-41	650 °C	10	2.89
Red Mud	650 °C	10	0.61
(2%) Al-MSU-S Foam	650 °C	10	1.94
(2%) Al-MSU-S Worm	650 °C	10	2.39

Therefore the experiments for selecting catalysts were repeated with the pyroprobe as the pyrolysis-catalysis unit (Setup 1).

4.3.6.2 Internal-bed catalytic pyrolysis GC/MS (Experimental Setup 1)

Catalytic pyrolysis-GC/MS experiments (internal bed or in-situ catalysis) were performed for biomass varieties with HZSM-5 by packing biomass (0.5 mg) between two layers of catalyst. a large increase in monoaromatics (BTEX) production (measured as wt. % of biomass) was observed (Table 4.10). HZSM-5 generated signifcantly higher aromatic yields that other catalysts and was selected as the best catalyst for use with spent coffee grounds as feedstock in the catalytic pyrolysis process.

Table 4.10. BTEX yields from catalytic pyrolysis-GC/MS of spent coffee grounds (SETUP 1)

Catalyst type	Pyroprobe Temp.	Catalyst: Biomass ratio	BTEX yield (wt.% biomass)	Relative BTEX yield
HZSM-5	650 °C	5	9.8	1
SO_4^{2-}-ZrO_2	650 °C	5	0.5	0.05
(20%) $SO_4^{2-}ZrO_2$ MCM-41	650 °C	5	0.9	0.09
Red Mud	650 °C	5	0.8	0.08
(2%) Al-MSU-S Foam	650 °C	5	2	0.20
(2%) Al-MSU-S Worm	650 °C	5	2	0.20

4.3.6.3 Analytical-scale external-bed catalyst reactor (Setup 3)

To explore catalysis reactions at higher catalyst temperatures (>350°C), an external catalyst reactor was designed. Similar in concept (separation of catalysis from pyrolysis) to setup 2, the external catalyst reactor enables "ex-bed" catalyst studies at high temperatures (>350°C) and different catalyst residence times. This modified analytical-scale method isolated the catalyst from biomass and allows independent temperature control of the catalyst bed to efficiently perform deactivation studies that are necessary for scale-up.

Preliminary runs with HZSM-5 as a catalyst produced reasonable yields of aromatics. There were losses due to cold spots in the system. To study the effect of residence time, the reactor was operated at different gas flow space velocities by varying the depth of catalyst bed (Table 4.11). As expected, higher bed depth gave a greater yield of aromatics due to increased residence time, i.e. contact time, between pyrolysis vapors and the catalyst bed. From our experiments and other studies, it is proposed that bed depth be atleast five times the reactor internal diameter for sufficient contact time between reactant gas and catalyst. The reactor was also operated at different catalyst temperatures. Although lower reactor temperatures (450 and 500 °C) produced more p-xylene, least amount of coke and maximum aromatics were observed at 550 °C. At 600 °C, the monoaromatics production was lower than at 550 °C and the production of naphthalene and its derivatives increased.

Catalytic pyrolysis experiments using the pyroprobe showed that HZSM-5 gave substantially higher aromatic yields compared to other catalysts when tested at the same pyroprobe conditions. The difference in yields was large and it was clear that HZSM-5 was the the best candidate for aromatics production. Therefore, catalyst selection experiments were not repeated with the external-bed catalyst reactor (setup 3). However, when HZSM-5 is used in a commercial process, it may be operated in a continuous mode and life of catalyst (on-stream time) and deactivation become important.

Therefore, the ex-bed setup was used to simulate a continuous process and test catalyst activity over a number of injections. The catalyst (0.005 g) is packed as a 1-cm high bed in a 3-mm ID quartz tube reactor heated by a coil at 550 °C. Over one hundred injections of pyrolysis vapors (~1 mg of spent coffee grounds for each injection) in a stream of He gas were made over this catalyst bed. Changes in BTEXN (benzene, toluene, ethylbenzene, xylenes, naphthalene) amongst other chemicals, were monitored (Figure 4.10). Deactivation of catalyst was observed after pyrolysis of biomass equivalent to 20 times catalyst weight. These data will be used to improve predictions of the techno-economic analysis since manufacturing cost is very sensitive to catalyst cost as well as catalyst deactivation.

Table 4.11. Py/Exbed-GC/MS method development: Yields are relative to Py/Exbed-GCMS analysis at 450 °C (SETUP 3)

Catalyst and Biomass type	Catalyst Reactor Temp.	Catalyst: Biomass ratio	Relative BTEX yield
HZSM-5 with Spent coffee grounds	450 °C	20	1
	500 °C	20	1.99
	550 °C	20	2.42
	600 °C	20	2.11

Figure 4.10. Change in yields of BTEXN (benzene, toluene, ethylbenzene, xylenes, naphthalene) measured as % weight of biomass for pyrolysis of spent coffee grounds over catalyst ZSM5. Biomass(g) x10 is the cumulative weight of spent coffee grounds

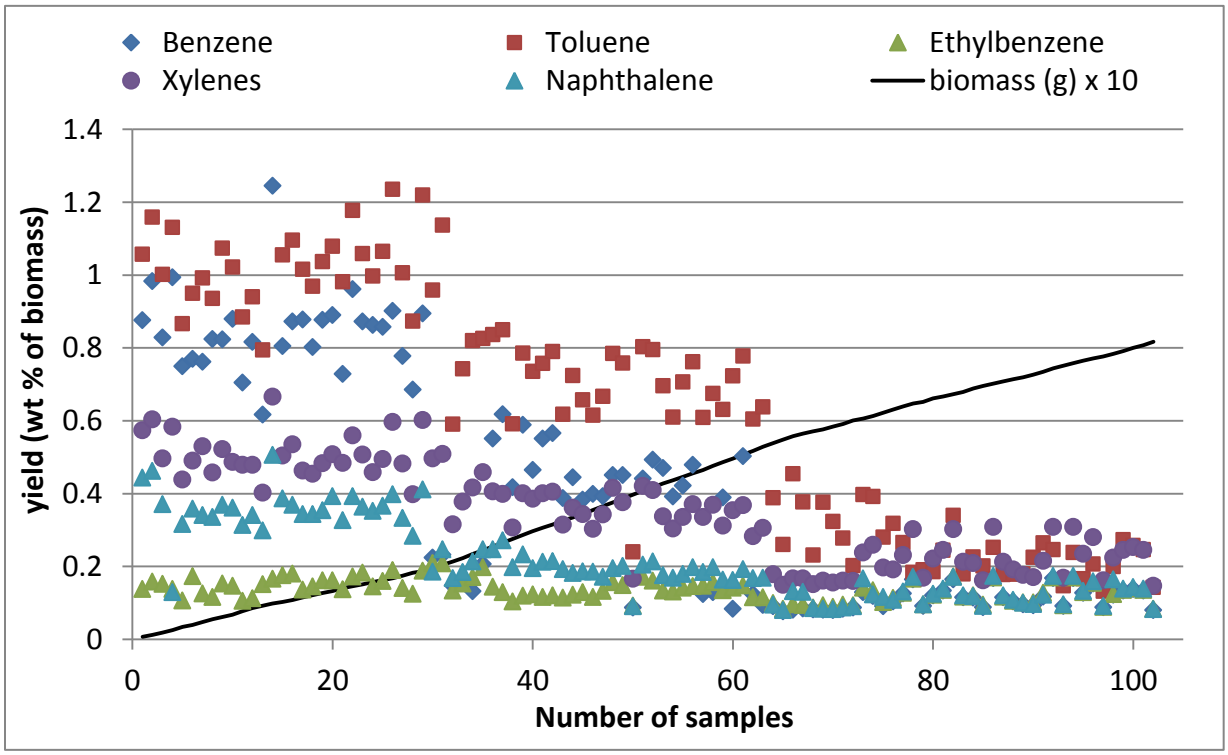

4.4 Conclusions

Different feedstocks were evaluated for their potential to produce aromatics from biomass pyrolysis reaction. Presence of inorganic minerals in ash present in biomass was found to act as a catalyst during pyrolysis leading to acceleration of degradation of biomass into smaller molecules. Catalytic pyrolysis experiments with HZSM-5 showed that spent coffee grounds produced the most aromatics compared to other feedstock. The use of shape-selective acidic catalyst post-pyrolysis deoxygenated the pyrolysis products and produced molecules of interest such as aromatics. Oxygen and lignin content, H:C molar ratio in biomass, and presence of aromatic precursors such as fatty acids and acetic acid were key to high aromatic yields.

CHAPTER 5. A SURVEY OF CATALYSTS FOR PRODUCING GREEN AROMATICS FROM BIOMASS

Authors:
Shantanu Kelkar, Christopher M. Saffron, Kevin Andreassi, Ambareesh Murkute, Zhenglong Li, Dennis J. Miller, Thomas J. Pinnavaia, Robert Kriegel

5.1 Abstract

Biomass fast pyrolysis and catalysis provides a renewable route to aromatic chemicals such as benzene, toluene and xylenes. As the choice of solid catalyst greatly affects the yield of aromatics, a comparison of catalysts and an explanation for their relative performance are needed to guide process development. Catalysts selected for this study exhibited prior success for making aromatics or were simply inexpensive. Ten catalysts were studied using poplar (DN-34) as the feedstock. Five of the ten catalysts consisted of HZSM-5 with different silica:alumina ratios (SAR, 23, 30, 50, 80 and 280). The other five catalysts were sulfated zirconia (SO_4^{2-} ZrO_2), 20% SO_4^{2-} ZrO_2 on MCM-41 support, Al-MSU-S exhibiting foam mesopores, Al-MSU-S exhibiting wormhole mesopores and a waste product from bauxite processing known as red mud. Analytical pyrolysis in tandem with GC/MS was used to identify the products of poplar (DN-34)-catalyst combinations. Product yields and carbon selectivities were evaluated after external calibration of gas chromatography with mass spectrometry detection. Additionally, the BET surface area, BJH pore volume and acidity using NH_3-TPD were measured for each catalyst. All of the catalysts except for HZSM-5 resulted in low aromatic chemical production, even the MSU mesoporous catalysts exhibiting high pore volume and acidity resulted in low aromatic yields. Of the HZSM-5 catalysts, those with the lowest SAR were the highest yielding for aromatics and produced the lowest levels of undesired coke with poplar DN-34 as feedstock.

5.2 Introduction

Monoaromatic compounds, such as benzene, toluene, ethylbenzene and xylenes (BTEX), are used as octane boosters in gasoline and as precursors to polymers such as polyethylene terephthalate. Renewable approaches for making aromatics from biomass will reduce the U.S. dependence on fossil petroleum and assuage the negative impacts of climate change. Fast pyrolysis offers one approach for depolymerizing biomass into the chemical precursors of aromatic compounds. Fast pyrolysis involves heat addition in the absence of oxygen to create a complex gas stream that can be catalyzed to aromatics and a solid co-product known as biochar. Previous research has demonstrated that pyrolysis gas can be converted into aromatics, especially by zeolite catalysts such as HZSM-5 [1,2] . This investigation considers five different varieties of HZSM-5 along with five additional catalysts that exhibit strong acidity, mesoporosity and low cost.

Several researchers have used zeolite catalysts to convert carbohydrate and biomass feeds into aromatics [1–5]. Acidic zeolite catalysts with microporous structure selectively produce aromatics versus non-acidic and non-microporous catalysts. Highly acidic catalysts promote cracking reactions that remove oxygen in the form of non-condensable gases [6]. HZSM-5 is a crystalline aluminosilicate where the ratio of silicon to aluminum in the crystal structure can be modified, affecting the hydrophilicity and the concentration of Bronsted acid sites [7]. The HZSM-5 catalyst is highly acidic, but is limited by low mass transfer rates due to its micropore dimensions of 5.5–5.6 Å, which are smaller than the kinetic diameters of most phenolic molecules produced from pyrolysis of lignin [8,9]. As acidity is important for producing high yield and selectivity, the silica:alumina ratio (SAR) of HZSM-5 was varied at five levels (23, 30, 55, 80, and 280) to study the catalysis of biomass pyrolysis products.

Although the use of heterogeneous catalysts for biomass conversion has been examined, many biomass-catalyst permutations warrant further study. In this regard, five additional catalysts are compared to HHZSM-5 for their potential to produce aromatics, namely mesoporous Al-MSU-S exhibiting cellular foam geometry, Al-MSU-S exhibiting wormhole geometry, highly acidic sulfated zirconia, sulfated zirconia deposited on highly porous MCM-41 support and inexpensive red mud.

Mesoporous catalysts that have large pores reduce diffusion limitations and increase available surface area for catalytic reactions. The greater surface area will also increase the acidic sites available on the external catalyst surface, which may increase conversion and reduce coke yields. Thus, mesoporous and non-zeolitic catalysts may be beneficial for generating valuable chemicals by biomass pyrolysis. Mesoporous catalysts such as Al-MSU-S catalysts and those based on MCM-41 support such as 20% SO_4^{2-} ZrO_2 MCM-41 (mesoporous sulfated zirconia), have a large pore volume and active acid sites spread over a uniform mesopore structure. These catalysts have a pore size of about 2.5 – 3 nm compared with about 0.6 nm for HZSM-5. However, MCM-41 supports are not considered to be hydrothermally stable [10,11]. Al-MSU-S Foam has an ordered hexagonal framework while the Worm exhibits wormhole geometry. Al-MSU-S catalysts have higher acidity as well as hydrothermal stability, which may be necessary for highly corrosive applications such as fast pyrolysis [12]. The larger pores and acidity of these mesoporous catalysts may allow cracking and deoxygenation reactions of large molecules (such as oligomers derived from lignin). Triantafyllides et al. [12] evaluated Al-MSU-S and Al-MCM-41 catalysts for upgrading pyrolysis vapors from Lignocel, a surrogate for biomass. They observed a high level of deoxygenation, an increase in the amount of non-condensable gas and more polyaromatic hydrocarbon (PAH) production. Pattiya et al. [13]

compared HZSM-5 (an acidic microporous catalyst), Al-MCM-41, Al-MSU-F and an alumina-stabilized ceria MI-575 (all mesoporous catalysts) using an analytical micro-scale pyrolysis reactor. All catalysts were found to reduce oxygenated lignin compounds in pyrolysis products with Al-MSU-F (150 Å pore diameter) outperforming HZSM-5 in terms of total xylene yield. Alumina-stabilized ceria was found to favor benzene and toluene formation in this study.

Sulfated zirconia (SO_4^{2-} ZrO_2) is an environmentally benign super acid shown to be active in a number of reactions such as isomerization, cracking, alkylation and acylation [14]. Its potential for pollution control such as selective NOx reduction has been demonstrated although its applications for upgrading pyrolysis oil have not been well explored [15].

To improve economic feasibility of the pyrolysis-catalysis process for biomass to aromatics, inexpensive catalysts are necessary. One such catalyst is red mud, which is produced as a toxic byproduct yet favors hydrogenation reactions [16]. Red mud is a by-product of bauxite refining for aluminum and is composed of oxides of many transition metals. It is an inexpensive catalyst that, in recent studies, showed potential for applications in upgrading of pyrolysis products [17]. Red mud is a hazardous waste due to its high alkalinity but is converted to a non-toxic waste by its use as a catalyst [18].

Though prior research has explored the use of HZSM-5 for converting neat sugars [3,19], cellulose, [20] lignin, [21]and biomass [4,22] as feedstock, the impact of catalyst properties such as surface area, pore volume and acidity has not been assessed in tandem with the use of raw biomass. This investigation begins to suture this knowledge gap by comparing several catalysts, such as sulfated zirconia, red mud and Al-MSU-S including several varieties of HZSM-5, in terms of catalyst properties and aromatic product yields.

5.3 Experimental

5.3.1 Catalysts

ZSM-5 catalysts (also referred to as ZSM5) with the following silica–alumina ratios 23, 30, 55, 80 and 280 were obtained from Zeolyst Co. (Conshohocken, PA) in ammonium cation form. In order to obtain the acidic HZSM5 form, the catalyst was calcined in air at 550 °C for 4 h prior to use. The properties of the catalysts, as measured by Zeolyst, were similar in surface area (400-425 m^2/g), pore size (~0.6 nm) and pore volume (~0.14 m^3/g).

The (2%) Al-MSU-S Foam (henceforth referred to as Foam) and (2%) Al-MSU-S Worm (Worm) were synthesized in the from zeolite beta seeds as precursors and the polymer, cetyltrimethylammonium bromide (CTAB) and tallow tetramine were used as structure-directing agents [125],[126]. Red mud was obtained from Professor Marcel Schlaf at the University of Guelph. The red mud was sourced as slurry from the Rio Tinto Alcan mining facility in Canada and contained about 50% w/w iron oxide. The slurry was water washed and dried at 120 °C [127]. This red mud had a significant concentration of Na_2O (5-10%) which has been known to act as a catalyst poison and significantly reduce activity [127], [128].

The standard sulfated zirconia catalyst (henceforth referred to as SZ) was prepared by hydrolysis of $ZrOCl_2 \cdot 8H_2O$ with aqueous ammonia, treating with 0.5 M H_2SO_4 and calcination at 650 °C. The sulfated zirconia supported in mesoporous material (20% SO_4^{2-} ZrO_2 MCM-41, henceforth referred to as MSZ) was prepared by dispersion of $ZrOCl_2 \cdot 8H_2O$ (20% ZrO_2) on to MCM-41 support using the incipient wetness method followed by drying at 105 °C for 12 h. The mixture was treated with ammonia gas leading to formation of amorphous $Zr(OH)_4$. The sample

was then water washed, treated with 0.5 M of H_2SO_4 solution at room temperature for 10 min and calcined at 650 °C in air for 3 h.

5.3.2 Catalyst characterization

Surface area measurements and pore size distribution analysis were done by nitrogen adsorption at 78 K (-195 °C) in a Micromeritics ASAP 2010 instrument. Prior to measurements, the sample was out-gassed in the degas port of the apparatus at 220 °C for 24 h. NH_3-TPD measurements were performed by volumetric adsorption in a Micromeritics AutoChem 2910 instrument. A thermal conductivity detector and an Ametek Dycor M100M Quadrupole Mass Spectrometer were used for continuous monitoring of the desorbed NH_3. Prior to NH_3 adsorption, approximately 0.5 g of catalyst was thermally pretreated in He (99.999%) at a flow rate of 50 cm^3min^{-1} at 410 °C for 1h followed by cooling to room temperature in He. After pretreatment, each catalyst was saturated at room temperature with NH_3 (99.998%) at a flow rate of 50 cm^3min^{-1} for 1h and then subsequently purged with He (50 cm^3min^{-1}) for 2 h to remove all physisorbed NH_3. Desorption of chemisorbed NH_3 was carried out in He flow with the catalyst being heated from ambient temperature to 700 °C at a rate of 10 °C min and held for 30 min. The resulting NH_3 peak was quantified by calibrating the area using a NH_3 gas standard.

5.3.3 Pyrolysis-GC/MS

Experiments were conducted using a microscale pyrolysis unit, CDS Pyroprobe 5250 (CDS Analytical Inc, Oxford, PA) interfaced to a Shimadzu QP-5050A gas chromatograph/mass spectrometer (Shimadzu Corp, Columbia, MD). A lignocellulosic feedstock, poplar (DN-34, *Populus x euramericana*, cv. 'Eugenei'), was used as biomass for all experiments. The poplar

was dried at 60 °C to a moisture content of ~8%, ground to a particle size of less than 0.5 mm and stored at room temperature [72]. For biomass pyrolysis experiments, approximately 0.5 mg of ground biomass sample was packed between quartz wool in a quartz tube with a filler rod. For catalytic pyrolysis experiments, approximately 0.5 mg of biomass was packed between quartz wool. Catalyst, with a 5:1 weight ratio of catalyst to biomass, was added on both sides followed by more quartz wool to hold the sample in place. Six or more replicates of each sample were run. Pyrolysis proceeded by setting the pyroprobe at 650 °C (pyrolysis temperature of 500-550 °C) with a hold time of 20 s at the maximum heating rate. The GC used a Restek rtx-1701 column (Restek, Bellefonte, PA), 60 m x 0.25 mm with a 0.25 μm film thickness. The column gas flow was 1 cm/s with a split ratio of 1:100 so as to not overwhelm the mass spectrometer. The GC oven temperature program began with a 1 minute hold at 40 °C followed by heating at 8 °C/min to 270 °C. The injector and detector temperature were set at 280 °C. Identification of compounds was performed by comparing the mass spectra of the peaks with standard spectra of other compounds using the NIST library to obtain the most probable matches. Pure compounds (Sigma-Aldrich Co., St Louis, MO) were then used to confirm the peak identities based on matching of retention times and mass spectra. Quantification was performed using external standards in acetonitrile and a four-point calibration curve was constructed relating concentration to peak area response. The mass spectra were recorded in electron ionization mode for *m/z* 28 to 300. In separate experiments to quantify non-condensable gases and volatile aromatics, an Agilent CP Porabond-Q column (25 m x 0.25 mm x 3 μm, Agilent Technologies, Santa Clara, CA) was used under identical experimental conditions. Char and coke were measured by burning off the solid pyrolysis product at 800 °C in a thermogravimetric analyzer with air (20 ml/min) as the carrier gas.

5.4 Results and Discussion

5.4.1 Catalyst properties

Table 5.1. Comparison of catalyst properties

Catalyst	Abbrev.	BET Surface Area (m^2/g)	Ext area surface (m^2/g)	Pore size (nm)	Pore Volume (cm^3/g)	Micropore Vol (cm^3/g)	Acid sites (*m*mol NH_3/g)
HZSM-5	ZSM5	404	135	0.6	0.25	0.121	0.40
SO_4^{2-} ZrO_2	SZ	63	61	3.6	0.08	0.001	0.37
(20%) SO_4^{2-} ZrO_2 MCM-41	MSZ	217	108	2.7	0.15	0.050	0.25
(2%) Al-MSU-S Foam	Foam	995	NA	3.0	0.96	NA	0.21
(2%) Al-MSU-S Worm	Worm	912	NA	3.5	1.49	NA	0.24
Red mud	RM	30	29	3.8	0.08	0.001	0.10

A comparison of nitrogen adsorption-desorption isotherms for catalysts is shown in Figure 5.1. Both MSU-S had a very high surface area, 995 m^2/g for Foam and 912 m^2/g for Worm **(**Table 5.1). Comparatively, sulfated zirconia (SZ) had a low BET surface area of only 63 m^2/g. Mesoporous sulfated zirconia (MSZ), 20% SO_4^{2-} ZrO_2 MCM-41, prepared using the highly porous silica support showed a low surface area of only 217 m^2/g, compared with over 1,000 m^2/g that was reported by Sigma-Aldrich for the batch of unmodified MCM-41 used in this study [68]. The pore volume for MSZ was only 0.15 cm^3/g. Deposition of zirconium oxide on MCM-41 may have blocked the pore openings reducing their volume. Red mud measured an even lower surface area of 24 m^2/g but this was in the range reported in literature [129], [130]. Comparatively, commercially prepared HZSM-5 has a much larger surface area of 404 m^2/g with a majority of the porosity being contributed by the micropores.

Figure 5.1. Isotherms for ZSM-5, sulfated zirconia (SZ), mesoporous sulfated zirconia (MSZ) and Red mud catalysts; isotherms for mesoporous MSU-S catalysts, 2% Al-MSU-S Worm and 2% Al-MSU-S Foam.

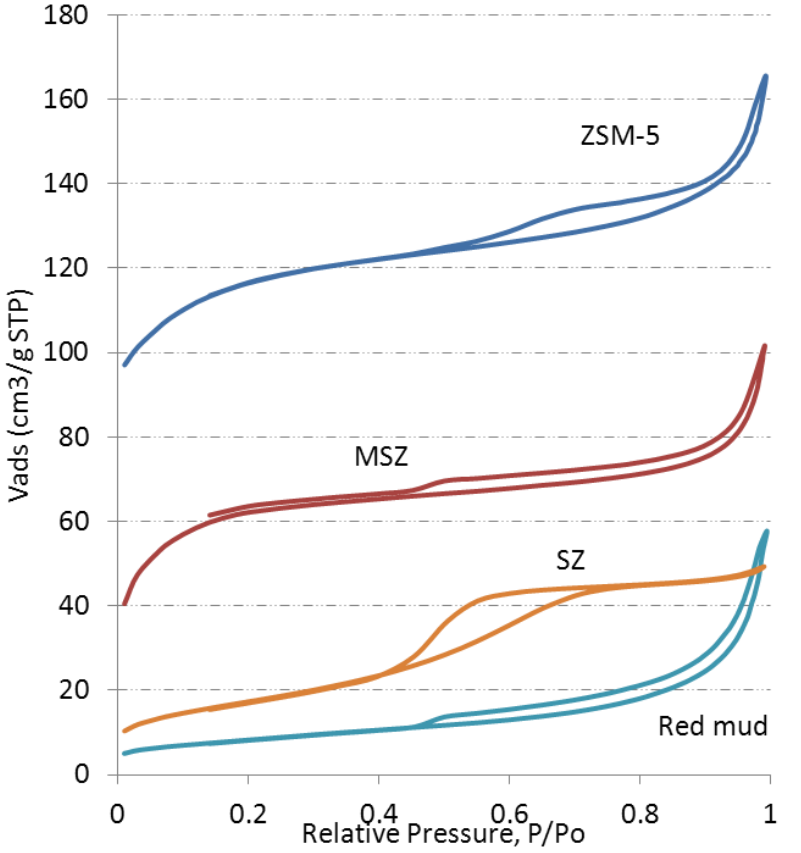

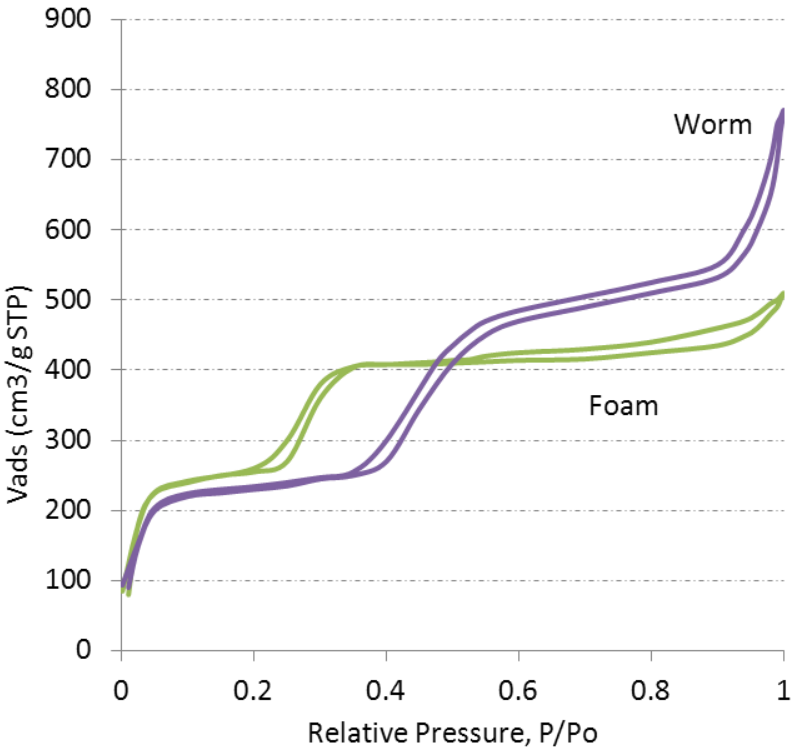

The MSU-S catalysts demonstrated isotherms of type II with the classical hysteresis loop of type H3 or H4, which is a characteristic of slit-shaped pores. The Worm catalyst showed a hysteresis loop but also some capillary condensation at high P/Po > 0.9 (Figure 5.1). This shows that large meso and macropores may exist due to the textural porosity provided by the worm-hole geometry [126]. This phenomena was also observed in red mud which showed a sharp rise in adsorption at P/Po > 0.8, which may be due to presence of meso or marcopores [128].

HZSM-5 had a median pore size of < 1 nm while the mesoporous catalysts had an average pore size between 2.4–3.5 nm. The large pore size of mesoporous catalysts is expected to reduce the diffusion resistance associated with transport of large pyrolysis products such as anhydrosugars, phenolics, and lignin oligomers. Reactivity is expected to increase as more reactive sites become available on the surface and in the mesopores [131]. The textural porosity and the 3D-wormhole-like geometry of the Worm catalyst is expected to facilitate easier transport of cracked molecules when compared with MCM-41 which has 1D channels as mesopores [126]. The mesoporous MSU-S catalysts had significantly higher pore volume ranging 0.96-1.49 cm^3/g compared with that for the microporous HZSM-5 (0.24 cm^3/g).

The microporous catalysts exhibited a higher concentration of acid sites when compared with the three mesoporous catalysts. The NH_3-TPD measurements (Table 5.1) showed the presence of both weak and strong adsorption sites of HZSM-5. Although SZ is considered a superacid, it showed a lower concentration of total acidic sites when compared with HZSM-5 as measurements were made below 700 °C. SZ has strongly bound acid sites that have been detected only at desorption temperatures of over 900 °C [132]. The mesoporous catalyst showed weaker acidity compared to HZSM-5 and SZ due to lower crystallanity and a lower concentration of active sites because of mesopores [126]. Red mud measured a reasonably high

acidity of 0.10 *m*mol/g (though still lower than other catalysts), which has been attributed to the presence of Si-O-Al or Si-O-S units in its structure [130].

5.4.2 Pyrolysis-GC/MS

The products of fast pyrolysis of poplar with and without catalyst were analyzed using a GC/MS (Figure 5.2). Pyrolysis yields a mixture of water, light gases such as carbon oxides, aldehydes, ketones, phenolics and anhydrosugars. Pyrolysis involves thermal decomposition of biomass into smaller oxygenated molecules. The small molecules diffuse into the catalyst pores and react at the active sites through a series of cyclo-oligomerization, decarbonylation and dehydration reactions to produce aromatics, CO, CO_2 and water [95], [133].

A representative pyrogram for catalytic pyrolysis of poplar with catalysts as analyzed by a CP-Porabond Q column is shown in Figure 5.3. Large peaks for oxygenates are observed in pyrolysis with all catalysts except HZSM-5, which produces mostly aromatics. Catalysis of these pyrolysis products with HZSM-5 produced a significant amount of aromatic molecules such as naphthalenes, xylenes and toluene. Phenolics and anhydrosugars are larger than the pore size of HZSM-5 and may be deposited in the form of coke on the catalyst surface or condensed on quartz wool and cooler surfaces encountered during flow in the analytical pyrolysis-GC/MS unit. SZ did not produce significant quantities of aromatics. Instead, many oxygenated molecules such as acetic acid and its derivatives, acetol, acetaldehyde and 2,5-dimethylfuran were observed.

Figure 5.2. A: Comparison of GC/MS chromatograms from pyrolysis of poplar (A) and catalytic pyrolysis with ZSM-5 (B) as analyzed by Restek Rtx-1701 column

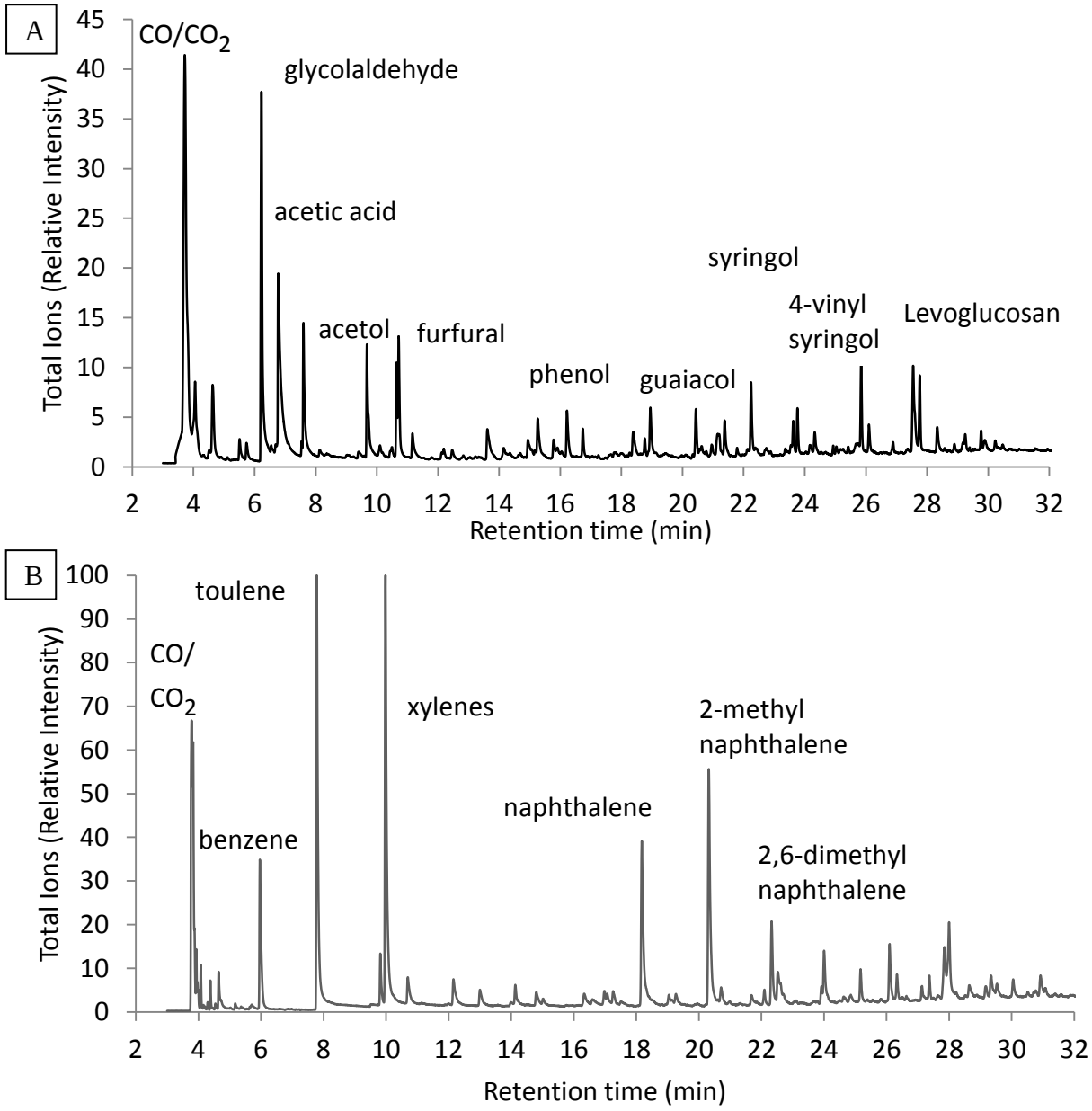

Figure 5.3. Representative pyrogram for catalytic pyrolysis of poplar with catalysts as analyzed by an Agilent CP-Porabond Q column. Large peaks for oxygenates are observed in pyrolysis with all catalysts except ZSM-5, which shows substantial peaks for aromatics.

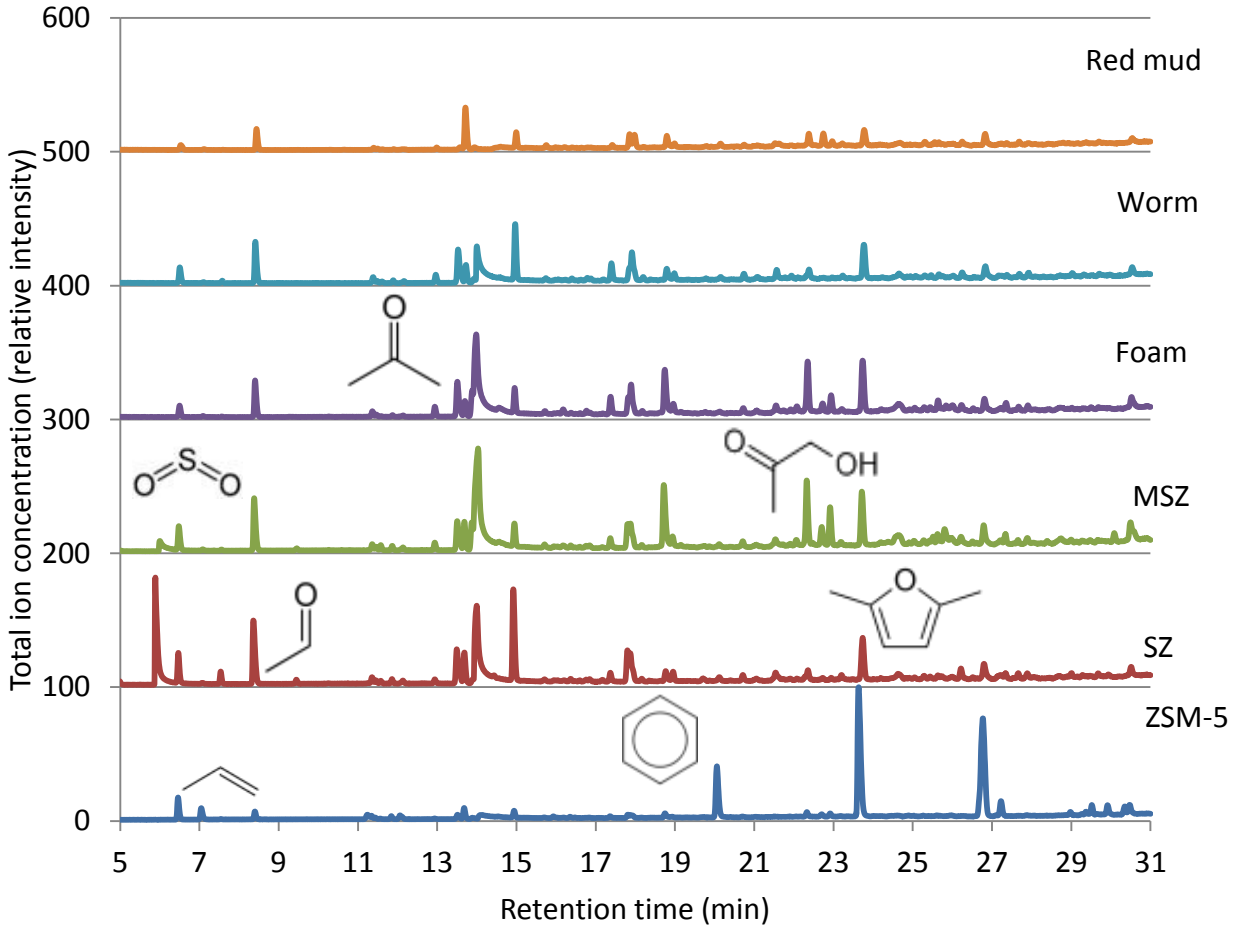

Note: chromatograms are offset by 100 data points on the Y-axis for clarity.

A quantitative comparison of catalytic pyrolysis products is shown in Figure 5.4. All catalysts reduced the condensable product yield due to thermal cracking of molecules, producing more non-condensable gas and coke. Deoxygenation and decarbonylation of the condensable fraction produced more CO, CO_2, other light gases and coke. Carbon selectivity is defined as the moles of carbon in the product divided by the total moles of carbon. The carbon selectivity of products found in catalytic pyrolysis vapors is shown in Figure 5.5.

In non-catalytic pyrolysis of poplar biomass, greater than 22% of the biomass carbon was found in oxygenated molecules and <2% in aromatics, mostly phenolics (Figure 5.5). On the other hand, in the catalytic pyrolysis with HZSM-5, up to 13% of the carbon ends up in aromatic molecules of which the C6–C8 monoaromatics were a large fraction. Cracking and deoxygenation reactions led to an increase in the carbon yield of non-condensable gases (i.e. CO, CO_2).

Figure 5.4. Mass balance for poplar catalytic fast pyrolysis in Py-GC/MS

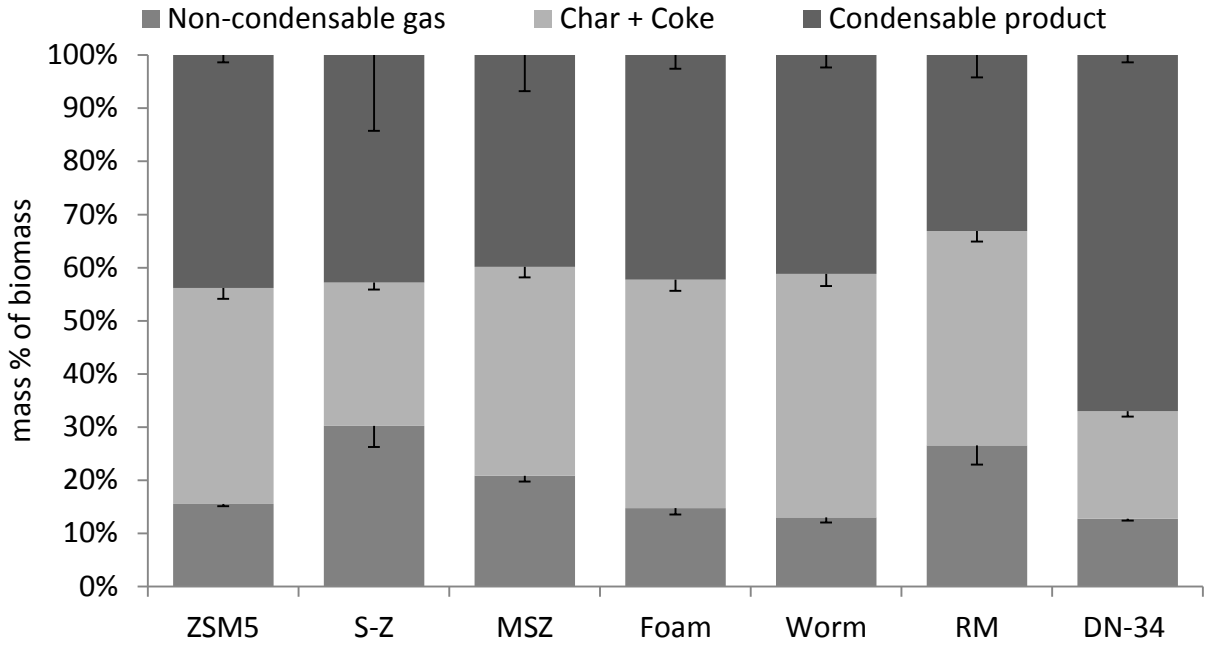

5.4.3 Non-condensable gases

Catalysis increased the production of non-condensable gases such as CO, CO_2 over that from biomass pyrolysis alone. Taarning et al.[95] noted that during catalytic pyrolysis, aldehydes, formates and carbohydrates lose oxygen in the form of CO and H_2O; and carboxylic acids lose oxygen as CO_2 and H_2O. Jae et al. [104] observed that small pore zeolites give the

maximum gas yields. In this study, the catalysts with the smallest pore volumes and surface areas, red mud and SZ, produced the greatest quantity of gases. All catalysts produced greater amounts of CO and CO_2 than HZSM-5, however ZSM5 produced a significant quantity (2–4 % mass) of alkanes and alkenes like propylene, unlike other catalysts. SZ and MSZ produced the most CO (7%), which is attributed to decarbonylation reactions. Higher CO production may be an indicator of higher O_2 removal and selectivity for aromatics [133]. Neither significant deoxygenation nor aromatic molecule production was observed with SZ and MSZ. In addition, the CO and CO_2 generation in SZ was accompanied by SO_2 evolution. The presence of SO_2 has been linked to the reaction of carbon atoms with oxygen atoms from the surface sulfate groups to form carbon oxides [134]. A large quantity of oxygenates and SO_2 in the products of SZ pyrolysis indicate that carbon from coke may have reacted with the catalyst surface, reducing coke yields and increasing gas.

Figure 5.5. Carbon selectivity for poplar catalytic fast pyrolysis in Py-GC/MS

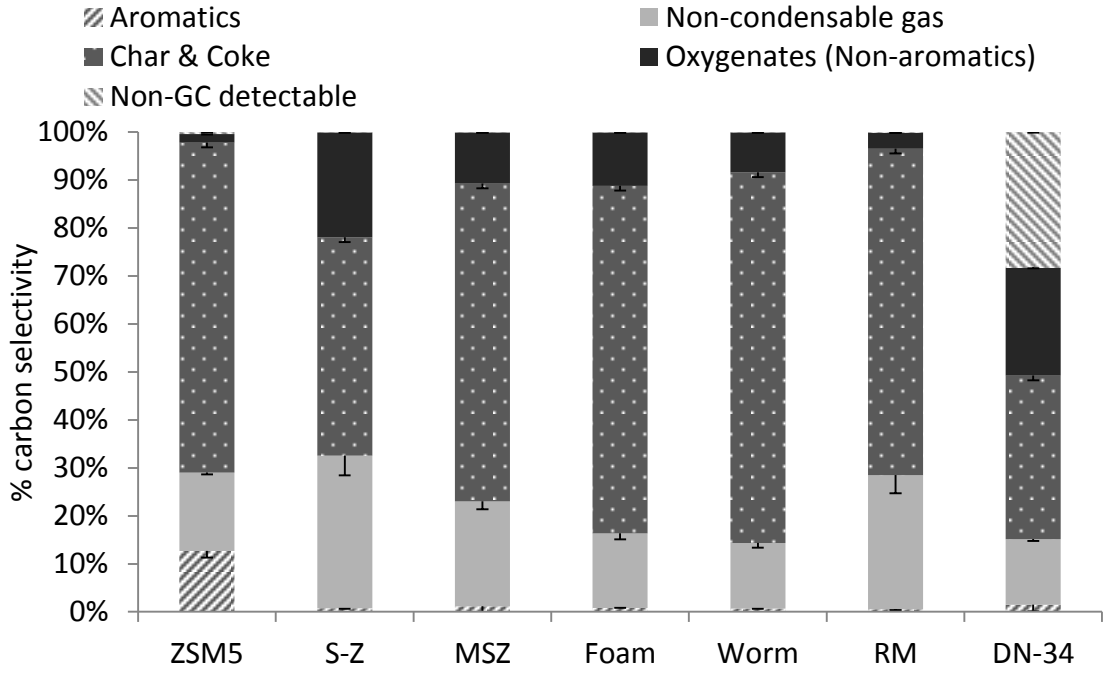

Red mud produced the most CO_2 (~10%), a likely result of cracking activity due to acidity and Red mud has cracking activity due to silica and alumina which may increase its acidity, while it also has a dehydrogenation activity due to ferric oxide[127], [128]. CO_2 yields have also been related to Al content in the catalyst which enhances the decarboxylation reactions by Bronsted acid catalysis [133]. SAR in red mud was 0.4 to 1.3, which is very low compared to HZSM-5 (SAR=23) [127]. Thus, red mud had much greater Al content compared with ZSM5 and may have produced more CO_2 from decarboxylation of acids in pyrolysis product.

5.4.4 Oxygenates

The amount of oxygenated molecules (condensable fraction which includes aldehydes, ketones, acids etc., but not including phenolics) produced upon poplar pyrolysis accounted for 23±1.4 % of the original carbon in biomass. For ZSM5 catalysis, oxygenates accounted for < 2 % of original biomass and ~ 3.5% for red mud. The mesoporous MSU-S and MSZ catalysts were less effective in deoxygenation; 8-11% oxygenated molecules by weight of the biomass was still observed in the catalytic pyrolysis products. The SZ catalyst was the least effective in deoxygenating pyrolysis products despite their high acidity, with over 17% of the carbon still present in the form of volatile oxygenates. Sulfated zirconia has been known to have a low tolerance for coking and much of its catalyst activity may have been lost at a much lower coking level than other catalysts [135].

5.4.5 Aromatics

“Aromatics” includes the aromatic hydrocarbons and phenolic molecules. Non–catalytic biomass (poplar DN-34) pyrolysis products contain a negligible amount of hydrocarbons but a significant amount of phenolics from lignin pyrolysis. The following major lignin derivatives

were observed: phenol, 2,6-dimethoxyphenol, 4-methylsyringol, 4-vinylsyringol, and 4-allylsyringol. ZSM5 catalysis generated significant quantities of aromatics, from decarboxylation and decarbonylation of oxygenates. Of the lignin derivatives, only syringol and 4-allylsyringol were observed in the products of ZSM5 and red mud catalysis. Aromatics such as trimethoxybenezene derivatives and methoxybenzaldehydes were also observed in ZSM5 catalysis.

None of the other catalysts produced significant aromatic molecules, although at lower split ratios for the GC/MS, traces of previously unseen hydrocarbons were observed. To summarize, catalysts other than ZSM5 were effective in deoxygenation but were not selective to aromatics production. High-angle X-ray diffraction of MSU-S catalysts has shown the absence of Braggs peaks and crystallite phases, both of which are present in ZSM5 and may be responsible for its shape selectivity and high aromatics production [125], [126]. Jae et al. [104] studied the kinetic diameters of benzene and p-xylene and observed that they were closest to the pore dimensions of ZSM5. They noted the importance of pore window size, internal pore space and steric hindrance in determining aromatic production. Therefore, if aromatics are desired, HZSM-5 or another-type catalyst with tunable porosity should be used.

5.4.6 Char and coke

Catalytic pyrolysis experiments in this study were conducted by packing biomass between layers of catalyst to simulate reaction of pyrolysis products with an external catalyst bed. Quartz wool was used to separate the layers and at the ends of the sample. As a result, coke was generated on catalyst surfaces and quartz wool in addition to the char produced due to biomass pyrolysis. ZSM5 and red mud also produced significant quantities of coke, although less than the MSU-S catalysts. The MSU-S catalysts produced the most coke (40-47%).

Even without the use of quartz wool with samples, the amount of char produced in the analytical filament pyrolysis reactor has been shown to be greater than that produced in bench-scale experiments[136]. In microporous catalysts such as ZSM5, under severe conditions (e.g. high temperature) favoring the desired reaction, there are often diffusion limitations due to coke molecules on the surface or in the pores, blocking access of the reactant to active sites [137]. Since phenolics are larger than the pore size of ZSM5 and SZ, they remain unconverted or produced coke precursor molecules [95], [113], [138]. Gayubo et al. [117] suggested removal of aldehydes and phenolics from the pyrolysis oil before zeolite catalysis to reduce coking. In this study, the quantity of phenolic compounds in catalytic pyrolysis was very low compared to non-catalytic biomass pyrolysis. A reason could be their conversion to coke or reactive molecules forming oligomers. The presence of coke precusors and acid sites on the catalyst surface may also have contributed to their condensation and conversion to coke molecules. Heavier compounds (part of the condensable product stream) may have deposited on cold spots on their way through the pyroprobe and transfer line to the inlet of GC column; they may have also formed coke on hot quartz wool.

Once the coke precursors are generated, they need to be retained on the catalyst. Steric hindrance, strong chemisorption and low volatility of molecules help retention of coke molecules[139]. Steric hindrance occurs due to the pore size (aperture size) and the cage size (intersection of pores, also known as channel intersections). Thus, coke production on MSU-S catalysts may be caused by their large pore size (3.0 – 3.5 nm) and cage size as the cages are sites for coke accumulation, effectively blocking access to strong active sites inside the pores[138], [139].

Highly acidic catalysts are good cracking catalysts and prone to heavy coke generation [139], [140]. Therefore it was surprising that the 'superacid' sulfated zirconia catalyst produced the least char and coke (27±10%). SZ also has a low resistance to coke and produced the highest amount of carbon oxides. It is speculated that carbon atoms from coke deposited on SZ surfaces may have reacted with oxygen atoms from the surface sulfate groups to form carbon oxides[134]. This not only decreased the measured coke amount but also increased the carbon and sulfur oxides in the gas product. Deactivation of SZ also led to lower deoxygenation and the greatest amount of oxygenated compounds in the catalysis product.

Although the above set of catalysts had many desirable properties such as mesoporosity, high pore volume and high acidity, they showed low selectivity for BTEX molecules. The large mesopores allowed production of undesirable polyaromatic hydrocarbons (PAH) leading to coke formation [138], [139]. The combination of high acidity with large pore volume induced severe cracking of pyrolysis products leading to greater production of non-condensable gases [141]. The BTEX yields were significantly low for all catalysts except ZSM5

5.4.7 Precursors to aromatic molecules and coke

Gayubo et al. [113] found that alcohols undergo dehydration at low temperatures (<250 °C) to form olefins, which were converted into alkanes and aromatics at higher temperatures. Acetaldehyde formed significant amount of coke; acetone was converted to isobutene and to heavier olefins, aromatics and alkanes at higher temperatures; while acetic acid ketonized to acetone and CO_2 [114]. Taarning et al.[95] also noted that alcohols and phenols lose oxygen in the form of H_2O, aldehydes, formates and carbohydrates in the form of CO and water and carboxylic acids lose oxygen as CO_2 and water. They concluded that acetic acid was important

for hydrocarbon generation as it improves the H/C ratio of pyrolysis products by removing oxygen in the form of CO_2, leading to less coke deposition. Willams and Horne observed that acetic acid and other low molecular weight bio-oil compounds over HZSM-5 catalyst give large amounts of aromatic hydrocarbons[107]. They suggested that primary pyrolysis products are directly catalyzed to aromatics, H_2O or CO_2, through deoxygenation and aromatization, bypassing the alkene route. Aromatics may also be produced via dehydrogenation of parrafins to olefins and the conversion of these olefins to aromatics occurs via oligomerization and cyclization [115],[108]. Methyl benzenes and poly-methyl benzenes are thought to be active species in the hydrocarbon pool and have been observed in products of methanol catalysis over HZSM-5 [142], [143]. Therefore it is possible that the methoxybenzenes detected in the current study may have been produced from catalytic cracking of lignin derivatives on surface active sites.

Phenolic compounds have been known to produce low yields of aromatics and higher coke than non-phenolic molecules [95], [115]. Phenol was found to be less reactive and only partially converted to propene and butenes at temperatures of 400 °C, while 2-methoxyphenol formed coke but did not decompose significantly over ZSM5 at 450 °C [113]. Mullen and Boateng suggested that simple phenolics like phenol do not lead to aromatics and may lead to coke production instead [116]. They also suggested that highly acidic sites (present inside ZSM5 pores, and therefore not accessible to phenolics) were necessary to crack lignin derivatives into olefins and allenes needed for aromatics production. Gayubo et al. [113] also showed that phenol and 2-methoxyphenol had low reactivity on ZSM5 and produced coke.

5.4.8 Optimizing aromatic yield by tuning Al content of HZSM-5

ZSM5 is a crystalline aluminosilicate zeolite with a high silica and lower aluminum content. The increase in aluminum content of ZSM5 increases its Bronsted acid sites. With change in the concentration and acidity of active sites, an effect on yields of aromatics is inevitable. Foster et al. [140] compared the X-ray diffraction and scanning electron microscopy images of four Zeolyst ZSM5 samples with SAR 23, 30, 50 and 80. They observed a highly crystalline framework typical of MFI type catalysts. No morphological differences between different SAR samples were observed. However the crystal particle size decreased with decreasing aluminum content and this led to a slight increase in inter-crystal porosity and mesoporosity.

For comparison of ZSM5 catalysts with different silica–alumina content, catalytic pyrolysis experiments were conducted with ground poplar wood under identical conditions described in the experimental section. For catalytic pyrolysis of glucose, Foster et al. [140] observed the highest aromatic and low coke yields for SAR30. In the present study with poplar, SAR23 and 30 did not produce significantly different ($p<0.05$) aromatic yields, but the aromatic selectivity varied (Figure 5.6 and 5.7). Another difference in the two studies concerns with sample preparation. Foster et al. [140] did their experiments by preparing mixtures of glucose and catalyst; in our study, lignocellulosic biomass was packed between layers of catalyst to simulate pyrolysis followed by catalysis.

Aromatic selectivity is defined as the moles of carbon in the product divided by the total moles of carbon in all aromatic molecules. SAR23 produced greater amount of smaller aromatics such as C6 (benzene) and C7 (toluene and methylphenols) while SAR30 produced larger quantities of C8 and C9 aromatics. Surprisingly, SAR23 also produced the most C10+

polyaromatics, which may be a result of its higher acidity and greater cracking activity, producing more coke and PAH precursor molecules. The C8 and C9 selectivity increased with SAR suggesting that lower acidity tends to produce greater amount of xylenes and tri-methylbenzene molecules, which was also observed in other studies [140]. SAR23 almost completely eliminated oxygenated molecules from the product and the yield of oxygenated molecules in products of catalytic biomass pyrolysis increased with SAR. SAR280 was particularly selective towards production of C9+ monoaromatics and not selective for C10+ polyaromatics. As a result of its large yield of C9 aromatics, SAR280 showed greater carbon selectivity for total aromatics over SAR55 and 80.

Figure 5.6. Carbon balance of catalytic biomass pyrolysis with ZSM-5 at different SAR

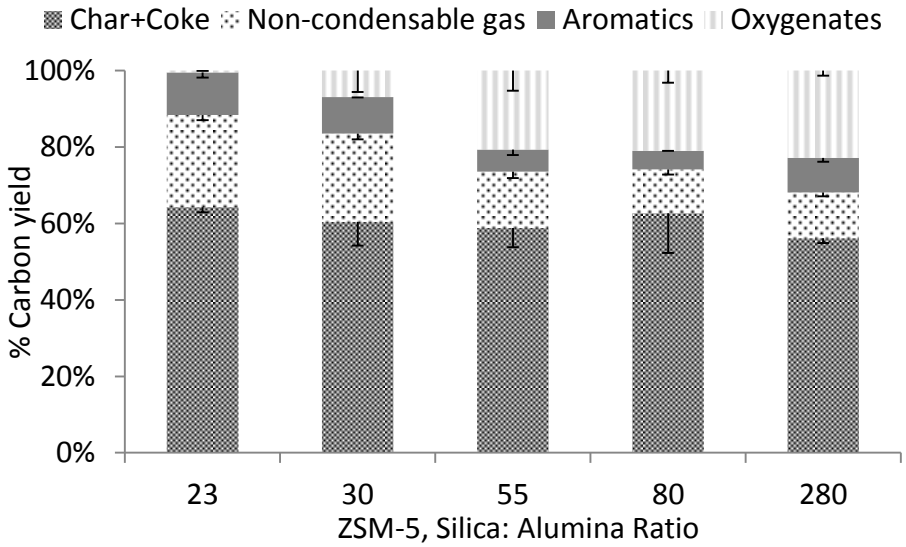

Figure 5.7. Aromatic selectivity of ZSM-5 at different SAR

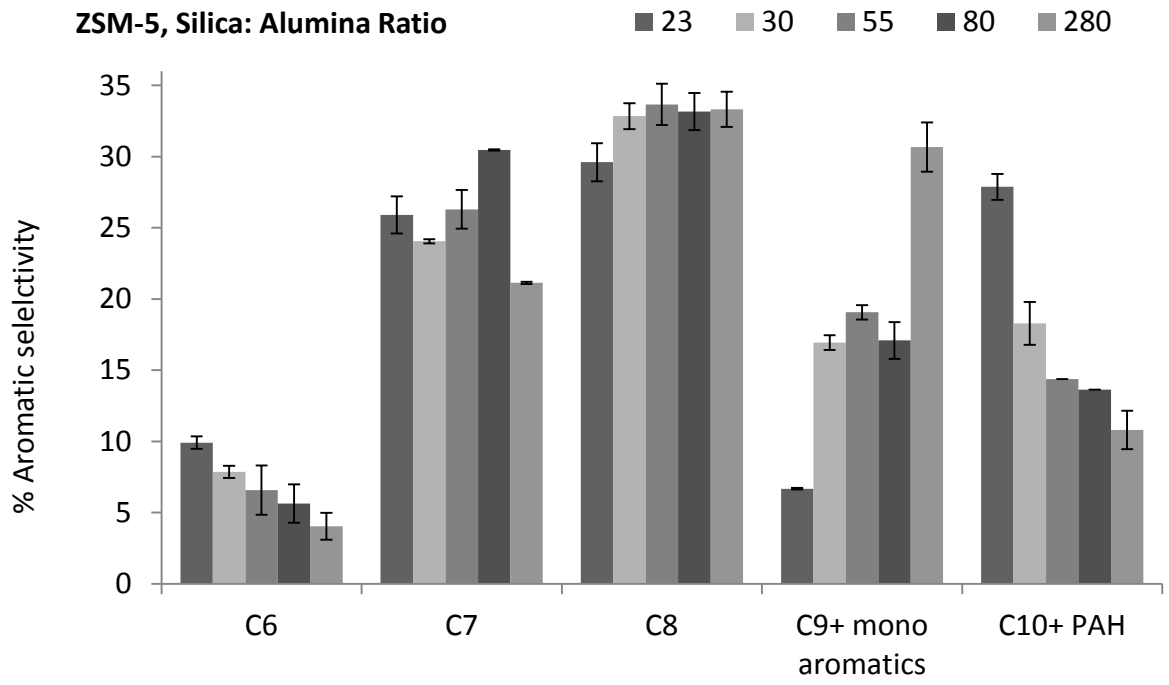

Figure 5.8. Gas composition of products of ZSM-5 catalytic pyrolysis

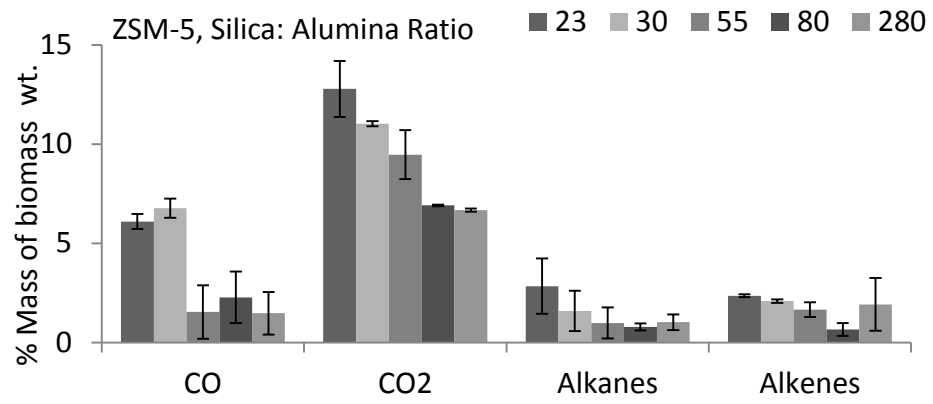

The non-condensable gases, CO and CO_2 are considered to be the products of decarbonylation and decarboxylation reactions, respectively [95], [140]. The non-condensable gas yield decreased with increasing SAR, although it was not significantly different between SAR23 and 30 (Figure 5.8). SAR30 produced the highest CO but was not significantly different

from SAR23, which produced the most carbon dioxide. Foster et al. [140] have proposed that the carbon dioxide production may be related to the aluminum content in the catalyst as its production correlated significantly with the SAR ratios. In the current study, carbon dioxide production decreased with increasing SAR. SAR23 and 30 both generated significant amounts of low molecular weight alkanes and alkenes that were present in the non-condensable gas.

The char and coke carbon yields were not significantly different between the five zeolites but showed a decreasing trend with increase in SAR. This was to be expected since at low SAR, the concentration and the acid strength of active sites increases, leading to greater cracking and secondary reactions that lead to coke precursors [138].

The results show that higher acidity, lower SAR HZSM-5 such as SAR23 and 30 need to be employed for catalytic conversion of biomass pyrolysis products to aromatics. There was no clear trend with regard to aromatic selectivity; however SAR23 and 30 produced greater of all aromatic types compared with the low acid varieties.

5.4.9 Pathways to production of aromatic molecules during catalytic upgrading of biomass pyrolysis

Catalytic upgrading of biomass pyrolysis has been well studied. Catalysts break down large molecules found in pyrolysis products to smaller hydrocarbon fragments forming a 'hydrocarbon pool' as shown in Figure 5.9 [102]. These intermediate oxygenates then diffuse into the catalyst pores and are condensed into aromatic molecules and olefins from the hydrocarbon pool due to the oligomerization and cyclization functionalities of the catalyst [91].

The hydrocarbon pool may consist of polymethylbenzene, benzenium cations, carbenium ions or naphthenes in pseudo-equilibrium [105], [106]. Monocyclic aromatics and their reaction with other oxygenates leads to the production of naphthalenes and other polycyclic aromatics. Wang et al. [103], [104] have suggested that the reactive hydrocarbon pool for the methanol to

olefins process is between 5.7 and 6.0 Å, i.e. similar to the kinetic diameters of benzene, indene, 2-furanmethanol and 4-methylfurfural. The intermediate oxygenates may exist in the hydrocarbon pool in the form of polymethylbenzene, benzenium cations, carbenium ions or naphtenes in pseudo-equilibrium[105], [106]. Olefins are precusors to producing aromatic molecules and many studies have shown that increasing the olefin content in catalyst feed increases the aromatics in catalysis products [91], [107], [108], [109]. However acidic catalysts are more selective towards cracking rather than dehydrogenating to produce olefins. Lewis acids sites may have a synergistic effect with Bronsted acid sites by converting a greater amount of alkanes to olefins for conversion to coke and aromatics. In the absence of these sites, free hydrogen ions may be attacking carbenium and benzenium ions and producing light olefins though β–scission, and eventually coke [105], [110]. Aromatics and coke production from polymerization of furans have been suggested to be the major competing reactions[91]. Tagliabue has proposed that the thermodynamics of catalytic reactions of hydrocarbon pool to aromatics is such that olefins production is preferred over aromatics and there is a greater tendency towards coke formation [108]. It is also speculated that coke is produced from acid catalyzed polymerization of furans to oligomers [111], [112].

5.5 Conclusions

Our experiments and previous studies show that microporous HZSM-5 catalysts have the desired shape selectivity and acidity to produce high aromatic yields from biomass pyrolysis, a renewable and environment friendly resource. In particular, zeolite catalysts have been shown to be effective at modest temperature, low pressure, and in the absence of molecular hydrogen as a co-feed. The silica-alumina ratio in HZSM-5 affects the aromatic product distribution and yield and SAR 23 and 30 were found to produce the highest aromatic yields from actual

lignocellulosic biomass. The product yields from catalytic pyrolysis of biomass are lower than those obtained when neat compounds such as glucose or cellulose were used as feedstock. Therefore, significant potential exists for improving product yield from MFI catalysts such as HZSM-5 by altering the pore structure and adding catalyst promoters and modifiers.

Although mesoporous catalysts remove diffusion resistance, low crystallinity and lack of shape selectivity leads to low aromatic yield. Large pores act as sites for coke generation and accumulation. Aromatics production and coke are both functions of catalyst acidity, shape selectivity and pore size. Mesoporous catalysts, such as the Al-MSU-S Foam and Worm catalysts used in this study, have large mesopores with bottlenecks and cages that may promote coke formation and reduce yields, negating the benefits offered by low diffusion resistance. A novel variant of sulfated zirconia on a mesoporous MCM-41 support was prepared, which increased its surface area. Although sulfated zirconia catalysts are superacids, they were not shape selective to aromatic molecules. They produced large quantities of coke and gases and may be unsuitable for upgrading biomass pyrolysis products. Red mud, an industrial waste, was rendered non-hazardous [144] by its use as a catalyst in biomass pyrolysis. Although the red mud used in this study was not highly selective to aromatic molecules, it demonstrated significant deoxygenating activity and may be useful for biofuel applications due is inexpensive availability.

Figure 5.9. Proposed pathways for cellulose to aromatics [91], [105], [108], [109]

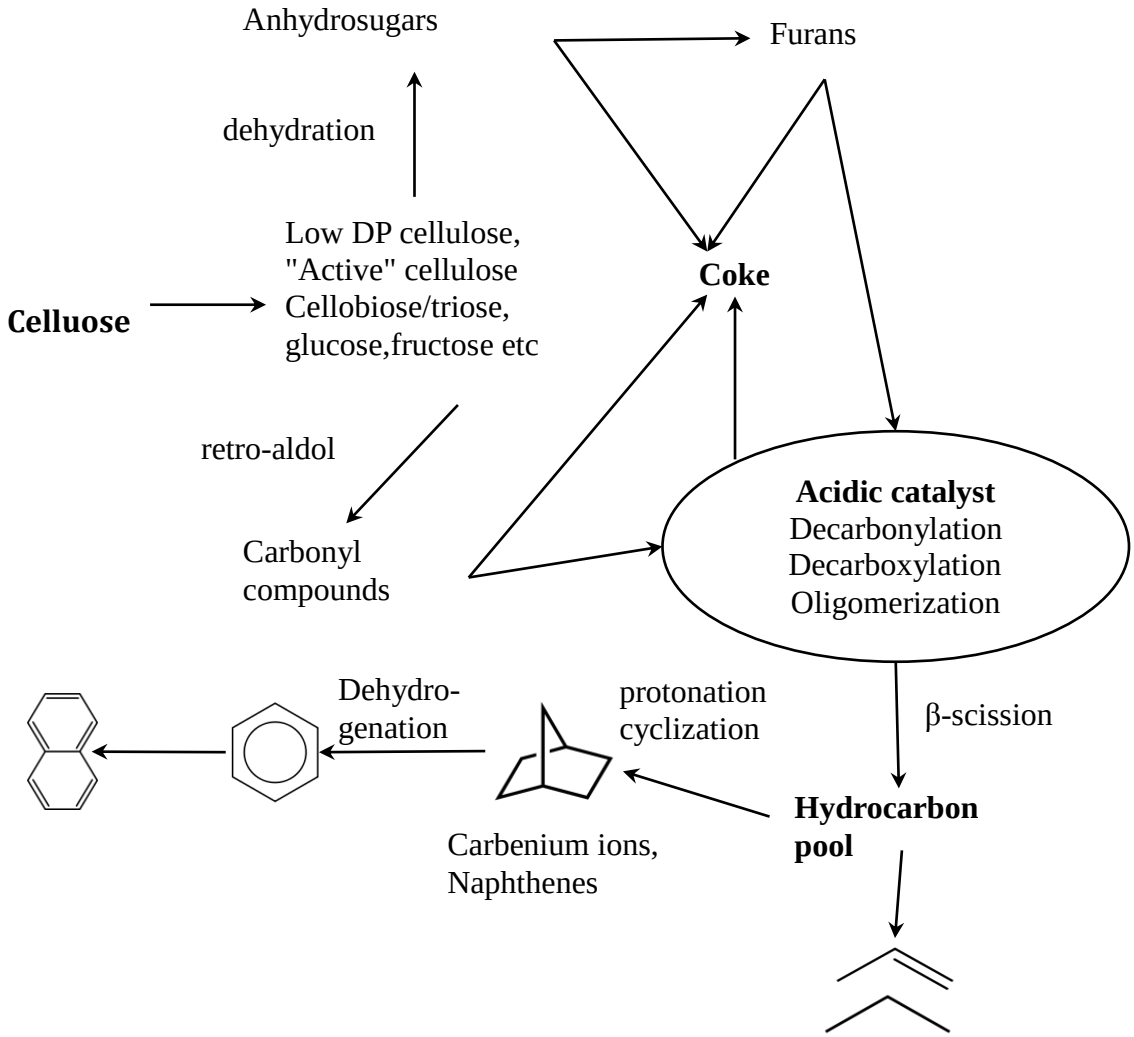

CHAPTER 6. A ZSM-5 CATALYST PELLET: DIFFUSION IN TWO REGIMES WITHIN A MACROPOROUS – MICROPOROUS SOLID

6.1 Introduction and Objective

Solid catalysts, for example zeolites, have microporous crystalline or semicrystalline structures where active sites of the catalyst are located. These microporous structures are often combined via thermal sintering, extrusion or compression with binders to form macroporous solid catalyst pellets required for heterogeneous reactor design. These pellets contain macropores between the microporous structures that facilitate transport of reactants and products in and out of the pellet. Therefore, many industrial catalysts such as zeolite pellets, supported alumina catalysts, molecular sieve pellets, and acid ion-exchange resin catalysts, have bidisperse pore size distributions containing micro- and macropores.

The pore size distribution of catalysts significantly affects diffusion in the macro- and micropores. Many approaches have been used to analyze diffusion and reaction in catalyst pellets with bimodal distribution including the pellet – particle model and random and geometrical pore distribution models [145],[146]. Another approach considers the catalyst pellet to have cylindrical macropores and cylindrical micropores that extend from the macropores into the pellet. This branched macropore – micropore model is an extension of Thiele's model for estimating effectiveness in a microporous catalyst. The goal of this chapter is to develop a simple, two-dimensional branched macropore – micropore model that describes mass transport in a catalyst pellet having the above properties, for a first order reaction with the pellet being isothermal [145], [147], as follows:

1. The effectiveness factor in the micropore region of the catalyst will be determined, using as a reference the reaction rate at the surface of the micropore region (z=L).

2. A differential equation for diffusion transport in the macropore and the overall effectiveness factor in the macroporous solid will derived
3. The effect of rate constant k for first order reaction on the two Thiele moduli (one for micropore region, one for macropore) will be studied.

6.2 Model development

6.2.1 Assumptions

A picture of the pellet pore structure is given below – it can be assumed that this "unit cell" of the pellet is of an arbitrary height H; this unit cell geometry can be repeated in three dimensions to form a macroscopic pellet. Therefore, only this geometry needs to be solved to characterize the system. Macroporosity (ε_M) can be determined from d_p and L.

Reactants diffuse from the bulk gas into the macropore of diameter d_p in the x-direction (negative x-direction). Along the macropore, reactants enter the microporous solid of depth L and diffuse through micropores while simultaneously reacting. At the edge of the micropore region (z=0) and at the end of the macropore (x=0), the flux of reactants can be assumed to be zero (symmetry). Note two diffusivities are present – bulk or Knudsen diffusion in the macropore, and single-file (configurational) diffusion in the micropores.

6.2.2 Effectiveness and Thiele modulus

Inside a catalyst pore, the concentration of the reactant drops progressively. This drop is a function of the dimensionless quantity $L\sqrt{(k/D)}$ where L=length of pore, k=rate constant, D=diffusivity, known as the Thiele modulus, ϕ [147]. Two Thiele moduli exist, one for the micropore and another for the macropore. The resistance offered to pore diffusion lowers the reaction rate. The extent of this effect on reaction rate due to diffusion resistance is measured by

effectiveness, η (Figure 6.3). In this report, η represents micropore effectiveness while ηm represents macropore effectiveness. ηm is affected by the micropore η as well as the dimensions of the catalyst pellet. For a unit cell of the pellet, the dimensions are determined by the diameter of macropore, d_p, and length of micropore, L, represented by the macroporosity, ε_m. ε_m in this case, is defined as the volume occupied by the macropores to the total pellet volume.

Figure 6.1 Micropore and macropore effectiveness and Thiele moduli

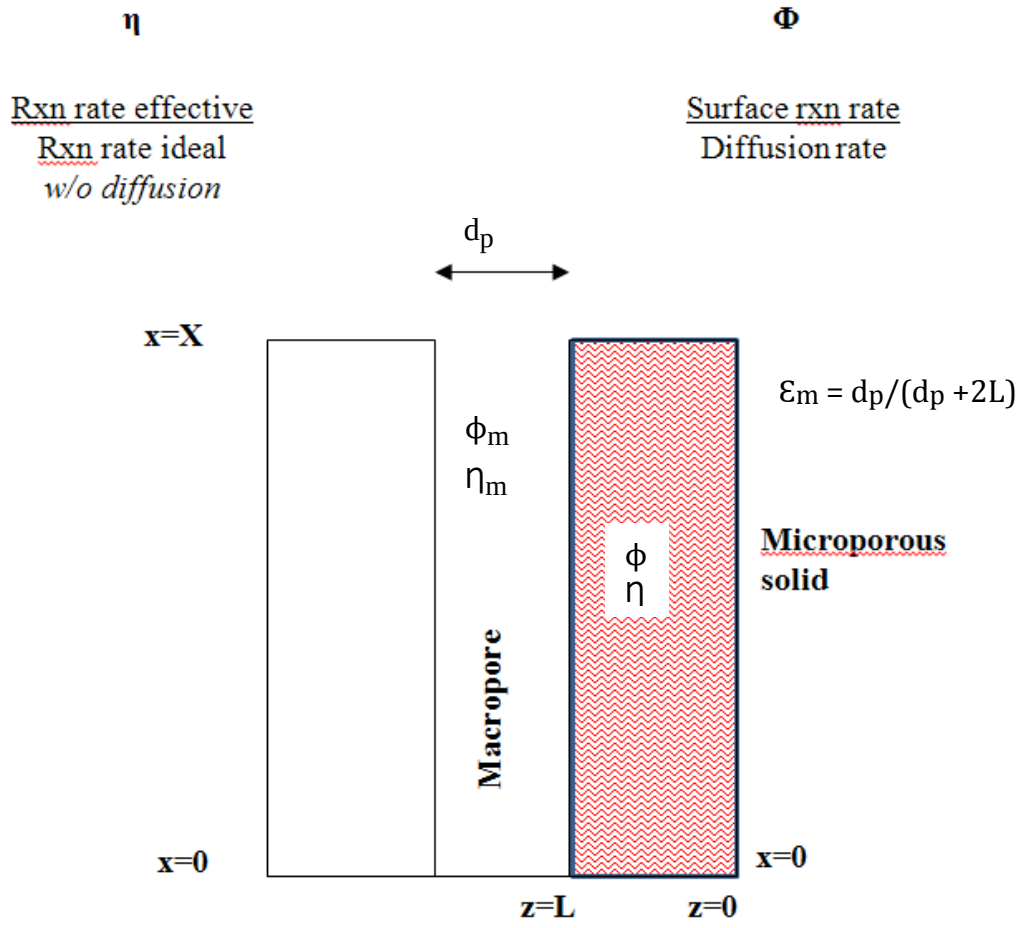

6.2.4 Shape normalization

Study of a catalyst pellet with simple 2-D slab geometry may seem simplistic but this model may be applied to other pellet shapes as well using the theory of shape normalization. Although catalyst pellets may be of different shapes, the reactant can only "see" a flat surface irrespective of pellet shape when diffusion-limited [149]. The distance from the pellet surface up to which the reactant can see the catalyst is given by the characteristic length of the catalyst, L, where $L=V_P/S$ (pore volume, surface area). When this characteristic length is used for estimating Thiele modulus, the product of effectiveness factor and Thiele modulus is unity for strongly diffusion-limited regimes. As a result of this relationship, the curves for η - ϕ are close to each other for a range of pellet shapes [149], [150]. For small $\phi < 1.5$, the reactant can see all the way to the pellet center. To account for this effect, Miller and Lee modified the calculation of L to ensure slab equivalence for small Thiele numbers by adding an additional thickness term [151]. This ensured that shape normalization of η and ϕ values was true over the entire range of values. Thus, for any time of regime – diffusion limited or not, the characteristic length L may be estimated for any shape such that we have its equivalent value for a slab geometry. This allows the simple 2D model developed in this study to be applied to all pellet shapes.

6.2.5 Derivation of micropore Thiele modulus and effectiveness factor

The micro Thiele modulus is a measure of the diffusion resistance in the micropore. Figure 6.2 shows the microporous area of the catalyst for which the Thiele modulus will be estimated.

Figure 6.2 Micropore Thiele modulus calculations

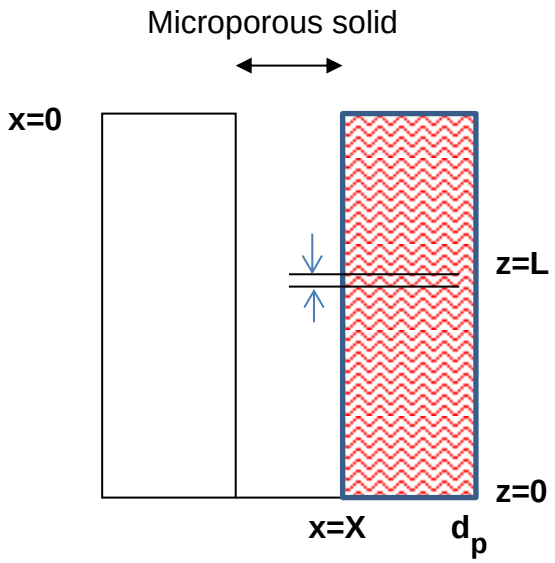

Output – input + rate of dissapearance from reaction = 0

$A * D * (dC_A/dz)_{z+\Delta z} - A * D * (dC_A/dz)_{z+\Delta z} = A * K * C_A * dz$

$d^2/dz^2\ C_A - k/D * C_A = 0$

Where A = area of cross-section of micropore, D = effective diffusivity in micropore, Dm = effective diffusivity in macropore, CA = concentration of reactant (1^{st} order reaction) in micropore, z= distance along length L, k=rate constant, X=length of macropore,

To make dimensionless and present the micropore Thiele modulus in terms of macropore dimensions, let

$d^2/d\lambda^2\ C_A - kX^2/D * C_A = 0$

where $\lambda = z/X$

The term kX^2/D represents ϕ^2, the square of a quantity known as the Thiele modulus. The analytical solution to the above 2nd order differential equation is given by:

$$C_A/C_{AS} = (e^{\wedge}(\emptyset\lambda) + e^{\wedge}(-\emptyset\lambda))/(e^{\wedge}(\emptyset L/X) + e^{\wedge}(-\emptyset L/X))$$

Where C_{AS}=reactant concentration in macropore equal to micropore-macropore interface,

$$\frac{C_A}{C_{AS}} = \frac{\cosh \emptyset\lambda}{\cosh \emptyset(\frac{L}{X})}$$

The effectiveness factor can then be calculated from the ratio of actual or effective reaction rate to the ideal rate that is the reaction rate in the absence of diffusion resistance.

$$\eta = (\int 0^{\wedge}(L/X)\ [C_A\ k\ V])/(\int 0^{\wedge}(L/X)[C_{AS}\ k\ V])$$

$$\eta = \ ([\tan[\emptyset\lambda]/\emptyset]\_0^{\wedge}(L/X))/[\emptyset\lambda]\_(L/X)$$

$$\eta = \frac{\tan \emptyset\lambda\ L/X}{\emptyset\lambda\ L/X}$$

The effect of diffusion and reaction on the effectiveness and Thiele modulus is demonstrated by the following plot. Thus the effective reaction rate comes closer to ideal when the diffusion resistance is low e.g. small pore length resistance to diffusion resistance is low e.g. small micropore length or interconnected pores. A change in volume of due to change in number of moles or partial pressure of species can also change the effectiveness.

Figure 6.3 The effectiveness factor as a function of Thiele modulus [147]

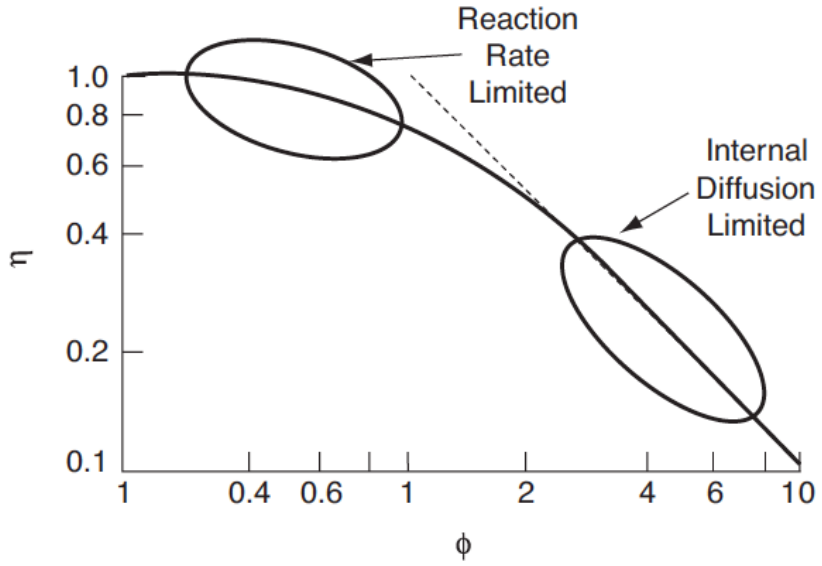

6.2.6 Derivation of macropore Thiele modulus and effectiveness factor

The macropore Thiele modulus is derived similarly:

Output – input + rate of dissapearance from reaction = 0

$$A_m * D_m * (dC_{Am}/dx)_{x+\Delta x} - A_m * D_m * (dC_{Am}/dx)_{x+\Delta x} = 2 * A * D * C_A$$

$$A_m = d_p * H$$

$$A = dx * H$$

Where Am= area of cross-section of macropore, H = third dimension of catalyst, Dm = effective diffusivity in the macropore, C_{AM} = concentration in macropore = C_{AS}, C_{bulk} = bulk conc.

To make the equation dimensionless, let

where λ = z/X and where λ’ = x/X

Therefore,

$d^2/d\lambda'^2\ (C_{Am}) = 2 * D / D_m * X / d_p *\ (dC_A/d\lambda)\ \lambda=L/X$

$C_A/C_{AS} = \cosh\ (\phi\lambda) / \cosh \phi L/X$

$C_A/C_{AS} = 2\ D/Dm\ \ X/(dp)\ \emptyset\hat{}(2)\ \ \tan\ [\![\emptyset L/X]\!]\ /(\emptyset L/X)\ \ L/X$

$= 2\ D/Dm\ \ k/(D)\ X\hat{}(2)\ \ X/dp\ \eta\ L/X\ \ Cas$

But $\varepsilon m = dp/(dp + 2L)$

Reorganizing and simplifying

$d^2/d\lambda'^2\ (C_{Am}) = k / D_m * n * X^2 * (1-\varepsilon_m/\ \varepsilon_m)* C_{Am})$

Similarly, the macropore effectiveness factor can then be calculated from the ratio of effective reaction rate to the ideal rate that is the reaction rate in the absence of diffusion resistance in the macropore.

Derivation for η_m

$C_{Am} = (e\hat{}(\emptyset\lambda') + e\hat{}(-\emptyset\lambda'))/(e\hat{}\emptyset + e\hat{}(-\emptyset))\ C_{bulk}$

$\eta m = \tanh\ [\emptyset m]/[\emptyset m]$

6.3 Model testing

6.3.1 Base case values

Standard values of variables in the model were obtained from literature (Table 6.1). When zeolite pellets with diameter > 2 mm are used, intercrystalline mass transfer had a dominating effect on catalytic activity and selectivity of the zeolite at <600 K [152]. Since we wish to study intracrystalline (micropore) diffusion as well, a smaller particle size of 1 mm was selected. The micropore length was determined for the approximate size of zeolite crystal (100 nm = 10^{-5} cm) and that of aggregates (1000 nm). The diffusivities were measured in studies by [145], [153] and were assumed to be effective diffusivities. The microporosity was fixed. Pellets would be made by compressing (for example) this microporous catalyst producing macropores which in turn will affect macroporosity and the volume occupied by solid catalyst. The toluene dealkylation reaction was selected as a model reaction. Data for the effect of temperature on reaction rate was obtained from Li et al. [152] and is plotted in Figure 6.4.

6.3.2 Macroporosity and overall effectiveness

Catalyst pellets are made from microporous structures. The porosity of microporous structures that form the pellet does not change; ε_{mic} (micropore effectiveness) is constant. The micropore length does not change either; the micropore values of Thiele modulus and effectiveness remain unchanged. The volume occupied by the macropores can be adjusted by controlling variables such as temperature and compression pressure during pellet production. As macroporosity increases, the amount of solid microprous content in the pellet decreases, leading to a loss in concentration of active sites. That is, for high macroporosity and the total volume occupied by the solid catalyst material represented by ε_m and ε_s, has to decrease to maintain

constant dimensions. However, increase in macroporosity allows easier transport of reactant molecules to micropores and increases the overall effectiveness factor. Thus it becomes necessary to model mass transfer in catalysts to determine their effectiveness in specific applications. Figure 6.5 below shows how the rate constant (reaction temperature) affects diffusion resistance and decreases the effectiveness factor.

Table 6.1 Standard values of model variables

Parameter	Name	Std Value	Reference
D	Dia of catalyst pellet	0.1 cm	[145]
X	Macropore length = D/6	0.017 cm	[154]
L	Length of micropore	$1x10^{-5}$ cm	[155]
d_p	Dia of macropore (ε_s=0.3)	$1.33x10^{-5}$ cm	ε_m
D_{eff}	micropore diffusivity	$1x10^{-10}$ cm^2/s	[145], [153]
D_m	macropore diffusivity	$1x10^{-2}$ cm^2/s	[145]
ε_s	Solid volume	0.01 – 0.7	-
ε_{mic}	Microporosity (fixed)	0.3	[152], [156], [157]
ε_m	Macroporosity	0.01 – 0.7	[152], [156], [157]

Figure 6.4 Effect of temperature on rate constant for toluene dealkylation [152]

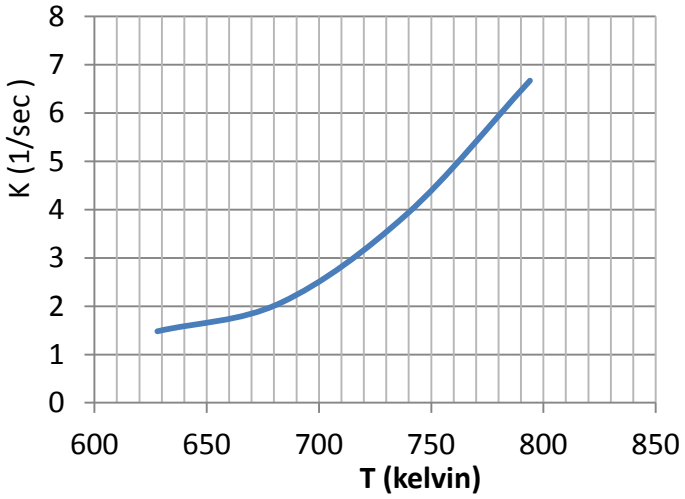

Figure 6.5 Macroporosity and effectiveness. Table shows values of variables used in the corresponding plots. Variables denoted in red (d_p, ε_s, ε_m) were varied to determine effect on diffusion.

Parameter	Std Value
D	1 cm
X	0.17 cm
d_p	1.33×10^{-5} cm
L	1×10^{-5} cm
D_{eff}	1×10^{-10} cm^2/s
D_m	1×10^{-2} cm^2/s
ε_s	0.05 – 0.65
ε_{mic}	0.3
ε_m	0.65 – 0.05

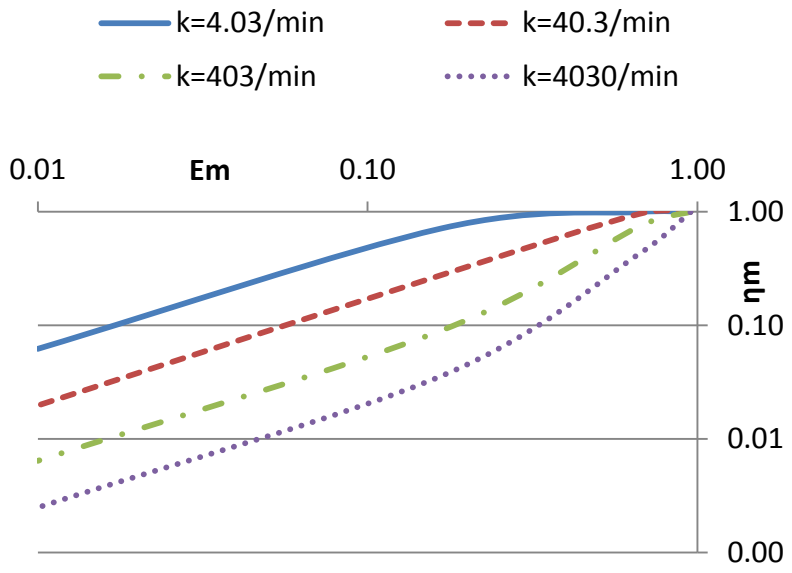

6.3.3 Effect of catalyst pellet diameter – macropore length

The plots in Figure 6.6 show the effect of changing pellet size on effectiveness, while keeping other factors such as ratio of the other internal dimensions (L, d_p) fixed. The size of pellet changes the length of the macropores and increases the overall diffusion resistance for reactants. As particle size grows, the macropore effectivness drops very quickly with temperature (i.e. reaction rate). The micropore effectiveness remains unchanged however as the micropore length, L, is not affected.

6.3.4 Effect of macropore diameter and micropore length

In previous plots, the pellet diameter was changed. If that dimension (and other factors such as porosities) is kept constant while changing the internal catalyst dimensions (d_p: L ratio), both ŋ are affected. The macropore diameter may be adjusted to a low value to have a large number of macropores with small diameter as well as smaller values of micropore length. The plots below show the effect on change in d_p on effectiveness factors. An increase in macropore diameter increases micropore length as the porosities are fixed, increasing ŋ (micropore). Figure 6.7 shows that as L increases, ŋ drops rapidly. The effect of reaction rate is also apparent: at high temperatures, even very short length of micropore is not sufficient to remove diffusion resistance. Therefore L has to be less than 5 μm for high ŋ i.e. the zeolite crystal may be of size as large as ~10 μm and there is no need to develop complicated synthesis techniques for nano-sized zeolite crystals.

Figure 6.6 η at ρ, porosity=constant: effect of X. Table shows values of variables used for obtaining the plots.

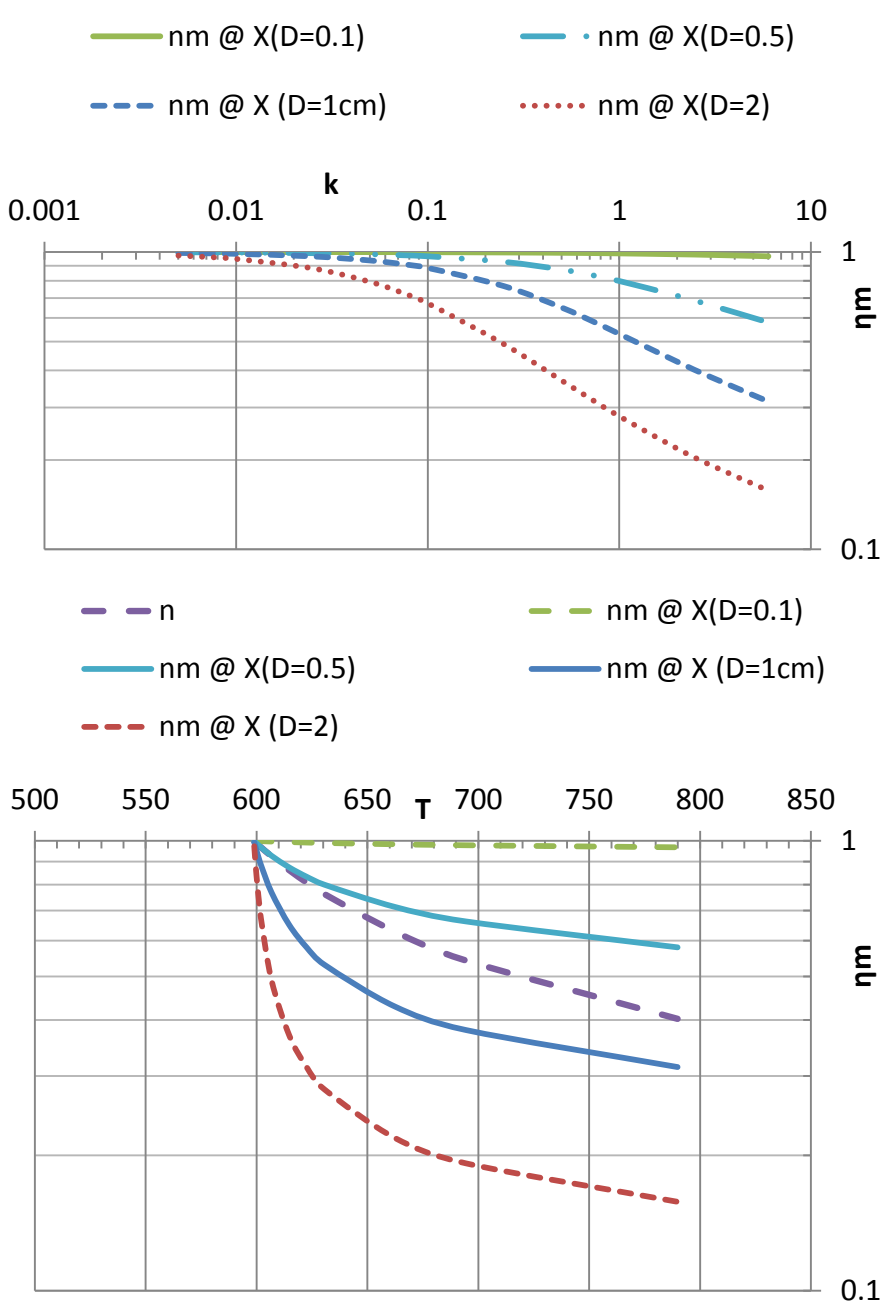

Para-meter	Std Value
D	1 cm
X	0.17 cm
d_p	1.33×10^{-5} cm
L	1.00×10^{-5}
D_{eff}	1×10^{-10} cm^2/s
D_m	1×10^{-2} cm^2/s
ε_s	0.3 (fixed ρ)
ε_{mic}	0.3
ε_m	0.3

Figure 6.7 η at ρ,porosity=constant: effect of d_p,L

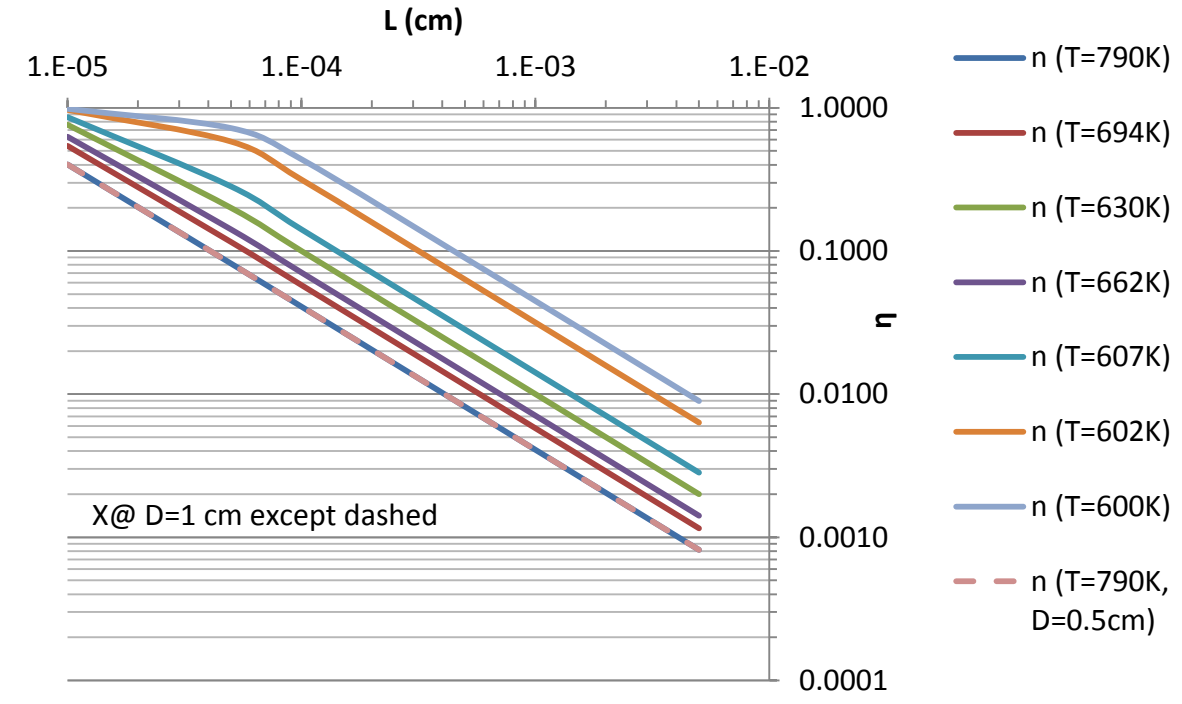

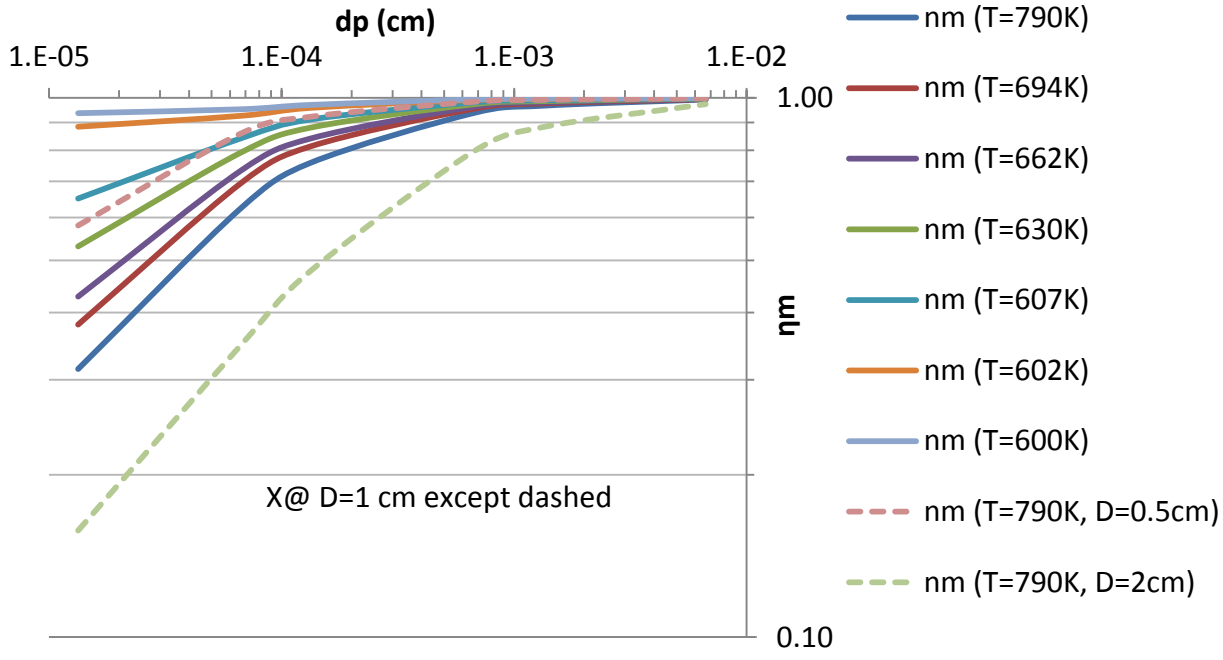

Figure 6.8 Diffusion-limiting regimes($\phi > 3$) begin at at L = 0.2 μm (700 K, red line) versus a much longer pore length of 2 μm at lower reaction temperatures (600 K, blue line)

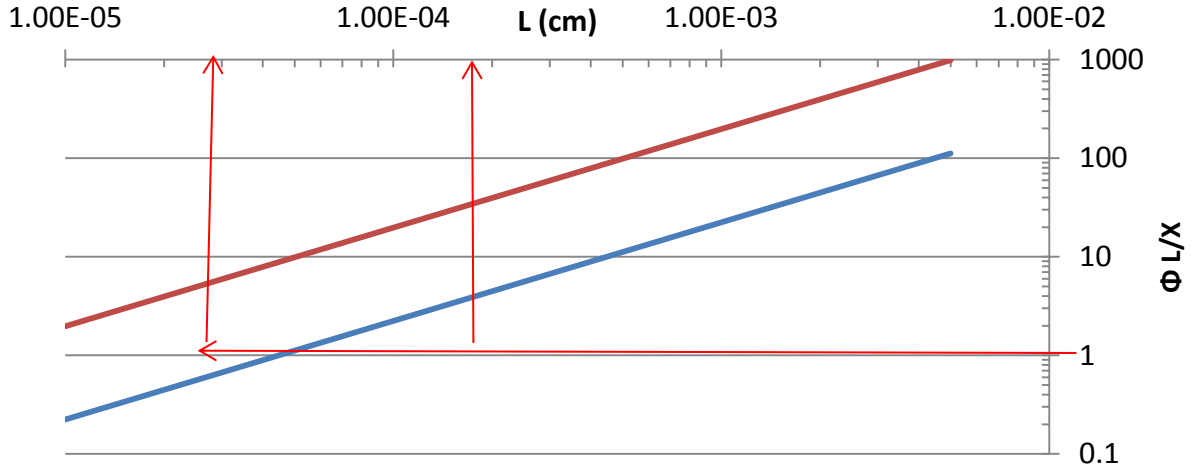

Another example of the importance of identifying the critical value of micropore length, L, for high effectiveness is given by Figure 6.8. This plot shows the effect of change in micropore length and reaction temperature on the Thiele modulus. To avoid operation of catalyst systems in the diffusion limited regimes ($\phi > 3$), a much shorter L is desired as the reaction temperature is increased. For low diffusion resistance, a length of 2 μm which is approximately the size of normal zeolite aggregates, is acceptable at 600 K. But of the reaction temperature is increased to 700 K, the length would have to be only 0.2 μm (the size of a single zeolite nanocrystal, which will have to be specially synthesized) to maintain $\phi < 3$.

6.3.5 Effect of pellet density

The pellet density (ε_s) may be increased by compression of catalyst. As solid becomes denser, macroporosity is lost leading to high diffusion resistance in the macropore (Figure 6.9). Microporosity remains unaffected and it is observed that η (micropore) is only a function of T, not of ε_s.

Figure 6.9 η at L, X=constant: effect of Ɛ

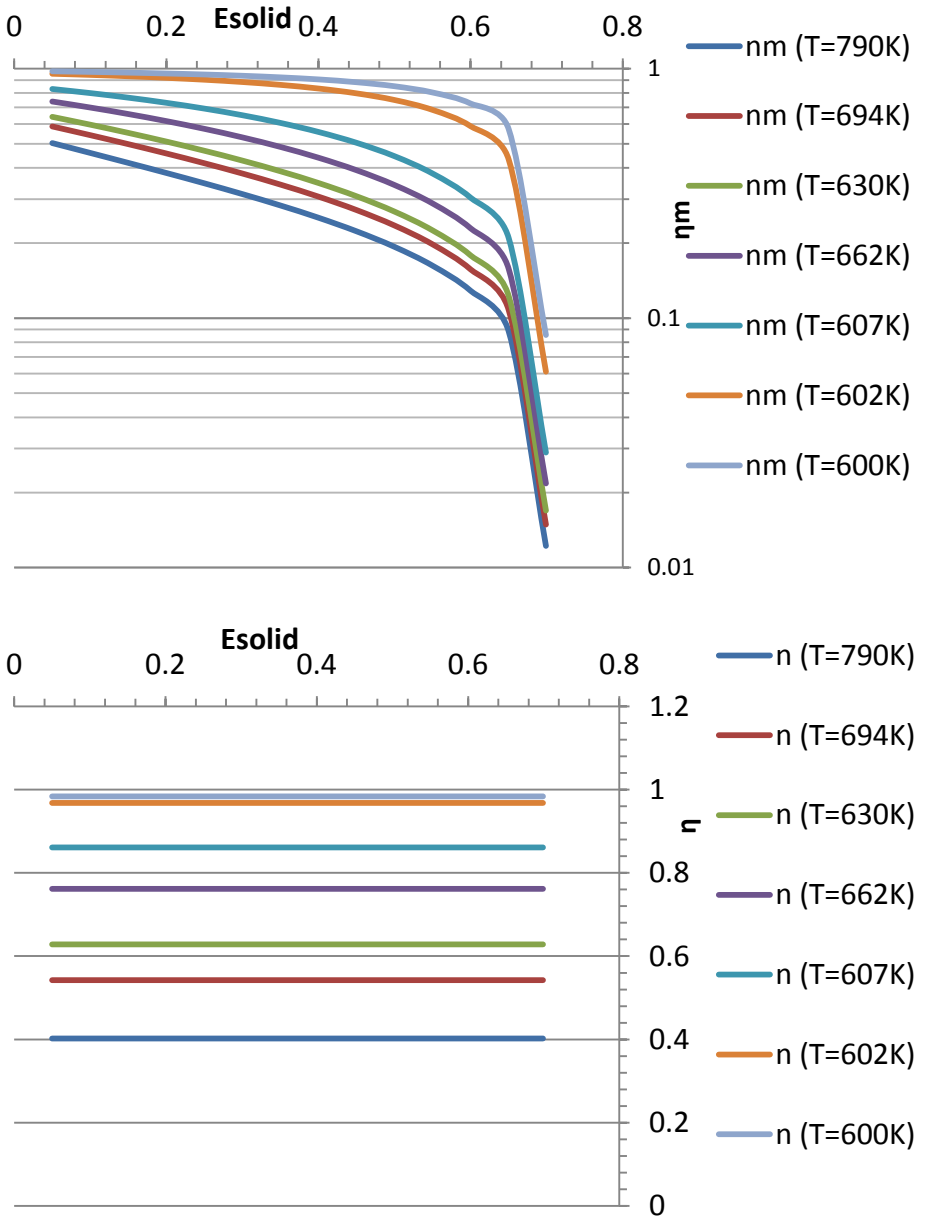

Para-meter	Std Value
D	1 cm
X	0.17 cm
d_p	1.33×10^{-5} cm
L	1×10^{-5} cm
D_{eff}	1×10^{-10} cm^2/s
D_m	1×10^{-2} cm^2/s
$Ɛ_s$	0.3
$Ɛ_{mic}$	0.3
$Ɛ_m$	0.3

6.3.6 Four regimes of macropore and micropore diffusion resistance

Pellet manufacturing can be adjusted to control its internal dimensions. As these dimensions change, the effectiveness factors for the pellet are affected. The pellet dimensions in this example are controlled by the macropore diameter, d_p, which also determines L, and the macropore length, X. X is determined from the pellet size while d_p can be adjusted by controlling the pellet composition and manufacturing process. As the pellet size grows, X increases and η_m decreases. As d_p increases, L increases and while the overall effectiveness is increased, micropore effectiveness is reduced. This gives rise to four diffusion regimes as shown in Figure 6.10.

Figure 6.10. Effect of internal pellet dimensions on diffusion resistance and effectivenss

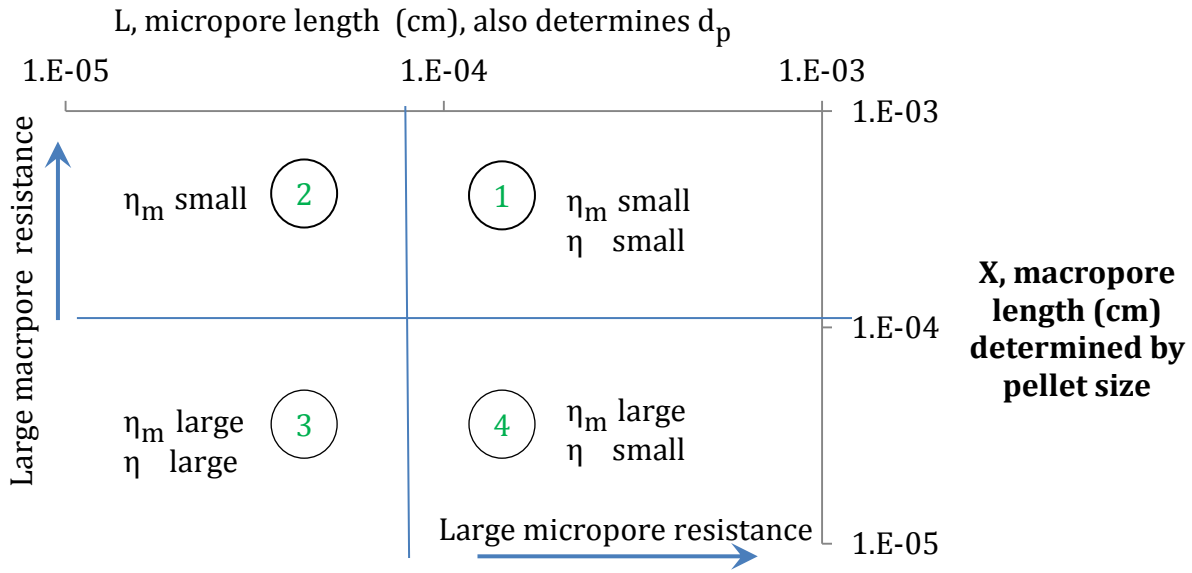

The effect of pellet dimensions on effectiveness values in micro and macropore is shown in Figure 6.11 and Figure 6.12. For example, effectiveness regime #4 (high η_m, small η) can be

identified by combining the observations from both the plots in each figure. It is possible to predict catalyst effectiveness factors using a program written for e.g., in MATLAB or such software, and identify them using 3D plots of X (or d_p) with η and η_m.

Figure 6.11. X effect on η – effectiveness factor regimes as described in Figure 6.10 can be identified from combining observations from both of the below plots.

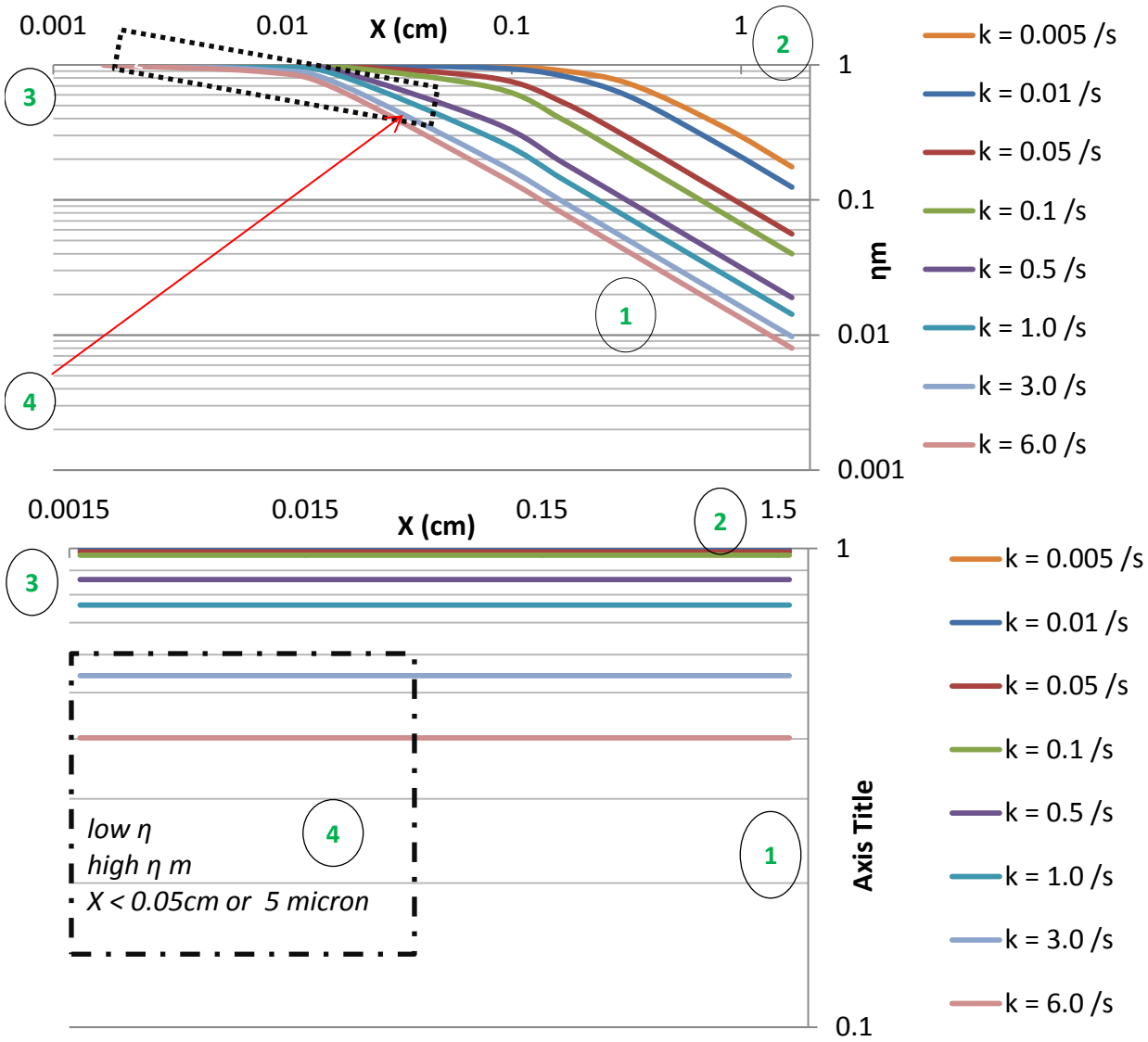

Figure 6.12 dp effect on η

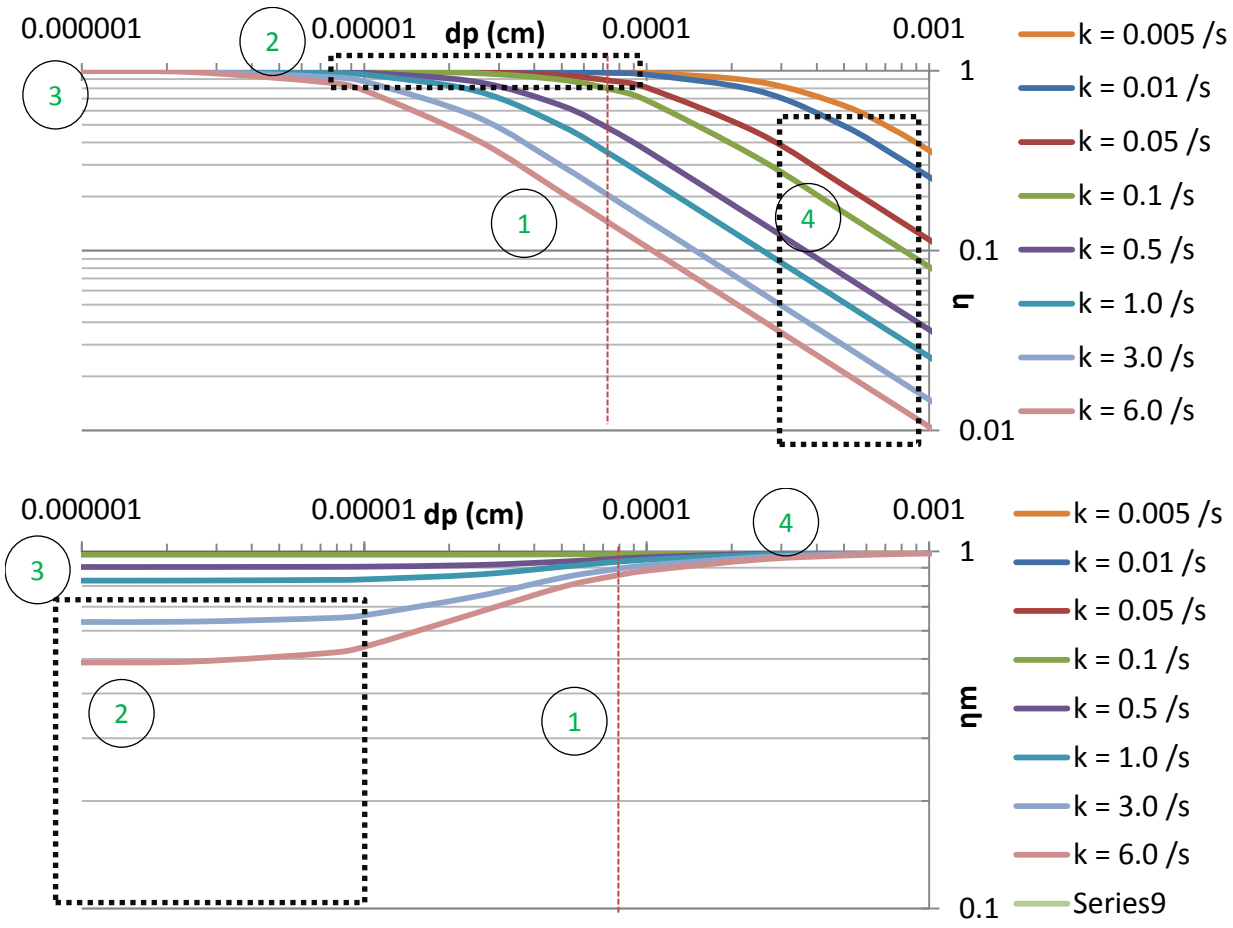

6.4 Conclusions

A simple, two-dimensional branched macropore – micropore model that describes mass transport in a catalyst pellet was proposed and tested for a 1st order reaction. The model helped study the effect of pellet properties on the Thiele moduli and effectiveness factors. Such a model can help us design catalyst pellets for aromatics production for high product yield and catalyst efficiency. For example, if pores are too small, mass transport is diffusion-limited, leading to low turnover at active sites as well as greater potential for coke generation. If pores are too large, the solid catalyst material is low and there are less active sites leading to reduced yields.

CHAPTER 7. GREEN AROMATICS FROM BIOMASS PYROLYSIS VAPORS USING A BIFUNCTIONAL MESOPOROUS CATALYST

Authors:
Shantanu Kelkar, Christopher M. Saffron,
Thomas J. Pinnavaia, Dennis J. Miller, Robert Kriegel

7.1 Abstract

Zeolites with uniform intracrystal mesopores, designated MSU-MFI, were prepared using silane-modified polymers as mesopore-generating agents. X-ray diffraction analysis of this catalyst showed Braggs peaks representative of MFI structure. Catalyst characterization by N_2 physisorption revealed a mesoporous structure with high surface area, pore size and volume. The MSU-MFI catalysts developed in this study were selective toward aromatic chemical production from poplar pyrolysis vapor. Yields of generalized products and aromatics were comparable to those obtained from conventional microporous ZSM-5 analogs as demonstrated by pyroprobe-gas chromatography/mass spectrometry and thermogravimetric analysis. While ZSM-5 was more selective to smaller C6 aromatics and naphthalenes, MSU-MFI catalysts were more selective to C8 and C9 monoaromatics. The incorporation of gallium (III) ions in MSU-MFI using the incipient wetness method increased aromatic yields by up to 20% over Ga-free catalysts and decreased the coke production by up to 6%. Due to high yields and low coke formation, Ga-MSU-MFI offers an improved option for making non-oxygenated aromatic chemicals from photosynthetic biomass.

7.2 Introduction

Biomass fast pyrolysis involves the rapid heating of biomass in an inert atmosphere to intermediate temperatures (~500 °C). The generalized products of pyrolysis include solid char, combustible gases and liquid bio-oil. Though pyrolysis is relatively simple and inexpensive to

deploy, its overall efficacy suffers from low product selectivity. Hundreds of chemical compounds are produced from pyrolysis of biomass, including highly oxygenated compounds such as anhydrosugars, carboxylic acids, aldehydes, ketones, furans, phenolics and a significant amount of water. Prior research shows that product selectivity can be improved using heterogeneous catalysts to convert pyrolysis vapors into products rich in aliphatic and aromatic hydrocarbons [3].

Both authentic carbohydrate compounds and biomass have been show to produce high levels of deoxygenated aromatic products using zeolite catalysts [68], [91], [94], [115], [142], [158], [159]. The selection of appropriate catalysts is crucial for high hydrocarbon or aromatic yields from biomass pyrolysis. Highly acidic catalysts are desired for accelerating the cracking reactions that remove oxygen in the form of small molecules as CO, CO_2, and H_2O. Historically, low hydrocarbon yields have been observed from catalytic pyrolysis of biomass due to the presence of highly oxygenated compounds in the pyrolysis vapors. This in turn, is due to high oxygen levels present in photosynthetic biomass.

Wang et al. have suggested that a reactive hydrocarbon pool of intermediates is generated in catalysts during the methanol to olefins process [103]. The intermediates in this pool have molecular dimensions between 5.7 and 6.0 Å, i.e. similar to the kinetic diameters of benzene, indene, 2-furanmethanol and 4-methylfurfural [103], [104]. Therefore it not surprising that ZSM-5 catalyst has demonstrated the highest aromatic yields from biomass catalytic pyrolysis. But with average pore dimensions of 5.5–5.6 Å, which is smaller than the kinetic diameters of most phenolic molecules and anhydrosugars produced during pyrolysis, ZSM-5 is limited by low reactant and product mass transfer rates, especially for larger molecules [104], [109]. Even for small molecules, the diameter of the pore may be smaller than the mean free path of the

molecule, reducing its diffusivity. Mesoporous catalysts such as Al-MCM-41, Al-MSU-S, alumina stabilized ceria have been synthesized in order to increase mass rates, but their pore sizes are often too large or they lack the shape selectivity to produce aromatics. MCM-41 supports, for example, are amorphous and lack the high acidity of zeolite catalysts[160]. They are also hydrothermally unstable and may be unsuitable for reactions such as pyrolysis upgrading, which occurs at medium to high temperatures and with an acidic and high moisture content feed. Catalysts that exhibit high acidity, high selectivity to desired products, reduced coke formation and hydrothermal stability are needed if biomass pyrolysis vapors are to be a source of aromatic chemicals.

Mesoporous aluminosilicates with zeolitic walls have been synthesized, but they were only partially crystalline, have had significantly reduced mesoporosity and unit wall thickness[161], [162]. Zeolitic nanostructures were synthesized by quenching the zeolite crystallization reaction and used the product as seeds to assemble hexagonal mesostructures, now known as MSU-S[125]. These materials showed significantly higher acidity and hydrothermal stability than MCM-41 type catalysts. Although the MSU-S catalysts have performed well for reactions such as cumene cracking, they showed low selectivity for aromatics production in our experiments, producing non-condensable gases and coke, possibly due to their high acidity and large mesoporosity.

Methods on synthesizing nano-sized zeolite crystals for inter-crystal mesopores have been developed through precise control of reactions conditions, while methods such as carbon templating, chemical leaching (steaming) or carbon nanoparticles have been used to develop zeolite crystals with intra-crystal mesopores[163], [164], [165], [166], [167]. However some of these techniques are laborious and expensive while others do not offer good control over the

zeolite particle size or textural porosity as well as affected the chemical structure; the mesopore size in some cases had a broad distribution (>10nm width at half maximum) [160]. The catalysts so developed are therefore not suitable for shape or size selective catalytic conversions.

Surfactant micelles such as those used for synthesizing highly ordered mesopores in MCM-41, are held together by Van der Waals forces of attraction that cannot withstand the forces due to zeolite crystallization. Therefore, when used for zeolite synthesis, the micelles collapse, inhibiting mesopore formation. In contrast, many soft templating techniques have been developed recently which use organosilicon polymer templates as mesopore and structure directing agents[160], [168], [169], [170], [171]. The polymers employed for such synthesis are organosilane polymers or surfactant polymers with a quaternary ammonium head similar to tetrapropylammonium used as an organic template for ZSM-5 synthesis. These polymers act as structure-directing agents due to the attached silane group, which can participate in Si-O-Si bond formation. At the same time, the rest of the surfactant polymer is able to form micelles to direct the formation of ordered, uniform mesopores comparable with MCM-41. The zeolites produced not only possess the micropores and crystallanity of conventional zeolites but also have ordered mesopores comparable to MCM-41 materials.

Catalysts break down large molecules found in pyrolysis products to smaller hydrocarbon fragments (cracking). These hydrocarbon fragments are condensed into BTEX molecules due to the oligomerization and cyclization functionalities in catalysts. Olefins are precusors to aromatic molecules and many studies have shown that increasing the amount of olefins fed increases the BTEX content in catalysis products [91], [107], [108], [109]. However acidic catalysts are selective towards cracking molecules rather than dehydrogenating to produce olefins. Hence a second functionality (in addition to the cyclo-oligomerization) is desired to promote olefin

production. Studies have demonstrated the dehydrogenating potential of gallium metal (Ga) doped on a shape-selective acidic catalyst [108], [119], [172], [173]. Ga incorporated in the zeolite structure increased catalyst acidity, selectivity for aromatics and reduced tar and coke production.

Thus, it is hypothesized that a bi-functional (capable of dehydrogenation and aromatization) MFI catalyst with tunable porosity may produce higher levels of mono-cyclic aromatics and decrease coke production. However, an off-the-shelf bi-functional catalyst is not available, therefore synthesis is required. Methods for synthesis of catalysts with dehydrogenation functionality and different porosities were identified [108], [109], [173], [174], [175], [176]. A method using silane-functionalized polymer as a mesoporogen was developed to synthesize mesoporous MFI catalysts (MSU-MFI) with different porosities [174]. The mesoporous catalysts were tested for aromatics production from biomass pyrolysis vapors. Gallium, a dehydrogenating metal, was deposited on the catalyst and its effect on the yield or aromatics and coke generation was tested and compared with conventional ZSM-5.

7.3 Experimental

7.3.1 Synthesis of MSU-MFI

MFI catalysts with different porosities were synthesized using organic polymers of polypropylene oxide α,ω-diamine, also known as polyetheramine (Jeffamine D-400 and D-4000, Huntsman Corp., The Woodlands, TX) with molecular weights of 430 and 4,000 Daltons, respectively, as mesopore generators. All other chemicals were obtained from Sigma Aldrich, St. Louis, MO. The silylated polymers were formed by reaction of all of the N-H groups of the polypropylene oxide diamine polymer with glycidoxypropyltrimethoxysilane (GOPTMS), at 80-85°C for 24 h to form C-N linkages to the GOPTMS units. A mixture of the mesoporogen,

tetrapolyammonium hydroxide solution (TPAOH), tetraethoxysilane (TEOS) and aluminum isopropoxide was prepared to obtain a gel with the molar composition 1 SiO_2: 0.010-0.012 Al_2O_3: 0.37 TPAOH: 20 H_2O: 4 EtOH: 0.10 to 0.025 polymeric organosilicon. The crystallization of the zeolite phase was carried out in a Teflon-lined autoclave at 100 to 150°C for 48 to 96 hours under static conditions. The products were washed, air-dried, and calcined at 600°C for 4 hours. Prior to use, the zeolites were converted to the protonated forms by treating the calcined zeolites with 10 % ammonium nitrate solution at 80°C for 8 hours.

Gallium loaded catalysts were prepared by the incipient wetness method 34 using an appropriate amount of aqueous gallium nitrate (Aldrich, 99.9%) solution. Gallium loaded catalysts were prepared using an appropriate amount of aqueous gallium nitrate (Aldrich, 99.9%) solution using the incipient wetness method [176]. The treated catalysts were dried overnight at 110°C, calcined in air at 550°C for 5 h, reduced in a hydrogen stream at 500°C for 4 h, and finally calcined in air at 550°C for 5 h to generate the highly dispersed active Ga^{3+} species [176].

7.3.2 Catalyst characterization

Catalysts were characterized for number and strength of active sites using BET surface area and BJH pore volume analysis. Surface area measurements and pore size distribution analysis were done by nitrogen adsorption at 195 °C (78 K) in a Micromeritics ASAP 2010 instrument. Prior to measurements, the sample was out-gassed in the degas port of the apparatus at 220°C for 24 h. The surface area originating from the framework micropores of the zeolite was determined from t- plots of the nitrogen adsorption data. XRD patterns were recorded on a Rigaku Rotaflex Diffractometer using $Cu_{K\alpha}$ radiation (λ=1.542A°). The Ga, Si and Al content for catalysts was determined by inductively coupled plasma (ICP) analysis performed by Galbraith

Laboratories (Knoxville, TN). Ga presence was also confirmed using X-ray photoelectron spectroscopy. X-ray photoelectron spectroscopy was performed on a Perkin Elmer Phi 5400 ESCA system equipped with a Magnesium K_α x-ray source. Samples were analyzed at pressures between 10^{-9} and 10^{-8} torr with a pass energy of 58.7 eV and a take-off angle of 45°.

7.3.3 Pyrolysis-GC/MS

Experiments were conducted using a microscale pyrolysis unit, CDS Pyroprobe 5250 (CDS Analytical Inc, Oxford, PA) interfaced to a Shimadzu QP-5050A gas chromatograph/mass spectrometer (Shimadzu Corp, Columbia, MD). A lignocellulosic feedstock, poplar (DN-34, *Populus x euramericana*, cv. 'Eugenei') was used as biomass for all experiments. The poplar was dried at 60°C and ground to a particle size of less than 0.5 mm and stored at room temperature. The moisture content, as measured by oven drying was approximately 8% [72]. For biomass pyrolysis experiments, approximately 0.5 mg of ground biomass samples were packed between quartz wool in a quartz tube with a filler rod. For catalytic pyrolysis experiments, approximately 0.5 mg of biomass was packed between quartz wool. Catalyst, at a 10:1 weight ratio of catalyst to biomass, was added on both sides followed by more quartz wool to hold the sample in place. Six or more replicates of each sample were run. Pyrolysis proceeded by setting the pyroprobe at 650°C with a hold time of 20 s at the maximum heating rate. The GC used a Restek rtx-1701 column (Restek, Bellefonte, PA), 60 m x 0.25 mm with a 0.25 μm film thickness. The column gas flow was 1 cm/s with a split ratio of 1:100 so as to not overwhelm the mass spectrometer. The GC oven temperature program began with a 1 minute hold at 40°C followed by heating at 8°C/min to 270°C. The injector and detector temperature was set at 280°C. Identification of compounds was performed by comparing the mass spectra of the peaks with standard spectra of other compounds using the NIST library to obtain the most probable

matches. Pure compounds (Sigma-Aldrich Co., St Louis, MO) were then used to confirm the peak identities based on matching of retention times and mass spectra. Quantification was performed using external standards in acetonitrile and a four-point calibration curve was constructed relating concentration to peak area response. The mass spectra were recorded in electron ionization mode for *m/z* 28 to 300.

7.4 Results and Discussion

7.4.1 Catalyst properties

Figure 7.1 shows the nitrogen adsorption-desorption isotherms for ZSM-5 and two mesoporous MFI catalysts made using polymers with different size and molecular weights. Unlike ZSM5, the mesoporous catalysts showed type IV isotherms analogous to that observed in the MCM-41 support. The average pore size was 2.6 – 4.0 nm (compared with 0.6 nm for ZSM5) and mesoporosity was observed with a distinguishable hysteresis loop between *P/Po*=0.5 to 0.8. Catalysts made using the smaller polymer, D400, as the mesoporogen showed an increased adsorption in the range of *P/Po*= 0.7 to 1 which may be attributed to greater textural porosity and capillary condensation in the mesopores. Textural porosity was observed above P/P_o>0.9 and this may be due to surface defects or inter-particle voids [160]. The surface areas and porosities of MSU-MFI catalysts were far higher than ZSM5 (Table 7.1). Nitrogen desorption isotherms of the catalyst showed that the external surface area was over three times that of ZSM-5. The mesopore volume was significantly increased at the expense of microporosity. The larger polymer, D4000 produced a catalyst with larger mesopores of size 3.9 nm compared with approx. 2.9 nm for D400. The BET surface area and pore volume increased with the amount of mesoporogen used during catalyst synthesis for both polymers.

The formation of mesopores is expected to result from the binding of units of silylated polypropylene oxide α,ω-diamine polymer to the zeolite matrix through SiO_3 linkages [160]. The polymer is thought to become phase-segregated as the zeolite crystal grows, forming the mesopores. Temperature seemed to have a greater effect than the size (molecular weight) of the mesoporogen on surface area and pore volume of catalysts. Higher reaction temperature produced catalysts with greater surface area and pore volume with the smaller D400 polymer when compared with the larger D4000. However, catalysts M5 and M6 made with D4000 did have a larger mean pore size of 3.8 nm compared with 2.9 nm for D400. Increasing the amount of mesoporogen in the catalyst synthesis mix did not affect the pore size but increased the volume and surface area.

X-ray diffraction was used to compare the structure of zeolites crystals. Figure 7.2 shows patterns for MFI1 (prepared with D400) with ZSM-5. The characteristic peaks for MFI catalysts are observed in both ZSM-5 and MFI1. No other crystalline phases were observed; therefore it is concluded that the catalyst produced is a mesoporous aluminosilicate with zeolite walls. The mesopores reduce the domain of zeolite crystals, therefore the peaks of MFI1 are of lower intensity [160].

Table 7.1 Properties of mesoporous MFI catalyst variants

ID	Polymer	Conc.(mol/ mol SiO_2)	Temp. (°C)	BET Surface Area (m^2/g)	Avg. Pore size (nm)	Pore Vol. (cm^3/g)	Micropore Vol. (m^3/g)	Ext. surface area (m^2/g)
M1	D400	0.05	150	514	2.6	0.47	0.084	327
M2	D400	0.1	150	520	2.9	0.65	0.059	455
M3	D400	0.05	120	480	2.9	0.63	0.063	404
M4	D400	0.1	120	523	2.9	0.66	0.062	385
M5	D4000	0.025	100	476	3.8	0.44	0.064	370
M6	D4000	0.05	100	569	3.9	0.58	0.063	481
ZSM5	-	-	-	396	0.6	0.24	0.119	135

Figure 7.1. Comparison of N_2 isotherms of ZSM-5 (continuous line), M4: MSU-MFI with D400 as mesoporogen (dashed line) and M6: MSU-MFI with D4000 (dotted line)

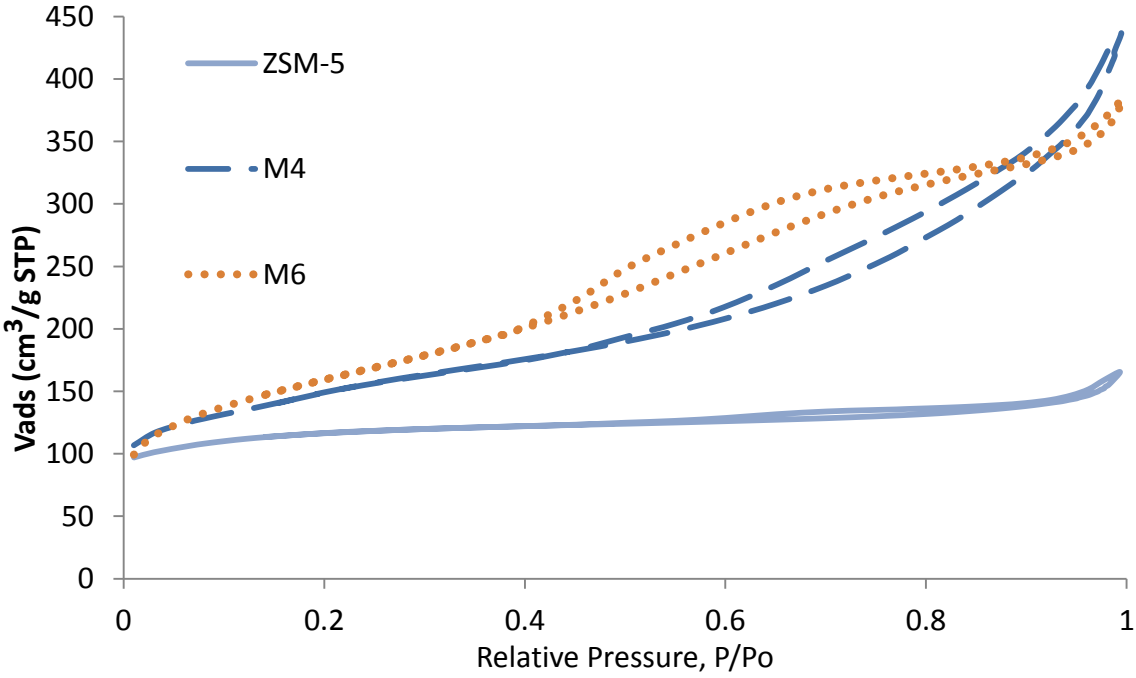

Figure 7.2. X-ray diffraction analysis: comparison of ZSM-5 (dotted, blue) with M4 (red, shorter peaks)

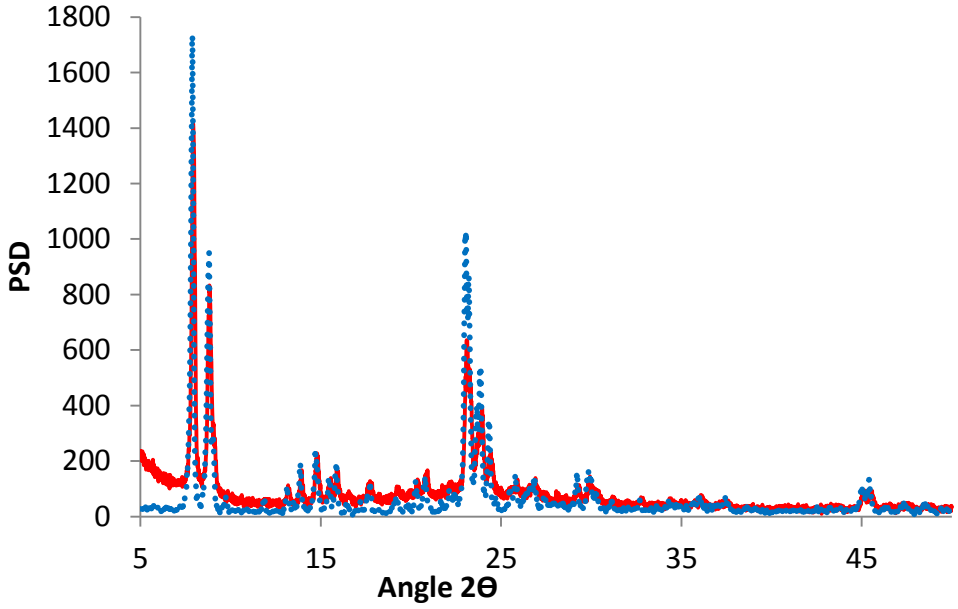

ZSM-5 had a median pore size of < 1 nm while the mesoporous catalysts had an average pore size between 2.6–4.0 nm. The large pore size of mesoporous catalysts is expected to reduce the diffusion resistance through the micropores to facilitate the transfer of the large molecules found in biomass pyrolysis products (e.g. anhydrosugars, phenols and oligomeric lignins). The apparent reactivity of these large molecules will be increased as more reactive sites are available on the surface and in the mesopores [131]. As the resistance to diffusion is reduced, larger molecules formed during pyrolysis are more likely to crack into smaller units that lead to aromatics rather than form coke outside the catalyst or remain unreacted [133]. The textural porosity of MSU-MFI is expected to facilitate easier transport of cracked molecules when compared with MCM-41 which as 1D channels as mesopores [126].

7.4.2 Pyrolysis-GC/MS

The products of fast pyrolysis of poplar with and without catalyst were analyzed using a GC/MS (Figure 7.4) Pyrolysis yielded a mixture of water, light gases such as carbon oxides, aldehydes, ketones, phenolics and anhydrosugars. Catalysis of pyrolysis products involves the homogeneous reactions of thermal decomposition of biomass into smaller oxygenated molecules. The small molecules diffuse into the catalyst pores and react at the active sites through a series of cyclo-oligomerization, decarbonylation and dehydration reactions to produce light hydrocarbons, aromatics, CO, CO_2 and water [95], [133].

Figure 7.3 Representative GC/MS chromatograms for comparison of products from (a) poplar pyrolysis (without catalyst) and (b) catalytic pyrolysis with M1

a

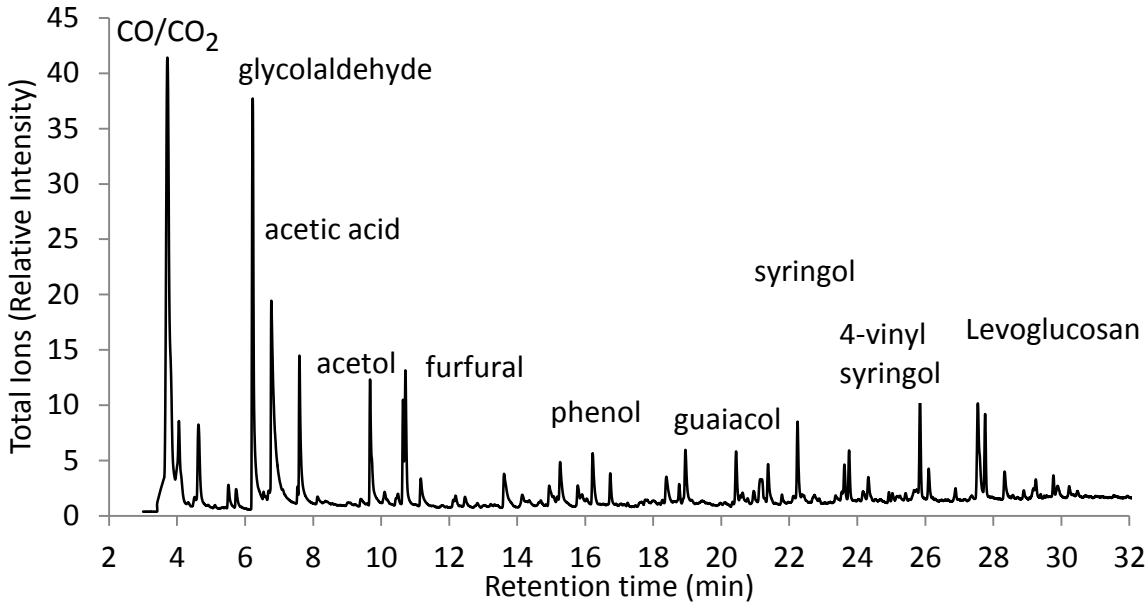

Figure 7.3 (cont'd)

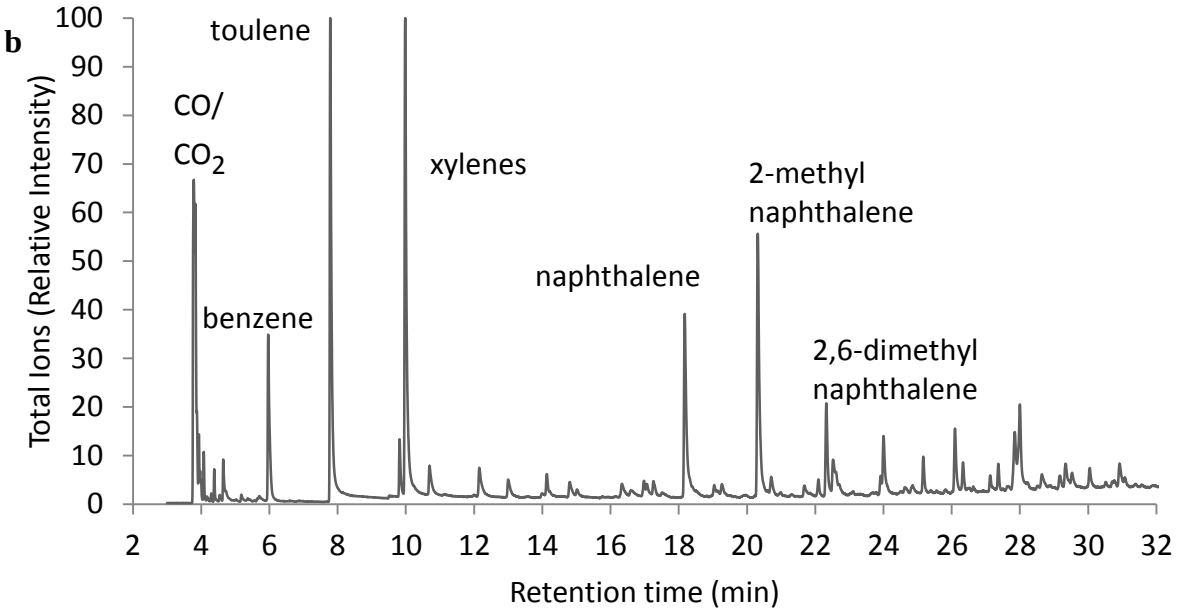

Compounds detected with retention times are as follows: (retention time)compound name, (4.0) Gases, CO, CO_2, (6.3) Glycolaldehyde, (7.1) acetic acid, (7.8) acetol, (8.1) 3-hydroxy-2-butanone, (9.9) acetic anhydride, (10.5) furfural, (11.2) 2-methyl-2-cyclopentenone, (12.1) cyclohexanone, (13.6) 3-methyl-1,2-cyclopentanedione, (15.5) phenol, (16.1) guaiacol, (16.5) 2-methoxy-4-methylphenol, (18.5) 4-ethyl-2-methoxy phenol, (19.0) 2-methoxy-4-vinylphenol, (20.5) eugenol, (22.1) syringol, (23.6) 2-methoxy-4-(1-propenyl)-phenol, (23.8) 1,2,4-trimethoxybenzene, (26.0) 5-tert-Butylpyrogallol, (25.8) 4-vinylsyringol derivatitive, (27.4) levoglucosan, (2738) 2,6-dimethoxy-4-(2-propenyl)-phenol.

Table 7.2. Comparative product yields for catalysis and pyrolysis of poplar with MFI catalysts (without Gallium)

Product distribution	M1	M2	M3	M4	M5	M6	ZSM5
Pyrolysis vapors	59.2±2.6	59.0±3.2	60.3±6.8	59.3±6.0	58.3±8.4	56.2±3.0	52.5±3.0
Char + Coke	40.8±1.9	41.0±3.9	39.7±6.2	40.7±3.9	41.7±6.2	43.81±3.9	47.5±3.0
Relative Aromatics yield	1.15±0.22	1.06±0.05	0.99±0.35	1.09±0.18	0.85±0.16	0.68±0.18	1.00±0.19

* Aromatic yield of 1.00 = 1.8% w/w dry biomass. All data in this study are an average of six replicates. Pyrolysis vapors includes condensable fraction (bio-oil) as well as non-condensable gases. Char + Coke includes char produced from pyrolysis and coke deposited on catalyst

Fig. 7.4. Carbon selectivity of condensable fraction for MFI catalysts (without Gallium). Carbon selectivity was defined as the moles of carbon in a chemical group divided by the total moles of carbon in the condensable product. *Average of six py-gcms replicates.

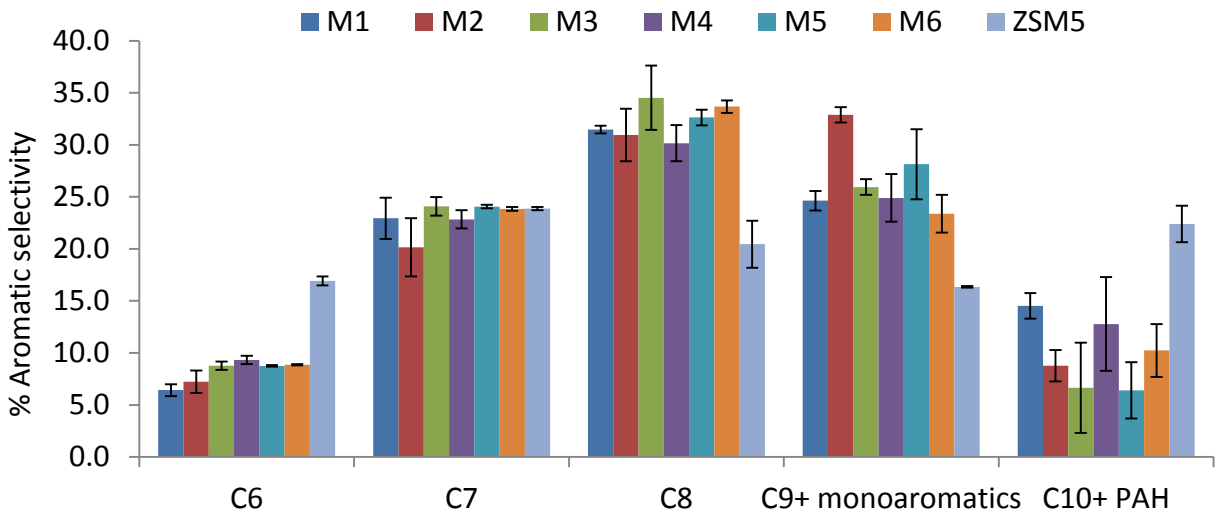

A comparison of the condensable product distribution is shown in Table 7.2 and Figure 7.4. The MSU-MFI catalysts produced less solid product (char and coke) and more vapors (condensable and non-condensable) than conventional ZSM5. The yield of aromatics was higher for the mesoporous catalysts M1 through M4 prepared with smaller polymer (by up to 15% for M1) when compared with microporous ZSM5. Catalysts M5 and M6 had larger pores and smaller micropore volume, which may have contributed to lower aromatic yields. Due to challenges associated with using the microscale setup of the pyroprobe-GC/MS system and inherent variability in biomass, the standard deviations on yield data were high [177], [178]. Therefore, a minimum of six replicates and often more, were tested to obtain more confident estimates of the average yield values (Table 7.2).

All mesoporous catalysts produced lower amounts of char and coke than microporous ZSM5. This corresponds with the results of a previous study with MSU-MFI catalyst for gas-oil cracking, where the coke accumulation was less than half of that of ZSM5 [174]. Additionally, the amount of coke on mesoporous catalysts is significantly affected by mesopore size,

recognizing that larger pores (5 nm and above) contribute to more PAH formation and coke, whereas all the catalysts in this study had pore sizes of less than 4 nm [109], [133]. Gayubo et al. have shown that part of the coke formed on zeolite catalyst surfaces is "soluble" and can be thermally disintegrated, especially at reaction temperatures of 650°C in a pyroprobe or 500-550°C in a reactor [179]. The "insoluble" coke deposits on the external surface and inside the micropores, where a combination of strong acidic sites with small apertures exists [138], [180]. Since the mesoporous MSU-MFI catalysts had lower microporosity, mesopore size less than 5 nm were used in a high temperature reaction, the combination of these factors may have assisted with lower coke accumulation on these catalysts compared with ZSM5.

Aromatic carbon selectivity is defined as the moles of carbon in an aromatic group divided by the total amount of carbon in the condensable product. The aromatic selectivity of C10 and higher polyaromatic molecules such as naphthalene and its derivatives was significantly higher for ZSM5. The pore diameter of ZSM5 is very close to the kinetic diameter of naphthalene at reaction temperatures. ZSM5 also has the largest volume of micropores which may have increased the selectivity for these molecules [104]. ZSM5 also showed a much greater selectivity for C6 (benzene) and C7 (toluene) while the larger pore MSU MFI catalysts were selective towards C8 (e.g. *p*-xylene) and C9 monoaromatics.

Correlation coefficients between the catalyst properties and pyrolysis products were determined (Table 7.3). Correlations may not provide conclusive evidence for proving a hypothesis but they may be used as quantitative indicators of trends observed in the dataset. The BET and external surface area, pore size and volume were positively correlated. Micropore volume and char plus coke production were negatively correlated to the surface area values while micropore volume itself showed a strong positive relationship with char and coke. Aromatics

production was negatively correlated with the pore size and surface area but showed positive relationship with micropore volume and total volume. Catalyst M6 with lowest micropore volume and largest pore size produced the highest coke and lowest aromatic yield amongst mesoporous catalyst varieties while ZSM5 with the largest micropore volume produced the highest amount of small aromatics such as C6 and C7 monoaromatics as well as coke.

Table 7.3. Correlations between catalyst properties and pyrolysis products

	BET Surface Area	Pore size	Pore Vol	Micropore Vol.	Ext surface area	Char+ Coke	Aromatics
BET Surface Area	1.00	0.79	0.77	-0.77	0.88	-0.53	-0.26
Pore size		1.00	0.65	-0.89	0.89	-0.62	-0.49
Pore volume			1.00	-0.89	0.88	-0.78	0.04
Micropore volume				1.00	-0.95	0.79	0.22
Ext surface area					1.00	-0.67	-0.33
Char + coke						1.00	-0.32
Aromatics							1.00

7.4.3 Gallium(III) Impregnated – MFI catalysts

We demonstrated above that a mesoporous MFI catalyst with tunable porosities may be used for catalytic fast pyrolysis to achieve BTEX yields greater than conventional ZSM5. Besides tunable catalyst porosity, the use of promoters (such as dehydrogenating metals on acidic catalysts) may further increase aromatic hydrocarbon yields. Gallium (Ga) is a byproduct of aluminum production from bauxite. It provides the dehydrogenation functionality in a catalyst and has been previously shown to enhance the catalytic transformation of compounds found in pyrolysis products to mono-aromatic molecules [109]. ZSM5 (0.5 and 2.5% Ga) and mesoporous MSU-MFI catalyst M1 (0.25, 0.5, 1, 2, 3% Ga), were doped with gallium in the form of aqueous gallium nitrate using the incipient wetness method. X-ray diffraction analysis showed no major in crystal structure due to presence of Ga. BET analysis showed that a 3% Ga deposition reduced the surface area by 10-30 m^2/g. ICP-OES was used to confirm the Ga loading on catalysts. X-ray

photoelectron spectroscopy confirmed the presence of Ga on catalyst surfaces with a binding energy of 1118 eV corresponding to Ga_2p_3, which may be attributed to an oxidation state of 3+ on catalyst surface [109], [122], [181]. Catalytic pyrolysis experiments were conducted with Ga loaded catalysts to evaluate its effect on the fast pyrolysis products of poplar.

Incorporation of gallium on ZSM5 catalyst produced a significant change in the yield of aromatics. In preliminary experiments with ZSM5 (not reported), 0.5% Ga showed a significant increase (~30%) in yields of aromatics over that without any Ga. However at a 2.5% loading a slight decrease of 5% in aromatic yields was observed. This may be a result of Ga ions replacing H^+ on the catalyst surface, thereby reducing its acidity as well as its cracking ability [109]. The overabundance of gallium, which acts as a Lewis acid, may reduce the Bronsted acidity of the catalyst. For highly acidic catalysts, a greater amount of Ga may be deposited without significant reduction in catalyst acidity; a less acidic catalyst may show loss of catalytic cracking activity even at low levels of Ga. Kwak et al. [182] have proposed that catalysts having $Ga/(Ga + H^+)$ ratios between 0.4 and 0.5 are desired, while Al-Yassir et al. [183] have shown that a ratio of Ga/(Al + Ga) equal to 0.3 gives optimum aromatization performance. Several researchers have studied metal loaded ZSM5 for applications in pyrolysis without giving due consideration to the above effect of metal loading on catalyst activity, and hence made conflicting observations about the effects of metals on zeolite catalysts [184].

To study the effect of Ga loading on the mesoporous MFI catalyst, M1 with five levels of Ga was tested: 0.25, 0.5, 1, 2, and 3%. Catalytic pyrolysis experiments with poplar as feedstock and Ga MFI catalyst showed that incorporation of Ga increased aromatic yields up to 1% loading, beyond which a decrease in yield was observed (Table 7.4). The char yield was also

affected and decreased with an increase in Ga loading. The selectivity for smaller C6 and C7 aromatics increased slightly with Ga loading, as shown in Figure 1.10. The change in aromatic selectivity due to the addition of Ga is strongly dependent on the preparation route and has been shown to be small when Ga is added post-catalyst synthesis [183]. The M1 catalyst without any Ga produced the highest yields of C8 aromatics.

Table 7.4 Comparison of aromatic yields from poplar fast pyrolysis with M1 catalyst loaded with different quantities of Gallium (by weight).

Product distribution	Control	0.25%-Ga	0.50%-Ga	1.0%-Ga	2.0%-Ga	3.0%-Ga
Pyrolysis vapors	59.2±2.26	59.9±0.9	59.4±0.11	60.8±1.7	61.4±0.9	61.6±1.28
Char + Coke	40.8±1.9	40.1±0.9	40.6±1.7	39.2±1.28	38.6±1.0	38.4±0.16
Relative Aromatics yield	1.00±0.09	1.15±0.04	1.16±0.12	1.21±0.05	0.97±0.30	1.01±0.07

* Aromatic yield of 1.00 = 2.1% w/w dry biomass.

Figure 7.5 Carbon selectivity of condensable fraction for MFI catalysts (with Gallium). Carbon selectivity was defined as the moles of carbon in a chemical group divided by the total moles of carbon in the condensable product. *Average of six py-GC/MS replicates.

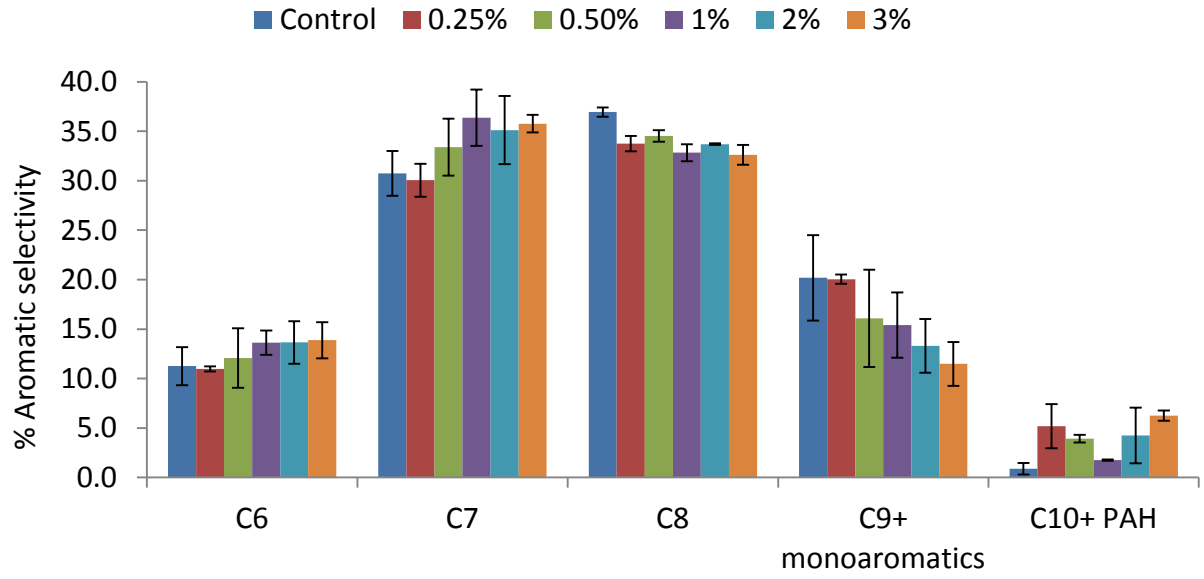

7.4.4 Pathways – Catalytic upgrading of biomass pyrolysis

Catalytic upgrading of biomass pyrolysis has been well studied. Catalysts break down large molecules found in pyrolysis products to smaller hydrocarbon fragments forming a

‘hydrocarbon pool’ [102]. These intermediate oxygenates then diffuse into the catalyst pores and are condensed into aromatic molecules and olefins due to the oligomerization and cyclization functionalities of the catalyst [91]. The hydrocarbon pool may consist of polymethylbenzene or benzenium cations or carbenium ions or naphtenes in pseudo-equilibrium [105], [106]. Monocyclic aromatics and their reaction with other oxygenates leads to the production of naphthalenes and other polycyclic aromatics. Wang et al. have suggested that the reactive hydrocarbon pool intermediates for the methanol to olefins process is between 5.7 and 6.0 Å, i.e. similar to the kinetic diameters of benzene, indene, 2-furanmethanol and 4-methylfurfural[103], [104]. The intermediate oxygenates may exist in the hydrocarbon pool in the form of polymethylbenzene or benzenium cations or carbenium ions or naphtenes in pseudo-equilibrium[105], [106].

Olefins are precusors to producing aromatic molecules and many studies have shown that increasing the olefin content in catalyst feed increases the aromatics in catalysis products [91], [107], [108], [109]. However acidic catalysts are more selective towards cracking rather than dehydrogenating to produce olefins. Hence a second functionality (in addition to the cyclo-oligomerization) is desired to promote olefin and aromatic production. Dehydrogenating metals provide the Lewis acid functionality to an acidic MFI (Mordenite Framework Inverted) type catalyst such as HZSM-5 with high Bronsted acid functionality (due to presence of protons)[183]. Bronsted acid sites catalyze oligomerization and ring closure, while metals act as dehydrogenating sites or as entrance sites for hydrogen spillover [109], [110], [173], [182]. Lewis acids sites may have a synergistic effect with Bronsted acid sites by converting a greater amount of alkanes to olefins for conversion to coke and aromatics. At the same time the presence of metals on zeolites reduces the available Bronsted acid sites, decreasing coke production.

Addition of a dehydrogenating metal on acidic zeolites promotes conversion of parrafins to olefins as well as olefins to aromatics by acting as a site for removal of excess hydrogen atoms produced as a result of the processes [185]. It also moderates the strong Bronsted acidity that is responsible for coke production on zeolites. Al-Yassir et al. concluded that the high aromatization acitivity of metal (Ga) loaded catalysts was primarily due to the presence of highly dispersed, reducible, extra-framework Ga_2O_3 species which act as Lewis dehydrogenating sites, in close proximity to zeolitic Bronsted acid sites [183]. Tagliabue noted that for dehydrogenation combined with cyclo-oligomerization activity, bi-functional catalysts that combine shape-selective acidic zeolites with a dehydrogenating metal or oxide were the most effective [108]. Metals may act as lewis acid sites (dehydrogenation effect), which are electron pair acceptors, and may have strong affinity for hydride ions released during the conversion of parrafins to olefins as well as the transformation of olefins to carbenium ions through intermediate dienes[110]. It has also been suggested that metals act as sites for combing hydrogen ions as molecules that can be desorbed, known as the back hydrogen spillover effect. In the absence of these sites, free hydrogen ions may be attacking carbenium and benzenium ions and producing light olefins though β–scission, and eventually coke [105], [110]. Aromatics and coke production from polymerization of furans have been suggested to be the major competing reactions[91]. Tagliabue suggested that olefins to aromatics is thermodynamically preferred and a tendency towards higher coke formation[108]. It is speculated that coke is produced from acid catalyzed polymerization of furans to oligomers [111], [112].

Todorova reviewed and studied the use of Pt to increase activity and stability of MFI catalysts [173]. However, Pt -loaded zeolite catalysts have a high, undesired selectivity for methane and ethane, due to strong hydrogenolysis [173], [186]. In contrast, Zn loaded zeolites

show high aromatization potential with lower hydrogenolysis activity [187]. However, for upgrading pyrolysis oil, Zn or Mn incorporated in HZSM-5 increased PAH production [115], [121]. French and Czernik observed that ZSM-5 loaded with Ni produced the least coke and highest hydrocarbon yields [184]. Many studies have demonstrated the dehydrogenating potential of Ga doped on a shape-selective acidic zeolite catalyst [108], [119], [172], [173], [182]. Tagliabue noted that for dehydrogenation combined with cyclo-oligomerization activity, bi-functional catalysts that have shape-selective acidic zeolites with a dehydrogenating metal or oxide were the most effective [108]. They presented two examples of bi-functional catalyst use: the Cyclar process, where Ga/ZSM-5 converts a saturated stream of LPG to BTEX; and the Alpha process where Zn/Al_2O_3/ZSM-5 converts olefins to BTEX. Park et al. observed that gallium (Ga) combined with strongly acidic zeolite such as ZSM-5 decreased catalyst coking, production of CO/CO_2 and alkanes but increased aromatics and alkenes such as ethene and propene for catalytic upgrading of pyrolysis vapors [109]. In addition, catalysts such as platinum-tin-alumina supported catalysts are widely used in the petroleum industry for paraffin dehydrogenation and have been extensively studied [188]. Platinum on gallium zeolites improve aromatic yields and reduce undesired reactions[189]. The deposition of bimetallic Pt/Ga on ZSM-5 has been shown to have greater selectivity for desired aromatic reaction over just Ga-ZSM-5 for ethane aromatization[189]. However such bimetallic zeolites have not been investigated for their effect on the selectivity of aromatics or coke production for biomass pyrolysis applications.

7.5 Summary

Zeolite catalysts such as ZSM-5 provide the functionality necessary to crack, deoxygenate and cyclize biomass pyrolysis products to aromatic hydrocarbons. Due to small pores (micropores) of ZSM-5 and absence of meso or macropores, many intermediate and primary products of pyrolysis remain unreacted. Therefore a mesoporous MSU-MFI catalyst was developed which possesses the activity and micropores of ZSM-5 catalyst but also the mesopores to facilitate transport and cracking of larger reactant molecules. We have demonstrated that such mesoporous MFI catalysts may be synthesized using silylated polymeric mesoporogens and the size of the polymer and reaction conditions may be adjusted to affect the size and volume of mesopores. These mesoporous MFI catalysts give higher yields of C8 and C9 mono-aromatics when compared with conventional ZSM-5. The overall aromatic yields for the mesoporous MSU-MFI catalyst are higher and the char yields are lower than that of the microporous ZSM-5. Addition of a dehydrogenating metal on such a catalyst further improves yield of aromatics. Gallium was deposited in ZSM-5 as well as the mesoporous MFI catalyst at various loadings and its effect on the products of catalytic fast pyrolysis of biomass was tested. Gallium (up to 1% w/w loading) increased aromatic yields significantly, while maintaining low char yields. Thus, a bifunctional mesoporous MFI catalyst may be used to increased conversion and aromatics yield over a conventional ZSM-5 catalyst. In addition, the decreased char production will ensure longer active life for catalysts and reduce losses due to deactivation and regeneration.

CHAPTER 8. ISOBUTYLENE CONVERSION TO AROMATICS USING A BIFUNCTIONAL MESOPOROUS AND OTHER CATALYSTS

8.1 Introduction

Aromatic hydrocarbons are basic building blocks of the petrochemical industry. They are also used as additives to gasoline to enhance the octane rating of fuels. The production of aromatics from renewable feedstocks will enable a sustainable route to chemical traditionally produced from petroleum sources. One such green process is biomass pyrolysis followed by catalysis. However, the yields of aromatics from this process are low for most biomass, making the process economically uncompetitive with traditional petrochemical sources. Biomass has a high O/C and a low H/C ratio, an indicator of its low potential to generate aromatics. On the other hand, C4 compounds like isobutylene are already hydrocarbons, which can be readily cyclized and dehydrogenated over zeolite catalysts to produce aromatics, specifically *p*-xylene. Isobutylene can obtained by the dehydration of isobutanol, which is turn, may be produced from biomass fermentation. Thus an alternative, green and sustainable route to aromatics not involving biomass pyrolysis can be developed. Therefore the objectives of this work were to assess the yields and economic feasibility of existing zeolite and novel metal-doped MSU-MFI catalysts for isobutylene conversion to aromatics.

Scheme 8.1 Isobutylene to aromatics

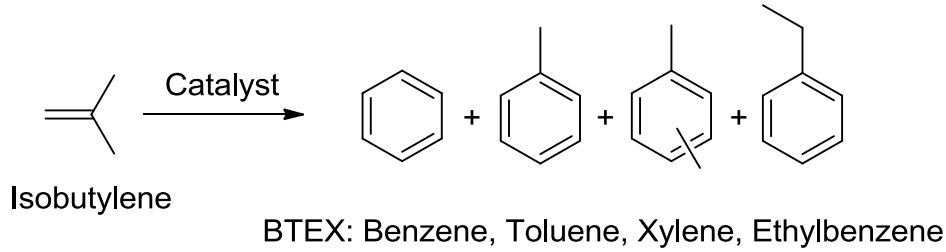

The maximum theoretical yield of a monoaromatic like *p*-xylene from isobutylene is 0.95 grams *p*-xylene per gram of isobutylene. Approaching this yield for a single type of molecule is

unlikely as the zeolite catalysts used are prone to the co-production of coke, polyaromatics such as naphthalene, benzene, toluene, ethylbenzene as well as *m*- and *o*-xylene. Though coke production is not as severe with isobutylene feeds when compared to biomass pyrolysis gas, significant coke encapsulation and catalyst deactivation does occur. Catalyst reactivation can be performed in a combustion unit at the expense of equipment capital and the need for a fresh catalyst feed stream to makeup for loss due to abrasion. As the overall process economics are strong functions of product yield and catalyst deactivation, catalysts were studied to determine product and coke yields when isobutylene is used as feedstock.

A review of literature showed that oligomerization of isobutylene to isooctane (C12-trimers) has been a subject of many studies [190], [191], [192]. However, only three studies were found on the conversion of isobutylene to aromatics [193], [194], [195]. A 2009 study reviewed the use of Mo_2C on ZSM5 for converting paraffins to aromatics and observed that reactions of isobutylene over ZSM5 at 500°C gave a conversion of over 90% with the main products being xylene (selectivity=26%) [195]. In another study from 2004, aromatization of isobutylene was investigated using ZSM5 as well as physical mixtures with metal oxides of Ga, Cu, and Zn [194]. High conversions (90.5%) were obtained at 500 °C with a high yield (28.5%) for aromatic molecules. For a 90 min catalyst on-stream time, no appreciable carbon deposition on the catalysts was observed. A 1978 study explored the use of bismuth oxide-Pt/Al catalyst and achieved conversion of 50% and a selectivity of 60% for *p*-xylene at 600 °C [193]. At MSU, our previous experiments with biomass pyrolysis and a mesoporous zeolite catalyst developed in our lab, Ga-MSU-MFI, showed that aromatic yields higher than ZSM5 could be obtained with reduced production of undesired coke. Building on the information presented above, the

following experiments explored bismuth oxide-Pt/Al, Ga-loaded ZSM5 and Ga-loaded MSU-MFI catalysts for conversion of isobutylene to aromatics.

8.2 Methodology

In order to determine the costs of isobutylene conversion to BTEX, mass and energy balances must be performed on key unit operations within the overall process. In particular, the reaction yields for aromatics and coke are needed in order to adequately assess the cost of feedstock. Higher yields of aromatics will result in lower feedstock flows and thus reduced feedstock costs. To this end, two bench-scale systems were devised to measure the yields of desired and undesired product. Figure 8.1 depicts the two systems that were constructed to gather the mass and energy balance data needed to inform the economic analysis.

Figure 8.1 A:Pulse injection system, B: Continuous flow system.

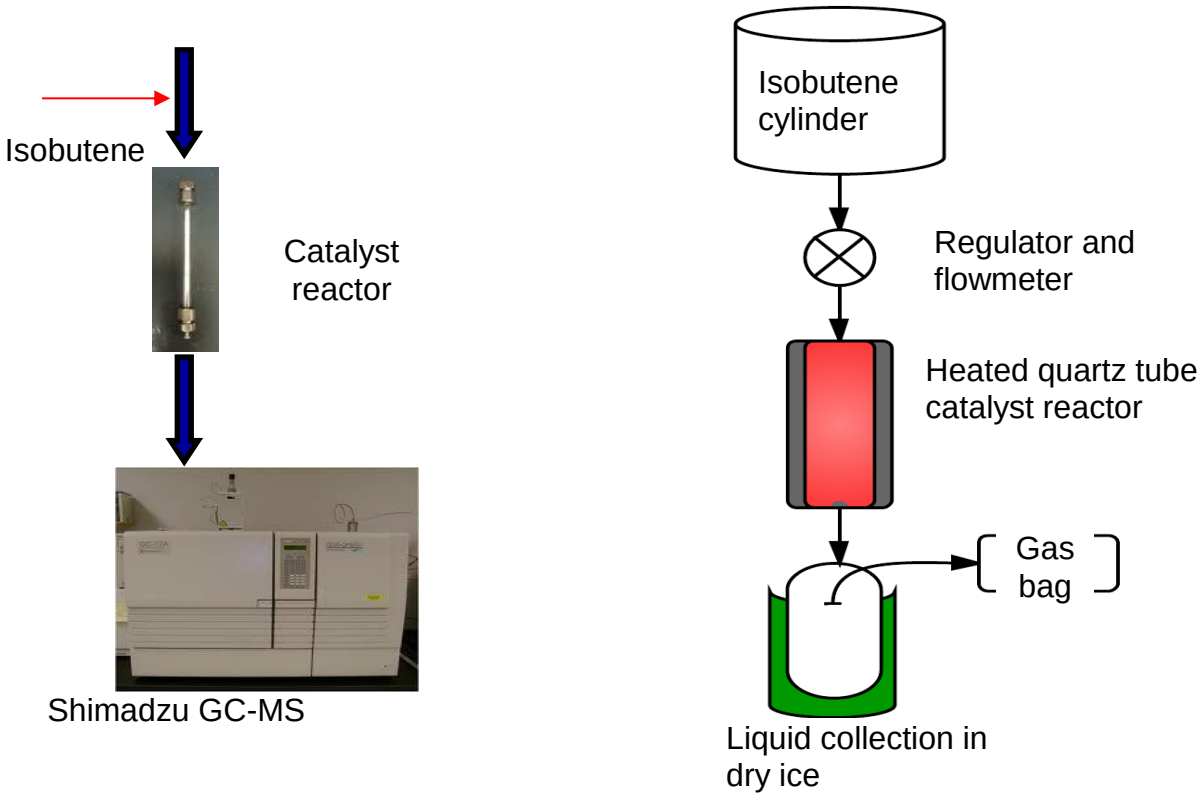

In the pulse injection system, catalyst was loaded the reactor connected at the inlet of the GC/MS. Helium flow was maintained at a zero split ratio. Sample was injected into the helium stream upstream of the catalyst reactor. The products formed over the catalyst carried over to the GC inlet and were analyzed by a rtx-1701 column and mass spectrometry. The GC/MS was run using the program described in earlier chapters. The continuous flow system consisted the catalyst reactor independent of the GC/MS. Isobutene gas at low space velocities (2 mL/min) was fed directly from a cylinder. After equilibration, samples were collected at the exit of the catalyst reactor using Tedlar gas bags for volatile gases and liquid collection vessel cooled with dry ice. Liquid and gas samples were both injected into the GC/MS for analysis.

8.3 Results

8.3.1 Pulse injection-GC/MS setup

An external catalyst reactor interfaced to a GC/MS (Figure 1A) was used for preliminary studies. Isobutylene gas (0.05 to 0.1 ml) was pulse injected (single shot) into a helium stream of gas that passed over a catalyst bed. The catalyst-bed reactor consists of a heated quartz tube that is 1 cm in height, and 3 mm in inside diameter. At 550°C, high yields of BTEX aromatics were observed as shown in Table 8.1.

Table 8.1. Mass yields from isobutylene catalysis. Yields are mass of product divided by mass of isobutylene reacted.

Reactant	Catalyst	BTEX Yield wt. %	Unknown Gases + Coke Yield (by difference) wt. %
Isobutylene	ZSM5	31.9	10.7
Isobutylene	1%Ga/ZSM5	43.3	8.0
Isobutylene	1%Pd/ZSM5	30.7	5.4
Di-isobutylene	1%Ga/ZSM5	10.4	NA

8.3.2 Continuous flow system

Though the pulse system is convenient for screening catalysts for isobutylene production, it is not convenient for examining coke yields or rates of product formation. In order to measure coke yields and catalyst deactivation rates, a flow reactor was assembled as shown in Figure 8.1. In this setup, a steady stream of isobutylene gas was reacted continuously with the catalyst over a known time as opposed to pulse injections. This setup is ideal for testing factors important for process design such as catalyst on-stream time, deactivation rate and aromatic yields at different gas flow rates. Unlike the pulse system, the continuous reactor setup produced a significant amount of liquid product after condensation. The condensed product was collected and diluted with methanol for analysis by GC/MS. Non-condensable product was collected in gas bags that were attached to the end of the condenser and gaseous product composition was determined using GC/MS. External standards for BTEX and isobutylene were used for calibration to quantify aromatics and olefins. After the reaction, the catalyst was recovered from the reactor and regenerated by combustion in a TGA (thermal gravimetric analyzer) to determine the coke yield. BTEX yields, coke yields, and gas composition are reported in Table 8.2.

Preliminary experiments with the catalyst reactor-GC/MS-pulse injection setup generated high product yields as shown in Table 8.1. However, as can be seen in Table 8.2, these results could not be replicated in the larger-scale continuous setup at this time, due to challenges with controlling feed rate, and losses during product condensation and collection. Improvements to the recovery yield of the condensation and collection system are being attempted.

ZSM5 produced higher BTEX yields of 17 % wt. of feed compared with ~13% for MSU-MFI (Table 8.2). However, MSU-MFI generated greater olefins of 48% compared with 33% for ZSM5. Addition of gallium (Ga, provides dehydrogenation functionality) improved BTEX as

well as olefin yields for both catalysts. Benzene selectivity was very high for ZSM5 and increased with addition of Ga. Xylene and C9 aromatics (e.g. trimethylbenzene) selectivity was higher for MSU-MFI. Although the ratio of *p*-xylene to ortho and meta isomers could not be determined in the current study, a significant fraction may be expected to be *p*-xylene, and may be expected to increase with decreasing feed rates. The 'effectiveness factor' for *m*-xylene on ZSM5 was found to be 0.1 indicating high diffusion resistance, 0.4 for *o*-xylene and 1.0 for *p*-xylene indicating negligible diffusion resistance, which means there is a very high probability of *p*-xylene being formed and desorbed from the catalyst surface compared with *m*- or *o*-xylene [153]. Polyaromatic hydrocarbons (PAH) such as naphthalenes were not observed in the condensed product from continuous experiments, although they were detected in the pulse GC/MS experiments. Low yields of condensed product and absence of PAHs may be a consequence of condensation on the cold tubing that connects the reactor to the condenser. Mass loss due to absorption to the rubber stopper on the top of the cold trap is a second explanation for low yields. Losses may also have occurred due to adsorption on the walls of gas bags and syringes used for transferring samples to the GC/MS for analysis. BTEX yields greater than 28% have been demonstrated in other studies [194], [195] for isobutylene over ZSM5.

One explanation for the difference in yields involves the contact time between the reactant and catalyst. The feed rate in our experiments was maintained at a weight hourly space velocity (a quotient) of 12.5 (or a gas hourly space velocity of 2,000). Due to limitations of the setup, the feed rate could not be controlled accurately at lower space velocities. In experiments by another group with ZSM5 and pyrolysis gas, it has been shown that very low space velocities (< 2) are necessary for high xylene yields and even small increases in feed rate alter the product composition drastically [91].

Table 8.2 Yields and product composition for the continuous reactor experiments involving isobutylene conversion over solid catalysts.

Product composition (wt. % of feed)	ZSM5	1%Ga-ZSM5	MSU-MFI	1%Ga-MSU-MFI
% Condensable (liquid) product	20.92	21.63	16.35	17.98
% Coke	0.97	0.82	0.67	0.55
% Gas (by difference)	78.11	77.55	82.98	81.47
Gas composition (% peak area)				
% Alkanes	39.30	32.93	33.77	27.64
% Olefins	52.22	56.15	57.78	66.39
% Misc. hydrocarbons	8.47	10.92	8.45	5.08
Liquid composition (% peak area)				
% C6 aromatics	36.88	44.09	5.37	12.52
% C7	16.46	20.72	25.40	26.50
% C8	28.51	24.14	45.70	44.65
% C9 + mono-aromatics	12.92	8.80	23.47	11.01
% C10+ poly-aromatics	0.0	0.0	0.0	0.0
% Unknown	5.23	2.25	0.06	5.31
BTEX yield (wt% of isobutylene)	17.12	19.24	12.50	15.04
Olefins yield (wt% of isobutylene)	32.90	43.55	47.95	54.09

Figure 8.2 Comparison of gas and liquid product chromatograms from continuous experiments.

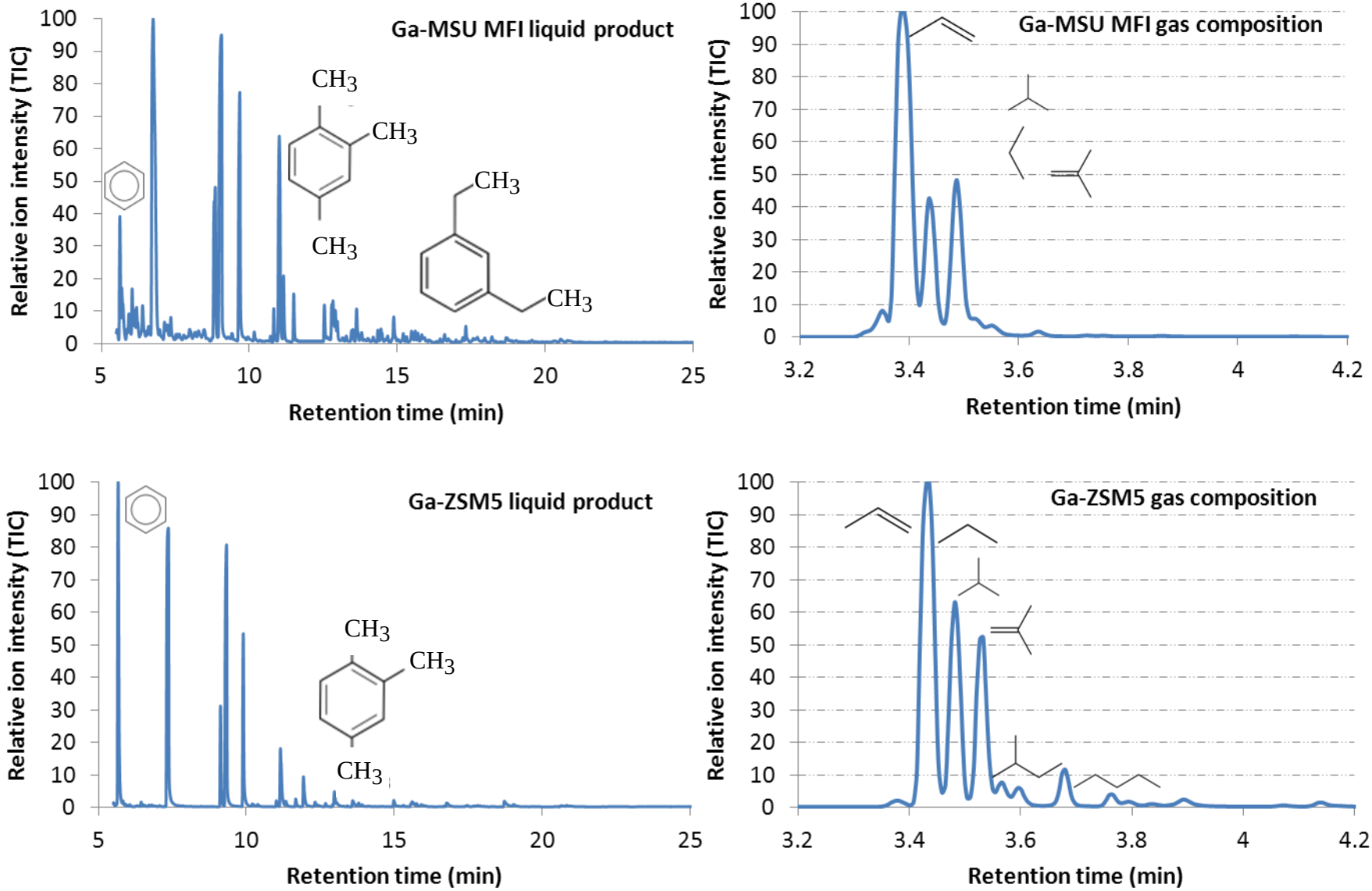

8.3.3 Other catalyst systems

Besides zeolite-type catalysts, a bismuth oxide-platinum-alumina catalyst was explored for *p*-xylene production [193]. In preliminary experiments in our lab using the pulse injection method, significant quantities of xylenes were produced with a large amount of isobutylene feed remaining unreacted (Figure 8.3). Quantification data for these experiments was not obtained with reasonable accuracy. However, this catalyst has been shown to have good selectivity to *p*-xylene in a previous study [193]. Because of the high apparent selectivity towards *p*-xylene, a new variant (composition) of this catalyst is being developed. (Compound) and (% area): Isobutylene 67.2, Benzene 1.82, Methyl hexadienes 9.77, Toluene 2.43, Xylenes 9.02, Naphthalenes 2.83.

Figure 8.3 Chromatogram and product composition for spike injection experiment with Bismuth oxide-Pt-Al catalyst.

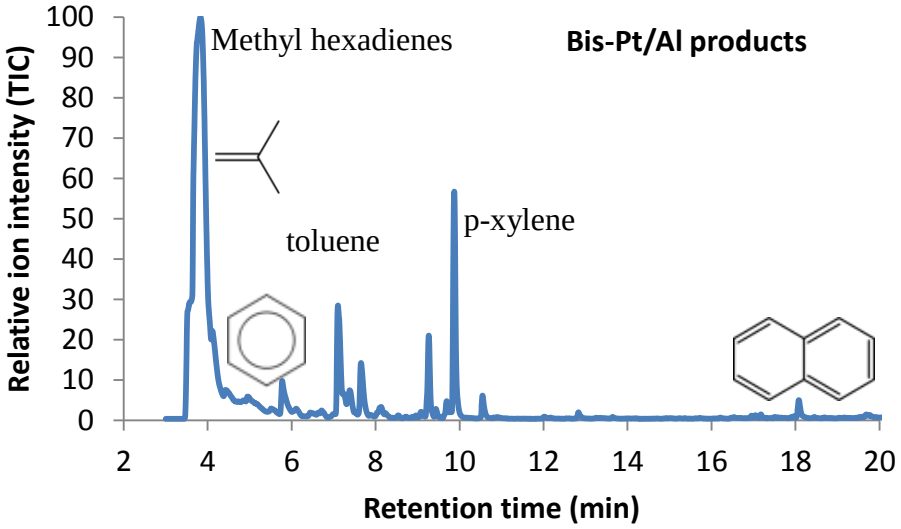

8.3.4 Preliminary Economic Analysis

A thorough technoeconomic analysis for the process is being developed by Mr. Chai Li and Dr. Chris Saffron. A preliminary evaluation of the minimum cost of *p*-xylene can be stoichiometrically made by calculating the cost contribution from the feedstock, i.e. isobutylene. Cost is minimized in the limiting case when isobutylene is completely converted to desired *p*-xylene without the formation of carbonaceous coke. Computation of the cost contribution of isobutylene to *p*-xylene is important as it provides the lowest possible cost for *p*-xylene. In order to determine the cost of isobutylene, ICIS Chemical Pricing was consulted to determine the price of *i*-butanol, which is the precursor to isobutylene (Scheme below).

Scheme 8.2 Bio-derived iso-butanol to p-xylene

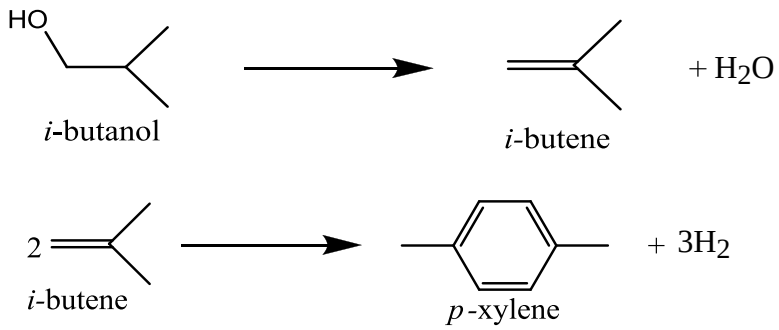

Using an *i*-butanol price of $0.60 per lb and assuming stoichiometric conversion, the cost of isobutylene is $0.79 per lb. Subsequent conversion of isobutylene results in a cost of $6.02 per gallon of *p*-xylene, which is much higher than the petroleum-based selling price of about $3.60 per gallon. Table 8.3 the effect of variable *i*-butanol price on the cost of isobutylene and *p*-xylene. This approach computes the minimum cost of *p*-xylene, and does not include utilities, labor, supervision, taxes, or depreciation.

Table 8.3. Cost of *p*-xylene assuming stoichiometric conversion of *i*-butanol to isobutylene.

i-butanol $/lb	*i*-butanol $/gal	*isobutylene* $/lb	*p*-xylene $/lb	*p*-xylene $/gal
0.2	1.34	0.26	0.28	2.01
0.4	2.67	0.53	0.56	4.01
0.6	4.01	0.79	0.84	6.02
0.8	5.34	1.06	1.12	8.03

From the stoichiometric analysis, clearly an inexpensive source of isobutylene is needed in order for this process to be cost competitive with petroleum-derived *p*-xylene.

8.4 Conclusions and continuing work

Aromatics may be generated from catalysis of bio-derived hydrocarbons (such as isobutylene from i-butanol) with higher yields compared to biomass pyrolysis–catalysis. Limitations of the continuous experimental setup hindered collection of good yield data. Experiments will be repeated once a new condenser system is installed. This may provide an explanation for the discrepancy between the pulse system and the continuous system as the full extent of the aromatic product formed is not being recovered during collection.

Gallium loaded MFI/ZSM5 catalysts were effective in improving aromatic yields and decreasing coke compared to catalyst without Ga. Bismuth oxide-Pt-Alumina catalyst system showed good activity for isobutylene to aromatics as well. A preliminary economic analysis showed that an inexpensive feedstock is desired to make the process competitive with existing petroleum-based aromatics.

CHAPTER 9. SCALE-UP EXPERIMENT: EFFECT OF TEMPERATURE AND RESIDENCE TIME IN A SCREW-CONVEYOR PYROLYSIS REACTOR

Abstract

The fast pyrolysis of spent coffee grounds using a compact, transportable, screw conveyor reactor for producing bio-oil was studied. A two-factor, five-level, central composite response surface experiment was completed to formulate a statistical model that relates reactor temperature (429-550 °C) and screw speed (40-75 rpm) to bio-oil yield and quality. Regression analysis of model fits with experimental data showed that temperature and screw speed had a significant effect ($p<0.05$) on bio-oil yield. Furthermore, the organic fraction of liquid bio-oil was more abundant when the reactor was operated at lower temperature. In addition to containing oxygenated organic compounds typical of bio-oils, spent coffee bio-oil also contains more hydrophobic compounds such as fatty acids, fatty acid esters, medium-chain parrafins, olefins, and caffeine. Because of the abundance of spent coffee grounds and the quality of its bio-oil, this waste stream offers potential as a valuable bioenergy feedstock.

9.1 Introduction

Plant biomass is currently the only renewable feedstock that can lead to hydrocarbon fuels and meet worldwide energy demands. Fast pyrolysis is an efficient technology for converting renewable plant biomass into bio-oil, which can be used as a fuel intermediate to displace petroleum in the liquid fuels supply chain. Biomass fast pyrolysis involves the rapid heating of biomass in an inert atmosphere at temperatures between 400 and 600°C to produce solid char, combustible gas and liquid bio-oil. The fast pyrolysis of biomass to bio-oil has many advantages, including the bulk and energy densification of biomass, simple operation, flexible conversion of different biomass varieties and relatively low capital costs. Further, the char co-product may be used as an energy source, adsorbent, soil amendment or for carbon sequestration.

For these reasons, this technology can be distributed into rural locations of the world that may be economically disadvantaged.

Coffee is one of the largest consumed agricultural products with over 20 billion pounds (9 billion kg) produced worldwide [196]. Although some waste coffee is used in composting and as animal feed, most is burned as a waste [197]. Coffee contains between 11 to 20% oil by weight while spent coffee grounds (SCG) have been found to contain around 15% [198]. Studies have evaluated biodiesel production [198], [199] and extraction of valuable chemicals such as palmitic acid from SCG [200], [201]. Charcoal produced from combustion of SCG has been used as an adsorbent [202] and has been used for removing pollutants such as phenol and harmful dyes such as indigo carmine from aqueous streams [203].

Fast pyrolysis of SCG using a fluidized bed reactor was used to study the bactericidal and insecticidal properties of bio-oil [204]. Pyrolysis of fresh coffee grounds in a fluidized-bed reactor has also been examined [205]. Unlike the previous studies of coffee pyrolysis, our study examines the use of a transportable screw-conveyor reactor instead of a fluidized-bed reactor (Figure 9.1). The pilot-scale screw-conveyor fast pyrolysis reactor is capable of processing one to ten kilograms of biomass per hour, depending upon the flowability of the feedstock. Because this reactor does not use a sand bed as a heat transfer medium, no inert gas is needed for fluidization. Instead, an extruder screw presses biomass against the heated surface of the reactor barrel. A variable speed motor controls the rotation rate of the screw and hence the residence time of the solid biomass. A gravimetric pre-feeder enables accurate biomass feeding without undesired solids bridging. Because of compact and simple design, this reactor could be made transportable or deployed in regional centers.

This study assessed the effects of reactor temperature and residence time on the overall and organic yield of SCG-derived bio-oil produced using a screw-conveyor pyrolysis reactor. The objectives were as follows: 1) demonstrate high bio-oil yields from SCG using a screw-conveyor pyrolysis reactor; 2) measure the effect of temperature and determine the optimum temperature for maximum bio-oil yield; 3) determine the effect of screw speed, which controls solids residence time on bio-oil yield; and 4) measure the quantity and examine the composition of the water-free, organic, bio-oil fraction. Experiments were conducted using a circumscribed central composite rotatable design (CCCRD) and response surface methodology (RSM) [206]. Response surface methods have been used in a wide variety of areas including agriculture, chemistry, chemical engineering, and mechanical engineering such as coal pyrolysis [207], biodiesel production [208] and adsorption [209]. A response surface model was used to predict bio-oil and biochar yields and to find the temperature and screw speed that maximizes these yields and improves the likelihood of establishing a commercial bioenergy system from SCG.

9.2 Materials and Methods

9.2.1 Biomass

SCG, a food waste, were used as feedstock for biomass pyrolysis experiments. Freshly spent coffee grounds were shipped frozen from The Coca-Cola Company (Atlanta, GA). The SCG were dried at 60°C and stored at that temperature to maintain low moisture content until usage in experiments. After drying, the moisture contents of duplicate 2.5 g samples were measured at 130°C using a moisture analyzer (Sartorius MA-30, Göettingen, Germany). Particle size distribution was estimated using ASTM D1511-10, in which biomass is passed through sieve trays of successively smaller mesh size on a shaker table [210]. A thermogravimetric analyzer (TGA, CH-8603 model, Mettler-Toledo, Schwerzenbach, Switzerland) was used to plot

the weight loss curves and derivative curves (DTG curves) for all samples. This analysis was used to adjust the temperature settings of the screw-conveyor reactor and negate premature pyrolysis in the feed port which results in undesired solids bridging. In the TGA, nitrogen was used as the purge gas with a cell and furnace flow rate of 20 mL/min. The furnace was initially purged with nitrogen for 10 minutes at the beginning of each experiment, and samples were then dried in the furnace for 25 minutes at 105 °C. DTG curves were obtained using a temperature profile of 10 °C/min, from 105°C to 800°C, directly following the drying phase.

9.2.2 Reactor

The major parts of this reactor include: gravimetric pre-feeder, screw-conveyor reactor, char trap, bio-oil condensors and traps, electrostatic precipitator (ESP) and a flame calorimeter as shown in Figure 9.1. Each reactor run was conducted with approximately 1 to 1.5 kg of SCG in the temperature range of 450 to 550 °C, as recommended for maximum bio-oil yields [211], [212]. Nitrogen was used only for purging oxygen from the system to provide an inert atmosphere before each run. Occasionally, nitrogen is pulsed through the reactor inlet to regain flow in the event of solids bridging. Six electrical band heaters were divided into three heating zones (1st, 2nd, 3rd), where each zone has two heaters (Figure 9.1). The temperatures of the band heater sections were monitored by thermocouples and controllers. The first two heating zones were set to 200 and 350 °C. The final heating zone temperature was varied from 450 to 550°C and is the input parameter to the CCCRD. The screw rotation rate was varied between 45 and 75 rpm.

Bio-oil yield was measured from the collection traps attached to the condensers and electrostatic precipitator. Most of the pyrolysis gas was condensed by the two bio-oil condensers and collected in the glass jars used as traps. The two condensers were controlled at 25°C and -

7°C, with most of the bio-oil collected in the first condenser. After operation, the collected bio-oil was weighed and stored in a refrigerator at 4°C. After cooling, the char trap was opened and the contents weighed to determine the char yield. A small amount of char was retained by a plate and hole array that is used to retain particles in the char trap and avoid char collection in the bio-oil traps. After ESP, the non-condensed gas was combusted in a flame calorimeter to measure its energy content and to close the energy balance.

Figure 9.1. A schematic of the screw conveyor pyrolysis reactor and downstream equipment

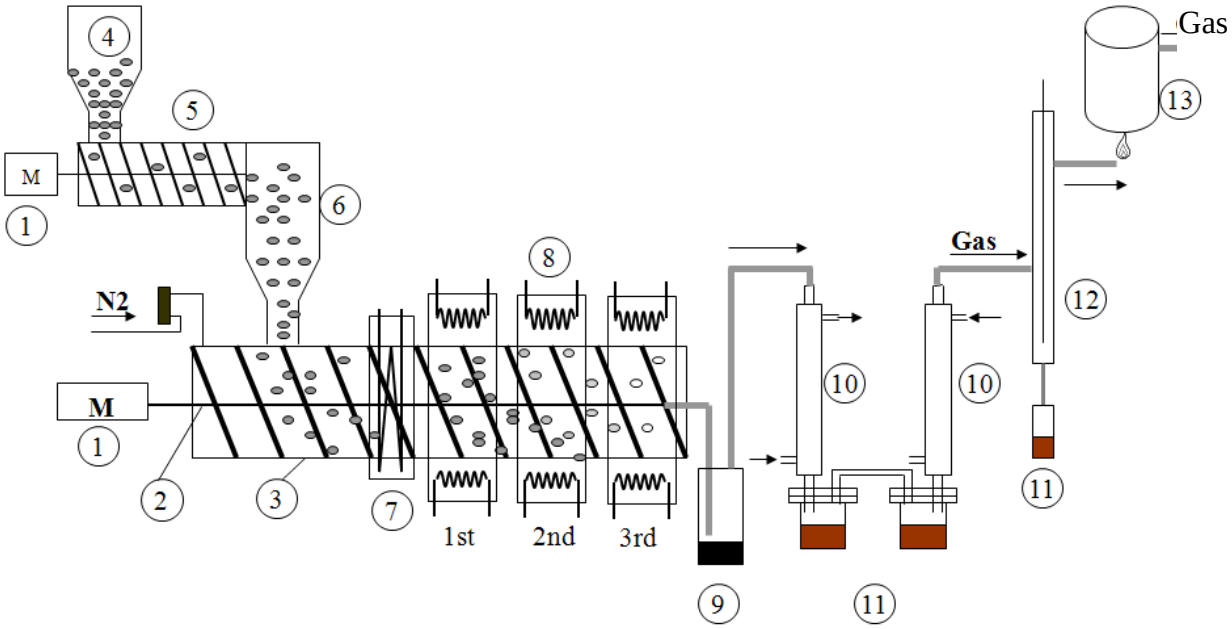

1. Motor, 2. screw conveyor, 3. pyrolysis reactor, 4. biomass feed hopper, 5. auger feeder, 6. feeding connection, 7. cooler, 8. heating zones, 9. char collector, 10. condenser, 11. bio-oil container, 12. electrostatic precipitator, 13. gas flame calorimeter.

9.2.3 Experimental design and statistical analysis

A five-level, two-factor, circumscribed central composite rotatable design (CCCRD) with three replicates at the center point was employed in this study, requiring 11 experiments [213]. The CCCRD is a quadratic polynomial response surface model of the form expressed in Equation 1:

$$Y = \beta_0 + \Sigma \beta_i x_i + \Sigma \beta_{ii} x_i^2 + \Sigma \Sigma \beta_{ij} x_i x_j$$

Where y = response (bio-oil yield), x_i, x_j = independent variables

β_0, β_i, β_{ii}, β_{ij} = intercept, linear, quadratic and interaction coefficients

CCCRD is a fractional factorial design that is improved with a group of 'star points' outside the square that allows estimation of curvature. The square is generated from values of independent variables (factors) as its corner points while the star points outside the square represent the extreme settings that can be applied for the factors. The distances from the design space center to a factorial point is ±1 unit for each factor while that to the start point is ±α with α > 1. The value of α is equal to the number of factorial runs to the one-quarter power. Regression analysis was used in an experimentally consistent way to identify and quantify statistically significant trends in the CCCRD. Model fits and the significance of predicted variable effects were analyzed by least-squares regression using JMP (SAS Institute, Cary, NC). Bio-oil and char yields were selected as the two response variables. Pyrolysis (third zone) temperature was selected as the first independent variable. Screw rotation rate, an indicator of biomass and pyrolysis vapor residence time in the reactor, was selected as the second variable. All experiments involving the pyrolysis reactor were executed in a randomized order.

Distinctions amongst bio-oils produced after pyrolysis were made using Principal Component Analysis (PCA). PCA has been previously used to simplify complex pyrolysis data, identify major products and observe commonalities amongst species [66], [67], [68], [69]. PCA of the experimental data simplifies vast amounts of data for observing trends by correlating chemical species that can be linearly combined into a new variable, known as a principal component (PC). Chemical species affect each new PC by a value known as the "loading." When

a chemical is highly correlated with a PC, either positively or negatively, they have a high loading for that PC. Thus, PCA reduces the dimensions of data consisting of a large number of variables to a new set of variables, i.e. PCs, ordered such that the first few components retain most of the variation present in the original variables. PCA was performed on the percentage peak area responses of more than 30 variables (chemical species) from the collected set of pyrograms using the JMP (SAS Institute, Cary, NC) software. The data were not scaled or normalized. Correlation analysis was used to examine the relationship between the key chemical markers and independent variables, that is, the reactor temperature and screw speed. The correlation coefficient measures the linear association between two variables on a scale of -1 to +1.

9.2.4 Characterization of bio-oil

The bio-oils obtained from the above experiments were diluted using a 1:1 mixture of 2-chloroethanol and trichloroethane (Hydranal-Working Medium K, Sigma Aldrich, St. Louis, MO), recommended for volumetric one-component Karl-Fischer (KF) titration of samples containing aldehydes and ketones. Bio-oil water content was determined by KF titration using a Volumetric Titrando instrument (Metrohm USA, Riverview, FL) and following the ASTM standard test method for water using volumetric Karl Fischer titration [214]. Bio-oil composition was analyzed using a Shimadzu QP-5050A gas chromatograph/mass spectrometer (Shimadzu Corp, Columbia, MD). Briefly, 1 g of bio-oil was solubilized in 25 mL methanol, of which 1 μL was injected into the GC. The GC used a Restek rtx-1701 column (Restek, Bellefonte, PA), 60 m x 0.25 mm with a 0.25 μm film thickness. The column gas flow was 1 cm/s with a split ratio of 1:100 so as to not overwhelm the mass spectrometer. The GC oven temperature program began with a 1 minute hold at 40°C followed by heating at 8°C/min to 270°C. The injector and detector

temperature was set at 280°C. Identification of compounds was performed by comparing the mass spectra of the peaks with standard spectra of other compounds using the NIST library to obtain the most probable matches. Pure compounds (Sigma-Aldrich Co., St Louis, MO) were then used to confirm the peak identities based on matching of retention times and mass spectra. Quantification was performed using external standards in acetonitrile and a four-point calibration curve was constructed relating concentration to peak area response. The mass spectra were recorded in electron ionization mode for *m/z* from 28 to 300.

9.2.5 Analytical Pyrolysis-GC/MS

Experiments with pure palmitic acid and potassium chloride (Sigma Aldrich, St. Louis, MO, USA) were done in an analytical pyrolysis unit known as the pyroprobe with a heated vapor line directly attached to a GC-MS. Palmitic acid samples were pre-mixed with potassium chloride in different physical ratios (9:1 and 99:1 approximately). Then weighed amount of those premixed samples (300-500 μg) were poured into quartz tubes containing quartz wool. These samples were pyrolyzed at 600 ^{o}C pyroprobe setting (500 °C pyrolysis temperature) for 20 s. Sample vapors were analyzed in GC using the same method described above and each peak was determined by mass-spectrometer and NIST database. Major compounds from mass-spectrometer were separately injected to GC to validate the presence of that compound.

9.3 Results and discussion

9.3.1 Biomass composition and characteristics

The stored SCG has a moisture content of about 3%. The results are normally distributed, with about 22% of SCG retained on a 1 mm mesh sieve, 48% on a 0.71 mm size and 18% on 0.5 mm mesh sieve. The sufficiently small particle size reduces heat and mass transfer resistances during pyrolysis and removes the need for further grinding [215], which reduces the capital and

operating costs needed for pyrolysis [216]. As further size reduction is unnecessary for this waste byproduct, the pyrolysis of SCG provides an inexpensive pathway for the production of biofuels and bioproducts.

The fiber composition of SCG is presented in Table 9.1. SCG has comparable lignin content to woody biomass such as poplar or pine wood but more than herbaceous grasses such as switchgrass and miscanthus. Bok et al. (2012) noted that due to a higher protein and caffeine content, coffee grounds contained a greater amount of nitrogen. Because of higher carbon content (52% compared with 47%), its heating value is greater than that of woody biomass. The alkali and alkaline earth metal content was higher than woody biomass but significantly lower than grasses [65]. Inorganic minerals may aid biomass pyrolysis by catalyzing reactions necessary for the breakdown of biomass components such as lignin and cellulose at a lower temperature [50], [59]. Many studies have reported the effect of inorganic minerals on the shift in biomass weight loss temperature identified by DTG analysis [53], [55], [59].

Table 9.1. Fiber analysis and elemental analysis (weight% of dry biomass)

Characteristic	Value
% Ash	1.52
% Cellulose	47.3
% Hemicellulose	23.4
% ADL[1]	19.8
% Lignin[2]	29.3
%C	52.2
%H	7.7
%N	2.0
%S	0.2
%O	37.9
% Ca	0.100
% P	0.070
% Mg	0.100
% K	0.210
% Na	0.013
% Cl	0.040
Fe (ppm)	69

1 ADL: acid-detergent lignin; 2 Acid hydrolysis lignin (soluble and insoluble)

Table 9.2 Bio-oil and char yields (% w/w biomass) from experimental matrix. A graphical representation of the CCCRD pattern is shown in supplementary figure

Sample ID	Temp. (°C)	Speed (rpm)	Bio-oil (%)	Char (%)	Gas (%)
429-58	429	58	59.6	20.6	22.3
450-45	450	45	57.3	19.9	20.2
450-70	450	70	60.7	18.9	25.6
500-40	500	40	55.5	18.6	19.7
500-58	500	58	61.5	18.3	25.9
500-58	500	58	60.0	17.7	20.4
500-58	500	58	59.8	18.2	22.0
500-75	500	75	61.7	18.6	22.9
550-45	550	45	54.5	18.1	19.8
550-70	550	70	60.8	13.6	27.4
571-58	571	58	57.8	17.3	24.9

As SCG is characterized by high lignin content, high heating value and modest metal contents, the components of bio-oil will reflect these attributes through the presence of phenolics, increased energy density and presence of metal-catalyzed cracking products.

A differential thermogravimetry (DTG) analysis was performed on the SCG. The onset of pyrolysis appeared to begin around 200 °C (473 K), which was used to determine the temperature of the first heating zone of the pyrolysis reactor. The maximum rate of weight loss was observed around 320°C (593 K) and represented the thermal decomposition of cellulose [78]. A second smaller peak or shoulder-like feature was observed after 410°C (683 K). This smaller peak may be partially related to the lignin content of SCG, which was comparable to woody biomass. Lignin decomposition occurs over a wide temperature range and a higher temperature than cellulose, contributing to the cellulose and hemicellulose decomposition peaks [77], [79]. Most of the weight lost during SCG pyrolysis was before 600 °C (873 K). Using these data and observations from previous studies, a temperature range of 450 to 550 °C (723 – 823 K) was selected for the pyrolysis trials.

9.3.2 Pyrolysis trials

Material balances and product yields were calculated for each screw-conveyor reactor trial using the bio-oil and solid char collected after every run. The liquid product was collected from three locations post-pyrolysis: two condenser collection vessels and one vessel attached to the electrostatic precipitator (ESP). The fraction of bio-oil condensed in the second and ESP vessels was very small compared to the first condenser, though the amounts in these fractions did increase with screw speed. Char was collected from the trap attached to the screw and represented all the solid product exiting the reactor after pyrolysis. Table 9.2 shows the bio-oil and char yields for pyrolysis of SCG. Overall, the bio-oil yield from the screw reactor compares favorably with previous studies. The highest yield reported by Bok et al. (2011) was 55 wt.% at 600 °C (873K) while Bedmutha et al. (2012) reported only 44 wt.% maximum liquid yield. The lowest char yield in Bok's study was 18% and in Bedmutha's study was 19.6%. In our experiments, the highest liquid yield was 61.5 % and the char yield averaged around 18%.

Bok et al. (2012) also noted that the pyrolysis of coffee grounds produced bio-oil with higher water content than woody biomass. At the same time, they observed that the higher heating value (HHV) for coffee ground bio-oil was higher than that of mallee wood bio-oil, probably due to the higher levels of fatty esters in the pyrolysis product and a higher C:O ratio of the feedstock itself [205]. In addition to observing a low liquid yield, Bedmutha et al. (2011), observed a high water content of 40-50%. Comparatively, in our study, the liquid product yield was in the range of 54.5 – 61.5% with an average total water content (feed + reaction water) of 13% of original biomass weight on a wet basis. The quality of biomass, its moisture content, the reactor design and vapor residence time (affecting the product distribution) may have played a role in achieving the high yields in this study.

9.3.3 Optimizing bio-oil yield

The CCCRD, a quadratic polynomial response surface model, was used to analyze the experimental data by least-squares regressions. The regression coefficients (β_0, β_i, β_{ii}, β_{ij}) of the CCCRD model are given in the supplementary tables and Table 9.3 along with the prediction errors and significances. The screw speed was a highly significant variable followed by temperature. Both the linear and quadratic effect terms for speed and temperature were significant ($p<0.05$) showing a strong influence of these factors on bio-oil yield. However the interaction effect was not significant at the 95% level. On the other hand, char yield was affected only by the temperature linear term but not by the quadratic term, showing a straightforward correlation between temperature and solid by-product.

Figure 9.3 shows how the predicted product liquid and char yields vary with reaction temperature at the residence time conditions. In these figures, experimental data is plotted to visualize goodness of regression fits. At the center point test condition, plotted data are averages of the three tests. Bio-oil yields are predicted with reasonable accuracy ($p<0.05$) but regression analysis shows that char yield predictions are less accurate ($p<0.11$, $R^2=0.77$). The 95% prediction interval was narrow for bio-oil predictions but quite large for char yield predictions, especially away from the center point, indicating loss of accuracy in model predictions. Error in char yield predictions may be due to data outliers which were not removed prior to the statistical analysis.

Figure 9.2 Comparison of product yields (% w/w biomass). Water content of bio-oil was determined by Karl Fisher titration. Feed water was equal to moisture content of biomass.

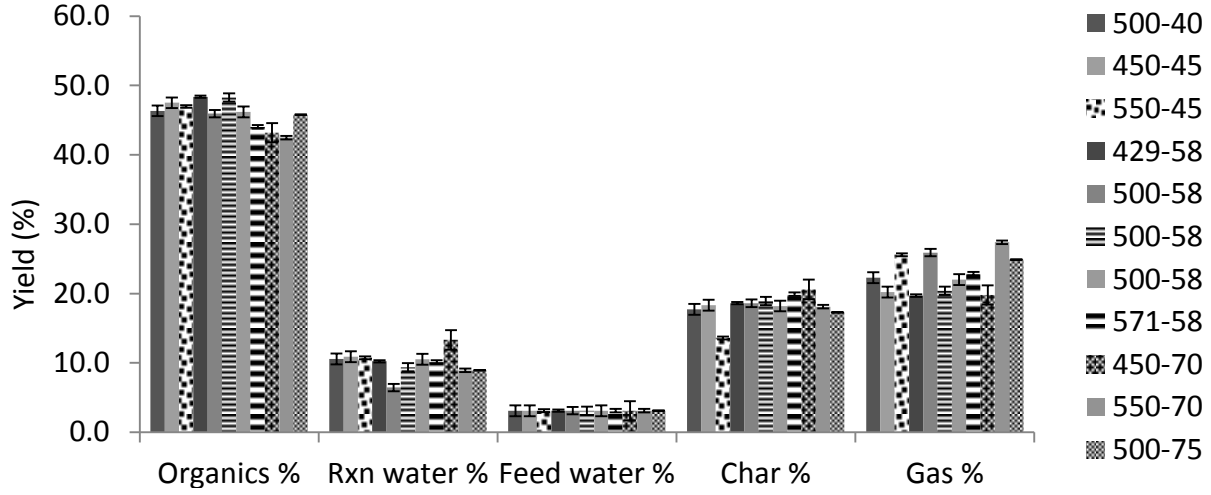

9.3.3.1 Effect of Temperature

In order to determine the effect of temperature on bio-oil yields and composition, all experiments were run in random order at the different temperatures and screw rates as specified by the CCCRD employed in this work. ANOVA on the CCCRD model showed that the liquid yield was significantly ($p<0.05$) affected by temperature. Bok et al. (2012) observed a significant effect of temperature in their study with fluidized bed reactors. Their yield varied from 36.75 weight % at 400 °C (673K) to 54.85 % at 550 °C (823 K). Similarly, Bedmutha et al. (2011) observed liquid yields of 32 to 44 % for a temperature range of 400 to 600 °C (673 – 873 K). Such high variability was not observed in the current study, where the yields were not only higher, but also in a narrower range of 54.5 to 61.5 %.

Temperature had a significant effect on both, bio-oil and char yields as seen in Figure 9.3. Up to a temperature of approximately 505 °C (778 K), the liquid and solid product showed an inverse relationship. Beyond this temperature, the non-condensable gas yield increases at the expense of both, liquid and solid product. The char produced was highest, 20.6 %, at the lowest temperature of 429 °C (702 K). Similar observations, i.e. high char yields at the lowest

temperature, were made by other researchers for various types of biomass including SCG, coffee grounds, sorghum, and mallee wood [204], [205], [212], [217]. Bedmutha et al. (2011) observed higher char yields, ranging from 35.2 % at 400°C (673 K) to 19.6 % at 600°C (873 K), than in this study for SCG. According to the CCCRD model, the predicted pyrolysis temperature for maximum oil yields was 505 °C (778 K). Interestingly, Piskorz et al. (1998) observed maximum liquid yield at 510 °C (783 K) with sorghum, Bok et al. (2012) found 550 °C (823 K) to give the maximum for coffee grounds, while Bedmutha (2011) observed a maxima between 500 to 510 °C (773 K) for SCG. All of these experiments were with fluidized bed reactors, unlike the current study which uses a screw-conveyor reactor.

Figure 9.3. Regression model predictions for bio-oil yield. Yields are in % w/w biomass. (–) shows model prediction, (.) experimental data points, (….) prediction bands

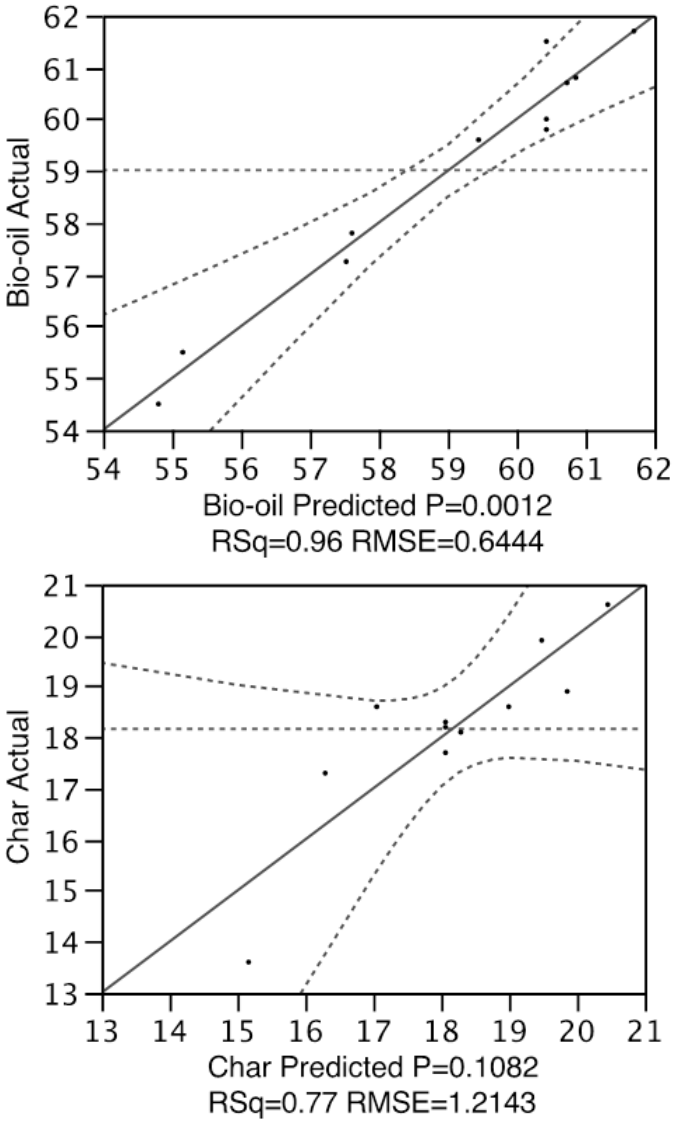

Figure 9.4. Model predictions and critical values of dependent variables for maximum for bio-oil yield. (–) model prediction, (- --) prediction bands, (…) critical values of temperature, speed and yields at model solution

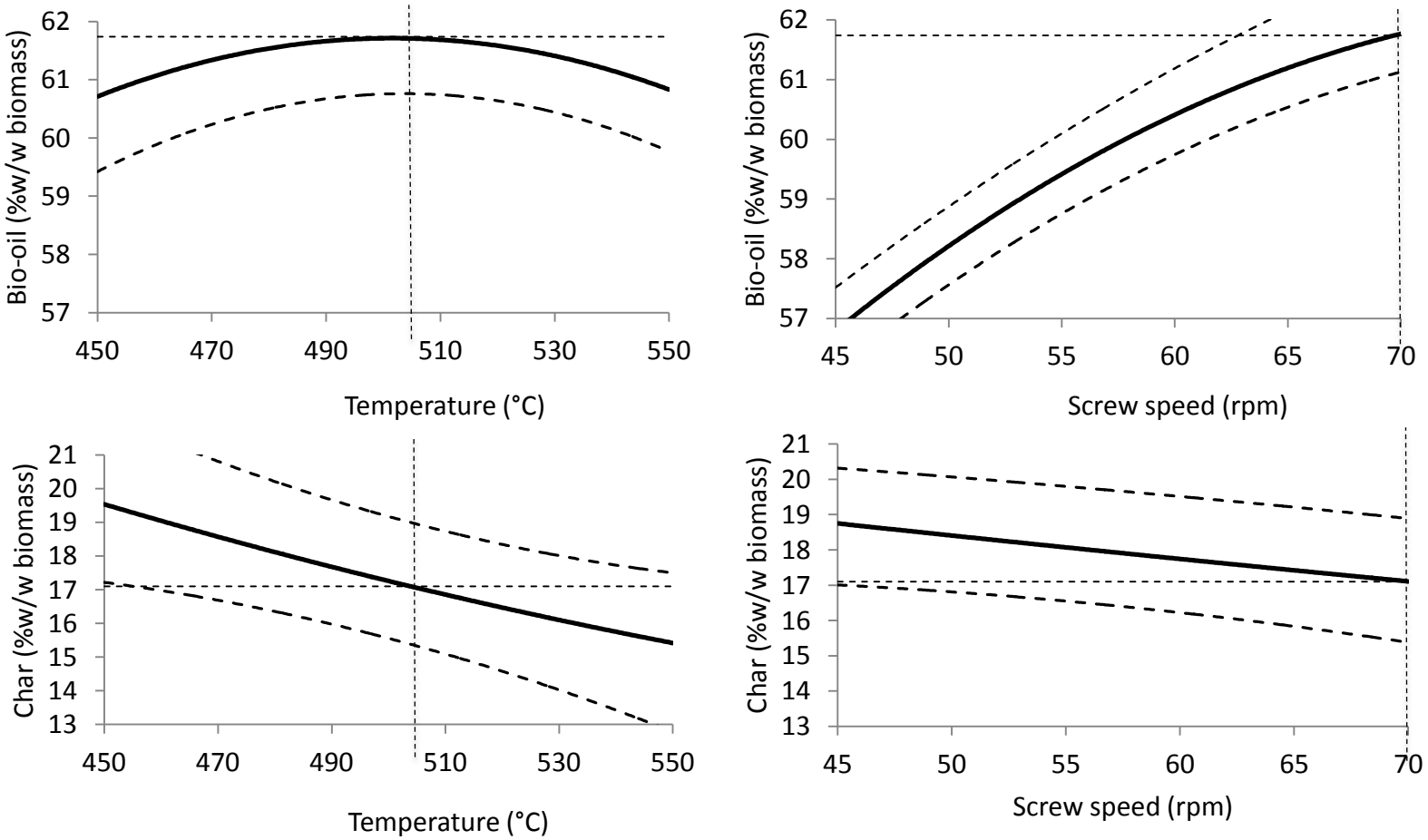

Table 9.3. Paramater estimates for regression analysis of CCCRD model for the response variables

BIO-OIL YIELD

Term	Estimate	Std Error	Prob>|t|
Speed(45,70)	2.31	0.22	0.0002
Speed*Speed	-1.00	0.27	0.01
Temp*Temp	-0.95	0.27	0.01
Temp(450,550)	-0.64	0.22	0.03
Temp*Speed	0.71	0.32	0.07

CHAR YIELD

Term	Estimate	Std Error	Prob>|t|
Temp(450,550)	-1.47	0.42	0.02
Speed(45,70)	-0.68	0.42	0.17
Temp*Speed	-0.87	0.60	0.20
Temp*Temp	0.15	0.51	0.77
Speed*Speed	-0.02	0.51	0.96

ORGANIC FRACTION OF BIO-OIL

Term	Estimate	Std Error	Prob>|t|
Temp(450,550)	-1.18	0.64	0.12
Speed(45, 70)	-0.92	0.64	0.21
Temp*Temp	-0.62	0.77	0.45
Speed*Speed	-0.55	0.77	0.50
Temp*Speed	-0.05	0.91	0.95

9.3.3.2 Effect of screw speed

Regression analysis of CCCRD model fits to experimental data showed that screw rotation rate had a highly significant ($p<0.05$) effect on liquid yield (Supplementary Tables). Unlike the temperature effect, where liquid yield went through a maximum, the bio-oil yield continues to increase while the char yield decreased as screw speed increased. A maximum screw speed of 70 rpm corresponds to the lowest biomass and pyrolysis vapor residence times in the reactor. Although screw speed affected char yields, the effect was not significant at a 95%

confidence level. It is speculated that longer residence times for char and pyrolysis vapors inside the reactor led to further cracking of pyrolysis products and a larger production of non-condensable gases and water. For example, experiments at the same temperature but lower screw speeds produced bio-oil with increased water content (Figure 9.2). High bio-oil yield is a pre-requisite for using SCG in bioenergy applications. The model predicts a maximum liquid yield of 61.7% and an accompanying char yield of 17.1% at independent variable values of 505 °C (778 K) and 70 rpm. Greater screw rotation rates, which lead to lower solid and vapor residence times, may lead to increased bio-oil yields.

9.3.4 Bio-oil characterization

Bio-oil from pyrolysis of SCG was dissolved in methanol and analyzed by GC/MS. A representative chromatogram and the list of major compounds detected along with retention times are presented in Figure 9.5. The top five chemicals, in terms of percent peak area, in this extract of bio-oil were acetol, palmitic acid, acetic acid, caffeine and pentadecane. The composition was different from that of bio-oil from woody or herbaceous biomass where carbonyl and phenolic group compounds, especially compounds like acetic acid, glycolaldehyde, acetol, furfural, guaiacol, and syringol dominate. A large number of medium-chain alkanes, alkenes, fatty acids, and fatty esters were observed in SCG bio-oil, unlike bio-oil from woody biomass.

Multivariate statistical analysis was employed to identify key factors affecting bio-oil composition (Figure 9.6). Principal component analysis (PCA) was used to study the correlations between data for percent peak area of chemicals in bio-oil. The first two principal components described 61.7% and 36.2% of the variability observed in bio-oils produced at different experimental conditions. The loadings plot (Figure 9.6 B) showed that fatty acids and carbonyl

compounds were the two variables that influenced the 1st principal component, i.e. affected the data spread along the x-axis in Figure 9.6 A. The y-axis representing the 2nd principal component showed the effect of carbonyls, fatty acids and hydrocarbons (Figure 9.6 B). PCA revealed that lower speeds (longer residence times) increased the amount of small carbonyl group compounds, increased the fraction of medium-length hydrocarbons and decreased the fraction of long-chain fatty acids and fatty esters in the bio-oil. Small carbonyl compounds such as acetic acid may be generated by the cracking of biomass components in the presence of inorganic minerals [48]. The same mechanism likely forms the medium-length hydrocarbons, as long-chain fatty acids are being similarly cracked. Long-chain fatty acids, along with fatty esters and caffeine, are correlated positively with screw speed, that is, lower residence time produced more of these compounds. To summarize, low residence time helps retain the fatty acid and fatty ester content in bio-oil while longer residence time results in cracking of primary pyrolysis products to smaller molecules such as carbonyl compounds and aliphatic hydrocarbons.

9.3.5 Pyrolysis of palmitic acid with an inorganic salt

To explore whether aromatics and long-chain alkanes were derivatives of palmitic acid in SCG bio-oil, neat palmitic acid was pyrolyzed in the presence of an inorganic salt, potassium chloride using the analytical pyroprobe-GC/MS. Pyrolysis of palmitic acid produced only palmitic acid and light gases. On reacting palmitic acid with potassium chloride, cracking of palmitic acid into alkenes and gases was observed. This correlates with observations from principal component analysis where the hydrocarbons and the fatty acid groups are aligned opposite and away from each other on the loading plot, confirming that palmitic acid produced during SCG pyrolysis may be catalytically cracking due to the presence of inorganic minerals present in the solid char byproduct.

Compounds detected with retention times in Figure 9.5 are as follows: (retention time)compound name, (7.1)Acetic acid, (7.6)Toluene, (7.7)1-hydroxy-2-Propanone(Acetol), (11.5)1-Nonanol, (12.0)3-methyl-Butanoic acid, (12.1)2-Furanmethanol (furfuryl alcohol), (12.2) 3-methyl-2-Butanone, (12.4)2-methyl-2-Cyclopenten-1-one, (13.6)Undecane, (13.7)octyl-Cyclopropane, (14.1)Propanoic acid, ethenyl ester, (14.2)2-Butanone, 1-(acetyloxy)-, (14.7)Butyrolactone, (15.7)Tridecane, (15.8)1-Undecene, (15.8)1,2-Cyclopentanedione, 3-methyl-, (17.7)Tridecane, (17.7)1-Dodecene, (18.0)Phenol, 4-methyl-, (19.1)Pentanal, (19.5)Tridecane, (19.6)1-Tetradecene, (21.3)Pentadecane, (21.3)1-Hexadecene, (22.9)Hexadecane, (23.0)1-Hexadecene, (24.3)8-Heptadecene, (24.4)Eicosane, (26.8) 1-Tetradecanol, 14-chloro- , (28.7)Hexadecanoic acid, methyl ester, (30.6)n-Hexadecanoic acid (palmitic acid), (30.7) Octadecanoic acid, 2-propenyl ester, (31.5)1H-Purine-2,6-dione, 3,7-dihydro-1,3,7-trimethyl- (caffeine), (33.3)12-Methyl-E,E-2,13-octadecadien-1-ol, (34.6)Palmitic acid vinyl ester.

Figure 9.5. Representative Chromatogram (A) of methanol extract of bio-oil from spent coffee grounds (500 °C pyrolysis temperature) and comparison with chromatogram (B) obtained for analytical pyroprobe-gc/ms at 650 °C (525-550 °C pyrolysis temperature)

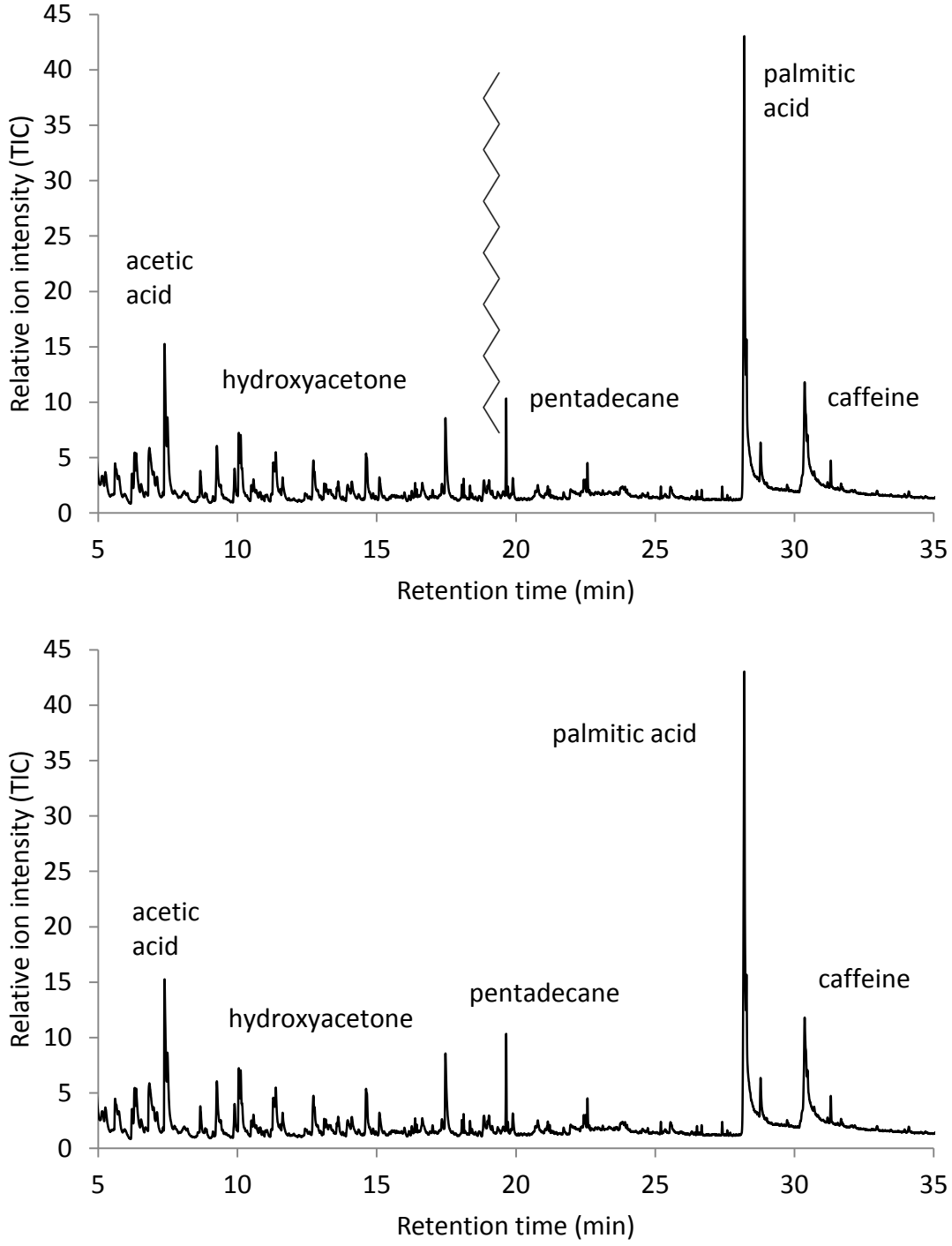

Table 9.4. Correlations between pyrolysis input variables and major chemicals and groups

	Carbo-nyls	Hydro carbons	Aromatic/ Phenolic	Fatty acids	Acetic acid	Acetol	Penta decane	Palmitic acid	Caffeine	Temp.	Speed
Carbonyls	1.0	-0.6	0.0	-0.5	0.8	0.5	-0.6	-0.5	-0.3	-0.3	0.0
Hydro-carbons		1.0	0.4	-0.3	-0.1	-0.7	0.9	-0.4	-0.1	0.0	-0.4
Aromatics			1.0	-0.6	0.5	-0.7	0.2	-0.5	-0.7	-0.3	-0.7
Fatty acid/ ester				1.0	-0.8	0.2	-0.2	1.0	0.6	0.3	0.6
Acetic acid					1.0	-0.1	-0.3	-0.7	-0.8	-0.5	-0.5
Acetol						1.0	-0.6	0.1	0.4	0.4	0.5
Penta-decane							1.0	-0.2	0.1	-0.1	-0.1
Palmitic acid								1.0	0.5	0.2	0.6
Caffeine									1.0	0.6	0.6
Temp.										1.0	0.0
Speed											1.0

Figure 9.6. Principal component analysis of bio-oil components – A: plot of principal components 1 and 2, B: Loadings plot

A

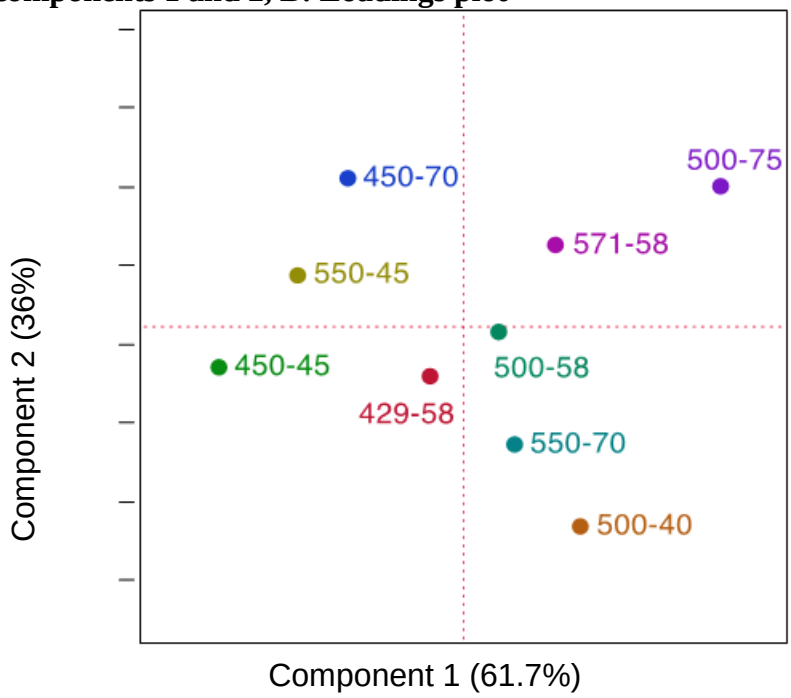

B

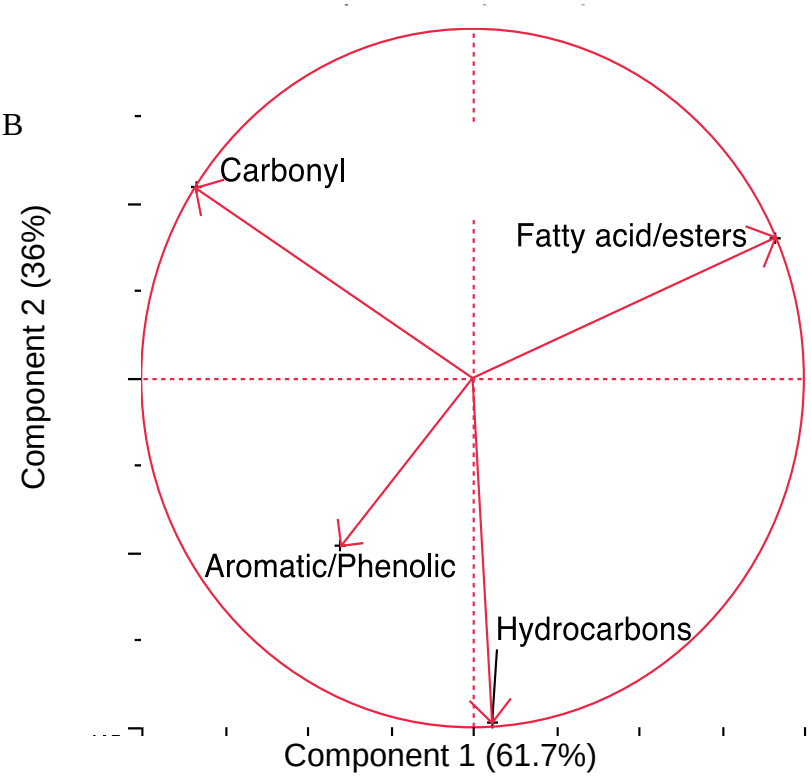

9.4 Conclusions

Pyrolysis of SCG using a screw-conveyor pyrolysis reactor produced higher bio-oil and lower char yield than fluidized bed reactors. A maximum bio-oil yield of 61.8% was obtained in a screw-conveyor reactor at 70 rpm and 500°C. To support adoption of screw conveyor reactors at small scales for bioenergy, SCG bio-oil needs to have a high yield, high HHV, low water content and low levels of carbonyl compounds to reduce corrosion and reactivity. This may be accomplished by running the screw conveyor reactor at maximum screw speed and an optimum temperature (500 °C). As a waste by-product with a small particle size, SCG is an ideal bioenergy feedstock for conversion to higher-value energy products using fast pyrolysis.

CHAPTER 10. CONLUSIONS AND FUTURE WORK

10.1 Conclusions

Pyrolysis technologies offer a potentially less expensive route to bio-based aromatic chemicals with minimal modifications required to the existing petroleum infrastructure.

For an efficient transition to a bio-based economy, it is necessary to select cheap and abundant source of biomass. Our experiments showed that it is the qualities, composition and thermal propertie of feedstock that determine the qualities and composition of pyrolysis products. Feedstock is the critical biological component of this process and it is important to select biomass varieties that lead to high aromatic yields. Although phenolics are produced from biomass pyrolysis, monocyclic aromatics such as BTEX, which are raw materials for many other chemicals, are not produced. Therefore catalysis in the form of solid acid catalysts has to be employed to crack and convert product molecules to aromatics. Of the dozen or more biomass studied, spent coffee grounds were found to be the most desirable feedstock for conversion to aromatics using pyrolysis and catalysis. Spent coffee grounds are an ideal bioenergy feedstock as they may be inexpensively obtained and eliminate the need for biomass size reduction before pyrolysis. Many catalysts were tested for aromatics production from biomass pyrolysis. Although the mesoporous catalysts in this study had many desirable properties such as high pore volume and high acidity, they showed low selectivity for hydrocarbons when compared with conventional ZSM-5 catalyst. However an improved option for making non-oxygenated aromatic chemicals from photosynthetic biomass is offered by mesoporous ZSM-5 type catalysts with dehydrogenating metal functionality. Zeolites with uniform intracrystal mesopores and loaded with Gallium (III) ions, designated Ga-MSU-MFI, were prepared using silane-modified polymers as mesopore-generating agents. Ga-MSU-MFI gave higher yields and lower coke formation than conventional ZSM-5 catalyst. Besides biomass pyrolysis, this catalyst was shown

to be effective in improving yields of aromatics from hydrocarbon feeds such as isobutylene. Pyrolysis of spent coffee grounds in a pilot-scale screw conveyor reactor was demonstrated. The screw conveyor reactor gave higher bio-oil yields than fluidized bed reactors at a pyrolysis temperature of 505 °C and maximum screw speed, which minimized residence time. Results from the pilot-scale demonstration are needed to de-risk the subsequent adoption of the proposed process. If deployed, positive socio-economic benefits include domestic and international jobs creation, capital retention and investment in rural communities, and increased profitability resulting from waste conversion into valuable chemicals. This process will exhibit simplicity in concept and flexibility across an array of plant biomass feedstock, cost-competitiveness when compared to the current petro-based supply chain is expected as is a reduction in environmental impacts associated with climate change.

10.2 Future work

The following research may be useful in expediting the commercialization of green aromatics from biomass pyrolysis and catalysis:

1. Techno-economic analysis and life-cycle assessment
2. Development of isotopically-labeled biomass to elucidate reaction pathways and kinetics of biomass to aromatics,
3. Catalyst design (pore size, acidity, dehydrogenating metals) to increase conversion and reduce coke generation,
4. Pyrolysis reactor design to increase liquid yield and reduce secondary reactions.

REFERENCES

REFERENCES

[1] U.S. Department of Energy, "U.S. Billion-Ton Update: Biomass Supply for a Bioenergy and Bioproducts Industry," Oak Ridge, TN, 2011.

[2] R. C. Brown, *Thermochemical Processing of Biomass*. Chichester, UK: John Wiley & Sons, Ltd, 2011.

[3] S. Czernik and A. V. Bridgwater, "Overview of Applications of Biomass Fast Pyrolysis Oil," *Energy & Fuels*, vol. 18, no. 2, pp. 590–598, Mar. 2004.

[4] D. Mohan, C. U. Pittman, and P. H. Steele, "Pyrolysis of Wood/Biomass for Bio-oil: A Critical Review," *Energy & Fuels*, vol. 20, no. 3, pp. 848–889, May 2006.

[5] P. Winsley, "Biochar and bioenergy production for climate change mitigation," *New Zealand Science Review Vol*, vol. 64, no. 1, 2007.

[6] T. R. Brown, M. M. Wright, and R. C. Brown, "Estimating profitability of two biochar production scenarios: slow pyrolysis vs fast pyrolysis," *Biofuels, Bioproducts and Biorefining*, vol. 5, no. 1, pp. 54–68, 2011.

[7] P. McKendry, "Energy production from biomass (Part 1): Overview of biomass.," *Bioresource technology*, vol. 83, no. 1, pp. 37–46, May 2002.

[8] R. P. Anex, A. Aden, F. K. Kazi, J. Fortman, R. M. Swanson, M. M. Wright, J. A. Satrio, R. C. Brown, D. E. Daugaard, A. Platon, G. Kothandaraman, D. D. Hsu, and A. Dutta, "Techno-economic comparison of biomass-to-transportation fuels via pyrolysis, gasification, and biochemical pathways," *Fuel*, vol. 89, pp. S29–S35, Nov. 2010.

[9] P. J. Dauenhauer, J. L. Colby, C. M. Balonek, W. J. Suszynski, and L. D. Schmidt, "Reactive boiling of cellulose for integrated catalysis through an intermediate liquid," *Green Chemistry*, vol. 11, no. 10, p. 1555, 2009.

[10] M. S. Mettler, D. G. Vlachos, and P. J. Dauenhauer, "Top ten fundamental challenges of biomass pyrolysis for biofuels," *Energy & Environmental Science*, vol. 5, no. 7, p. 7797, 2012.

[11] D. Shen, R. Xiao, S. Gu, and K. Luo, "The pyrolytic behavior of cellulose in lignocellulosic biomass: a review," *RSC Advances*, vol. 1, no. 9, p. 1641, 2011.

[12] J. Lédé, "Cellulose pyrolysis kinetics: An historical review on the existence and role of intermediate active cellulose," *Journal of Analytical and Applied Pyrolysis*, vol. 94, pp. 17–32, Mar. 2012.

[13] P. R. Patwardhan, J. A. Satrio, R. C. Brown, and B. H. Shanks, "Product distribution from fast pyrolysis of glucose-based carbohydrates," *Journal of Analytical and Applied Pyrolysis*, vol. 86, no. 2, pp. 323–330, Nov. 2009.

[14] G. R. Ponder and G. N. Richards, “A review of some recent studies on mechanisms of pyrolysis of polysaccharides,” *Biomass and Bioenergy*, vol. 7, no. 1–6, pp. 1–24, Jan. 1994.

[15] D. K. Shen and S. Gu, “The mechanism for thermal decomposition of cellulose and its main products.,” *Bioresource technology*, vol. 100, no. 24, pp. 6496–504, Dec. 2009.

[16] J. C. Irvine and J. W. H. Oldham, “CXCVIII.?The constitution of polysaccharides. Part III. The relationship of l-glucosan to d-glucose and to cellulose,” *Journal of the Chemical Society, Transactions*, vol. 119, p. 1744, 1921.

[17] G. A. Byrne, D. Gardiner, and F. H. Holmes, “The pyrolysis of cellulose and the action of flame-retardants,” *Journal of Applied Chemistry*, vol. 16, no. 3, pp. 81–88, May 2007.

[18] R. S. Assary and L. A. Curtiss, “Thermochemistry and Reaction Barriers for the Formation of Levoglucosenone from Cellobiose,” *ChemCatChem*, vol. 4, no. 2, pp. 200–205, Feb. 2012.

[19] S. Li, J. Lyons-Hart, J. Banyasz, and K. Shafer, “Real-time evolved gas analysis by FTIR method: an experimental study of cellulose pyrolysis,” *Fuel*, vol. 80, no. 12, pp. 1809–1817, Oct. 2001.

[20] F. Shafizadeh, R. H. Furneaux, T. G. Cochran, J. P. Scholl, and Y. Sakai, “Production of levoglucosan and glucose from pyrolysis of cellulosic materials,” *Journal of Applied Polymer Science*, vol. 23, no. 12, pp. 3525–3539, Jun. 1979.

[21] S. Madorsky, S. L., Hart, V. E., & Straus, “Pyrolysis of Cellulose in a Vacuum,” *Journal of research of the National Bureau of Standards*, vol. 56, no. 6, pp. 343–354, 1956.

[22] P. M. Molton and T. F. Demmitt, “Reaction Mechanisms in Cellulose Pyrolysis,” 1977.

[23] G. R. Ponder, G. N. Richards, and T. T. Stevenson, “Influence of linkage position and orientation in pyrolysis of polysaccharides: A study of several glucans,” *Journal of Analytical and Applied Pyrolysis*, vol. 22, no. 3, pp. 217–229, Mar. 1992.

[24] G. R. Ponder and G. N. Richards, “Thermal synthesis and pyrolysis of a xylan,” *Carbohydrate Research*, vol. 218, pp. 143–155, Sep. 1991.

[25] T. L. Lowary and G. N. Richards, “Cycloheptaamylose as a model for starch in the pyrolysis of polysaccharides,” *Carbohydrate Research*, vol. 218, pp. 157–166, Sep. 1991.

[26] F. Shafizadeh, R. A. Susott, and G. D. McGinnis, “Pyrolysis of substituted phenyl β-d-glucopyranosides and 2-deoxy-α-d-arabino-hexopyranosides,” *Carbohydrate Research*, vol. 22, no. 1, pp. 63–73, Apr. 1972.

[27] P. Köll, G. Borchers, and J. O. Metzger, “Thermal degradation of chitin and cellulose,” *Journal of Analytical and Applied Pyrolysis*, vol. 19, pp. 119–129, Jul. 1991.

[28] R. Vinu and L. J. Broadbelt, “Unraveling Reaction Pathways and Specifying Reaction Kinetics for Complex Systems.,” *Annual review of chemical and biomolecular engineering*, vol. 3, no. January, pp. 29–54, Jan. 2012.

[29] H. B. Mayes and L. J. Broadbelt, “Unraveling the reactions that unravel cellulose.,” *The journal of physical chemistry. A*, vol. 116, no. 26, pp. 7098–106, Jul. 2012.

[30] D. Gardiner, “The pyrolysis of some hexoses and derived di-, tri-, and poly-saccharides,” *Journal of the Chemical Society C: Organic*, p. 1473, 1966.

[31] K. Kato, “Pyrolysis of Cellulose Part III. Comparative Studies of the Volatile Compounds from Pyrolysates of Cellulose and its Related Compounds,” *Agr. Biol. Chem*, vol. 31, p. 657, 1967.

[32] M. S. Mettler, S. H. Mushrif, A. D. Paulsen, A. D. Javadekar, D. G. Vlachos, and P. J. Dauenhauer, “Revealing pyrolysis chemistry for biofuels production: Conversion of cellulose to furans and small oxygenates,” *Energy & Environmental Science*, vol. 5, no. 1, p. 5414, 2012.

[33] M. Moliner, Y. Román-Leshkov, and M. E. Davis, “Tin-containing zeolites are highly active catalysts for the isomerization of glucose in water.,” *Proceedings of the National Academy of Sciences of the United States of America*, vol. 107, no. 14, pp. 6164–8, Apr. 2010.

[34] J. N. Chheda, Y. Rom?n-Leshkov, and J. A. Dumesic, “Production of 5-hydroxymethylfurfural and furfural by dehydration of biomass-derived mono- and poly-saccharides,” *Green Chemistry*, vol. 9, no. 4, p. 342, 2007.

[35] J. B. Paine, Y. B. Pithawalla, and J. D. Naworal, “Carbohydrate pyrolysis mechanisms from isotopic labeling,” *Journal of Analytical and Applied Pyrolysis*, vol. 82, no. 1, pp. 10–41, May 2008.

[36] E. B. Sanders, A. I. Goldsmith, and J. I. Seeman, “A model that distinguishes the pyrolysis of D - glucose , D -fructose , and sucrose from that of cellulose . Application to the understanding of cigarette smoke formation,” *Journal of Analytical and Applied Pyrolysis*, vol. 66, pp. 29–50, 2003.

[37] J. B. Paine, Y. B. Pithawalla, and J. D. Naworal, “Carbohydrate pyrolysis mechanisms from isotopic labeling,” *Journal of Analytical and Applied Pyrolysis*, vol. 83, no. 1, pp. 37–63, Sep. 2008.

[38] Y.-C. Lin, J. Cho, G. A. Tompsett, P. R. Westmoreland, and G. W. Huber, “Kinetics and Mechanism of Cellulose Pyrolysis,” *The Journal of Physical Chemistry C*, vol. 113, no. 46, pp. 20097–20107, Nov. 2009.

[39] M. S. Mettler, A. D. Paulsen, D. G. Vlachos, and P. J. Dauenhauer, “Pyrolytic conversion of cellulose to fuels: levoglucosan deoxygenation via elimination and cyclization within molten biomass,” *Energy & Environmental Science*, vol. 5, no. 7, p. 7864, 2012.

[40] Y. Zhu, J. Zajicek, and A. S. Serianni, “Acyclic Forms of [1- 13 C]Aldohexoses in Aqueous Solution: Quantitation by 13 C NMR and Deuterium Isotope Effects on Tautomeric Equilibria,” *The Journal of Organic Chemistry*, vol. 66, no. 19, pp. 6244–6251, Sep. 2001.

[41] F. Shafizadeh, “Alternative Cellulose pathways,” *Fuel*, vol. 75, 1983.

[42] F. Shafizadeh and Y. L. Fu, “Pyrolysis of cellulose,” *Crabohydrate Research*, vol. 29, pp. 113–122, 1973.

[43] T. Hosoya, H. Kawamoto, and S. Saka, “Cellulose–hemicellulose and cellulose–lignin interactions in wood pyrolysis at gasification temperature,” *Journal of Analytical and Applied Pyrolysis*, vol. 80, no. 1, pp. 118–125, Aug. 2007.

[44] S. Wang, X. Guo, K. Wang, and Z. Luo, “Influence of the interaction of components on the pyrolysis behavior of biomass,” *Journal of Analytical and Applied Pyrolysis*, vol. 91, no. 1, pp. 183–189, May 2011.

[45] T. Hosoya, Y. Nakao, H. Sato, H. Kawamoto, and S. Sakaki, “Thermal degradation of methyl beta-D-glucoside. a theoretical study of plausible reaction mechanisms.,” *The Journal of organic chemistry*, vol. 74, no. 17, pp. 6891–4, Sep. 2009.

[46] M. A. Sanderson, P. R. Adler, A. A. Boateng, M. D. Casler, and G. Sarath, “Switchgrass as a biofuels feedstock in the USA,” *Canadian Journal of Plant Science*, vol. 86, no. Special Issue, pp. 1315–1325, Dec. 2006.

[47] D. Tilman, J. Hill, and C. Lehman, “Carbon-negative biofuels from low-input high-diversity grassland biomass.,” *Science (New York, N.Y.)*, vol. 314, no. 5805, pp. 1598–600, Dec. 2006.

[48] P. R. Patwardhan, J. A. Satrio, R. C. Brown, and B. H. Shanks, “Influence of inorganic salts on the primary pyrolysis products of cellulose,” *Bioresource Technology*, vol. 101, no. 12, pp. 4646–4655, Jun. 2010.

[49] D. Mourant, Z. Wang, M. He, X. S. Wang, M. Garcia-Perez, K. Ling, and C.-Z. Li, “Mallee wood fast pyrolysis: Effects of alkali and alkaline earth metallic species on the yield and composition of bio-oil,” *Fuel*, vol. 90, no. 9, pp. 2915–2922, Sep. 2011.

[50] R. Fahmi, A. V. Bridgwater, L. Darvell, J. Jones, N. Yates, S. Thain, and I. Donnison, “The effect of alkali metals on combustion and pyrolysis of Lolium and Festuca grasses, switchgrass and willow,” *Fuel*, vol. 86, no. 10–11, pp. 1560–1569, Jul. 2007.

[51] M. Nik-Azar, M. R. M. R. Hajaligol, M. Sohrabi, and B. Dabir, “Mineral matter effects in rapid pyrolysis of beech,” *Fuel Processing Technology*, vol. 51, no. 1–2, pp. 7–17, Mar. 1997.

[52] M. Mullerhagedorn, H. Bockhorn, L. Krebs, and U. Muller, “A comparative kinetic study on the pyrolysis of three different wood species,” *Journal of Analytical and Applied*

Pyrolysis, vol. 68–69, pp. 231–249, Aug. 2003.

[53] D. J. Nowakowski and J. M. Jones, "Uncatalysed and potassium-catalysed pyrolysis of the cell-wall constituents of biomass and their model compounds," *Journal of Analytical and Applied Pyrolysis*, vol. 83, no. 1, pp. 12–25, Sep. 2008.

[54] K. Raveendran, A. Ganesh, and K. C. Khilart, "Influence of mineral matter pyrolysis characteristics on biomass," *Fuel*, vol. 74, no. 12, pp. 1812–1822, 1995.

[55] A. Jensen, K. Dam-Johansen, M. A. Wójtowicz, and M. A. Serio, "TG-FTIR Study of the Influence of Potassium Chloride on Wheat Straw Pyrolysis," *Energy & Fuels*, vol. 12, no. 5, pp. 929–938, Sep. 1998.

[56] J. Wang, M. Zhang, M. Chen, F. Min, S. Zhang, Z. Ren, and Y. Yan, "Catalytic effects of six inorganic compounds on pyrolysis of three kinds of biomass," *Thermochimica Acta*, vol. 444, no. 1, pp. 110–114, May 2006.

[57] Z. Wang, F. Wang, J. Cao, and J. Wang, "Pyrolysis of pine wood in a slowly heating fixed-bed reactor: Potassium carbonate versus calcium hydroxide as a catalyst," *Fuel Processing Technology*, vol. 91, no. 8, pp. 942–950, Aug. 2010.

[58] M. Chen, J. Wang, M. Zhang, M. Chen, X. Zhu, F. Min, and Z. Tan, "Catalytic effects of eight inorganic additives on pyrolysis of pine wood sawdust by microwave heating," *Journal of Analytical and Applied Pyrolysis*, vol. 82, no. 1, pp. 145–150, May 2008.

[59] N. Shimada, H. Kawamoto, and S. Saka, "Different action of alkali/alkaline earth metal chlorides on cellulose pyrolysis," *Journal of Analytical and Applied Pyrolysis*, vol. 81, no. 1, pp. 80–87, Jan. 2008.

[60] K. O. Davidsson, J. G. Korsgren, J. B. C. Pettersson, and U. Jäglid, "The effects of fuel washing techniques on alkali release from biomass," *Fuel*, vol. 81, no. 2, pp. 137–142, Jan. 2002.

[61] M. E. Fuentes, D. J. Nowakowski, M. L. Kubacki, J. M. Cove, T. G. Bridgeman, and J. M. Jones, "Survey of influence of biomass mineral matter in thermochemical conversion of short rotation willow coppice," *Journal of the Energy Institute*, vol. 81, no. 4, pp. 234–241, Dec. 2008.

[62] R. He, X. P. Ye, B. C. English, and J. A. Satrio, "Influence of pyrolysis condition on switchgrass bio-oil yield and physicochemical properties.," *Bioresource technology*, vol. 100, no. 21, pp. 5305–11, Nov. 2009.

[63] E. M. Hodgson, D. J. Nowakowski, I. Shield, A. Riche, A. V. Bridgwater, J. C. Clifton-Brown, and I. S. Donnison, "Variation in Miscanthus chemical composition and implications for conversion by pyrolysis and thermo-chemical bio-refining for fuels and chemicals," *Bioresource Technology*, vol. 102, no. 3, pp. 3411–3418, Feb. 2011.

[64] E. Butler, G. Devlin, D. Meier, and K. McDonnell, "A review of recent laboratory

research and commercial developments in fast pyrolysis and upgrading," *Renewable and Sustainable Energy Reviews*, vol. 15, no. 8, pp. 4171–4186, Oct. 2011.

[65] S. V. Vassilev, D. Baxter, L. K. Andersen, and C. G. Vassileva, "An overview of the chemical composition of biomass," *Fuel*, vol. 89, no. 5, pp. 913–933, May 2010.

[66] R. J. Evans and T. a. Milne, "Molecular characterization of the pyrolysis of biomass," *Energy & Fuels*, vol. 1, no. 2, pp. 123–137, Mar. 1987.

[67] H. L. C. Meuzelaar, W. Windig, A. M. Harper, S. M. Huff, W. McClennen, J. M. Richards, and H. Mcclennen, "Pyrolysis Mass Spectrometry of Complex Organic Materials," *Science*, vol. 226, no. 4672, pp. 268–274, Oct. 1984.

[68] A. Pattiya, J. O. Titiloye, and A. V. Bridgwater, "Evaluation of catalytic pyrolysis of cassava rhizome by principal component analysis," *Fuel*, vol. 89, no. 1, pp. 244–253, Jan. 2010.

[69] D. Meier, I. Fortmann, J. Odermatt, and O. Faix, "Discrimination of genetically modified poplar clones by analytical pyrolysis–gas chromatography and principal component analysis," *Journal of Analytical and Applied Pyrolysis*, vol. 74, no. 1–2, pp. 129–137, Aug. 2005.

[70] P. J. Soest and H. K. Goering, "{VAN} Forage fiber analyses. {(Apparatus,} reagents, procedures, and some applications.)." 1970.

[71] A. Sluiter, B. Hames, R. Ruiz, C. Scarlata, J. Sluiter, D. Templeton, and D. Crocker, "Determination of Structural Carbohydrates and Lignin in Biomass," National Renewable Energy Laboratory, Jun. 2010.

[72] ASTM International, "ASTM D4442 - 07 Standard Test Methods for Direct Moisture Content Measurement of Wood and Wood-Base Materials," 2007.

[73] ASTM International, "ASTM D1102 - 84(2007) Standard Test Method for Ash in Wood," 2007.

[74] ASTM International, "ASTM E711 - 87(2004) Standard Test Method for Gross Calorific Value of Refuse-Derived Fuel by the Bomb Calorimeter," 2004.

[75] E. M. Hodgson, R. Fahmi, N. Yates, T. Barraclough, I. Shield, G. Allison, A. V. Bridgwater, and I. S. Donnison, "Miscanthus as a feedstock for fast-pyrolysis: does agronomic treatment affect quality?," *Bioresource technology*, vol. 101, no. 15, pp. 6185–91, Aug. 2010.

[76] B. Jenkins, "On the properties of washed straw," *Biomass and Bioenergy*, vol. 10, no. 4, pp. 177–200, 1996.

[77] C. E. Greenhalf, D. J. Nowakowski, A. V. Bridgwater, J. O. Titiloye, N. Yates, A. Riche, and I. Shield, "Thermochemical characterisation of straws and high yielding perennial

grasses," *Industrial Crops and Products*, vol. 36, no. 1, pp. 449–459, Mar. 2012.

[78] G. Varhegyi, M. J. Antal, T. Szekely, F. Till, and E. Jakab, "Simultaneous thermogravimetric-mass spectrometric studies of the thermal decomposition of biopolymers. 1. Avicel cellulose in the presence and absence of catalysts," *Energy & Fuels*, vol. 2, no. 3, pp. 267–272, May 1988.

[79] M. Garcia-Perez, S. Wang, J. Shen, M. Rhodes, W. J. Lee, and C.-Z. Li, "Effects of Temperature on the Formation of Lignin-Derived Oligomers during the Fast Pyrolysis of Mallee Woody Biomass," *Energy & Fuels*, vol. 22, no. 3, pp. 2022–2032, May 2008.

[80] B. F. Tjeerdsma and H. Militz, "Chemical changes in hydrothermal treated wood: FTIR analysis of combined hydrothermal and dry heat-treated wood," *Holz als Roh- und Werkstoff*, vol. 63, no. 2, pp. 102–111, Feb. 2005.

[81] M. Kleen and G. Gellerstedt, "Influence of inorganic species on the formation of polysaccharide and lignin degradation products in the analytical pyrolysis of pulps," *Journal of Analytical and Applied Pyrolysis*, vol. 35, no. 1, pp. 15–41, Oct. 1995.

[82] J. Piskorz, D. Radlein, and D. S. Scott, "On the mechanism of the rapid pyrolysis of cellulose," *Journal of Analytical and Applied Pyrolysis*, vol. 9, no. 2, pp. 121–137, Jan. 1986.

[83] F. Shafizadeh, "Introduction to pyrolysis of biomass," *Journal of Analytical and Applied Pyrolysis*, vol. 3, no. 4, pp. 283–305, Apr. 1982.

[84] G. Dobele, G. Rossinskaja, T. Dizhbite, G. Telysheva, D. Meier, and O. Faix, "Application of catalysts for obtaining 1,6-anhydrosaccharides from cellulose and wood by fast pyrolysis," *Journal of Analytical and Applied Pyrolysis*, vol. 74, no. 1–2, pp. 401–405, Aug. 2005.

[85] G. N. Richards and G. Zheng, "Influence of metal ions and of salts on products from pyrolysis of wood : applications to thermochemical processing of newsprint and biomass," *Journal of Analytical and Applied Pyrolysis*, vol. 21, no. 1–2, pp. 133–146, Sep. 1991.

[86] H. Kawamoto, D. Yamamoto, and S. Saka, "Influence of neutral inorganic chlorides on primary and secondary char formation from cellulose," *Journal of Wood Science*, vol. 54, no. 3, pp. 242–246, Dec. 2007.

[87] W.-P. Pan and G. N. Richards, "Influence of metal ions on volatile products of pyrolysis of wood," *Journal of Analytical and Applied Pyrolysis*, vol. 16, no. 2, pp. 117–126, Jun. 1989.

[88] P. de Wild, H. Reith, and E. Heeres, "Biomass pyrolysis for chemicals," *Biofuels*, vol. 2, no. 2, pp. 185–208, Mar. 2011.

[89] S. Thangalazhy-Gopakumar, S. Adhikari, R. B. Gupta, M. Tu, and S. Taylor, "Production of hydrocarbon fuels from biomass using catalytic pyrolysis under helium and hydrogen

environments.," *Bioresource technology*, vol. 102, no. 12, pp. 6742–9, Jun. 2011.

[90] T. R. Carlson, "Catalytic fast pyrolysis of biomass for production of fuels and chemicals," University of Massachusetts Amherst, 2010.

[91] T. R. Carlson, Y.-T. Cheng, J. Jae, and G. W. Huber, "Production of green aromatics and olefins by catalytic fast pyrolysis of wood sawdust," *Energy & Environmental Science*, vol. 4, no. 1, p. 145, 2011.

[92] W. D. Van Krevelen, "Graphical-statistical method for the study of structure and reaction processes of coal," *Fuel*, vol. 29, pp. 269–284, 1950.

[93] N. H. Bostick and T. A. Daws, "Relationships between data from Rock-Eval pyrolysis and proximate, ultimate, petrographic, and physical analyses of 142 diverse U.S. coal samples," *Organic Geochemistry*, vol. 21, no. 1, pp. 35–49, Jan. 1994.

[94] N. Y. Chen, T. F. Degnan, and L. R. Koenig, "Liquid fuel from carbohydrates," *Chemtech*, vol. 16, p. 506, 1986.

[95] E. Taarning, C. M. Osmundsen, X. Yang, B. Voss, S. I. Andersen, and C. H. Christensen, "Zeolite-catalyzed biomass conversion to fuels and chemicals," *Energy & Environmental Science*, vol. 4, no. 3, p. 793, 2011.

[96] H. Zhang, Y.-T. Cheng, T. P. Vispute, R. Xiao, and G. W. Huber, "Catalytic conversion of biomass-derived feedstocks into olefins and aromatics with ZSM-5: the hydrogen to carbon effective ratio," *Energy & Environmental Science*, vol. 4, no. 6, p. 2297, 2011.

[97] G. W. Huber, S. Iborra, and A. Corma, "Synthesis of Transportation Fuels from Biomass: Chemistry, Catalysts, and Engineering," *Chemical Reviews*, vol. 106, no. 9, pp. 4044–4098, Sep. 2006.

[98] J. P. Diebold, "A Review of the Chemical and Physical Mechanisms of the Storage Stability of Fast Pyrolysis Bio-Oils," 2000.

[99] G. Varhegyi, M. J. Antal, T. Szekely, and P. Szabo, "Kinetics of the thermal decomposition of cellulose, hemicellulose, and sugarcane bagasse," *Energy & Fuels*, vol. 3, no. 3, pp. 329–335, May 1989.

[100] T. Fisher, M. Hajaligol, B. Waymack, and D. Kellogg, "Pyrolysis behavior and kinetics of biomass derived materials," *Journal of Analytical and Applied Pyrolysis*, vol. 62, no. 2, pp. 331–349, Feb. 2002.

[101] J. J. M. Orfão, F. J. A. Antunes, and J. L. Figueiredo, "Pyrolysis kinetics of lignocellulosic materials—three independent reactions model," *Fuel*, vol. 78, no. 3, pp. 349–358, Feb. 1999.

[102] M. Stöcker, "Methanol-to-hydrocarbons: catalytic materials and their behavior," *Microporous and Mesoporous Materials*, vol. 29, no. 1–2, pp. 3–48, Jun. 1999.

[103] Q. Wang, Z. Cui, C. Cao, and W. Song, “0.3 Å Makes the Difference: Dramatic Changes in Methanol-to-Olefin Activities between H-ZSM-12 and H-ZSM-22 Zeolites,” *The Journal of Physical Chemistry C*, p. 111116154640001, Nov. 2011.

[104] J. Jae, G. A. Tompsett, A. J. Foster, K. D. Hammond, S. M. Auerbach, R. F. Lobo, and G. W. Huber, “Investigation into the shape selectivity of zeolite catalysts for biomass conversion,” *Journal of Catalysis*, vol. 279, no. 2, pp. 257–268, Apr. 2011.

[105] C. Liu, Y. Deng, Y. Pan, Y. Gu, B. Qiao, and X. Gao, “Effect of ZSM-5 on the aromatization performance in cracking catalyst,” *Journal of Molecular Catalysis A: Chemical*, vol. 215, no. 1–2, pp. 195–199, Jun. 2004.

[106] M. Bjorgen, S. Svelle, F. Joensen, J. Nerlov, S. Kolboe, F. Bonino, L. Palumbo, S. Bordiga, and U. Olysbye, “Conversion of methanol to hydrocarbons over zeolite H-ZSM-5: On the origin of the olefinic species,” *Journal of Catalysis*, vol. 249, no. 2, pp. 195–207, Jul. 2007.

[107] P. A. Horne, N. Nugranad, and P. T. Williams, “Catalytic coprocessing of biomass-derived vapours and methanol pyrolysis,” *Journal of Analytical and Applied Pyrolysis*, vol. 34, pp. 87–108, 1995.

[108] M. Tagliabue, A. Carati, C. Flego, R. Millini, C. Perego, P. Pollesel, B. Stocchi, and G. Terzoni, “Study on the stability of a Ga/Nd/ZSM-5 aromatisation catalyst,” *Applied Catalysis A: General*, vol. 265, no. 1, pp. 23–33, Jun. 2004.

[109] H. J. Park, H. S. Heo, J.-K. Jeon, J. Kim, R. Ryoo, K.-E. Jeong, and Y.-K. Park, “Highly valuable chemicals production from catalytic upgrading of radiata pine sawdust-derived pyrolytic vapors over mesoporous MFI zeolites,” *Applied Catalysis B: Environmental*, vol. 95, no. 3–4, pp. 365–373, Apr. 2010.

[110] R. Fricke, H. Kosslick, G. Lischke, and M. Richter, “Incorporation of gallium into zeolites: syntheses, properties and catalytic application.,” *Chemical reviews*, vol. 100, no. 6, pp. 2303–406, Jun. 2000.

[111] M. Choura, N. M. Belgacem, and A. Gandini, “Acid-Catalyzed Polycondensation of Furfuryl Alcohol: Mechanisms of Chromophore Formation and Cross-Linking,” *Macromolecules*, vol. 29, no. 11, pp. 3839–3850, Jan. 1996.

[112] S. Bertarione, F. Bonino, F. Cesano, A. Damin, D. Scarano, and A. Zecchina, “Furfuryl alcohol polymerization in H-Y confined spaces: reaction mechanism and structure of carbocationic intermediates.,” *The journal of physical chemistry. B*, vol. 112, no. 9, pp. 2580–9, Mar. 2008.

[113] A. G. Gayubo, A. T. Aguayo, A. Atutxa, R. Aguado, J. Bilbao, and M. Olazar, “Transformation of Oxygenate Components of Biomass Pyrolysis Oil on a HZSM-5 Zeolite. I. Alcohols and Phenols,” *Industrial & Engineering Chemistry Research*, vol. 43, no. 11, pp. 2610–2618, May 2004.

[114] A. G. Gayubo, A. T. Aguayo, A. Atutxa, R. Aguado, M. Olazar, and J. Bilbao, "Transformation of Oxygenate Components of Biomass Pyrolysis Oil on a HZSM-5 Zeolite. II. Aldehydes, Ketones, and Acids," *Industrial & Engineering Chemistry Research*, vol. 43, no. 11, pp. 2619–2626, May 2004.

[115] P. T. Williams and P. A. Horne, "The influence of catalyst type on the composition of upgraded biomass pyrolysis oils," *Journal of Analytical and Applied Pyrolysis*, vol. 31, pp. 39–61, Feb. 1995.

[116] C. A. Mullen and A. A. Boateng, "Catalytic pyrolysis-GC/MS of lignin from several sources," *Fuel Processing Technology*, vol. 91, no. 11, pp. 1446–1458, Nov. 2010.

[117] A. G. Gayubo, B. Valle, A. T. Aguayo, M. Olazar, and J. Bilbao, "Pyrolytic lignin removal for the valorization of biomass pyrolysis crude bio-oil by catalytic transformation," *Journal of Chemical Technology & Biotechnology*, vol. 85, no. 1, pp. 132–144, Jan. 2010.

[118] R. Fahmi, A. V. Bridgwater, S. C. Thain, I. S. Donnison, P. M. Morris, and N. Yates, "Prediction of Klason lignin and lignin thermal degradation products by Py–GC/MS in a collection of Lolium and Festuca grasses," *Journal of Analytical and Applied Pyrolysis*, vol. 80, no. 1, pp. 16–23, Aug. 2007.

[119] J. D. Adjaye and N. N. Bakhshi, "Production of hydrocarbons by catalytic upgrading of a fast pyrolysis bio-oil. Part II: Comparative catalyst performance and reaction pathways," *Fuel Processing Technology*, vol. 45, no. 3, pp. 185–202, Dec. 1995.

[120] M. C. Samolada, A. Papafotica, and I. A. Vasalos, "Catalyst Evaluation for Catalytic Biomass Pyrolysis," *Energy & Fuels*, vol. 14, no. 6, pp. 1161–1167, Nov. 2000.

[121] H. L. Dao, M. Haniff, A. Houle, and D. Lamothe, "Reactions of Model Compounds of Biomass-Pyrolysis Oils over ZSM—5 Zeolite Catalysts," in *Pyrolysis Oils from Biomass: Producing, Analysing and Upgrading*, J. Soltes and T. A. Milne, Eds. Washington, DC: American Chemical Society, 1988, pp. 328–341.

[122] Z. X. Gao, C. R. Chang, and C. Y. Tan, "The oxidation state of Gallium in Ga/HZSM-5 light alkane aromatization catalysts," *ACS Fuel Preprint for Dallas Spring Meeting*, vol. 43, no. 2, pp. 283–286, 1998.

[123] V. Srinivasan, S. Adhikari, S. A. Chattanathan, and S. Park, "Catalytic Pyrolysis of Torrefied Biomass for Hydrocarbons Production," *Energy & Fuels*, vol. 26, no. 12, pp. 7347–7353, Dec. 2012.

[124] M. . Nokkosmäki, E. . Kuoppala, E. . Leppämäki, and a. O. . Krause, "A novel test method for cracking catalysts," *Journal of Analytical and Applied Pyrolysis*, vol. 44, no. 2, pp. 193–204, Jan. 1998.

[125] Y. Liu, W. Zhang, and T. J. Pinnavaia, "Steam-Stable MSU-S Aluminosilicate Mesostructures Assembled from Zeolite ZSM-5 and Zeolite Beta Seeds," *Angewandte*

Chemie International Edition, vol. 40, no. 7, pp. 1255–1258, 2001.

[126] Y. Liu and T. J. Pinnavaia, "Assembly of wormhole aluminosilicate mesostructures from zeolite seeds," *Journal of Materials Chemistry*, vol. 14, no. 7, p. 1099, 2004.

[127] E. Karimi, A. Gomez, S. W. Kycia, and M. Schlaf, "Thermal Decomposition of Acetic and Formic Acid Catalyzed by Red Mud—Implications for the Potential Use of Red Mud as a Pyrolysis Bio-Oil Upgrading Catalyst § § Dedicated to Prof. Ulf Schuchardt on the occasion of his retirement.," *Energy & Fuels*, vol. 24, no. 4, pp. 2747–2757, Apr. 2010.

[128] A. Lopez, I. de Marco, B. M. Caballero, M. F. Laresgoiti, A. Adrados, and A. Aranzabal, "Catalytic pyrolysis of plastic wastes with two different types of catalysts: ZSM-5 zeolite and Red Mud," *Applied Catalysis B: Environmental*, vol. 104, no. 3–4, pp. 211–219, May 2011.

[129] S. Sushil, A. M. Alabdulrahman, M. Balakrishnan, V. S. Batra, R. A. Blackley, J. Clapp, J. S. J. Hargreaves, A. Monaghan, I. D. Pulford, J. L. Rico, and W. Zhou, "Carbon deposition and phase transformations in red mud on exposure to methane.," *Journal of hazardous materials*, vol. 180, no. 1–3, pp. 409–18, Aug. 2010.

[130] S. Wang, H. M. Ang, and M. O. Tadé, "Novel applications of red mud as coagulant, adsorbent and catalyst for environmentally benign processes.," *Chemosphere*, vol. 72, no. 11, pp. 1621–35, Aug. 2008.

[131] G. Fogassy, N. Thegarid, Y. Schuurman, and C. Mirodatos, "From biomass to bio-gasoline by FCC co-processing: effect of feed composition and catalyst structure on product quality," *Energy & Environmental Science*, vol. 4, no. 12, p. 5068, 2011.

[132] Y. Sun, L. Zhu, H. Lu, R. Wang, S. Lin, D. Jiang, and F. Xiao, "Sulfated zirconia supported in mesoporous materials," *Applied Catalysis*, vol. 237, pp. 21–31, 2002.

[133] A. J. Foster, P. T. M. Do, and R. F. Lobo, "The Synergy of the Support Acid Function and the Metal Function in the Catalytic Hydrodeoxygenation of m-Cresol," *Topics in Catalysis*, vol. 55, no. 3–4, pp. 118–128, Mar. 2012.

[134] B. Li and R. D. Gonzalez, "TGA/FT-IR studies of the deactivation of sulfated zirconia catalysts," *Applied Catalysis A: General*, vol. 165, no. 1–2, pp. 291–300, Dec. 1997.

[135] B. Li and R. D. Gonzalez, "The effect of coke deposition on the deactivation of sulfated zirconia catalysts," *Applied Catalysis A: General*, vol. 174, no. 1–2, pp. 109–119, Nov. 1998.

[136] E. Biagini, F. Lippi, and L. Tognotti, "Characterization of a lab-scale platinum filament pyrolyzer for studying the fast devolatilization of solid fuels," *Fuel*, vol. 85, no. 17–18, pp. 2408–2418, Dec. 2006.

[137] I. Graça, J. M. Lopes, M. F. Ribeiro, F. Ramôa Ribeiro, H. S. Cerqueira, and M. B. B. de Almeida, "Catalytic cracking in the presence of guaiacol," *Applied Catalysis B:*

Environmental, vol. 101, no. 3–4, pp. 613–621, Jan. 2011.

[138] M. Guisnet, L. Costa, and F. R. Ribeiro, "Prevention of zeolite deactivation by coking," *Journal of Molecular Catalysis A: Chemical*, vol. 305, no. 1–2, pp. 69–83, Jun. 2009.

[139] M. Guisnet and P. Magnoux, "Organic chemistry of coke formation," *Applied Catalysis A: General*, vol. 212, no. 1–2, pp. 83–96, Apr. 2001.

[140] A. J. Foster, J. Jae, Y.-T. Cheng, G. W. Huber, and R. F. Lobo, "Optimizing the aromatic yield and distribution from catalytic fast pyrolysis of biomass over ZSM-5," *Applied Catalysis A: General*, vol. 423–424, pp. 154–161, May 2012.

[141] K. S. Triantafyllidis, E. Iliopoulou, E. Antonakou, A. Lappas, H. Wang, and T. J. Pinnavaia, "Hydrothermally stable mesoporous aluminosilicates (MSU-S) assembled from zeolite seeds as catalysts for biomass pyrolysis," *Microporous and Mesoporous Materials*, vol. 99, no. 1–2, pp. 132–139, Feb. 2007.

[142] J. P. Diebold and J. Scahill, "Biomass to gasoline (BTG): upgrading pyrolysis vapors to aromatic gasoline with zeolite catalysis at atmospheric pressure," *ACS, Div. Fuel Chem.*, vol. 32, no. 2, pp. 297–307, Feb. 1987.

[143] J. F. Haw, W. Song, D. M. Marcus, and J. B. Nicholas, "The mechanism of methanol to hydrocarbon catalysis.," *Accounts of chemical research*, vol. 36, no. 5, pp. 317–26, May 2003.

[144] E. Karimi, C. Briens, F. Berruti, S. Moloodi, T. Tzanetakis, M. J. Thomson, and M. Schlaf, "Red Mud as a Catalyst for the Upgrading of {Hemp-Seed} Pyrolysis Bio-oil," *Energy & Fuels*, vol. 24, no. 12, pp. 6586–6600, Dec. 2010.

[145] T. Dogu, "Diffusion and reaction in catalyst pellets with bidisperse pore size distribution," *Ind. Eng. Chem. Res.*, vol. 37, pp. 2158–2171, 1998.

[146] E. Johannessen, G. Wang, and M.-O. Coppens, "Optimal Distributor Networks in Porous Catalyst Pellets. I. Molecular Diffusion," *Industrial & Engineering Chemistry Research*, vol. 46, no. 12, pp. 4245–4256, Jun. 2007.

[147] O. Levenspiel, *Chemical Reaction Engineering*. John Wiley & Sons, Ltd., 1972.

[148] M. E. Davis and R. J. Davis, *Fundamentals of Chemical Reaction Engineering*. McGraw Hill Higher Education, 2003.

[149] R. Aris, "On shape factors for irregular particles I," *Chemical Engineering Science*, vol. 6, pp. 262–268, 1957.

[150] S. Reseter and R. Aris, "Communications on the theory of diffusion and reaction - II The effect of shape on the effectiveness factor," *Chemical Engineering Science*, vol. 24, pp. 793–795, 1969.

[151] D. J. Miller and H. H. Lee, “Shape normalization of catalyst pellet,” *Chemical Engineering Science*, vol. 38, no. 3, pp. 363–366, Jan. 1983.

[152] Y. Li, X. Chang, and Z. Zeng, “Kinetics Study of the Isomerization of Xylene on HZSM-5 Zeolite . 1 . Kinetics Model and Reaction Mechanism,” *Ind. Eng. Chem. Res.*, vol. 31, no. 1, pp. 187–192, 1992.

[153] S. Al-Khattaf, “Xylenes Reactions and Diffusions in ZSM-5 Zeolite-Based Catalyst,” *Industrial & Engineering Chemistry Research*, vol. 46, no. 1, pp. 59–69, Jan. 2007.

[154] H. S. Fogler, *Elements of chemical reaction engineering*. Englewood Cliffs, NJ: Prentice-hall, 1986, p. 769.

[155] W. Song, R. E. Justice, C. a Jones, V. H. Grassian, and S. C. Larsen, “Synthesis, characterization, and adsorption properties of nanocrystalline ZSM-5.,” *Langmuir : the ACS journal of surfaces and colloids*, vol. 20, no. 19, pp. 8301–6, Sep. 2004.

[156] F. a. Da Silva and A. E. Rodrigues, “Adsorption Equilibria and Kinetics for Propylene and Propane over 13X and 4A Zeolite Pellets,” *Industrial & Engineering Chemistry Research*, vol. 38, no. 5, pp. 2051–2057, May 1999.

[157] C. Ercan, F. M. Dautzenberg, C. Y. Yeh, and H. E. Barner, “Mass-Transfer Effects in Liquid-Phase Alkylation of Benzene with Zeolite Catalysts,” *Industrial & Engineering Chemistry Research*, vol. 37, no. 5, pp. 1724–1728, May 1998.

[158] D. Fabbri, C. Torri, and I. Mancini, “Pyrolysis of cellulose catalysed by nanopowder metal oxides: production and characterisation of a chiral hydroxylactone and its role as building block,” *Green Chemistry*, vol. 9, no. 12, p. 1374, 2007.

[159] J. D. Adjaye and N. N. Bakhshi, “Upgrading of a wood-derived oil over various catalysts,” *Biomass and Bioenergy*, vol. 7, no. 1–6, pp. 201–211, Jan. 1994.

[160] H. Wang, “Synthesis , characterization , and catalytic application of strongly acidic mesoporous aluminosilic ...,” Michigan State University, 2007.

[161] D. T. On and S. Kaliaguine, “Large-Pore Mesoporous Materials with Semi-Crystalline Zeolitic Frameworks,” *Angewandte Chemie International Edition*, vol. 40, no. 17, p. 3248=3251, 2001.

[162] X. Lin, A. J. Blake, C. Wilson, X. Z. Sun, N. R. Champness, M. W. George, P. Hubberstey, R. Mokaya, and M. Schröder, “A porous framework polymer based on a zinc(II) 4,4’-bipyridine-2,6,2',6'-tetracarboxylate: synthesis, structure, and ‘zeolite-like’ behaviors.,” *Journal of the American Chemical Society*, vol. 128, no. 33, pp. 10745–53, Aug. 2006.

[163] X. Lai, X. Li, W. Geng, J. Tu, J. Li, and S. Qiu, “Ordered mesoporous copper oxide with crystalline walls.,” *Angewandte Chemie (International ed. in English)*, vol. 46, no. 5, pp. 738–41, Jan. 2007.

[164] J. C. Groen, L. A. A. Peffer, J. A. Moulijn, and J. Pérez-Ramírez, "Mechanism of hierarchical porosity development in MFI zeolites by desilication: the role of aluminium as a pore-directing agent.," *Chemistry (Weinheim an der Bergstrasse, Germany)*, vol. 11, no. 17, pp. 4983–94, Aug. 2005.

[165] J. R. Matos, M. Kruk, L. P. Mercuri, M. Jaroniec, L. Zhao, T. Kamiyama, O. Terasaki, T. J. Pinnavaia, and Y. Liu, "Ordered mesoporous silica with large cage-like pores: structural identification and pore connectivity design by controlling the synthesis temperature and time.," *Journal of the American Chemical Society*, vol. 125, no. 3, pp. 821–9, Jan. 2003.

[166] C. Madsen and C. J. H. Jacobsen, "Nanosized zeolite crystals—convenient control of crystal size distribution by confined space synthesis," *Chemical Communications*, no. 8, pp. 673–674, 1999.

[167] S. Mintova, "Mechanism of Zeolite A Nanocrystal Growth from Colloids at Room Temperature," *Science*, vol. 283, no. 5404, pp. 958–960, Feb. 1999.

[168] K. Na, C. Jo, J. Kim, K. Cho, J. Jung, Y. Seo, R. J. Messinger, B. F. Chmelka, and R. Ryoo, "Directing Zeolite Structures into Hierarchically Nanoporous Architectures," *Science*, vol. 333, no. 6040, pp. 328–332, Jul. 2011.

[169] D. P. Serrano, J. Aguado, G. Morales, J. M. Rodríguez, A. Peral, M. Thommes, J. D. Epping, and B. F. Chmelka, "Molecular and Meso- and Macroscopic Properties of Hierarchical Nanocrystalline ZSM-5 Zeolite Prepared by Seed Silanization," *Chemistry of Materials*, vol. 21, no. 4, pp. 641–654, Feb. 2009.

[170] H. Wang and T. J. Pinnavaia, "MFI Zeolite with Small and Uniform Intracrystal Mesopores," *Angewandte Chemie International Edition*, vol. 45, no. 45, pp. 7603–7606, Nov. 2006.

[171] M. Choi, H. S. Cho, R. Srivastava, C. Venkatesan, D.-H. Choi, and R. Ryoo, "Amphiphilic organosilane-directed synthesis of crystalline zeolite with tunable mesoporosity.," *Nature materials*, vol. 5, no. 9, pp. 718–23, Sep. 2006.

[172] V. R. Choudhary, "Low-Temperature Nonoxidative Activation of Methane over H-Galloaluminosilicate (MFI) Zeolite," *Science*, vol. 275, no. 5304, pp. 1286–1288, Feb. 1997.

[173] S. Todorova and B.-L. Su, "Effects of acidity and combination of Ga and Pt on catalytic behavior of {Ga-Pt} modified {ZSM-5} catalysts in benzene alkylation with pure propane," *Catalysis Today*, vol. 93–95, pp. 417–424, Sep. 2004.

[174] D. H. H. Park, S. S. S. Kim, H. Wang, T. J. J. Pinnavaia, M. C. C. Papapetrou, A. A. a Lappas, and K. S. Triantafyllidis, "Selective Petroleum Refining Over a Zeolite Catalyst with Small Intracrystal Mesopores," *Angewandte Chemie International Edition*, vol. 48, no. 41, pp. 7645–7648, Sep. 2009.

[175] D. P. Serrano, J. Aguado, J. M. Escola, A. Peral, G. Morales, and E. Abella, "Synthesis of

hierarchical ZSM-5 by silanization and alkoxylation of protozeolitic units," *Catalysis Today*, vol. 168, no. 1, pp. 86–95, Jun. 2011.

[176] V. Shetti, J. Kim, R. Srivastava, M. Choi, and R. Ryoo, "Assessment of the mesopore wall catalytic activities of {MFI} zeolite with mesoporous/microporous hierarchical structures," *Journal of Catalysis*, vol. 254, no. 2, pp. 296–303, Mar. 2008.

[177] S. Thangalazhy-Gopakumar, S. Adhikari, and R. B. Gupta, "Catalytic Pyrolysis of Biomass over HZSM-5 under Hydrogen Pressure," *Energy & Fuels*, vol. 26, no. 8, pp. 5300–5306, Aug. 2012.

[178] F. Ronsse, D. Dalluge, W. Prins, and R. C. Brown, "Optimization of platinum filament micropyrolyzer for studying primary decomposition in cellulose pyrolysis," *Journal of Analytical and Applied Pyrolysis*, vol. 95, pp. 247–256, May 2012.

[179] B. Valle, P. Castaño, M. Olazar, J. Bilbao, and A. G. Gayubo, "Deactivating species in the transformation of crude bio-oil with methanol into hydrocarbons on a HZSM-5 catalyst," *Journal of Catalysis*, vol. 285, no. 1, pp. 304–314, Jan. 2012.

[180] G. T. Neumann and J. C. Hicks, "Novel Hierarchical Cerium-Incorporated MFI Zeolite Catalysts for the Catalytic Fast Pyrolysis of Lignocellulosic Biomass," *ACS Catalysis*, vol. 2, no. 4, pp. 642–646, Apr. 2012.

[181] S. B. A. Hamid, E. G. Derouane, G. Demortier, J. Riga, and M. A. Yarmo, "State, activation, and migration of gallium in Ga H-MFI(Si,Al) propane aromatization catalysts," *Applied Catalysis A: General*, vol. 108, no. 1, pp. 85–96, Jan. 1994.

[182] B. Kwak, "Effect of Ga/Proton Balance in Ga/HZSM-5 Catalysts on C3 Conversion to Aromatics," *Journal of Catalysis*, vol. 145, no. 2, pp. 456–463, Feb. 1994.

[183] N. Al-Yassir, M. N. Akhtar, and S. Al-Khattaf, "Physicochemical properties and catalytic performance of galloaluminosilicate in aromatization of lower alkanes: a comparative study with Ga/HZSM-5," *Journal of Porous Materials*, vol. 19, no. 6, pp. 943–960, Dec. 2011.

[184] R. French and S. Czernik, "Catalytic pyrolysis of biomass for biofuels production," *Fuel Processing Technology*, vol. 91, no. 1, pp. 25–32, Jan. 2010.

[185] A. I. Serykh, "On the formation of surface gallium hydride species in supported gallium catalysts," *Applied Surface Science*, vol. 259, pp. 252–255, Oct. 2012.

[186] G. Price, "On the Mechanism of Propane Dehydrocyclization over Cation-Containing, Proton-Poor MFI Zeolite," *Journal of Catalysis*, vol. 173, no. 1, pp. 17–27, Jan. 1998.

[187] W.-L. Fanchiang and Y.-C. Lin, "Catalytic fast pyrolysis of furfural over H-ZSM-5 and Zn/H-ZSM-5 catalysts," *Applied Catalysis A: General*, vol. 419–420, pp. 102–110, Mar. 2012.

[188] Z. Nawaz, T. Xiaoping, and W. Fei, “Influence of operating conditions, Si/Al ratio and doping of zinc on Pt-Sn/ZSM-5 catalyst for propane dehydrogenation to propene,” *Korean Journal of Chemical Engineering*, vol. 26, no. 6, pp. 1528–1532, Feb. 2010.

[189] M. N. Mikhailov, I. V. Mishin, L. M. Kustov, and A. L. Lapidus, “Structure and reactivity of Pt/GaZSM-5 aromatization catalyst,” *Microporous and Mesoporous Materials*, vol. 104, no. 1–3, pp. 145–150, Aug. 2007.

[190] D. H. Park, S. Kim, T. J. Pinnavaia, F. Tzompantzi, J. Prince, and J. S. Valente, “Selective Isobutene Oligomerization by Mesoporous MSU-S,” *Langmuir*, pp. 5809–5816, 2011.

[191] J. Yoon, J. Chang, H. Lee, T. Kim, and S. Jhung, “Trimerization of isobutene over a zeolite beta catalyst,” *Journal of Catalysis*, vol. 245, no. 1, pp. 253–256, 2007.

[192] K. Hauge, E. Bergene, D. Chen, G. R. Fredriksen, and a. Holmen, “Oligomerization of isobutene over solid acid catalysts,” *Catalysis Today*, vol. 100, no. 3–4, pp. 463–466, Feb. 2005.

[193] M. R. Goldwasser and D. L. Trimm, “The oxidation of isobutene to p-xylene over bismuth oxide-based catalysts,” *Journal of Chemical Technology and Biotechnology*, vol. 28, no. 11, pp. 733–739, Nov. 1978.

[194] N. M. Al-Otaibi and G. Hutchings, “Aromatization of Isobutene Using H-ZSM-5/Oxide Composite Catalysts,” *Catalysis Letters*, vol. 134, no. 3–4, pp. 191–195, Dec. 2009.

[195] F. Solymosi and A. Széchenyi, “Aromatization of isobutane and isobutene over Mo2C/ZSM-5 catalyst,” *Applied Catalysis A: General*, vol. 278, no. 1, pp. 111–121, Dec. 2004.

[196] USDA Foreign Agricultural Service, “Coffee: World Markets and Trade,” 2012.

[197] I. Safarik, K. Horska, B. Svobodova, and M. Safarikova, “Magnetically modified spent coffee grounds for dyes removal,” *European Food Research and Technology*, vol. 234, no. 2, pp. 345–350, Dec. 2011.

[198] N. Kondamudi, S. K. Mohapatra, and M. Misra, “Spent Coffee Grounds as a Versatile Source of Green Energy,” *Journal of Agricultural and Food Chemistry*, vol. 56, no. 24, pp. 11757–11760, Dec. 2008.

[199] Z. Al-Hamamre, S. Foerster, F. Hartmann, M. Kröger, and M. Kaltschmitt, “Oil extracted from spent coffee grounds as a renewable source for fatty acid methyl ester manufacturing,” *Fuel*, vol. 96, pp. 70–76, Jun. 2012.

[200] A. Zuorro and R. Lavecchia, “Spent coffee grounds as a valuable source of phenolic compounds and bioenergy,” *Journal of Cleaner Production*, vol. 34, pp. 49–56, Oct. 2012.

[201] R. Cruz, M. M. Cardoso, L. Fernandes, M. Oliveira, E. Mendes, P. Baptista, S. Morais, and S. Casal, “Espresso coffee residues: a valuable source of unextracted compounds.,”

Journal of agricultural and food chemistry, vol. 60, no. 32, pp. 7777–84, Aug. 2012.

[202] A. Nakanishi, M. Tamai, N. Kawasaki, T. Nakamura, M. Araki, and S. Tanada, "Characterization of Water Adsorption onto Carbonaceous Materials Produced from Food Wastes," *Journal of Colloid and Interface Science*, vol. 255, no. 1, pp. 59–63, Nov. 2002.

[203] T. Nakamura, M. Hirata, N. Kawasaki, S. Tanada, T. Tamura, and Y. Nakahori, "Decolorization of Indigo Carmine by Charcoal from Extracted Residue of Coffee Beans," *Journal of Environmental Science and Health, Part A*, vol. 38, no. 3, pp. 555–562, Apr. 2003.

[204] R. Bedmutha, C. J. Booker, L. Ferrante, C. Briens, F. Berruti, K. K.-C. Yeung, I. Scott, and K. Conn, "Insecticidal and bactericidal characteristics of the bio-oil from the fast pyrolysis of coffee grounds," *Journal of Analytical and Applied Pyrolysis*, vol. 90, no. 2, pp. 224–231, Mar. 2011.

[205] J. P. Bok, H. S. Choi, Y. S. Choi, H. C. Park, and S. J. Kim, "Fast pyrolysis of coffee grounds: Characteristics of product yields and biocrude oil quality," *Energy*, vol. 47, no. 1, pp. 17–24, Nov. 2012.

[206] R. G. Petersen, *Design and analysis of experiments*. Marcel Dekker, Inc, 1985, p. 429.

[207] L. A. Bissett and S. C. Lamey, "Flash pyrolysis of Montana Rosebud coal. 1. Experimental data and response surface model predictions for product gas and char," *Energy & Fuels*, vol. 2, no. 6, pp. 819–827, Nov. 1988.

[208] S. V. Ghadge and H. Raheman, "Process optimization for biodiesel production from mahua (Madhuca indica) oil using response surface methodology.," *Bioresource technology*, vol. 97, no. 3, pp. 379–84, Feb. 2006.

[209] K. Ravikumar, S. Krishnan, S. Ramalingam, and K. Balu, "Optimization of process variables by the application of response surface methodology for dye removal using a novel adsorbent," *Dyes and Pigments*, vol. 72, no. 1, pp. 66–74, Jan. 2007.

[210] ASTM International, "Standard Test Method for Carbon Black-Pellet Size Distribution—D 1511-10," 2010.

[211] A. V. Bridgwater, "The production of biofuels and renewable chemicals by fast pyrolysis of biomass," *Internation Journal of Global Energy Issues*, vol. 27, pp. 160–203, 2007.

[212] J. Piskorz, P. Majerski, D. Radlein, D. S. Scott, and A. V. Bridgwater, "Fast pyrolysis of sweet sorghum and sweet sorghum bagasse," *Journal of Analytical and Applied Pyrolysis*, vol. 46, no. 1, pp. 15–29, Jun. 1998.

[213] NIST/SEMATECH, *e-Handbook of Statistical Methods*, April 2012. National Institute of Standards and Technology, 2012.

[214] ASTM International, "ASTM E203 - 08 Standard Test Method for Water Using

Volumetric Karl Fischer Titration," 2008.

[215] C. Di Blasi, "Modelling the fast pyrolysis of cellulosic particles in fluid-bed reactors," *Chemical Engineering Science*, vol. 55, no. 24, pp. 5999–6013, Dec. 2000.

[216] A. V. Bridgwater, A. J. Toft, and J. G. Brammer, "A techno-economic comparison of power production by biomass fast pyrolysis with gasification and combustion," *Renewable and Sustainable Energy Reviews*, vol. 6, no. 3, pp. 181–246, Sep. 2002.

[217] M. Garcia-Perez, X. S. Wang, J. Shen, M. J. Rhodes, F. Tian, W.-J. Lee, H. Wu, and C.-Z. Li, "Fast Pyrolysis of Oil Mallee Woody Biomass: Effect of Temperature on the Yield and Quality of Pyrolysis Products," *Industrial & Engineering Chemistry Research*, vol. 47, no. 6, pp. 1846–1854, Mar. 2008.